The runup of long waves

by

Constantine Emmanuel Synolakis

Project Supervisor:

Fredric Raichlen
Professor of Civil Engineering and Mechanical Engineering

Supported by:
National Science Foundation Awards No.
ENV77-20499, CEE79-1234, CEE81-15457 and CEE84-10087

W. M. Keck Laboratory of Hydraulics and Water Resources
Division of Engineering and Applied Science
California Institute of Technology
Pasadena, California 91125
Report No. KH-R-61 January 1986/September 2007

This work is dedicated to Irene Davos.

This report is essentially the thesis of the same title submitted by the author on January 1986 to the California Institute of Technology, in partial fulfillment of the requirements for the degree of Doctor of Philosophy in Mechanical Engineering. This material is based upon work supported by the National Science Foundation under Awards ENV77-20499, CEE79-1234, CEE81-15457 and CEE84-10087. Any opinions, findings, and conclusions or recommendations expressed in this publication are those of the author and do not necessarily reflect the views of the National Science Foundation.

ACKNOWLEDGEMENTS

I would like to acknowledge the support of my adviser Fred Raichlen throughout the progress of my work. I would also like to thank him for arranging for a major part of the funding for this study. In this regard, I acknowledge the support of the National Science Foundation through the following contracts : ENV77–20499, CEE79–1234, CEE81–15457 and CEE84–10087. I am also grateful for the partial support of the Alexander Onassis Public Benefit Foundation. I would like to thank John List and Norman Brooks for supporting my earlier work with the contracts CME77–27398 and ENG77–10182 and EPA/CH2M Hill ENG–238.

In his "Postscript to the Name of the Rose", Umberto Eco writes: *The writer (or painter or sculptor or composer) always knows what he is doing and how much it costs him. He knows he has to solve a problem. Perhaps the original data are obscure, pulsive obsesive, no more than a yearning or a memory. But then the problem is solved at the writer's desk as he interrogates the material on which he is working–material that reveals natural laws of its own, but at the same time contains the culture with which it is loaded (the echo of intertextuality).* It is for his benefit and that of other period historians that I will now provide a record of this study to identify the contributions of my colleagues and my peers ; after all, academic life is often similar to life in a Benedictine monastery.

My interest in science was aroused early in my life. My mother's laboratory was a wimsical world where centrifuges, microscopes, scales, photometers, and my mother constantly conspired to convince me that there was order in the world around me. It was my desire to prove her wrong that led me in my present career. It is with regret and with relief that I confess that what I achieved to demonstrate is that there is order some of the time and no order the rest of the time.

Paul Dimotakis picked up where my mother and father had left. He challenged all of my adolescent beliefs. His persistence in teaching me that computers never knowingly make mistakes paid off; the

graphics software I developed from scratch is there to show it. Alan Acosta and Rolf Sabersky were my first fluid mechanics teachers. I thank them both for stimulating my curiosity.

Next came three great teachers : Cathy Van Ingen, John List and Michael Hoffman. Cathy taught me everything I always wanted to know about being a graduate student at Keck labs, and, regrettably, many things I never wanted to know. Not only did she teach me the elements of style in computer programming, but also how to be software and hardware independent. She also galvanised me to be vigilant towards charlatanism. Thank you, Cathie. John List taught me the basic methods of applied mathematics. His lectures on contour integration so impressed me, that, without any difficulty, I proceeded to derive the long sought exact solution of the runup integral. I dedicate the solution to him and his powers of instruction. I also want to pay tribute to his talent to recognise talent. Thank you, John. Michael Hoffman influenced my intellectual development in many ways. I thank him for being the model of the consumate scientist, for assembling what is undoubtedly one of the brightest group of graduate students at Caltech (as evidenced by the fact that most of them became my best friends), and for stoically permitting me to use and abuse his computer hardware. Thank you, Michael.

Talking about friends, colleagues and peers, use and abuse. Without Martha Conklin, Jed Waldman and Panos Papanicolaou I would not have written my magnus opus. Leonidas and Constantine Vokas, Mike Lewy, Bruce Faust, Alan Stone, Johanna Wiebe, Sophie Lazarides, Edie Moore, Gina Christoula and Irene Andersen all pulled me through, each at different stages of my life. I love them all and I promise to let them pull me through again, when the need arises.

Other people have contributed significantly in my thesis work and my student life. I thank Norman Brooks for his contagious enthusiasm and his profound physical insight; he was of great help in probing the tangible unknown; Rick Flagan for his valuable advice for probing of the intagible known; Jim Morgan for letting me be Adso of Melk to his William of Baskerville; Jim Skjelbreia for his macros that made data acquisition a snap and his strange humor that made it a strange

pleasure ; Joan Mathews for all her help ; she made the interaction with the invisible and invincible powers much easier ; Rayma Harisson and Gunilla Halstrup for being a faithful audience ; Elton Daly, Jo Fontana, Rich Eastvedt, Leonard Montenegro and their little shop of horrors for always producing the ultimate contraption for the problem at hand, and for managing to satisfy my insatiable appetite for gadgetry (not always an easy feat).

On the serious side. Howell Peregrine, Gerry Whitham, George Carrier, Bob Guza, and Philip Liu provided varying amounts of criticism and suggestions for proceeding in this study. Carrier's, Peregrine's and Whitham's work has profoundly influenced my understanding of long waves. (As Woody Allen says, we must all choose our role models.)

On the more serious side. I want to thank Rena Davos, Cliff Ossorio, Bob Taub and Mel Avedon for providing the moral support and proper care for the past fifty four months. I cannot speculate where I would be without them; it is still too painful. Maybe, in six months, it will be less painful.

On the dead serious side. I am grateful to Rena Davos and Martha Conklin. Their commitment and dedication to their work is a continuous source of inspiration and encouragement in my own life. Thank you, Martha and Rena. Thank you, Martha, for sharing with me my life and times.

Finally, I want to thank my parents. They provided the intellectual encouragement and the proper emotional support that is necessary in any academic endeavour. Their generosity in providing a significant part of the computer hardware used in this study is deeply appreciated. Their vision made all this possible. Thank you, Mary and Manoli.

Abstract

The runup of long waves

This is a study of the fundamental physical processes of the runup of long waves with the objective to understand some coastal effects of tsunamis.

The runup of nonbreaking long waves on plane beaches is studied and an exact solution is developed for the runup of solitary waves. The maximum runup predicted by this solution is compared to laboratory data from this and other investigations and it is found to be in good agreement. A runup transducer was developed and deployed in the laboratory to provide data for the shape of the runup tongue. The exact solution is shown to model the details of the climb of the wave satisfactorily.

The runup of breaking long waves on plane beaches is investigated in the laboratory by studying different long waves and bores of finite volume. The runup is shown to be a function of a momentum scale determined from the generation characteristics of the incoming wave. The runup number is introduced and it is demonstrated that it models the runup process adequately. It is also observed that arbitrary long waves have runup numbers smaller than, or at most equal to, the runup number of breaking solitary waves, suggesting that on a given plane beach breaking solitary waves run-up further than other long waves with similar generation characteristics.

An exact result is established for the force on an accelerating plate in a fluid with a free surface. The result is used to explain some of the results of this study and other results on the hydrodynamic forces on moving partitions.

A technique is developed to generate arbitrary, long, continuously evolving waves at any desired location in a laboratory model. The technique is applied in the laboratory and it is shown to be successful in reproducing complex waveforms.

Table of Contents

Table of contents, continued

Table of contents, continued

Table of contents, continued

List of symbols

If a particular symbol is defined by an equation the number of the defining equation is preceded by the letter E. *If the symbol is defined in a figure, the figure number is preceded by the letter* F. *Otherwise, a page number is given preceded by the letter* p.

English symbols	Explanation of symbol	Defined by
a_n	: the residue of the integrand (3.4.4) at the nth pole.	E (3.4.14)
A_i	: the dimensionless amplitude of the incident wave to the beach.	E (3.2.2)
A_r	: the dimensionless amplitude of the wave reflected from the beach.	E (3.2.2)
b_n, b_0	: the coefficients in the series expansion of the velocity potential.	E (A2.3)
B	: the dimensionless amplitude of the wave transmitted to the beach .	E (3.2.2b)
c	: the dimensionless speed of propagation of shallow water waves over constant depth.	E (3.2.2)
c*	: the dimensional phase speed.	p 14
c_n	: the nth coefficient in a Fourier Bessel series.	E (3.2.5)
C	: a contour in the complex plane.	E (3.4.4)
C_m, C_e	: arbitrary constants used in dimensional analysis.	E (4.3.1)
d	: the depth of the constant depth region, always dimensional.	F (1.1.1)
D	: a domain in the complex plane.	p 61
$\mathbf{E}_p$	: the dimesional integral of the power imparted by the plate to the fluid.	E(4.4.11)
Fr	: the generation number $S/[T\sqrt{(gd)}]$.	p 113
F	: the boundary condition for solving the long wave equations.	p 58
$\underline{\mathbf{F}}$	: the dimensional force, a vector.	E (4.4.1)
$\mathbf{F}_{px}$	: the dimensional force on the wave plate per unit width in the x-direction, a scalar.	E (4.4.4)
$\mathbf{F}_{sx}$	: the dimensional force per unit width in the x-direction on the seaward boundary of volume ABCD of figure (4.1.1), a scalar.	E (4.4.7)

List of symbols, continued

$\mathbf{F}_{bx}$	: the dimensional force per unit width on the beach in the x-direction due to the hydrodynamic pressure of the fluid on the beach, a scalar.	E (4.4.9)
g	: the acceleration of gravity.	p 11
h	: the dimensionless total depth of the flow.	p 53
h_0	: the dimensionless undisturbed water depth.	E (3.1.2)
$\hat{h}$	: the dimensionless depth multiplied by $\cos\beta$.	E (B1.3)
H	: the wave height, always dimensional.	F (1.1.1)
H_{dr}	: the dimensional height of the positive wave of the dipole-shaped reflected wave.	E (3.8.1)
i	: the square root of (-1).	p 53
I_n	: the modified Bessel function of order n.	p 63
$\mathbf{I}_c$	: a contour integral.	E (3.4.4)
$\mathbf{I}_r$	: the part of a contour integral evaluated along the real axis.	p 61
$\mathbf{I}_\theta$	: the part of a contour integral evaluated along an arc of a circle.	p 61
j_n	: the nth zero of J_0.	p 54
$\boldsymbol{J}$	: the Jacobian of the Carrier and Greenspan transformation.	p 88
J_n	: the Bessel function of order n.	E (1.2.2)
k	: the wavenumber (dimensionless)	E (3.2.2)
K	: a dimensionless constant used in runup relationships.	E (1.3.2)
l	: a dimensional propagation distance.	p 111
L	: a measure of the horizontal extent of a solitary wave.	E (3.5.1)
L	: the dimensional long wave wavelength.	F (1.1.1)
L_0	: the dimensional deep water wavelength.	p 7
$\underline{\mathbf{M}}$	: the wave momentum, a vector.	E (4.4.2)
$\mathbf{M}_x$	: the dimensional wave momentum per unit width and in the x-direction.	E (4.4.4)
$\mathbf{M}_{vx}$	: the dimensional momentum per unit width contained in the control volume ABCD of figure (4.1.1).	E (4.4.6)
n	: the index of power series.	E (3.4.15)
N	: the number of zeroes in contour integrals.	p 62
p	: the dimensional fluid pressure.	E (A1.9)
P	: number of poles in contour integrals.	p 56
$\mathbf{P}_f$	: the integral of the momentum flux per unit width and per unit mass at the plate.	E (4.4.12)

List of symbols, continued

R	: the dimensional surface elevation at the initial position of the shoreline.	E (3.4.3)
$\mathbf{R}$	: the dimensional maximum vertical shoreline excursion, the wave runup.	F (1.1.1)
Ru	: the runup number $\mathbf{R}g^{1/5}/(S^2d/T)^{2/5}$.	E (4.3.5)
s	: a generic variable name used in integral substitutions.	p 54
S	: the dimensional piston stroke.	p 112
t	: the dimensionless time (dimensional in appendix A).	E (3.1.1)
t*	: the dimensional time.	E (3.1.1)
t_{max}	: the dimensionless time when a wave reaches its maximum runup.	E (3.4.18)
t	: the dimensionless time multiplied by $\sin\beta$.	E (B1.3)
T	: the duration of the piston motion (dimensional).	p 96
T_h	: the dimensional period of the periodic wave that is the best fit to the Boussinesq profile.	p 14
u	: the dimensionless horizontal water particle velocity.	E (3.1.1)
u*	: the dimensional horizontal water particle velocity.	E (3.1.1)
u_s	: the dimensionless instantaneous velocity of the shoreline.	p 59
U	: the dimensionless speed of propagation of discontinuities.	E (1.3.3)
U	: the dimensional speed of propagation of a bore when it reaches the shoreline.	E (1.3.4)
υ	: a dimensionless long wave parameter.	p 4
v	: the dimensional vertical particle velocity.	F (A1.1)
V	: the dimensionless plate velocity.	p 190
v_p	: the dimensionless plate velocity.	E (A3.1)
x	: the dimensionless horizontal coordinate, (dimensional in appendix A).	F (3.1.1)
x*	: the dimensional horizontal coordinate.	E (3.1.1)
x	: The dimensionless distance multiplied by $\sin\beta$	E (B1.3)
X_1	: the dimensionless x-location where the offshore height of a solitary wave is defined, dimensionless.	F (3.1.1)
X_0	: the location of the toe of the sloping beach, dimensionless. ($X_0 = \cot\beta$)	F (3.1.1)
y	: the dimensional vertical coordinate.	F (3.1.1)
z	: a generic complex variable name.	p 61

List of symbols, continued

Greek Symbols

α	:	a dimensionless solitary wave parameter.	p 60
β	:	the angle of the sloping beach.	F (1.1.1)
β	:	the dimensionless Riemann invariant.	E (B2.2)
γ	:	the dimensionless wavenumber of solitary waves.	E (3.4.1b)
δ	:	the dimensionless frequency squared = $\omega^2 d/g$.	E (A3.5)
ε	:	the dimensional bed roughness height.	p 111
ε	:	the ratio of wave height to water depth.	p 184
ζ	:	a real variable used in substitutions in integral evaluations.	p 54
η	:	the dimensionless wave amplitude.	E (3.1.1)
η^*	:	the dimensional wave amplitude.	E (3.1.1)
η_p	:	the dimensional surface elevation at the plate.	F (A1.1)
η_{rs}	:	the dimensionless height of the shelf behinf a solitary wave at the toe of the beach.	F (3.5.7)
θ	:	a phase difference.	p 61
κ	:	a dimensionless wavenumber in the (σ,λ) plane.	p 57
λ	:	the Carrier and Greenspan time-like coordinate.	E (3.3.1)
μ	:	the dimensional fluid viscocity.	p 111
ν	:	the dimensional kinematic viscocity.	E (4.2.2)
ξ	:	the dimensional plate path or plate trajectory. (dimensionless in appendix C)	E (A1.1)
π	:	3.14159265358979323846264 3	p 60
ρ	:	the dimensional fluid density.	p 111
σ	:	the Carrier and Greenspan x-like coordinate.	E (3.3.1)
σ	:	the rato of the water depth to the wavelength.	p 184
Σ_{max}	:	a generic name for the maximum value of a series.	E (A3.5)
ϕ	:	an arbitrary function used in empirical runup relationships.	E (1.3.2)
Φ	:	the Fourier transform of the wave amplitude.	p 56
χ	:	a variable used for change of variables for integral evaluation or substitutions in series.	p 64
ψ	:	the Carrier and Greenspan function.	F (3.3.1)
Ψ	:	the Fourier transform of ψ.	p 57
ω	:	the dimensional frequency.	p 14

List of figures

List of figures, continued

List of figures, continued

page **Chapter 3**

List of figures, continued

List of figures, continued

List of figures, continued

List of figures, continued

List of figures, continued

List of figures, continued

List of figures, continued

page Appendix B

page Appendix C

List of figures, continued

Chapter 1

Introduction

The objective of this study is the theoretical and experimental investigation of the runup of long waves on plane beaches. This problem arises in the evaluation of the coastal effects of tsunamis. Tsunamis are long water waves generated either by submarine tectonic displacements, or landslides. At generation, tsunamis are waves of small amplitude with wavelength large compared to the local depth ; they are essentially shallow water waves. Shallow water waves propagate at a speed approximately equal to the square root of the product of the depth and the acceleration of gravity. In a water depth of 4 km a tsunami travels at a speed of 200 m/sec or 720 km/hour. As a tsunami approaches coastal waters refraction and shoaling may amplify the wave appreciably. The flooding usually associated with tsunamis causes significant damage to structures and beaches in coastal areas.

1.1 Tsunamis and tsunami runup. It is conjectured that the first historical reference to coastal inundation by a tsunami is an episode associated with the eruption of the Thira volcano in the eastern Mediterranean, about 1500BC-1450BC. The event coincides with the devastation of the highly developed Minoan civilization on the northeastern coast of the island of Crete [Warren (1985)]. Although the immediate agent of the catastrophe was fire, it is hypothesized that a tsunami destroyed whatever had survived the fire. More recently, there are accounts of tsunamis in Japan dated back at least 1300 years. According to a current compilation of historical occurrences of tsunamis there have been 143 reported tsunamis between 1861 and 1961 [Camfield, (1980)]. The most recent major tsunami occurred in 1983 in the sea of Japan, and it resulted in the loss of about 100 lives.

The process of tsunami generation and propagation is now well understood. The runup process is not. There is consensus that one suitable physical model for the process of tsunami runup is the formalism of long waves propagating through a constant depth region and encountering a sloping beach [Meyer, (1972)]. This geometry is shown in figure (1.1.1). It represents a two-dimensional model, and it is frequently justified by arguing that wave refraction turns the wave crests, so that in the final stages of approach to the shoreline the runup process is essentially two-dimensional. The two-dimensional model has been shown to produce realistic results [Hammack, (1972)], except in cases of tsunami runup in estuaries, bays and harbors.

Historically, there have been two types of long waves used in the investigations of tsunami runup. A small number of studies have used solitary waves and undular bores. The others have used periodic long waves. Since there are no records of the surface elevation of a tsunami close to its source, there is little agreement about which model best describes a tsunami.

1.2 The runup of periodic long waves. Linear theory. The first study on tsunami runup was that of Kaplan (1955) who generated periodic waves that climbed a sloping beach after travelling over a constant depth region. He derived two empirical relationships from his experiments, of the form :

$$\frac{\mathbf{R}}{\mathrm{H}} = 0.381 \left(\frac{\mathrm{H}}{\mathrm{L}}\right)^{-0.316}, \qquad \text{when } \tan\beta = 1/30, \qquad (1.2.1a)$$

and

$$\frac{\mathbf{R}}{\mathrm{H}} = 0.206 \left(\frac{\mathrm{H}}{\mathrm{L}}\right)^{-0.315}, \qquad \text{when } \tan\beta = 1/60, \qquad (1.2.1b)$$

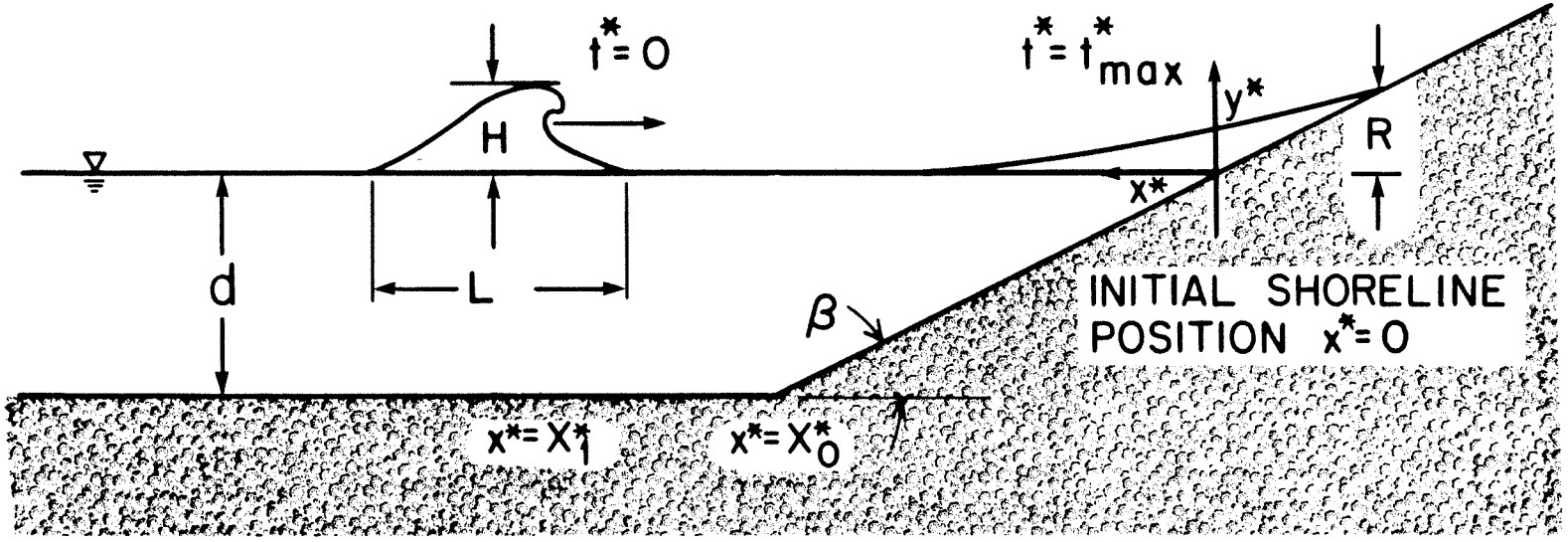

Figure 1.1.1 A definition sketch.

where **R** is the maximum wave runup, H is the offshore wave height, L is the offshore wavelegth, and β is the beach angle. The ratio **R**/H can be thought of as an amplification factor; for a vertical wall and inviscid flow conditions, **R**/H = 2. Unfortunately tables of data were not published, so that it is not possible to determine whether the waves used in the experiments were breaking or nonbreaking, or whether they were long or short waves. The only information available is that the wave-steepness parameter H/L was in the range $(2\times10^{-3}, 10^{-1})$. Nevertheless, equations (1.2.1) have been used extensively since, both for verification of theoretical models and for comparison with other laboratory studies within and beyond the range of Kaplan's data set.

The first analytical investigation of the propagation problem over the bathymetry defined in figure (1.1.1) was that of Keller and Keller (1960). They derived the following expression for the runup of periodic waves on a sloping beach using the linear nondispersive theory :

$$\mathbf{R}/H = 1/\{ J_0^2(\upsilon) + J_1^2(\upsilon)\}^{1/2} , \qquad (1.2.2)$$

where $\upsilon = 4\pi H/(L\tan\beta)$. Shuto (1967) solved the linearized form of the equation of motion for inviscid flow in Lagrangian coordinates and derived a similar expression, of the form :

$$\mathbf{R}/H = 1/ J_0(\upsilon) \qquad (1.2.3)$$

The three relationships (1.2.1), (1.2.2) and (1.2.3) have formed the basis of most studies in periodic long wave runup. Many studies have included the effects of bottom roughness, composite beaches, irregular waves, and varying channel widths. An extensive review of the literature of the subject can be found in the work of Togashi (1981),

who did a systematic compilation of the predictions of various laboratory investigations and compared them amongst themselves and with the analytical results (1.2.2) and (1.2.3). Figure (1.2.1) shows one comparison for wave runup on a 1:30 beach, exactly as presented by Togashi.

This figure is indicative of the state of the art and it has appeared in several review articles in the last ten years. It does not provide confidence in using any of the models presented, except perhaps in the range of values of wave steepness where the models do not contradict each other. One possible explanation is that the models represent data for different types of waves . In the nonbreaking wave region, Shuto's laboratory data are in the same range as Togashi's. Both seem to agree with the analytical results (1.2.2) and (1.2.3) in that range, which is reasonable since both analytical results refer to nonbreaking waves. These predictions are inconsistent with the data in the figure attributed to Kishi and Hanai, and to Kaplan (1955). Although it is not clear whether the latter are derived from breaking or from nonbreaking waves, one can hypothesize that they were derived from breaking wave data. This would be consistent with the other breaking wave data shown in the figure. Indeed, if this is the case, then it is obvious that different functional variations exist for the different breaking categories rather than the "unifying" fit reported by Togashi : $\mathbf{R}/H=46.0(H/L)^{0.468}$. There appears to be no apparent physical reason why runup data derived from experiments with breaking and nonbreaking waves should follow the same quantitative relationship.

It is interesting to attempt to reconstruct figure (1.2.1) by examining the data in groups depending on their breaking characteristics. For nonbreaking waves, and when $H/L < 0.001$, the Bessel functions of equation (1.2.2) can be replaced with their expansions for small arguments. This reduces (1.2.2) to $\mathbf{R}/H = 1$, a relationship which agrees with

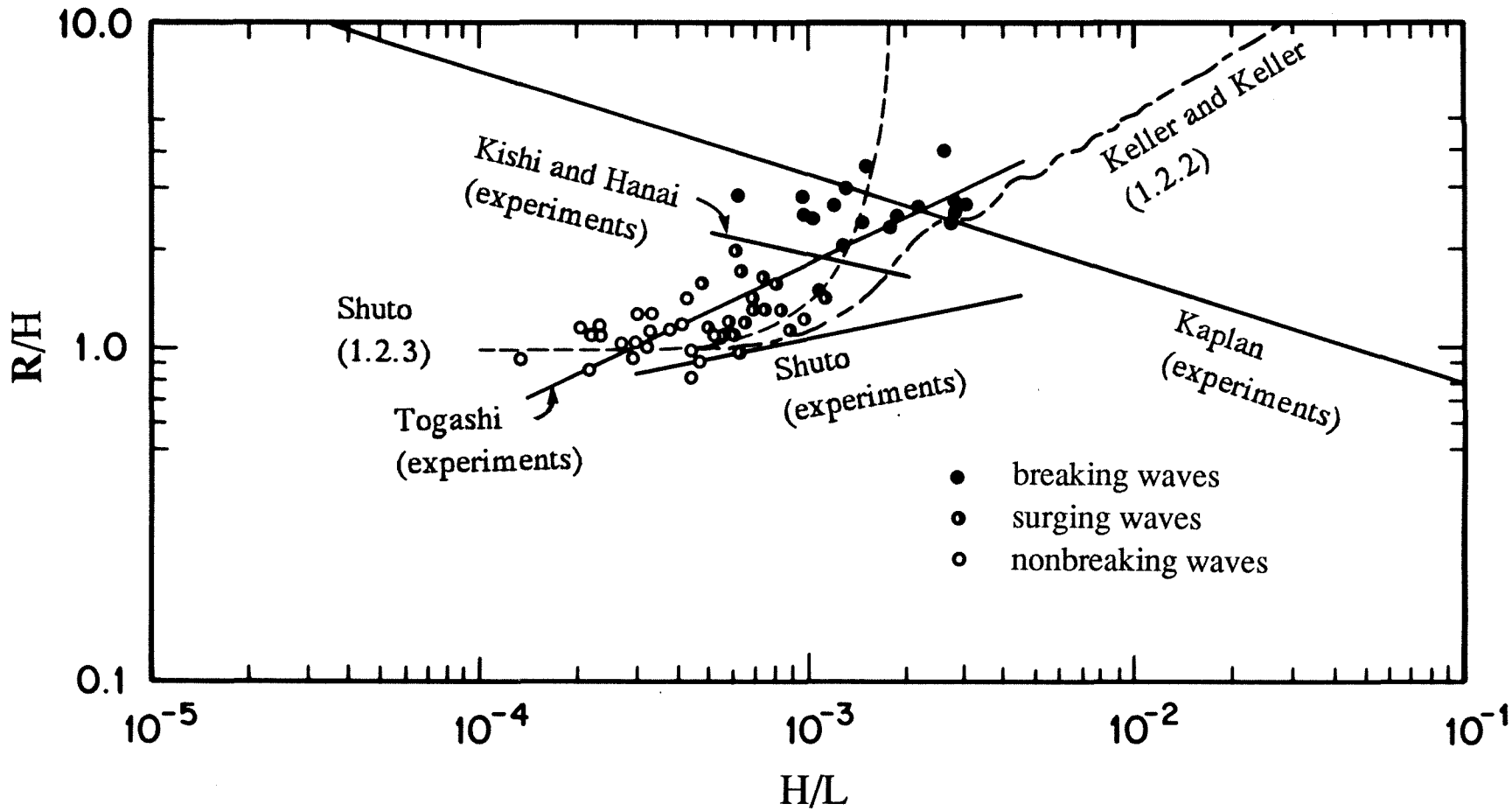

Figure 1.2.1 The runup of periodic waves on a 1:30 beach. The solid lines represent empirical fits of laboratory data. The solid line identifying Kaplan's data is drawn as presented by Kaplan (1955), although it extends beyond the range of his data set. The dashed lines represent two linear theory models (1.2.2) and (1.2.3). After Togashi (1981).

the data in the figure. The data also indicate that **R**/H is constant for surging waves and constant for breaking waves, although the scatter of the data does not permit positive identification of the values of these two constants. This observation is also consistent with data presented by Kishi (1962), for values of H/L in the range ($6x10^{-4}$, $1.5x10^{-3}$), but inconsistent with the extrapolated fit of Kaplan's data in that range. [Kaplan's experiments were conducted with H/L in the range ($2x10^{-3}$, 10^{-1}).]

To obtain further insight in Kaplan's data, one can use some of the results of the runup of waves on steep beaches. Battjes (1971) argued that for deep water waves climbing on steep beaches,

$$\frac{R}{H} = K \tan\beta \frac{1}{\sqrt{H/L_0}} \qquad (1.2.4)$$

where K is a constant that was set equal to one, and L_0 is the deep water wavelength. He named the parameter $\tan\beta / \sqrt{H/L_0}$ the Irribarren parameter, after Irribarren and Nogales (1949) who were the first to present it. Equation (1.2.4) was shown to agree well with breaking wave data for slopes in the range (1/3,1/7). Battjes (1971) was also able to derive breaking criteria based on this parameter. Although equation (1.2.4) with K=1 is not compatible with Kaplan's data, it seems reasonable to assume a variation of the same form and determine the constant K. Using equations (1.2.1a) and (1.2.1b), one finds that K=11.43 for the 1/30 beach slope and K=12.36 for the 1/60 slope. Averaging the two values, Kaplan's result can be restated as follows :

$$\frac{R}{H} = 11.89 \tan\beta \left(\frac{H}{L}\right)^{-0.316}, \quad \text{when } \tan\beta = 1/30,\ 1/60. \qquad (1.2.5)$$

If Kaplan's data represented deep water waves, then $L \approx L_o$, and equation (1.2.5) would be consistent with the analysis of Battjes, equation (1.2.4). In any case, there is no contradiction if one asserts that the experimental data for breaking waves of figure (1.2.1) indicate that the runup to height ratio is a constant for values of the wave steepness less than 0.004.

It is interesting to note that this behaviour was also noticed by Hunt (1959). Hunt did a comprehensive study of periodic wave runup on gentle beaches. He concluded that, "*for slopes of* $\tan\beta$ *less one half, the ratio* **R**/H *will increase slightly for values of* $(H/T^2)^{1/2}$, *then level off at its maximum value; and finally* **R**/H *will decrease with decreasing values of the wave steepness* ". The region where the "leveling off" of Hunt's data occured is the long wave region. Possibly because his work had always been synonymous with "regular" wave runup, this result has never been used in the studies of long wave runup.

A similar conclusion can be drawn from figure (1.2.2), which depicts the variation of the runup to height ratio with the parameter $(d/L)\cot\beta$, where d is the depth. This parameter is the ratio of the horizontal distance from the initial shoreline to the toe of the sloping beach over the wavelength, and in the Japanese literature it is referred to as the long wave parameter. It has the distinct advantage that the ratio d/L is proportional to the square root of the coefficient of the correction term for the vertical acceleration in the approximation of the equations of motion presented by Boussinesq (1872). The figure is taken directly from a review article by Togashi (1983), where he presented a best fit of the data of the form :

$$\log(\mathbf{R}/H) = 0.421 - 0.095 \log\{(d/L)\cot\beta\} - 0.254 \log\{(d/L)\cot\beta\}, \qquad (1.7.1a)$$

in the case $0.1 < (d/L)\cot\beta$. Otherwise, he found that :

$$\log(\mathbf{R}/H) = 0.421 - 0.109 \log\{(d/L)\cot\beta\} - 0.286 \log\{(d/L)\cot\beta\}. \qquad (1.7.1b)$$

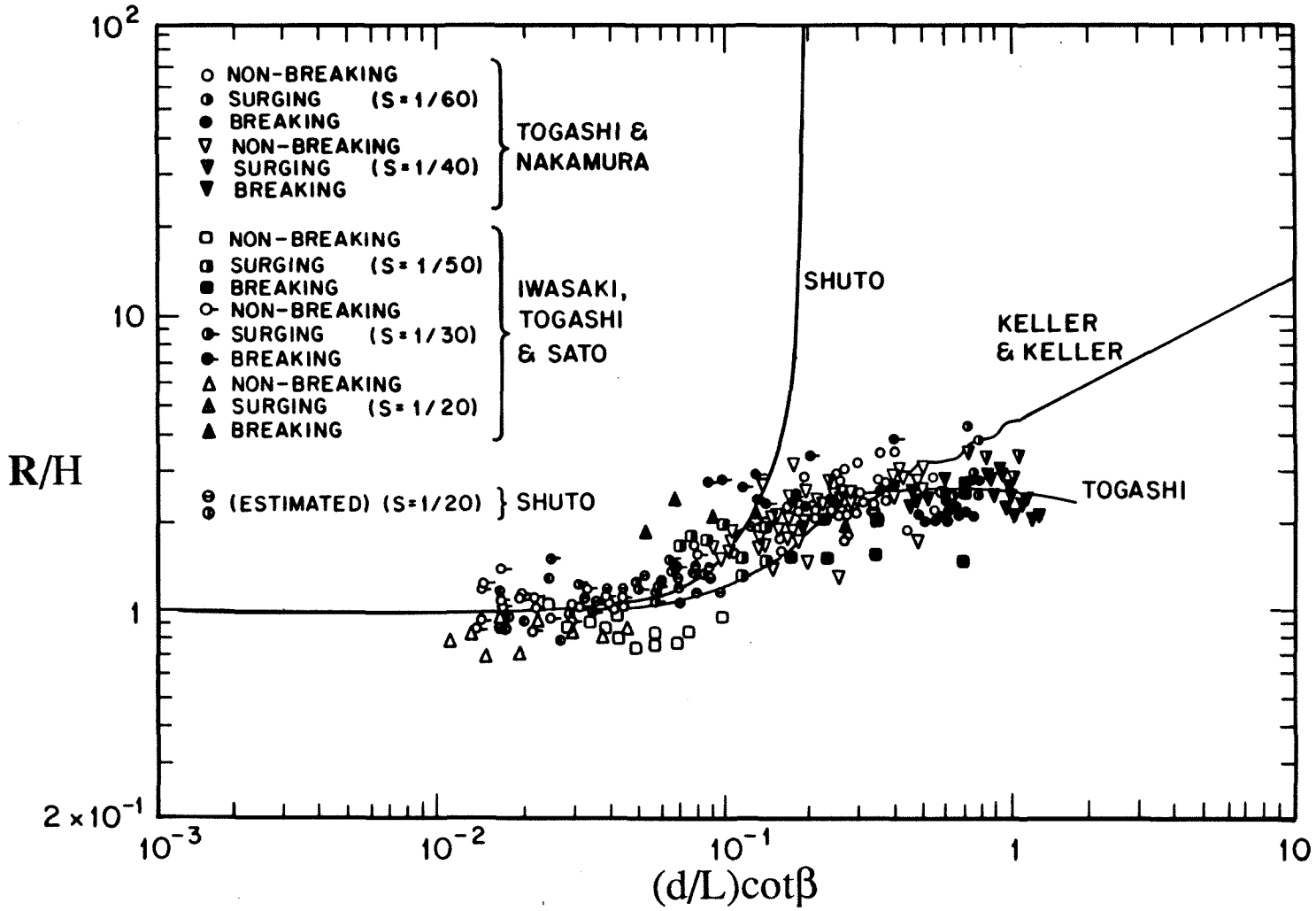

Figure 1.2.2 The runup of periodic waves on different beaches. After Togashi (1983). The solid line identified as Togashi's represents his best fit (1.7.1). The lines identified as Keller's and Shuto's represent (1.2.2) and (1.2.3) respectively.

Togashi's empirical fit was an attempt to derive a single functional variation for different wave types and different slopes; it is identified in the figure (1.2.2) with a solid line. There is no physical reason why such a relationship should exist. In fact, the figure indicates that, for each beach slope and each category of breaking and nonbreaking waves represented in the figure, the ratio **R**/H is a constant.

On the basis of the analytical results and of the laboratory data presented, one may assert that for long *periodic* waves the ratio of the runup to wave height depends explicitly on the beach slope and on the breaking character of the incoming wave. It depends implicitly on parameters such as $\cot\beta(d/L)$ and H/L; whether a wave breaks or not and the breaking wave type is a function of these parameters. If there is an expilicit dependence, it has not been demonstrated yet in the laboratory. However, it is clear that further detailed investigations are neccessary to qualify these statements.

1.3 The runup of periodic and nonperiodic long waves. Nonlinear theory. The other long wave model that has been used in studying the runup of tsunamis is the model of nonperiodic long waves. Strictly, a nonperiodic long wave is any wave of infinite period. In practice, the name is used to refer either to single long waves of translation, or to solitary waves, or to undular bores.

1.3.1 The runup of periodic long waves. Nonlinear theory. The foundations of the study of the runup of nonperiodic long waves were laid with the work of Carrier and Greenspan (1959). They derived a nonlinear transformation to commute the nonlinear shallow water wave equations into a single linear equation. Their equation is quite general and it describes the motion of any nonbreaking wave on a sloping beach. The transformation is discussed in detail in chapter 3. Carrier and Greenspan applied their method to calculate

the runup of a periodic wave and solved several other initial value problems. Carrier (1966) used the transformation to calculate the evolution of a long wave generated by a bottom displacement, propagating over varying topography, and then climbing up a sloping beach. Spielvogel (1979) assumed an exponentially shaped surface profile at maximum runup and derived the evolution of the wave during the rundown. Although the transformation is a very powerful tool for calculating the runup of nonbreaking waves, no further work has been reported to derive other exact solutions.

1.3.2 The runup of solitary waves. Solitary waves are waves consisting of a single volume of fluid propagating entirely above the undisturbed free surface. A solitary wave was first observed by Scott Russell (1844), who described it and who suggested various methods for generating one in the laboratory. In the present study, the name solitary wave is used to describe the permanent form wave with a surface profile $\eta^*(x^*,t^*)$ defined by :

$$\eta^*(x^*,t^*) = H\,\mathrm{sech}^2[\gamma(x^*-c^*t^*)]\,, \quad \text{where } \gamma = \sqrt{\frac{3H}{4d}}. \qquad (1.3.1)$$

c^* is the local phase velocity. This profile was derived by Boussinesq (1872), and it is also an exact solution of the KdV equation, developed by Korteweg and deVries (1895). In inviscid flow, the solitary wave propagates over constant depth without any change in its shape; it is a permanent form wave. As it is evident from (1.3.1), two variables, the wave height H and the water depth d, define this wave uniquely. Figure (1.3.1) shows the propagation of a solitary wave in an inviscid fluid over constant depth and with H/d=0.1

The first investigation on the runup of solitary waves was the laboratory study of Hall and Watts (1955). They used a rectangular channel with a plane beach and established a

relationship between wave height H/d, the beach slope β, and the dimensionless runup R/d of the form :

$$\frac{R}{d} = K(\beta) \left(\frac{H}{d} \right)^{\phi(\beta)}, \tag{1.3.2}$$

where K and ϕ were reported to be functions of the beach angle β. This result was later confirmed in the experimental studies of Camfield and Street (1966), Kishi and Saeki (1966)

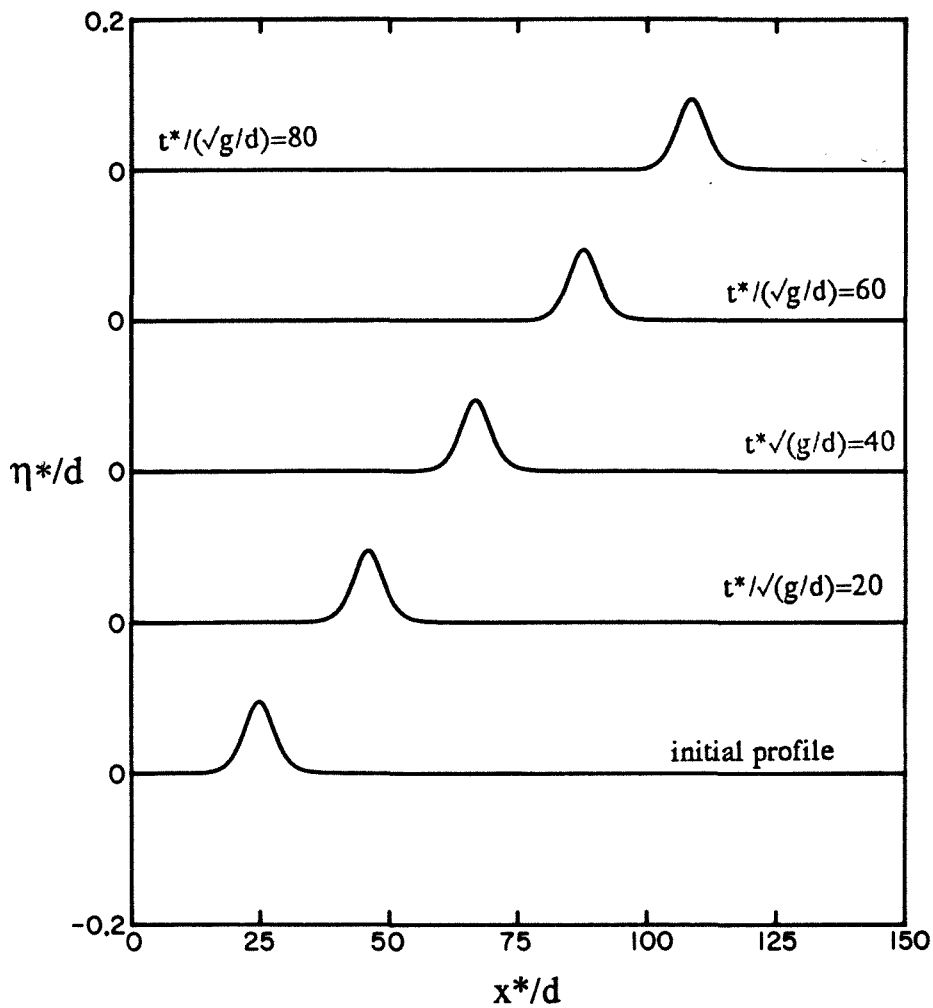

Figure 1.3.1 The propagation of a solitary wave with H/d=0.1 over constant depth, according to the KdV equation (C1.1). The Peregrine (1966) algorithm was used with $\Delta x = \Delta t = 0.1$

and Saeki et al (1971). Since then, equation (1.3.2) has been used extensively to check numerical calculations. The relationship can be justified by dimensional analysis, but until the present investigation there has been no attempt to explain its origin analytically.

The first attempt to find a numerical solution to the problem of a solitary wave propagating over constant depth, and then climbing a sloping beach was Heitner's (1969). He solved the shallow water wave equations including a term to correct for friction by using the finite element method. He presented some surface profiles for the propagation and runup of solitary waves and infinite bores and reported good agreement with the experimental data on maximum runup. However, the solution does not appear to reproduce the flow details well, a possible manifestation of the computational constraints of that time. Gopalakrishnan (1978) used a semi-discrete method (finite elements in space and finite differencing in time) to solve a modified form of the shallow water wave equations that included a term to account for vertical accelerations. He proceeded to calculate runup profiles of oscillatory waves, solitary waves, and waves that he referred to as bores. He reported good agreement with the Camfield and Street (1966) data. Although both finite element models appear to be capable of solving the problem, it is difficult to evaluate their advantages in problems with simple boundaries relative to finite difference models.

The current state-of-the-art numerical solutions were accomplished in the studies of Pedersen and Gjevik (1983), and Kim, Liu and Ligett (1983). Pedersen and Gjevik derived the equations of motion for long waves in an arbitrary channel in Lagrangian coordinates and solved them numerically. They presented results for the maximum runup of solitary waves on plane beaches in rectangular channels. Their numerical data are in good agreement with experiments for some cases and in poor agreement in others; the cause of the discrepancy is explained in chapter 3. Kim, Liu and Ligett (1983) used a boundary integral

method to solve the equations of motion for the problem of a runup of a solitary wave generated by a piston movement in a numerical wave tank. They presented data for the maximum runup of solitary waves and reported good agreement with the Hall and Watts (1955) data.

One common feature of the numerical studies referred to is that it is impossible to obtain any quantitative information from the computational models without repeating the solution procedure, except for those values of the parameters for which the equations were integrated in each study. This is unfortunate because it does not allow for an independent comparison of the solutions among themselves and with the appropriate laboratory data. The qualifier *appropriate* refers to the fact that, with the possible exception of Heitner's (1969) study where it was attempted to model the formation of shocks, all numerical studies have modelled nonbreaking waves and have used the Hall and Watts (1956) laboratory-data set to verify their results. However, Hall and Watts do not distinguish between breaking and nonbreaking waves in their presentation, and, as shown in chapter 3, the behaviour of breaking and nonbreaking solitary waves is different. This observation renders inconclusive any comparisons that have used extrapolations from the Hall and Watts data set. A comparison with the appropriate data for each model will be presented in section (3.5.1).

It appears that the only attempt to derive an exact solution to calculate the runup of solitary waves is that of Gjevik and Pedersen (1981). They used Carrier's hypothesis, discussed in section (3.5.2), to assign a boundary condition to the shallow water wave equations form for waves propagating on plane beaches. By using Laplace's transform techniques, they derived a solution for the runup of the monochromatic wave that best fits the Boussinesq solitary wave profile (1.3.1). The profile of the monochromatic wave they used is given by : $\eta^*(X_0, t)=(H/2)\,(1 - \cos\omega t)$, where $\omega T_h=\pi/2$, $T_h=1.018(c^*/H)\sqrt{(H/d)}$,

ω is the wave frequency, and where X_0 is the distance from the shoreline to the toe of the sloping beach. They also derived a breaking wave criterion and reported good agreement with some unpublished experiments.

1.3.3 The runup of bores. A bore is one of the natural phenomena that can best be defined by describing it. Peregrine (1967) describes a bore as a transition between two different uniform flows of water. " *In its most common form a bore is a turbulent, breaking zone of water whose length is a few times the depth of water* . " Meyer (1972) describes a bore as a " *region of steeper surface slope of relatively short horizontal extent [where] it is found that the study of the water motion in such a region can be avoided by combining the use of nonlinear beach equations (whenever they are valid) with an assumption of overall conservation of mass and momentum in the region of steeper surface slope.* ". Whitham (1974) defines bores as the discontinuities described by the following equations :

$$U[uh] + [u^2h + (1/2)h^2] = 0 \qquad (1.3.3a)$$

$$-U[h] + [uh] = 0 \ , \qquad (1.3.3b)$$

where U is the *dimensionless* speed of the bore, h is the *dimensionless* total depth of the flow, u is the *dimensionless* water particle velocity, and the brackets indicate the difference of the quantity inside when evaluated just ahead and just behind the discontinuity. These discontinuities " *are in reality the turbulent bores familiar from water wave theory as 'hydraulic jumps' or breakers on a beach* ". Hibberd and Peregrine (1979) distinguish between a bore and a bore region. "*Waves break in various ways, but in most circumstances there is a region near the shoreline where the waves have short steep turbulent fronts, that is bores, and otherwise have very gentle slopes. This region which we call the 'bore region' can be large or small depending on the slope of the beach and of the incident*

waves ". Bores are also caused at tidal inlets when an incoming tide travels up a river. Lynch (1982) describes a tidal bore as " *a solitary wave that carries a tide upstream* " . He continues : " *the formation of bores represents the turn of the tide* ". A useful idealization is the concept of a uniform bore. It refers to a bore that propagates into still water with uniform flow conditions behind the bore front. [Peregrine (1966)] Figure (1.3.2) shows an infinite bore propagating over constant depth.

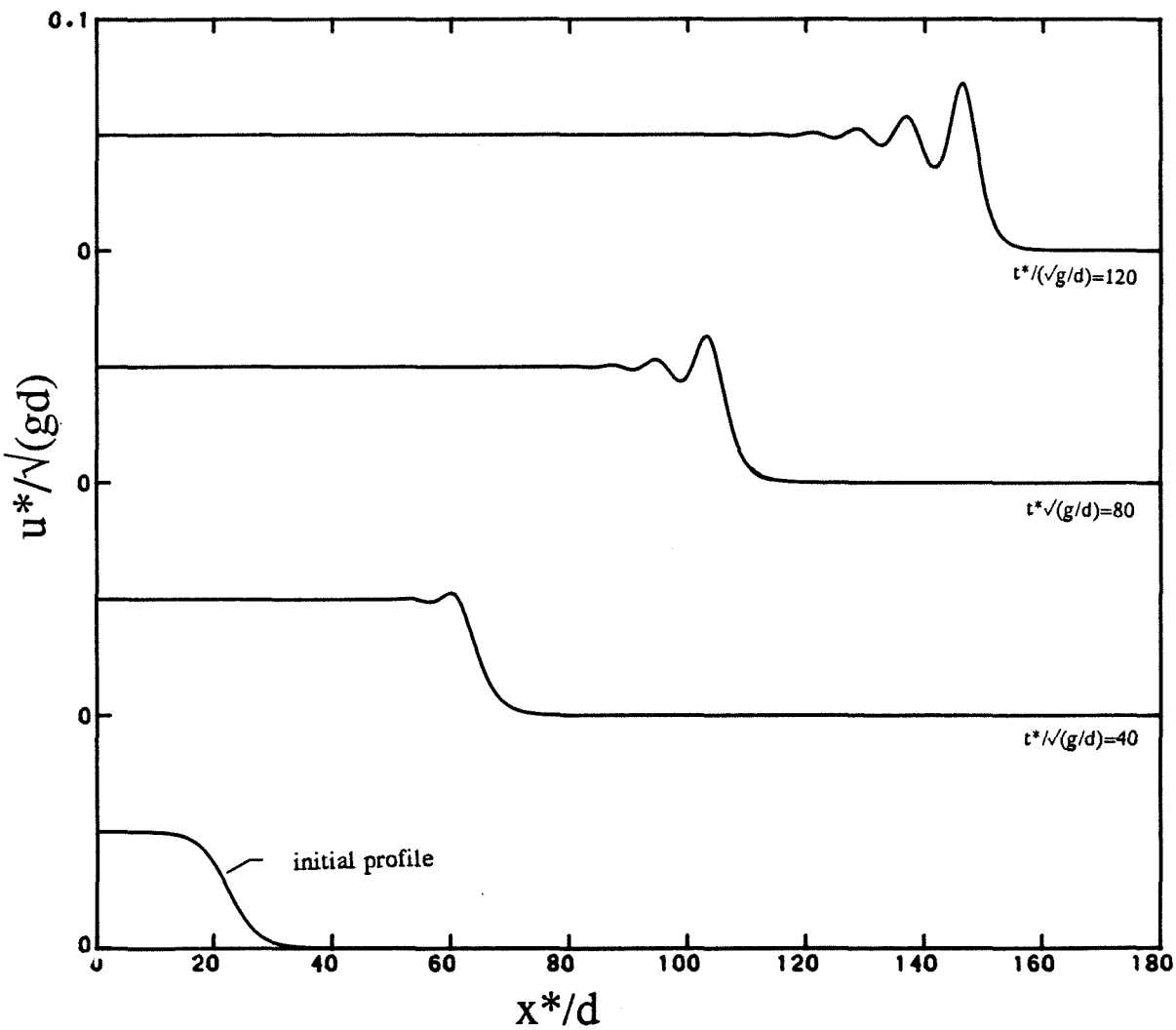

Figure 1.3.2 The evolution of a uniform bore propagating over constant depth. The inital velocity profile is given by $u^*(x^*,t^*) = 0.5gH[1-\tanh(x^*/5d)]$ with $H/d = 0.1$. The Peregrine (1966) algorithm was used with $\Delta x = \Delta t = 0.1$.

Although these definitions describe seemingly different natural phenomena, one common characteristic of the range of waves identified as bores is the manner with which the bore propagates until it reaches the shoreline where the bore collapses. The bore front may change shape, but the bore does not evolve into another type of wave until it collapses. It seems therefore most reasonable to define a bore as a long breaking wave of sufficient volume so that it propagates over considerable distances without reforming into a nonbreaking wave. Since it is not easy to generate uniform and tidal bores in the laboratory, in this study the name *bore* will refer to *a wave that is generated broken and propagates as a breaking wave until it collapses close to the shoreline.*

The study of the runup of bores has been profoundly influenced by the work of Whitham (1958). While working on the problem of shock wave propagation through nonuniform regions of flows, he suggested a method to circumvent the difficulty of evaluating differential relationships on a discontinuity. His idea was to apply the differential relationships which must be satisfied by the flow variables on the shock wave, immediately behind it. This practice has become known as the *Whitham bore rule*. Whitham derived approximate formulae for the variation of the height and the strength of a bore. He observed that for strong bores, the bore height η varies like the square root of the depth, and, consequently, the bore collapses as it approaches the shoreline. His result was verified by numerical methods by Keller, Levine and Whitham (1960). They also remarked on the insensitivity of the solution to detailed initial conditions. Whitham's approximate result was verified to a higher order by Ho and Meyer (1962). They did not assume any detailed initial conditions, but only a monotoneity property for the wave propagation to reflect the requirement that there is shoreward flux of mometum. They were able to determine an approximate bore path. Shen and Meyer (1963) extended Ho's and Meyer's result, and they calculated the bore path after the bore collapses. Their result implies that the maximum

runup is related simply to the speed of the bore as follows :

$$\mathbf{R} = \mathbf{U}^2/2g\ ; \tag{1.3.4}$$

U is the speed of the bore when the bore reaches the shoreline. They also discovered the existence of a singularity in the solution, occuring during the backwash. They interpreted it as representing the hydraulic jump that forms during the rundown of breaking waves. Barker and Whitham (1980) rederived Ho and Meyer's results with a more intuitive method.

It is evident that the climb of bores on sloping beaches is now well understood analytically. Unfortunately this understanding does not simplify the numerical calculation of the runup of bores. In computational terms, the runup process is a moving boundary problem. Any finite difference type of solution of such problems must first establish suitable criteria for introducing new grid points in the solution domain in order to account for the new boundary position. The state of the art of the numerical solutions was achieved with the work of Hibberd (1977) and Packwood (1980). Hibberd used tools developed in the last three decades for solving moving boundary problems in other fields, but he was the first to successfully complete the calculation of the climb of a uniform bore on a sloping beach. His algorithm is known as the Hibberd and Peregrine solution. Packwood used the same computational approach, but improved the details of the shoreline solution procedure. He proceeded to calculate the runup of a periodic waveform consisting of a series of bores climbing up a beach with the objective to model the climb of breaking periodic long waves; his numerical results agreed well with laboratory data during the climb of the waves on the beach indicating the power of the Hibberd and Peregrine. Hibberd's solution was reproduced in the present study, and it is presented in detail in appendix B. Figure (1.3.3) shows an example of a uniform bore climbing up a sloping beach. Iwasaki and Mano (1979)

presented another numerical scheme and claimed good agreement with experimental data. Mano (1983) did further unpublished work and was able to expand on the Hibberd and Peregrine solution by using different conditions at the shoreline.

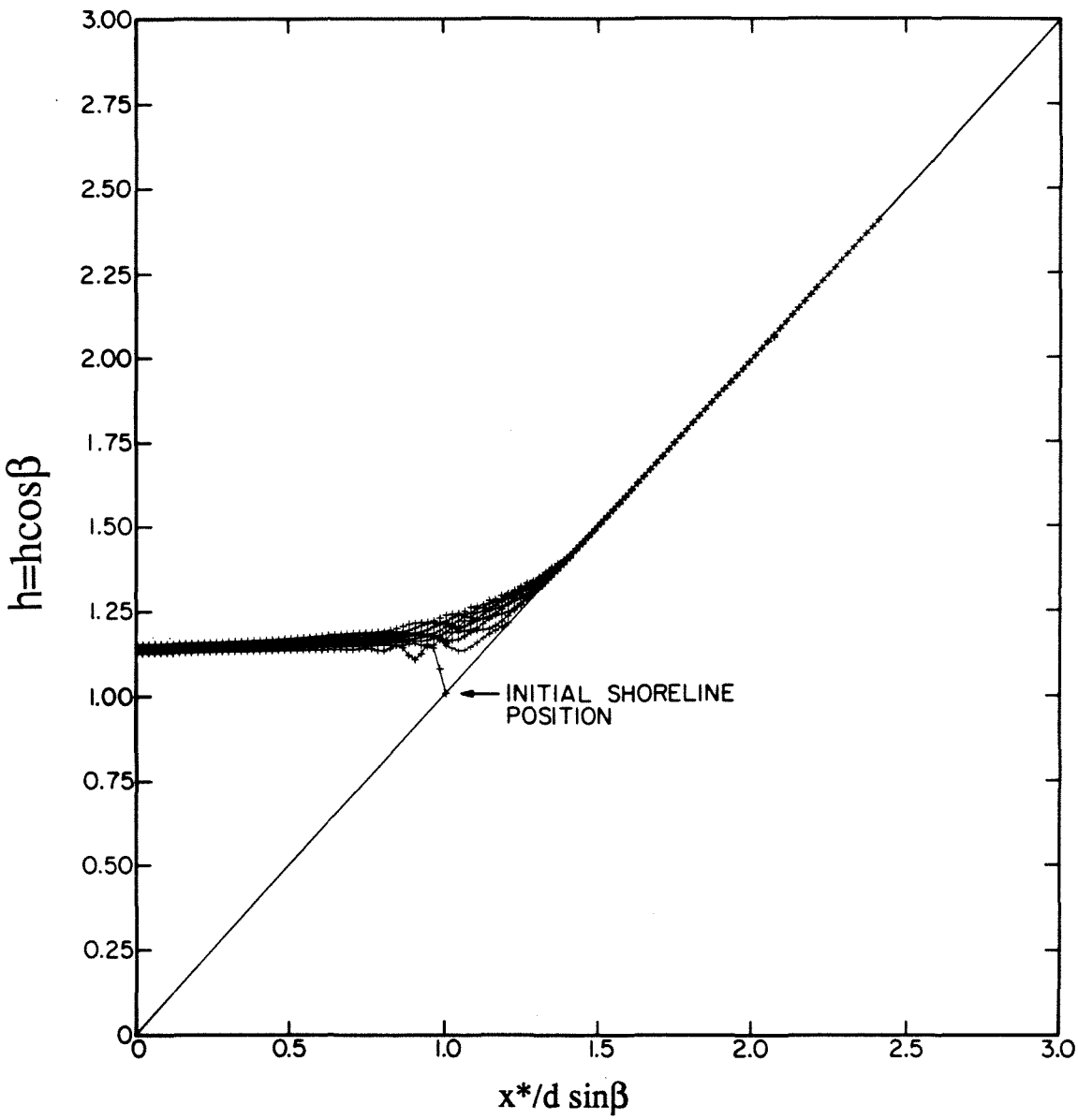

Figure 1.3.3 The climb of a uniform bore with initial H/d = 0.2. The Hibberd and Peregrine (1979) algorithm was used with Δx =0.01 and Δt = 0.04. (See appendix B)

Both the analytical methods and the numerical solutions described appear adequate to solve the problem of a bore propagating up a sloping beach, but only when boundary conditions are specified at some location on the beach for all times. Because of this limitation, it has only been possible to solve problems that allow for this specification, i.e., periodic waves or uniform bores. Using these solutions, it is not yet possible to calculate the runup of the bore that forms after a wave breaks on the beach, or the runup of a single breaking wave climbing up a beach.

Given the mathematical interest that bores have generated, it is quite surprising to discover that there seem to be only two experimental studies in the runup of bores. This can be attributed to the fact that bores are generally difficult to generate repeatably in the laboratory. Also, there is the widely held belief that the bore theory has been verified in the laboratory; this belief has been based on experiments with breaking periodic waves designated as bore experiments and compared with results from the bore theory.

The first laboratory study is that of Shen (1965), who worked on developing a bore generator to model the process of tsunami runup in a model of Hilo bay in the island of Hawaii. He experimented with three different waves generators, and he produced bores of finite volume in a rectangular channel with strengths H/d in the range [0.1 to 0.3] and measured their runup on a 1:33 beach. He presented his results in the form :

$$\mathbf{R}/H = \mathbf{f}\,(H/d,\ c^*\mathbf{T}\,/d\,), \qquad (1.3.5)$$

where H is the bore height before it starts climbing on the beach, and c* is the wave speed at that location, while **T** is a measure of the duration of the wave motion. To his surprise, he found the **R**/H ratio to be a constant with values in the range [2.0 , 2.4] for rough beach

surfaces and (2.6, 3.0) for smooth surfaces. Larger values of the duration parameter c*T/d produced slightly larger runup excursions than smaller values did. However, the variations were well within the experimental errors.

The other bore generation and runup study was that of Miller (1968). He used the apparatus developed by Miller and White (1966) to generate strong bores in a rectangular channel and then measured their runup. He reported his results in the form : **R**/d = **f** (1+H/d), where 1+H/d is the bore strength. He found strong correlation between **R**/d and the bore strength, for different slopes and surfaces. Many attempts have been made to use his result for the purpose of verifying numerical calculations for the runup of uniform bores, but with little success. One can speculate that this is the case because of the particular geometry of Miller's experiment. The wavemaker was operated in such a location that at maximum stroke the piston was only 0.76 m (2.5 ft) from the toe of the beach. The water depth in these experiments varied from 6.1 cm (2.40 in) to 12.2 cm (4.80 in), thereby allowing approximately ten depths through which the wave could propagate before reaching the shoreline. The stroke of the piston was 2.44 m (8.0 ft), and the generated waves were such that H/d ~ 1. A simple calculation shows that it is quite likely that the piston was still in motion by the time the wavefront reached its maximum runup point and this may have interfered with the reflection process. If this observation is correct, then Miller's data cannot be compared directly with analytical models of infinite bores.

1.4 The present study. It is quite obvious that the current understanding of the runup process is fragmented and incomplete. There exist analytical results for the runup of nonbreaking periodic waves and for the runup of uniform bores. There exist numerical data for the runup of nonbreaking periodic waves, nonbreaking solitary waves, and uniform bores. There exist laboratory data for the runup of periodic waves, for the runup of solitary waves, and for the runup of bores. There exist no data on the runup of long nonperiodic breaking waves (that are *not* solitary waves), or on the runup of bores of finite volume. There has been no verification of the linear or nonlinear theory of wave runup for nonperiodic waves. There is no realization of the differences between the runup of breaking and nonbreaking waves. There is little physical understanding of the runup process and there has been no attempt to explain the empirical results.

This study attempts to resolve some of these questions and to provide a more coherent approach to long wave runup problems. It is the first study to examine nonbreaking waves, breaking waves, and bores of finite volume.

The experimental equipment used in the study is described in chapter 2. In chapter 3, solitary waves are used as a long wave model to establish differences between breaking and nonbreaking waves, and to evaluate the relevance of the nonlinear theory in the runup process. An exact result is derived to explain the empirical relationships regarding solitary wave runup. In chapter 4, single long waves and bores of finite volume are used to determine appropriate invariants to describe the runup. It is found that a single parameter based on the generation characteristics of a wave maybe be sufficient to determine its runup. Conclusions are stated in chapter 5. Appendix A presents an exact theory to calculate the forces on an accelerating plate. Appendix B presents an algorithm to calculate the runup of uniform bores. Appendix C presents a method for generating arbitrary waves in the

laboratory. Appendix D presents a calculation for the Fourier transform of a solitary wave.

The composite picture that emerges is that, during runup, waves behave differently according to their breaking characteristics. The runup of nonbreaking waves can be predicted accurately from the linear theory. The climb of nonbreaking waves can be modelled adequately with the nonlinear theory. The runup of any single long wave can be determined from its generation characteristics. Solitary waves provide a limiting case for the runup of breaking long waves. There exist maximum runup values that nonbreaking waves, breaking waves and bores may achieve on any given beach.

Chapter 2

Experimental apparatus and procedures

This chapter describes the experimental equipment used in this investigation and its operation. The equipment consists of a wave tank, a wave generation system, a plane beach to study runup, a force measuring system, and different tranducers to monitor the wave motion.

The wave tank is decribed in section 2.1. The wave generation system consists of a piston attached to a wave carriage that carries a vertical plate. As the piston moves, the plate translates horizontally and displaces the adjacent fluid, thereby generating waves. The piston is driven by a hydraulic system. The hydraulic system and the wave carriage are described in section 2.2 They are controlled by a servo-system, operated by a function generator ; section 2.3 describes the servo-system, and section 2.4 describes the function generator. The force measurement system was developed to determine the force on the accelerating piston due to the hydrodynamic pressures on its front face; it is described in section 2.5. Three different wave transducers were used, and their design and operation is discussed in section 2.6. Section 2.7 gives an account of the experimental procedures.

In this chapter all dimensions are stated in the system of units used in the construction of the particular piece of equipment described, or in the measurement of the particular variable being discussed. The equivalent dimension in SI or in US customary units is given in parentheses.

2.1 The wave tank. The wave tank used in this investigation is a 123.8 ft (31.73 m) long, 2.0 ft (60.96 cm) deep and 15.5 in (39.37 cm) wide tank consisting of 12 identical sections. It has been described by French (1969), Hammack (1972), and Goring (1979). A schematic drawing of the wave tank is shown in figure (2.1.1), and a typical section is shown in figure (2.1.2). The side walls of each section consist of plate glass panels measuring 5.0 ft (1.52 m) long, 25.0 in (63.50 cm) high, and 0.5 in (1.27 cm) thick. The bottom of each section consists of painted steel channel section 1.0 in (2.54 cm) thick. There are carriage rails running along the whole length of the tank.

A ramp was installed at one end of the tank to model the bathymetry consisting of a plane beach joined to a constant depth region as in figure (1.1.1). The beach had a slope of 1 vertical to 19.85 horizontal and it was constructed out of four anodized aluminum plate sections, each measuring 8.0 ft (2.44 m) long by 15.0 in (0.38 m). The ramp was sealed to the tank walls by inserting a polysterene rod in between the edges of the ramp and the side walls, and then filling the gap with silicone. The toe of the ramp was distant 14.95 m (48.19 ft) from the rest position of the piston. A schematic drawing of the side view of the tank with the ramp is also shown in figure (2.1.1). Figure (2.1.3) is a photograph of a view of the wave tank.

In one of the later stages of this investigation it became necessary to determine the force on the plate due to the hydrodynamic pressures on its front face. To perform this measurement with a force cell, the fluid behind the plate must be drained rapidly ; otherwise the force cell would measure the difference between the forces on the front and the back face of the plate. To this end, the tank was modified by installing a bulkhead 2.0 in (5.08 cm) behind the rest position of the piston. A drainage hole of 1.0 in (2.54 cm) diameter was drilled on the flume bottom with its center distant 1.0 in (2.54 cm) from the bulkhead.

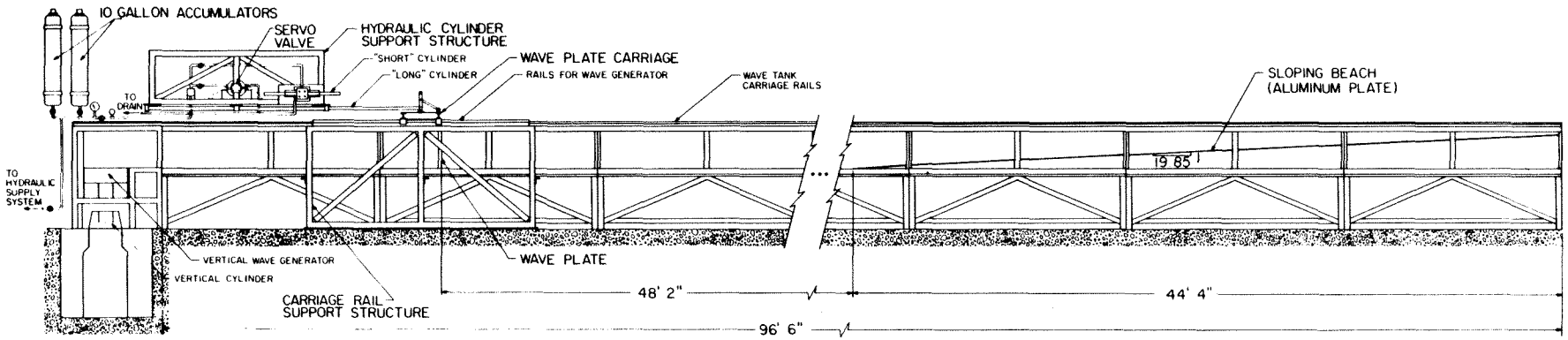

Figure 2.1.1 A schematic diagram of the wave tank and its appurtenances.

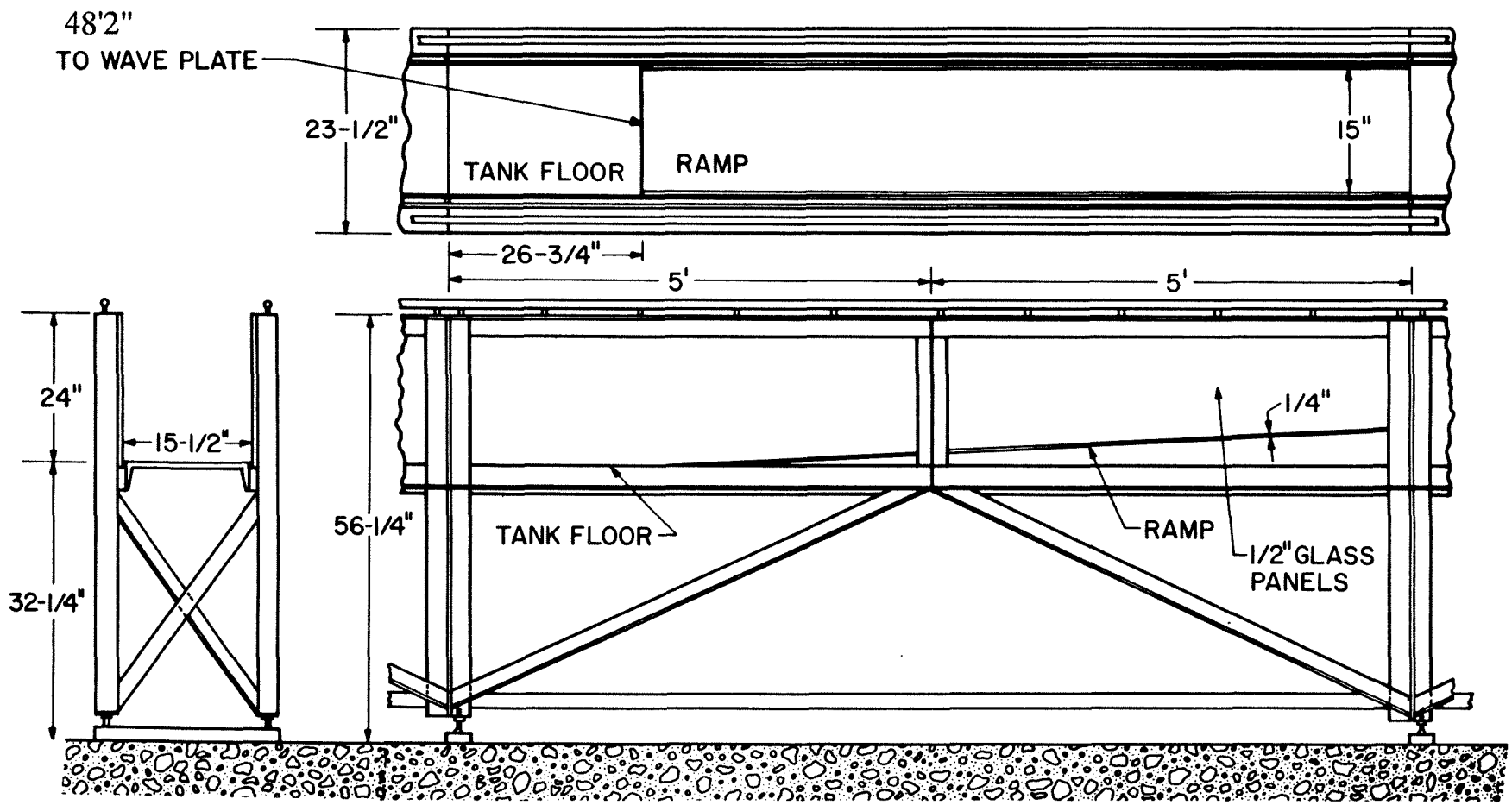

Figure 2.1.2 A schematic diagram of a typical section of the wave tank.

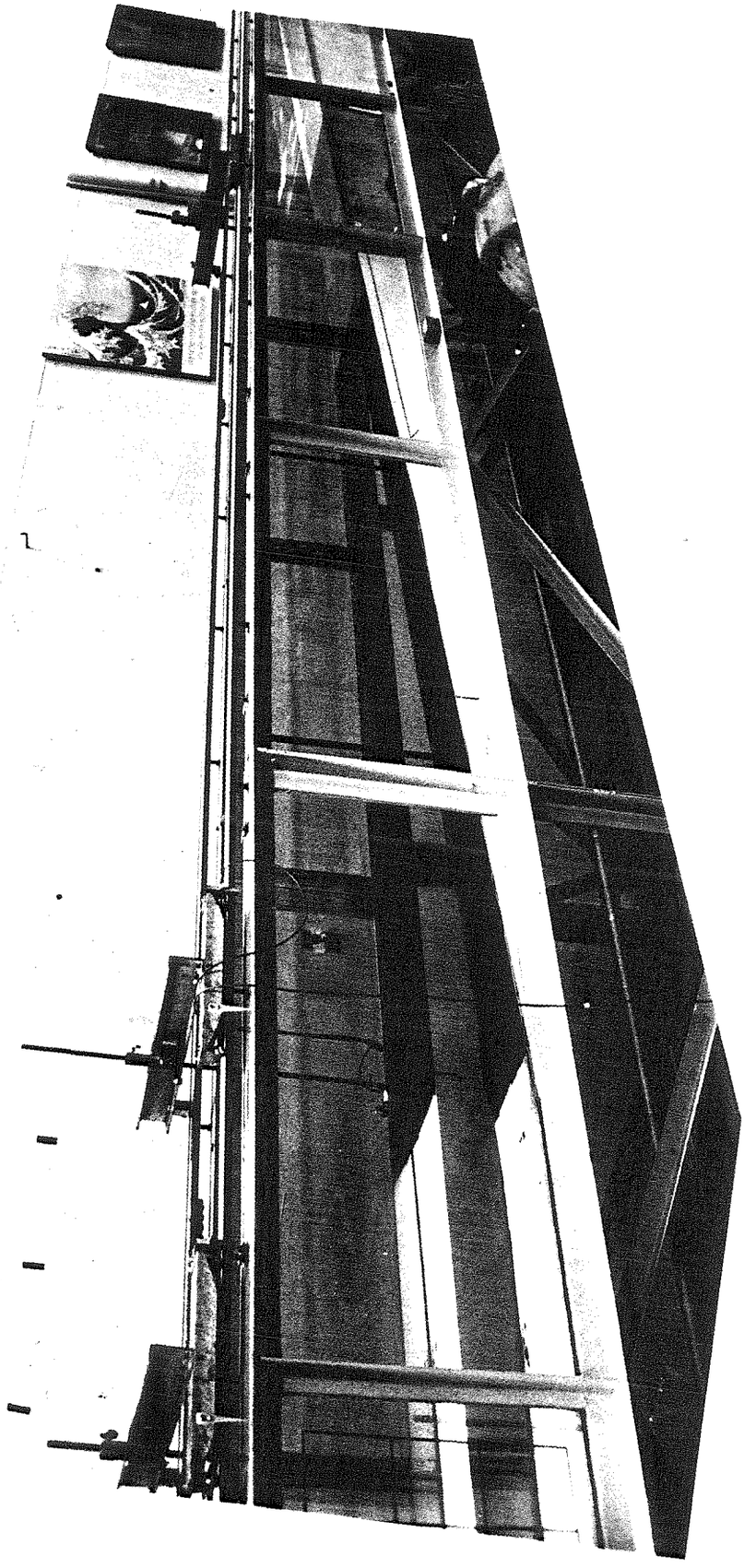

Figure 2.1.3 A photograph of a view of the wave tank.

2.2 The hydraulic system. The hydraulic system is described in detail by Goring (1978). Its most important element is an electromechanical servo-valve that controls the flow of hydraulic oil into a hydraulic cylinder. The piston moves in response to the oil flow in the cylinder. Oil flows to the valve from two oil accumulators which hold the fluid under pressure. The oil is supplied to the accumulators from an oil reservoir through an axial flow pump. The servo-valve is a Moog Model 72-103 and it is rated at 60 gpm (0.227 m^3/min) at 40 ma current. The accumulators are two ten gallon pressure vessels containing rubber bladders filled with nitrogen gas. The accumulators hold about 7.0 gal (0.026 m^3) of oil at the rated pressure of 3000 psi (20.68 MPa). The oil reservoir has a capacity of 40 gal (0.152 m^3) and the oil pump is a Denison constant flow pump rated at 2.9 gpm (0.011 m^3/min) at 3000 psi (20.68 MPa). It is powered by a 7.5 hp (5.6kW), 1800 rpm motor.

Two hydraulic cylinders were used, alternately. One cylinder, referred to as " the long cylinder", is a Miller Model DH77B cylinder with 2.5 in (6.35 cm) bore and 1.375 in (3.49 cm) rod and permits piston strokes up to 96 in (2.44m). The other, referred to as " the short cylinder " is a Miller Model DER-77 cylinder with a 5.0 in (12.7 cm) bore and 1.75 in (4.45 cm) rod, and it permits a stroke of 16.0 in (40.6cm). Either cylinder can be connected to the wave carriage through a vertical post on the carriage. In the schematic diagram in figure (2.1.1) the long cylinder is shown connected to the wave plate carriage.

The wave plate carriage carries the plate that generates the waves. The wave carriage is borne on rails supported on a steel truss that is structurally independent from the wave tank. The rails are Pacific-Bearings hardened steel rods of 1.250 in (3.175 cm) diameter, Model No SA-20-120. Four Pacific-Bearings linear roll bearings, Model No SPB-20-OPN, are used for the ride of the carriage on the rails.

2.3. The servo-system. The purpose of the electro-mechanical servo-system is to supply the servo-valve with the electric current necessary to drive the piston to follow a specified trajectory. In the absence of frictional forces this process has a linear transfer function; the piston velocity is proportional to the hydraulic oil flow rate through valve, which is itself proportional to the voltage applied across the valve. Then, to move the piston one would only have to apply a voltage proportional to the desired piston trajectory. However, the force required to get the piston moving from its at rest position and the other dynamic frictional forces distort the transfer function. If the piston is to follow a specified trajectory accurately, feedback must be provided to correct the motion in real time. This is the function of the servo-controller, which compares the current position of the piston to the desired position and adjusts its output so that there is no difference between the two positions.

The servo-controller used in this study is a Moog AC/DC controller Model No 82-151, with its power supply, model no 82-152. The controller was modified by the addition of a resistor array to allow fine tuning of the system damping and of a Dither oscillator to provide a 600 Hz excitation to the valve. The continuous excitation reduces the force required to overcome static friction and enables smoother movements from rest. The amplitude and the frequency of this excitation do not produce any free surface motions.

Two different transducers are used to measure the plate position and to output the feedback voltage. When the long cylinder is driving the wave carriage, a ten-turn potentiometer riding on a precision rack is used, in a rack and pinion arrangement. (The potentiometer is shown in the schematic drawing in figure (2.5.1).) When the short cylinder is in place, a linear variable differential transformer (LVDT) is used. Details of both systems maybe found in Goring (1978).

In the course of this study it became obvious that the LVDT device is the superior transducer for this application. It measures the position of the piston directly, while the potentiometer measures the position of the wave plate carriage to infer the piston position. The two measurements are equivalent only when the piston is attached to the carriage; when the carriage is disconnected from the piston for servicing, the feedback voltage of the potentiometer informs the controller of the carriage position which the controller interprets as the piston position. The controller forces the piston to move to the carriage position, an action with unpredictable results when the carriage is not in place. Also, the potentiometer requires tedious readjustment of its backlash gear when reinstalling the wave carriage.

2.4 The function generator. The purpose of the function generator is to store a specified trajectory in binary form and then convert the data to a voltage signal. It consists of a digital to analog converter with a buffer that stores data and was manufactured by Shapiro Scientific Instruments (SSI), Corona del Mar, California. The generator accepts data either manually or from a tape reader. The generator stores the data in memory and displays them sequentially with an LCD display. The rate with which data is dumped to the controller may vary continuously from 1 byte/sec to 10^6 bytes/sec and this rate determines the duration of motion. Since the memory buffer holds 1kbytes, the generator can create trajectories of duration from 0.001024 sec to 1024 sec. The system also allows sequential access of the memory to change data in specific data addresses.

The generator is connected to an amplifier to adjust the gain of the generated signal. This amplifier is called the "*wave form conditioner* " and was also designed by SSI. It allows adjustment of the gain of the voltage signal, so that the complete range of motions possible with the cylinder in operation can be realized. It also permits adjustment of the initial piston position and it resets the piston to its initial position. Details of the design of the system can be found in Goring (1978).

The introduction of microcomputers in the laboratory has rendered devices like the function generator and the tape reader obsolete. The digital-to-digital (DTD) or digital-to-analog (DTA) interfaces of a microprocessor perform the same functions easier and faster. Two microcomputers were available for this study, a PDP11/60 processor running under the RSX-11M operating system and an LSI-11/23 running under the RT-11 operating system. Both CPU's are manufactured by the Digital Equipment Corporation. The 11/60 is equipped with an AD11-K and an AA11-K interface, while the 11/23 is equipped with a DRV11-J and an AD11-J board. In early stages of the investigation, the AA11-K interface was used to transmit a voltage signal directly to the wave form conditioner bypassing the function-generator. Later, the DRV11-J interface was used to transmit trajectory data to the function generator memory, thereby replacing the tape-reader. The macro routine used to control the DRV11-J was written by Skjelbreia (1982).

The use of the two interfaces has certain advantages but also disadvantages compared to using the function generator. The DRV11-J interface allows fine tuning of the trajectory in essentially real time. However, it is rated for a communications distance of 10 ft (3.28 m). This distance is quite restrictive in the laboratory, where the LSI11/23 system is often used elsewhere. Communication over a distance of 100 ft (32.81 m) was often achieved, but the operation was erratic. The problem was solved by keeping the 11/23 and the function generator physically near, when a particular experiment required continuous adjustment of the trajectory. The AA11-K interface is not restricted by its distance from the signal destination, when operating in the DTA mode. It allows resolution up to four times higher than the one possible when using the function generator. However it must be operated in real time, thereby prohibiting the checking of the integrity of the incoming signal.

2.5 The force measuring system. For this investigation the wave carriage was instrumented with a force measuring system with the objective to determine the force on the piston plate due to the hydrodynamic pressures exerted when the fluid is displaced. The system consists of a load cell mounted in line between the piston and the piston mount in the wave carriage, and a calibration scale. The arrangement is shown in figure (2.5.1).

The load cell is a universal load cell rated at 100 lbs (22.4 Nt) and is a model 34b force tranducer, manufactured by West Coast Research Company, Santa Monica, California. The cell is temperature compensated and its electrical output is 3.0 mv/Volt. Its full load deflection is 0.012 in (0.030 mm). Its physical presence does not interfere with the operation of the feedback loop. The load cell is excited with an 8805A Hewlett Packard Carrier preamplifier (HP 8805A), which also demodulates and amplifies the output signal. The signal is simultaneously recorded by the AD11-J interface of the 11/23 system.

A calibration system was designed so that the cell can be calibrated in place so as to include any effects from side loading. It consists of a low-friction pulley with its axis perpendicular to the side rails and a scale, as shown in figure (2.5.1) . A steel wire [tensile strength 2500 psi (17.2 MPa)] rides over the pulley and connects the wave plate carriage with an aluminum bucket. The force cell is calibrated by placing lead weights in the bucket and recording the cell ouput. When the bucket is loaded, a force is applied through the wire to the wave carriage. This force is transmitted to the load cell, which then compresses between the stationary piston and the wave plate carriage. This method calibrates the cell in compression only, which is not a severe limitation since the hydrodynamic force on the plate is usually compressive. When calibration in tension was required, the calibration was extrapolated. This practice was in accordance with the manufacturer's recommendations.

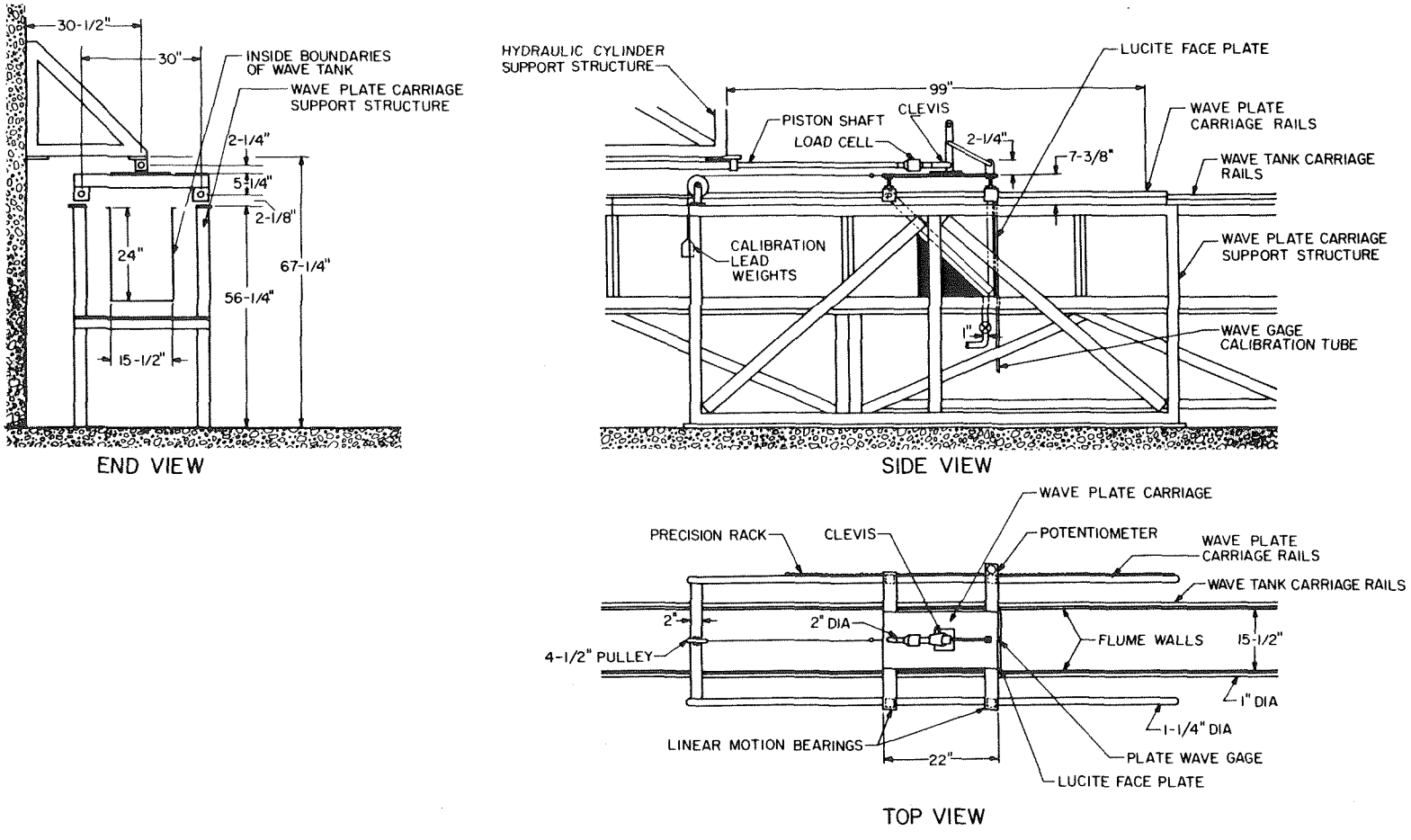

Figure 2.5.1 A schematic diagram of the wave plate carriage and the force measuring system.

2.6 The wave transducers. Three different wave transducers were deployed in this study. One transducer is the π-frame resistance-type wave gage. The two other gages were developed during the course of this investigation. They are the plate wave gage and the runup gage array. The next sections describe the principles of operation of these gages. Calibration curves are presented in section 2.7.

2.6.1 The π-frame wave gage. The π-frame wave gage used in this study is an instrument that measures water surface elevation. It consists of a pair of stainless steel wires of diameter 0.01 in (0.254 mm) spaced 0.16 in (4.06 mm) apart. The wires are insulated from each other and are streched taught between the open ends of a thin rod bent in a π-shape. When the wires are immersed in a conducting fluid, they form a resistor; the level of immersion is the resistance load. The gage is placed on a Wheatstone bridge to enable adjustment of the base level of resistance. Details may be found in Okoye (1970). Excitation is provided from an HP 8805A preamplifier. As the fluid level changes, the bridge becomes unbalanced and the preamplifier monitors the output voltage, demodulates it, and amplifies it. The output is recorded by the AD11-J interface of the 11/23.

In this study the gage was calibrated by immersing it in the wave tank and recording the immersion depths and the output voltage. The calibration device described in Goring (1978) and Lepelettier (1980) was used in some preliminary experiments. It consists of an array of syncronous motors. Each motor has appropriate gearing to allow linear motion of a gear shaft on which the wave gage is mounted. The motion of the motors is adjusted by a control motor which is rotated manually. This calibration system has the disadvantage of producing calibration curves with non-uniform density of data points. Since the AD11-J allows external starts for sampling data, the point-gage method was used for calibration. The wave gage is immersed a given depth in the tank and the AD11-J is

triggered to record a sample of the voltage output. The procedure is repeated until the calibration is completed. Then the 11/23 produces the calibration curve and an HP7470A plotter plots it.

2.6.2 The plate wave gage. The plate wave gage was developed with the objective to measure the water surface elevation on the face of the wave plate while the plate is in motion. It was designed to enable calibration for measuring elevations up to 30 cm (11.81 in). It is a 50 cm (19.68 in) long plexiglass rod with T-shaped crossection. Its front face is 0.375 in (9.52 mm) wide. Two 0.01in (0.254 mm) diameter steel wires were embedded in the rod inside two 0.005 in (0.127 mm) diameter grooves, 0.187 in (0.48 cm) apart. To provide lateral support to the gage, a lucite plate of 0.50 in (1.27 cm) thickness and with dimensions 23.00 in (58.42 cm) by 15.25 in (38.73 cm) was mounted flush on the piston plate. The wave gage rod slides inside a groove machined with a dove tail drill on the front surface of the lucite plate. When the gage is not being calibrated, the front face of the plate appears as a flat surface with two wires protruding a distance of 0.005 in (0.127 mm) from it. The location of the wave gage is shown in figure (2.5.1).

The plate gage operates as a resistance-type wave gage. To measure surface elevations of the same order as the local depth, the gage has to be calibrated in depths larger than the local depth. To enable such calibration depths, a hole was drilled in the bottom of the wave tank to create a well. A 30 cm (11.81 in) long piece of brass pipe of 0.5 in (1.27 cm) diameter was mounted beneath the hole. A valve was installed at the free end of the pipe for drainage. (See figure (2.5.1)) Tests were conducted to determine the influence of the proximity of the walls of the pipe to the electrostatic field set by the wires and no observable effects were noted for the combination of 0.5 in (1.27 cm) pipe with the pair of 0.01 in (0.254 mm) wires. During calibration, the wave gage is immersed in the wave tank

and eventually it enters the pipe. A typical calibration curve is shown in figure (2.7.4b). From the data points in the figure it is not possible to determine when the wave gage entered the pipe, indicating that the pipe did not interfere with the calibration process. The gage was immersed in the well only when measuring surface elevations larger than 20 cm (7.87 in).

2.6.3 The runup gage. Parallel wire resistance wave gages cannot be used for wave measurements close to the shoreline. As with the case of measuring wave heights on the piston plate, the small local depths (relative to the surface elevations to be measured) do not permit in situ calibration. Also, the gages cannot be calibrated in deeper water and then moved back, because of the strong boundary effects arising when the wave gage is in close proximity with the surface of the beach. These problems have discouraged measurements of wave height close to the shoreline with conventional techniques.

The most notable success in such measurements was the study of Battjes and Roos (1974). They developed a transducer that consisted of a parallel wire wave gage immersed in a tray filled with water and with a cover flush with the ramp face. The arrangement of their gages resembles the geometry of the plate wave gage calibration system, differing only by the fact that their wave gages are partially immersed in their "wells" continuously. Their instrument produced good results in measuring the wave heights of periodic waves climbing up sloping beaches. However, it has not been copied in other investigations, possibly because of construction difficulties.

A new type of transducer was developed in this study for the measurement of runup heights. It will be referred to as the *runup gage* . It consists of an array of capacitance wave gages mounted on an aluminum frame, as shown in the schematic drawing in figure (2.6.1). The distance between the probes can be varied from a minimum of 3 in (7.62 cm) in 3 in

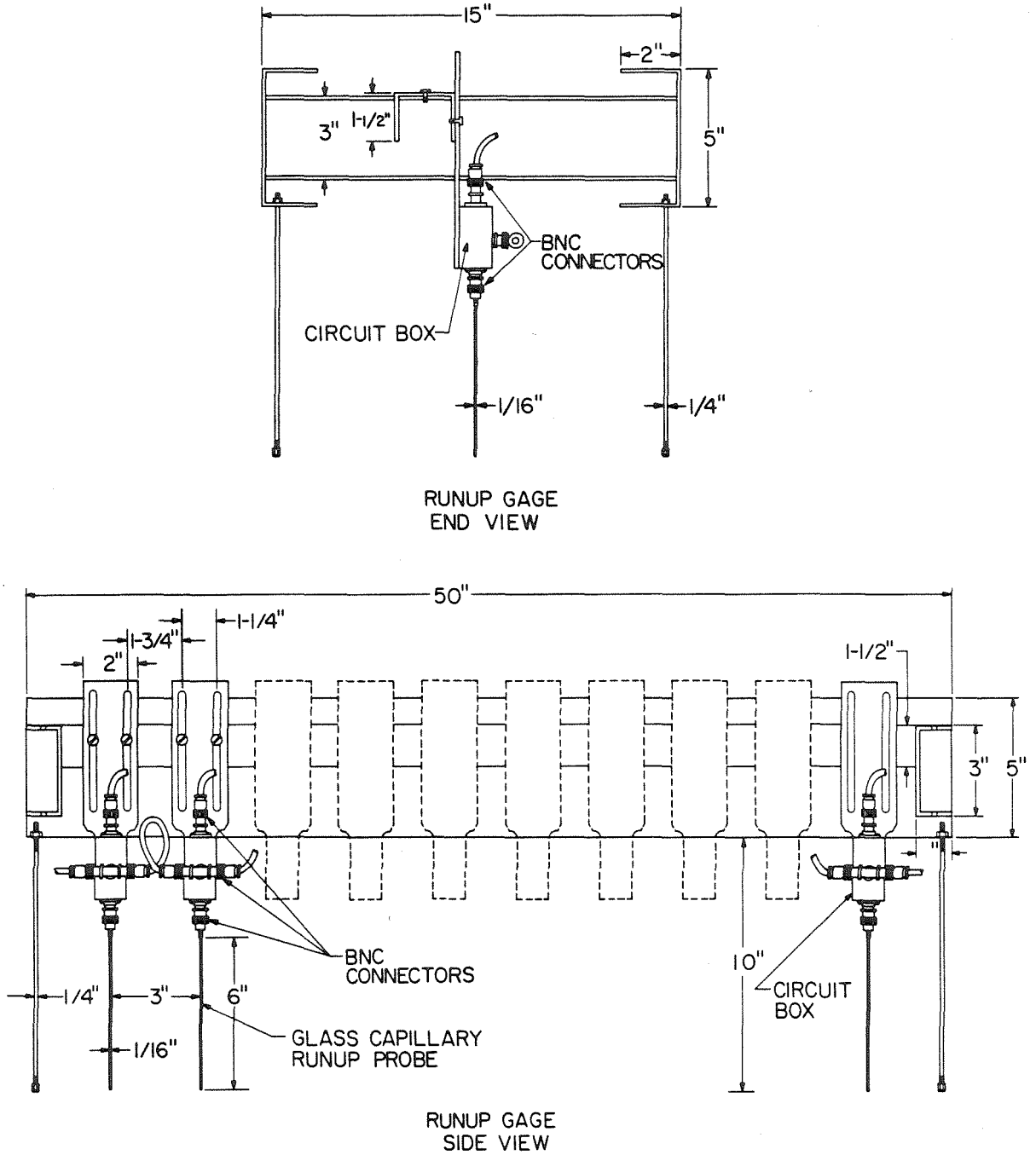

Figure 2.6.1 A schematic diagram of the runup gage.

(7.62 cm) increments. (These distances reflect topological limitations imposed by the support bracket of each gage.) In all cases in this study, the transducer was used with the probes mounted with equal spacing between them. The effective length of the probes is adjusted by sliding the gage inside its support bracket. Figure (2.6.2) shows a photograph of the runup gage.

Each gage consists of a wave probe and an electronics box. Each probe is made of steel rod of 0.030 in (0.76 mm) diameter and is fitted in a glass capillary tube with 0.062 in (1.58 mm) outside diameter. The glass tube acts as the dielectric. The probe is attached to the electronics box with a BNC connection. This arrangement permits rapid replacement of the probe when one of the capillary tubes breaks.

The gage operates as a capacitance wave gage. The electronic circuit that drives it is shown in figure (2.6.3a). An external oscillator is used to drive the gates of a field effect transistor (FET) which provides alternating current to the the wave probe. The output current passes through a radio frequency choke and then returns to a current to voltage converter. The circuit diagram for the current to voltage converter is shown in figure (2.6.3). [Montenegro, (1984)]. The output voltage is recorded directly by the AD11-K interface of the 11/23. Since the FET has high input impedance, there is practically no loading effect. As a result, there is no cross-talk between probes even at the smallest interprobe spacing permitted by the geometry of the runup gage, i.e., 1.5 in (3.81 cm).

One basic advantage of this system is that the transducers always maintain the same distance from the surface of the beach, thereby eliminating the need to account for wall effects during calibration; to calibrate the runup gage the entire frame is moved down the ramp, and changes in the local depth and voltage for each gage are recorded.

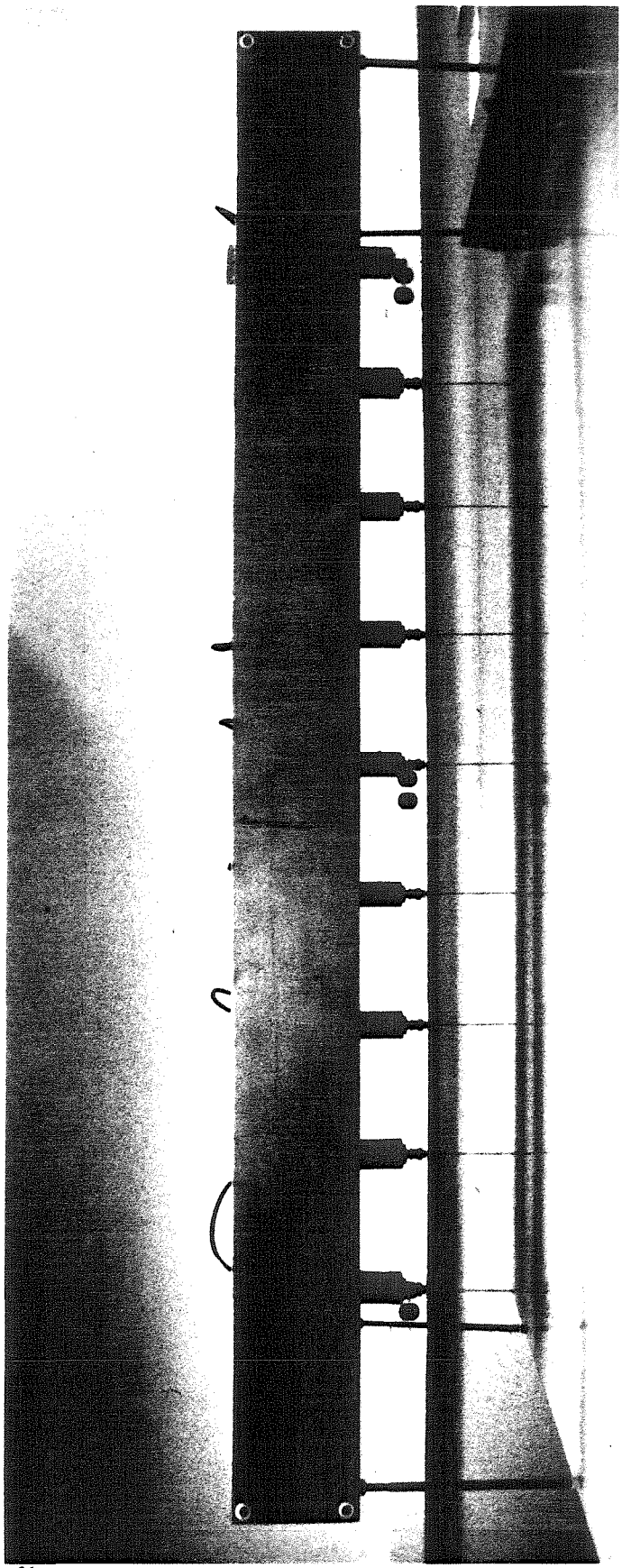

Figure 2.6.2 A photograph of a view of the runup gage.

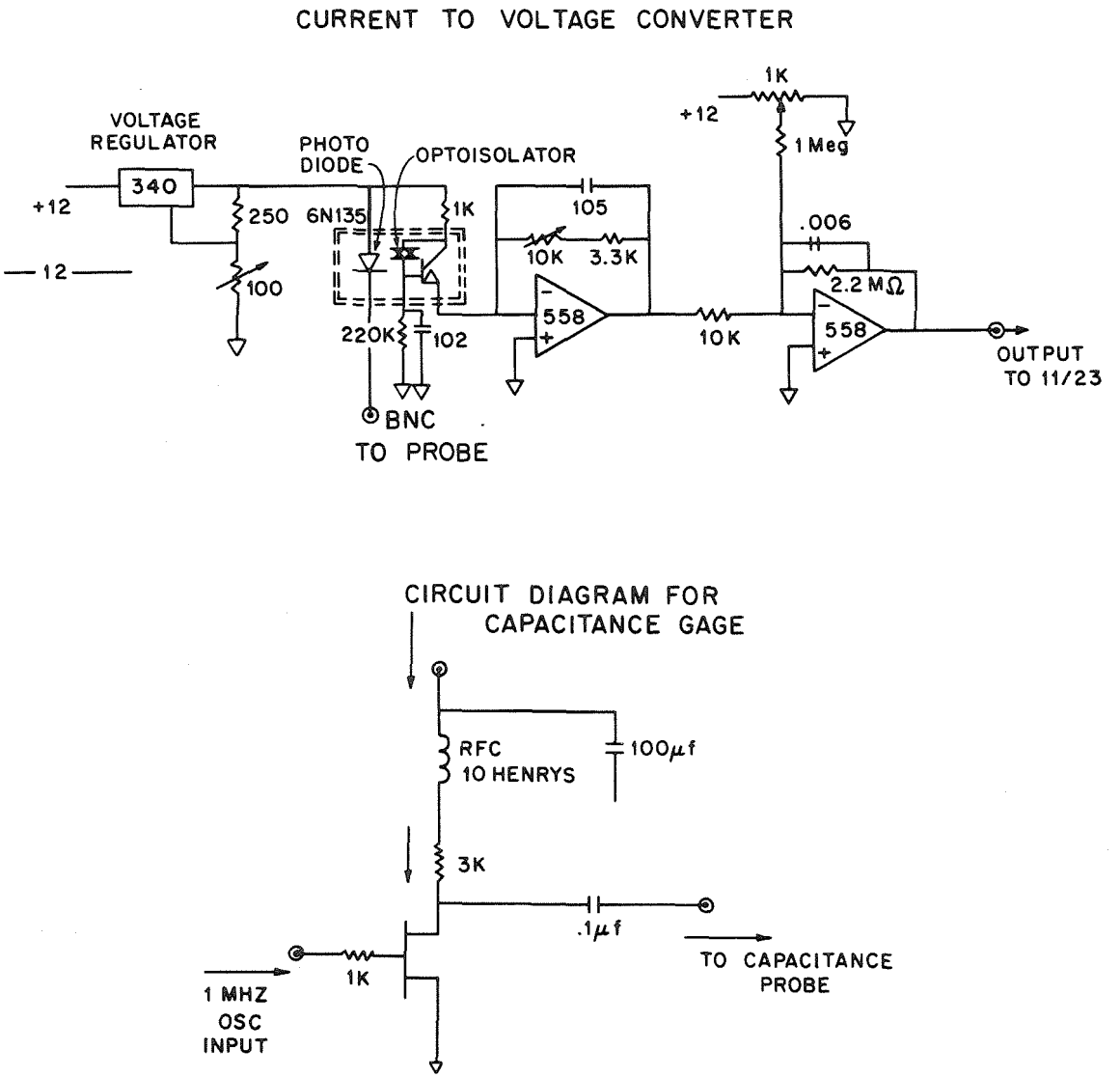

Figure 2.6.3 The circuit diagrams for the runup gages probes and the current to voltage converter.

The runup gage was tested dynamically by comparing its output with that of conventional π-frame gages. The comparison was done at a location near the toe of the ramp where both instruments could be deployed. It was accomplished by reproducing the same wave in the laboratory and by measuring it at the same location twice, once with the π-frame gage and then again with one of the runup probes. The comparison produced identical results. To test the performance of the runup gage when measuring surges on a dry bed, the gage was deployed at a distance of 0.06 depths seaward from the initial shoreline. A 16mm movie camera operating at 63.25 frames per second was used to record the climb of a wave on the beach, simultaneously with the runup gage. Figure (2.6.4) shows the comparison between the cinematographic data and the runup gage data. The data agree well during runup, but differ slightly during rundown. This may be attributed to the difficulty of identifying accurately the position of the free surface in the movie frames when digitizing images of flows with small depths ; this identification is harder during rundown than during runup, because then the windows of the tank have been wetted from the runup of the wave.

2.7 Experimental procedures. This section describes some of the laboratory procedures and software to collect data and do the analysis. Four different types of measurement were performed: measurements of the piston position, of the force on the piston, of wave heights using π-frame gages, and of wave heights using the runup gage.

2.7.1 The piston motion measurements. The measurement of the piston position is performed with either the potentiometer or the LVDT described in section 2.3. When the piston moves, the output voltage of the appropriate transducer is recorded first by an HP 8802A medium gain amplifier and then by the AD11-K interface of the 11/23.

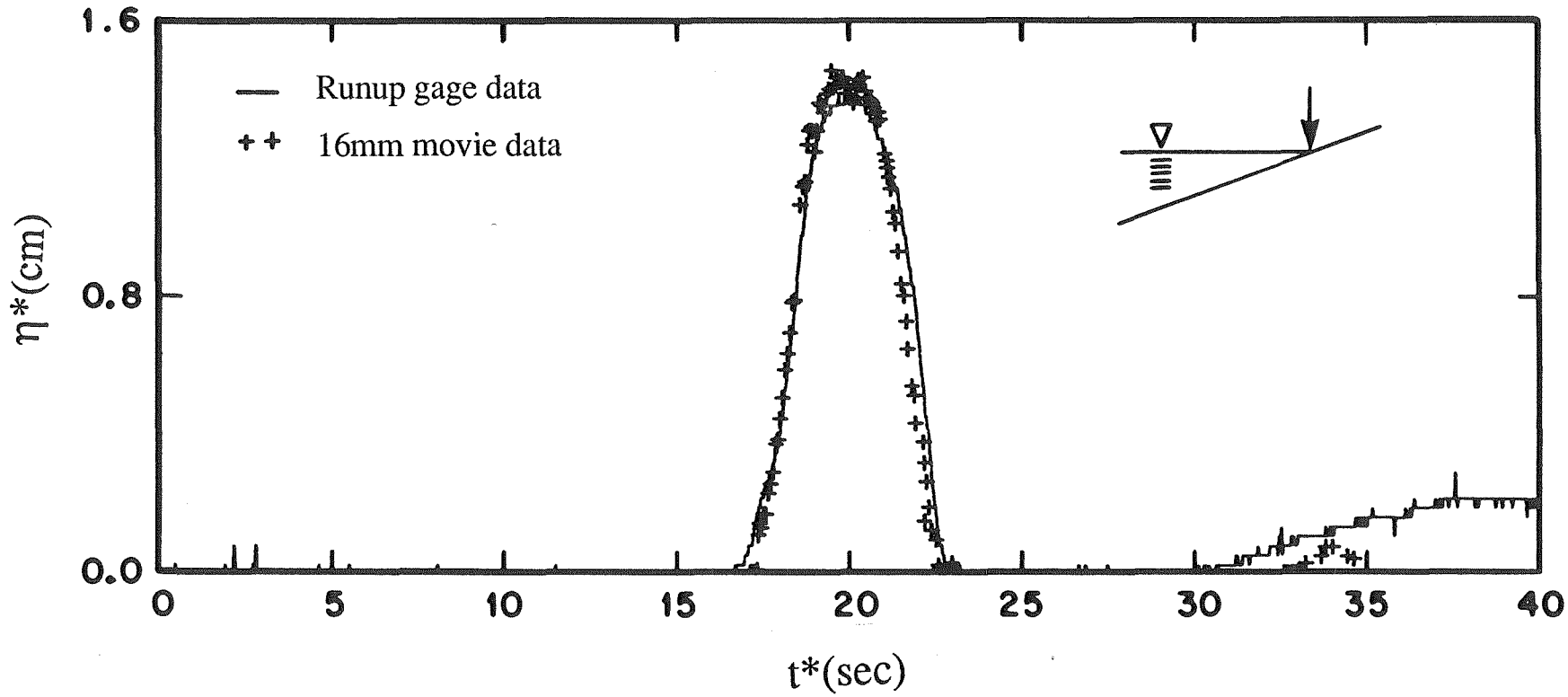

Figure 2.6.4 A comparison between surface elevations at x*/d=-0.06 measured with the runup gage and with a 16mm movie camera.

The stroke of the piston is defined as its maximum excursion and it is also recorded. The stroke divided by the maximum amplitude of the voltage signal is used to convert the latter into a trajectory time history, in a linear fashion. This practice was possible because the piston trajectory for all applications in this study was a monotonically increasing function of time. The measurement of the actual piston stroke in every experiment was necessitated by the fact that the piston motion was found to be a function of the pressure existing in the hydraulic system and the characteristic time of the motion. Tmes shorter than 1.000 sec produced distorted trajectories and produced strokes up to 5% off the intented ones. Depending on the stroke length, the error in measuring the piston motion varied between one to five percent. The noise level of the signal was in the same range.

2.7.2 The force measurements. The force measurements were performed with the force cell described in section 2.5. The force cell was calibrated before each run by adding lead weights on the bucket. To facilitate the data reduction, weights were added up to the anticipated loading level on the plate. A typical calibration curve is shown in figure (2.7.1). The force cell was proven to be a superb instrument, with highly repeatable calibration and performance. The error in the instrument calibration was less than one percent of the maximum load used in the calibration curve.

The force cell data were used to derive the force on the front face of the plate. When the piston moves, the recorded force is the vector sum of the hydrodynamic pressure forces on the front and rear of the plate and the "tare" force (which is the force necessary to move the piston). The hydrodynamic forces on the rear of the plate were reduced substantially by draining the fluid behind the plate rapidly. The drainage network is described in section 2.1. Initially the water level behind the plate is at the same level as the free surface on the front. The bulkhead behind the plate (shown in figure (2.5.1)) limited the volume of fluid between

the plate and the bulkhead to about a gallon (3.785 l). After the gate valve was opened, the fluid drained within 3 or 4 seconds to a level of 0.5 in (1.27 cm). The force due to this remaining fluid is easy to calculate, given the total force measurement, and the fact that the pressure on the front face, when the piston is not moving, is hydrostatic. When the piston starts moving, the volume behind the piston expands and the water level drops even further. The remaining fluid and any fluid leaking from the sides of the piston plate drains rapidly and does not contribute appreciably to the net hydrodynamic pressure force on the piston.

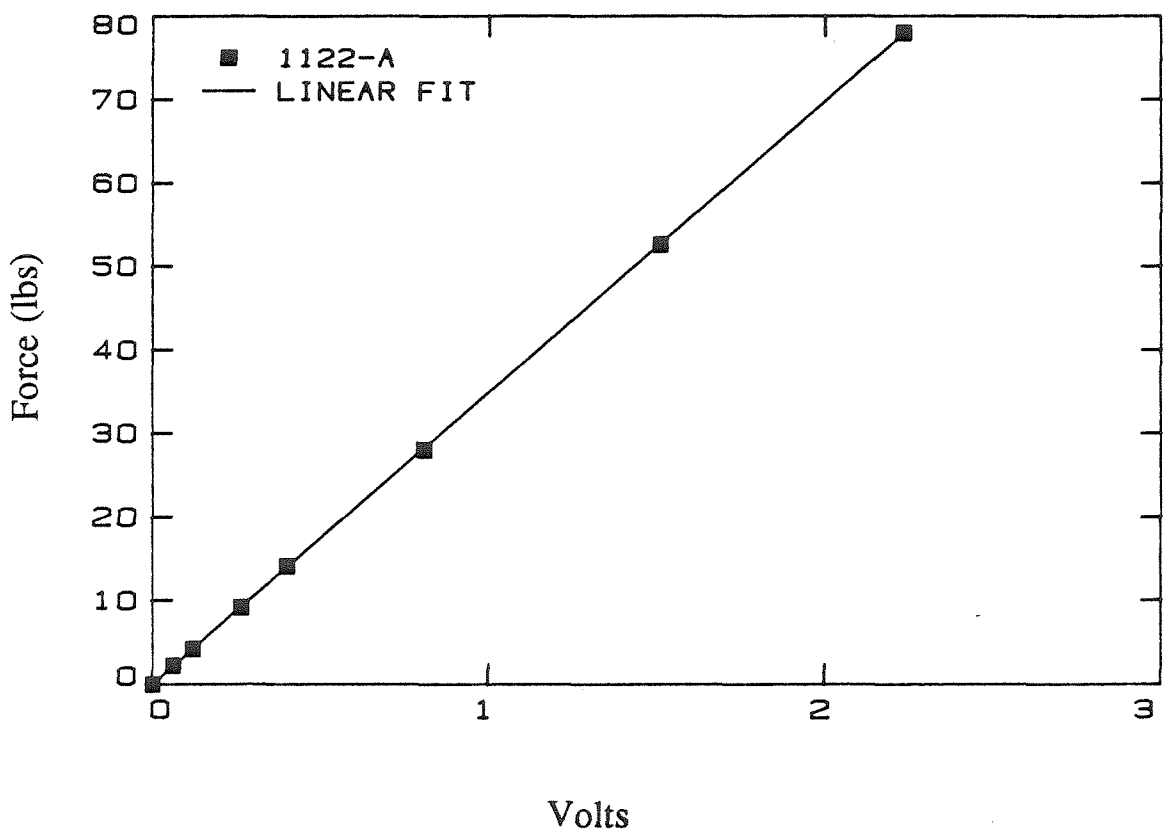

Figure 2.7.1 A typical calibration curve for the force cell.

The other quantity needed to determine the force on the front face is the "tare" force of the piston. In an ideal system, this force would be the product of the plate acceleration with the plate carriage mass. However, the action of static and dynamic friction forces necessitates the explicit measurement of the force for every possible trajectory to be used for the piston motion. To perform this measurement the tank is completely drained and the side walls are wetted with a spray bottle ; the plate is then moved with the trajectory whose associated tare force is to be determined, and the resulting force time history is recorded.

Although the measurement of the force on the piston plate was repeatable when water was in the tank, the measurement of the tare force did not produce reproducible results. Figure (2.7.2) shows the force required to move the piston, a measure of the piston velocity, and the associated impulse of the motion, as functions of time, for three realizations of the same linear piston motion. The actual piston velocity was determined by numerical differentiation of the motion signal and the impulse by numerical integration of the force signal. As it can be seen from the figure, there is a 72% difference between the impulse results associated with that motion.

The behaviour shown in figure (2.7.2) was persistent for many of the trajectories tested. In an effort to understand this apparent paradox, that the same motion under identical conditions required different impulse in different realizations, the wave generation system was stripped down. First the wiper blades were removed from the sides of the piston plate; then the seals of the linear motion bearings on which the piston carriage is riding were also removed. The reproducibility of the impulse of the motion did not improve substantially. Then an effort was made to calculate the transfer function of the system by determining the delta function response. However, it failed to reveal any characteristics of the wave generation system responsible for the poor results.

Because of this limitation, only data from runs where the tare force was reproducible in at least ten realizations of the same motion will be presented in the subsequent discussion of the laboratory results.

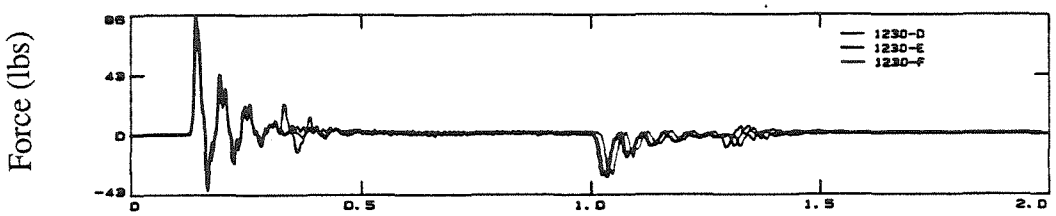

Figure 2.7.2a Three tare force measurements under identical plate motions. The stroke is equal to 12.55 cm (4.94 in) and the generation time is 1.000 sec. The plate is moving with a ramp motion. (See section 4.2.2.)

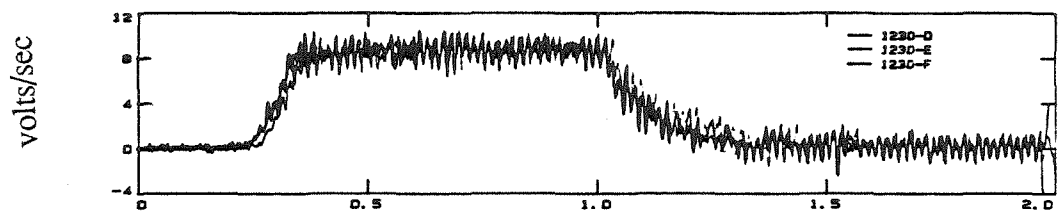

Figure 2.7.2b A measure of the plate velocity.

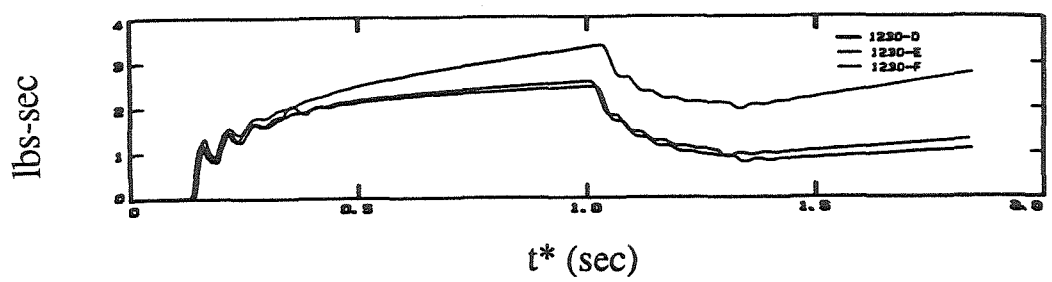

Figure 2.7.2c The impulse associated with the force measurements of figure (2.7.2a). Note how small changes in the force signals produce large differences in the impulse.

2.7.3 The wave height measurements. Wave height in the constant depth region of the tank were measured using resistance type wave gages as described in section 2.6. Any wave transducers deployed in a given experiment were balanced and calibrated before each experiment. The calibration was performed by varying the elevation of the wave gage sequentially and then triggering the 11/23 to record the corresponding voltage. The software displayed different degree polynomial fits for the calibration data, and the user was prompted to select the desired fit . Then the calibration curve was plotted on an HP 7470 plotter. Usually the fit selected was of degree four. Figure (2.7.3a) shows a typical calibration curve for one of the π-frame gages, and figure (2.7.3b) shows a typical calibration curve for the plate wave gage. The calibration of the resistance wave gages was accurate to within 0.5% of the maximum elevation included in the calibration curve.

2.7.4 The runup height measurements. The runup height measurement is performed in a different fashion than the other wave height measurements because all ten transducers are calibrated simultaneously. The runup gage includes its own excitation system, and no balancing of the system is necessary. The output signal is recorded directly, i.e., without amplification.

The gage was calibrated before each run as follows. The gage was moved sequentially down the ramp and the 11/23 was triggered to record the voltage data from all gages. As the runup gage became immersed in the fluid, not all of the probes were immersed in the same depth. The software inquired for the interprobe separation distance, and the initial immersion depth of the first gage in the array, and then monitored whether a given probe was immersed in the water and its immersion depth. Then the calibration curve was constructed for each gage and then was plotted on the HP 7470A plotter. A typical calibration curve is shown in figure (2.7.4). The calibration of each probe was accurate to within five percent of the maximum elevation.

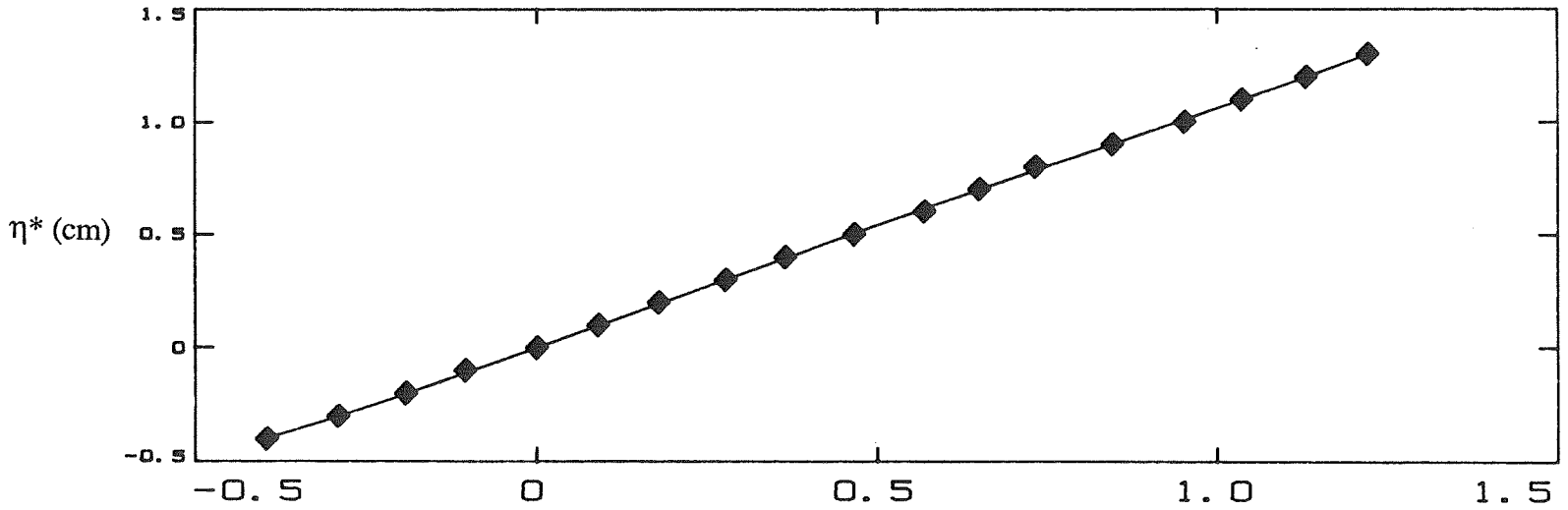

Figure 2.7.3a A typical calibration curve for π-frame gage.

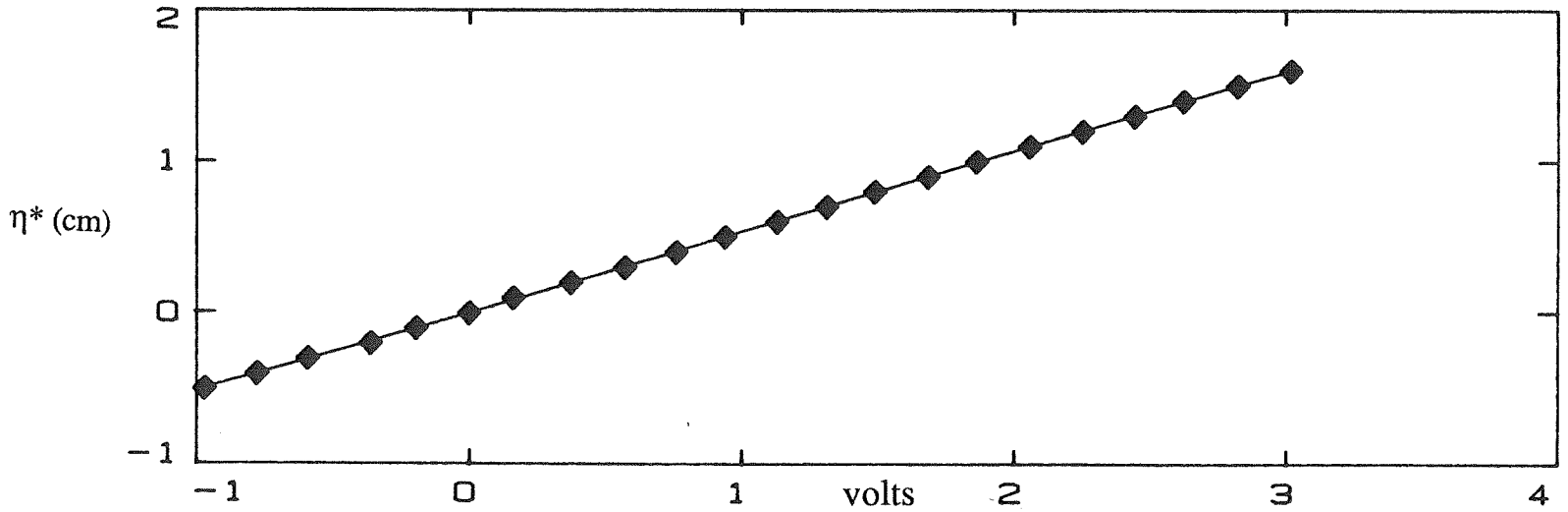

Figure 2.7.3b A typical calibration curve for the plate wave gage.

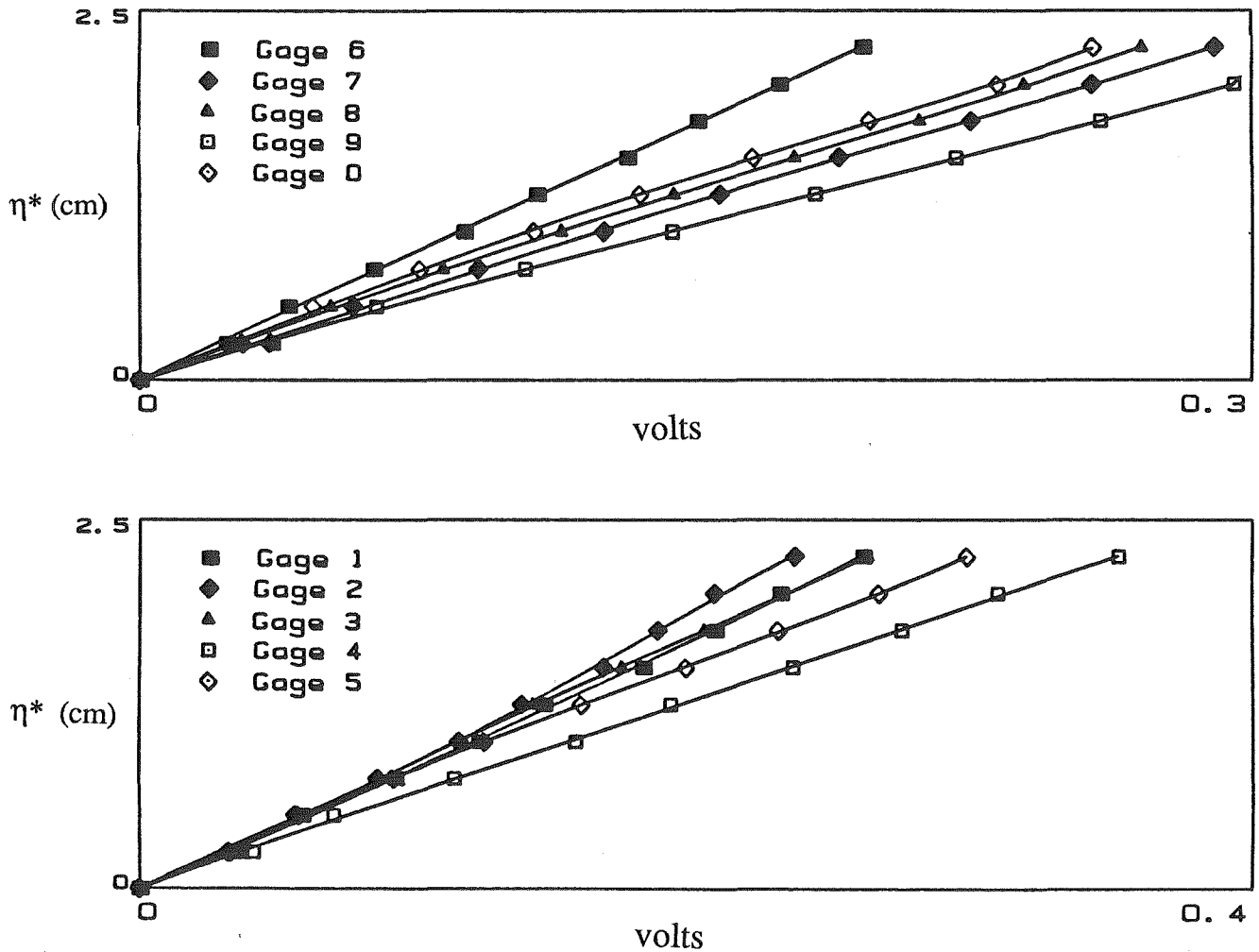

Figure 2.7.4 A typical calibration curves for the runup gage probes.

2.7.5 General specifications of the data acquisition. All of the wave data collected in this investigation were in the form of voltages recorded by the AD11-J interface board of the 11/23. The board specifications indicate conversion accuracy to 0.001 volts. This value was checked periodically with precision voltmeters, and the AD11-J gave results repeatable to 0.005 volts.

All calibrations described in sections 2.7.2, 2.7.3, and 2.7.4 involved measurements of voltages. The average of ten samples was used to establish a particular voltage value for each calibration point. The voltage range used in the calibrations was typically between -2.0 to 4.0 volts, except in the runup gage, where the range was from 0.0 to 1.4 volts.

Data was collected from 16 channels simultaneously. The macro routine that performed the data sampling was written by Skjelbreia (1982). The number of data collected imposed an effective limit on the sampling rate, even when virtual arrays were used for temporary data storage. The sampling rate used ranged from 2000 Hz to 125 Hz per channel.

The data were converted in real-time to dimensionless numbers, using the calibration coefficients of each run. It was stored in FILES-11 format, and it was displayed on the HP 7470 plotter as soon as the data acquisition of each run was completed. (Budget limitations did not permit the acquisition of a graphics display.) All software used in this study for data acquisition, reduction, analysis, display and plotting were developed by the author.

Chapter 3

The runup of solitary waves

In this chapter an exact solution of the linear and a nonlinear shallow water wave equations is derived for the climb of long waves on plane beaches. An exact result is developed for calculating the runup of nonbreaking solitary waves and is compared with experimental data. It is found that the linear theory predicts the maximum runup of solitary waves well, and that the nonlinear theory describes the climb of solitary waves up sloping beaches equally well. Some differences between breaking and nonbreaking solitary waves are discussed and some of the unresolved questions posed in the introduction are explained.

3.1 Basic equations and solutions. Consider a topography consisting of a plane beach of slope 1 : cotβ adjacent to a constant depth region, as shown in figure (3.1.1). Non-dimensional variables are now introduced as follows :

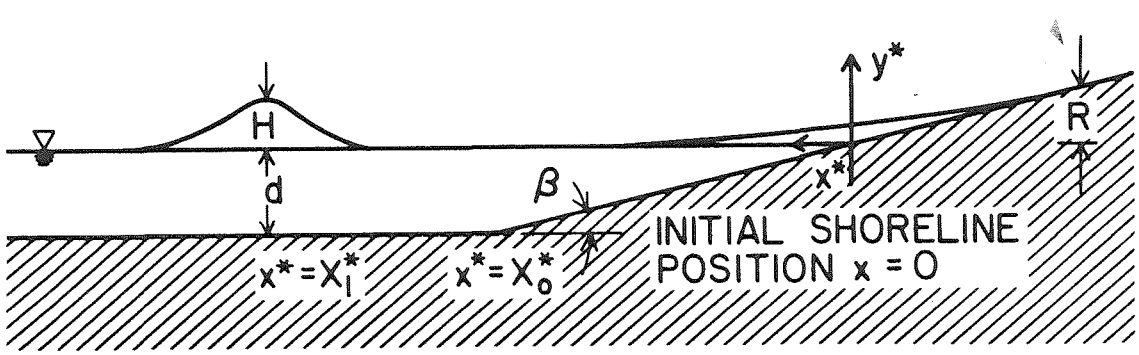

Figure 3.1.1 A definition sketch for a solitary wave climbing up a sloping beach.

$$x = x^*/d, \quad h = h^*/d, \quad \eta = \eta^*/d, \quad t = t^* \sqrt{g/d}, \quad \text{and} \quad u = u^* / \sqrt{gd}, \tag{3.1.1}$$

where the star indicates dimensional variables and d is the characteristic depth of water. The origin of the coordinate system is at the initial position of the shoreline and x increases seaward. The topography is described as follows :

$$h_0(x) = x \tan \beta \qquad \text{when} \qquad x \leq \cot\beta, \tag{3.1.2a}$$

and

$$h_0(x) = 1 \qquad \text{otherwise.} \tag{3.1.2b}$$

The local undisturbed water depth is h_0 . Consider a propagation problem in this region described by the nonlinear shallow water wave equations :

$$h_t + (hu)_x = 0 \tag{3.1.3a}$$

$$u_t + uu_x + h_x = 0 \tag{3.1.3b}$$

$$h(x,t) = h_0(x) + \eta(x,t) \quad . \tag{3.1.3c}$$

3.2 Linear theory. The system of equations (3.1.3) can be linearised by retaining the first order terms. The following equation results :

$$\eta_{tt} - (\eta_x h_0)_x = 0 \quad . \tag{3.2.1}$$

When the undisturbed depth h_0 is constant, equation (3.2.1) reduces to the classical wave equation, with the steady state solution :

$$\eta(x,t) = A_i e^{-ik(x+ct)} + A_r e^{ik(x-ct)} \quad , \text{ when } h_0(x) = 1 \ . \tag{3.2.2a}$$

When $h_0 = x \tan\beta$, then the substitution $\chi = 2\omega\sqrt{x}\cot b$, transforms (3.2.1) into a Bessel equation of order zero. The steady solution is :

$$\eta\,(x,t) = B\,(k,\beta)\,J_0\,(2k\sqrt{x}\cot\beta)\,e^{-ikct}\ ,\ \text{when}\ h_0\,(x) = x\tan\beta. \qquad (3.2.2b)$$

Note that, with the normalization used, the phase velocity is unity, i.e., c = 1. However, c is retained for compatibility with other formulations. Solutions for arbitrary boundary conditions can be derived for both cases, $h_0(x) = 1$ and $h_0(x) = x\tan\beta$, by standard methods. An elegant solution method for the case $h_0(x) = x\tan\beta$ will be outlined presently. Let $\zeta = \sqrt{x}$. Then (3.2.1) becomes :

$$\eta_{\zeta\zeta} + (1/\zeta)\eta_\zeta = 4\cot\beta\,\eta_{tt}\,. \qquad (3.2.3)$$

Expanding $\eta\,(\zeta,t)$ in a Fourier-Bessel series one obtains :

$$\eta\,(\zeta,t) = \sum_{n=1,\infty} c_n(t)\,J_0(j_n\zeta)\ , \qquad (3.2.4)$$

where j_n is the nth zero of J_0. Multiplying (3.2.4) by $s\,J_0\,(j_m s)$, integrating from 0 to 1 and using the orthogonality condition of the Bessel functions results into :

$$c_n\,(t) = \frac{2}{[J_1(j_n)]^2}\int_0^1 s\,J_0(j_n s)\,\eta\,(s,t)\,ds\,. \qquad (3.2.5)$$

Using the identity $d/dz\,\{J_1(j_n z)\} = j_n J_0(j_n z) - (1/z)\,J_1(j_n z)$ and substituting (3.2.4) into (3.2.3) the following differential equation is obtained for the coefficients of the series :

$$\frac{d^2c_n}{dt^2} = -\frac{j_n^2}{4}c_n . \qquad (3.2.6)$$

Once an initial value $\eta(\zeta,t_0)$ is specified, then $c_n(t_0)$ can be derived explicitly from (3.2.5) ; then $c_n(t)$ follows directly from (3.2.6). For example, the steady state solution can be derived immediately by letting $\eta(\zeta,t) = a(\zeta)e^{-i\omega t}$. Then (3.2.6) becomes $j_n^2 = 4\omega^2 \cot\beta$ and then $\eta(\zeta,t) = B\, J_0(\omega\zeta)\, e^{-i\omega t}$, where B is an arbitrary constant. A similar solution is presented in Carrier, Krook and Pearson (1966), page 372, for an equation that describes the free vibrations of a hanging chain.

A solution for the combined topography (3.1.2) can be derived by matching the outer solution (the solution in the constant depth region (3.2.2a)) and its x-derivative, to the inner solution (the solution on the sloping beach (3.2.2b)) and its x-derivative at $x = X_o$, the toe of the beach. Let constant A_i be the amplitude of the incident wave, A_r be the amplitude of the reflected wave, $B(k,\beta)$ be the amplitude of the wave transmitted to the beach, referred to as *the amplification factor* , and k be the wavenumber. This matching was first performed by Keller and Keller (1960). Given an incident wave of the form $\eta(x,t) = A_i e^{-ik(x+ct)}$, the following expressions are obtained for B and A_r :

$$B(k,\beta) = \frac{2A_i e^{-ikX_0}}{J_0(2X_0k) - i\,J_1(2X_0k)} , \qquad (3.2.7a)$$

and

$$A_r(k,\beta) = A_i\, e^{-2ikX_0} . \qquad (3.2.7b)$$

This solution can be used to study the behaviour of more general waveforms approaching the sloping beach. As Stoker (1947) pointed out, the standing wave solution (3.2.2) can be used to obtain travelling wave solutions by linear superposition, since the

governing equation (3.2.1) is linear and homogeneous. For an incident wave of the form : $\eta(x,t) = \int_{-\infty}^{\infty} \Phi(k)\, e^{-ikct}\, dk$, the transmitted wave to the beach has the form :

$$\eta(x,t) = 2\int_{-\infty}^{\infty} \Phi(k) \frac{J_0(2k\sqrt{xX_0})\, e^{-ik(X_0+ct)}}{J_0(2X_0k) - i\, J_1(2X_0k)}\, dk \quad . \tag{3.2.8}$$

This solution is only valid for $0 \leq x$. When $x < 0$, then (3.2.1) does not reduce to Bessel's equation. In order to obtain details of the wave in the region $x < 0$ one must solve the nonlinear set (3.1.2).

3.3 Nonlinear theory. To solve the nonlinear set (3.1.3) for the sloping beach case, where $h_0(x) = x \tan\beta$, Carrier and Greenspan (1959) introduced the following hodograph transformation,

$$u = \psi_\sigma/\sigma, \tag{3.3.1a}$$

$$x = \cot\beta\ [\sigma^2/16 - \psi_\lambda/4 + u^2/2], \tag{3.3.1b}$$

$$t = \cot\beta\ [\psi_\sigma/\sigma - \lambda/2], \tag{3.3.1c}$$

and

$$\eta = \psi_\lambda/4 - u^2/2\ . \tag{3.3.1d}$$

This reduces the set (3.1.3) to a single linear equation,

$$(\sigma\psi_\sigma)_\sigma = \sigma\psi_{\lambda\lambda}. \tag{3.3.2}$$

The transformation is such that in the hodograph plane, i.e., the (σ,λ) space, the shoreline is always at $\sigma=0$. This can be seen by observing that when $\sigma= 0$, (3.3.1b) implies that $\eta = -x\tan\beta$, which is a relationship valid only at the shoreline tip.

Equation (3.3.2) can be solved with standard methods. In its steady state form, it is Bessel's equation of order zero. If an initial condition is available, one can use Hankel transform techniques, as demonstrated by Carrier (1966). If a boundary condition is available, then the method of choice is the Fourier transform technique. Let κ be the transform variable, the wavenumber in the (σ,λ) space, distinct from k the wavenumber in the (x,t) space. Define the Fourier transform of $\psi(\sigma,\lambda)$ as $\Psi(\sigma,\kappa) = \int_{-\infty}^{\infty} \psi(\sigma,\lambda)\, e^{-i\lambda\kappa}\, d\lambda$. If initially, $\Psi(\sigma_0,\kappa) = F(\kappa)$, then the solution bounded at $\sigma = 0$ and $\sigma = \infty$ has the form :

$$\psi(\sigma,\lambda) = \int_{-\infty}^{\infty} F(\kappa) \frac{J_0(\sigma\kappa)}{J_0(\sigma_0\kappa)} e^{i\kappa\lambda} d\kappa. \qquad (3.3.3)$$

To complete the solution of (3.3.2) an appropriate initial or boundary condition must be specified. Carrier and Greenspan (1958) presented a general solution to the initial value problem when the velocity $u(x,t_0)$ is initially zero (t_0 is the initial time). Spielvogel (1974) used that solution to derive the evolution of the wave during rundown, assuming initially an exponentially shaped runup profile. Carrier and Greenspan (1958) also presented solutions with $u(x,t_0) \neq 0$, but for specific initial conditions. In general, it is difficult to specify initial conditions on a sloping beach, without making restrictive assumptions for the incoming and reflected waveforms. For similar reasons, a boundary condition for all times can not be specified apriori for an arbitary incoming wave. Even when boundary or initial conditions are available in the (x,t) space, the process of deriving the equivalent conditions in the (σ,λ) space is not trivial. Also, matching of an inner solution with an outer solution is not easy, because the resulting equations cannot be solved by simple elimination as in the derivation of equations (3.2.2).

These difficulties have restricted the use of the Carrier and Greenspan formalism.

This is quite unfortunate because the problems described can be circumvented. Carrier (1966) demonstrated how to specify a boundary condition when available or when reflection is negligible. Another method will be described presently for specifying such a condition, including reflection.

Carrier (1966) pointed out that far from the shoreline nonlinear effects are small. (The validity of this statement will be examined later, when the results of this theory are compared with experiments.) The transformation equations can then be simplified by neglecting terms $\sim O(u^2)$. To the same order, $\psi_\lambda/4 << \sigma^2/16$ (since $\sigma^2/16 \sim O(1)$), and $|\psi_\sigma/\sigma| << |\lambda/2|$, since $|\lambda/2| \sim O(10)$. This reduces (3.3.1) to :

$$u = \psi_\sigma/\sigma, \qquad \eta = \psi_\lambda/4,$$
$$x = \cot\beta\ (\sigma^2/16) \text{ and } \quad t = -\cot\beta\ (\lambda/2)\ . \tag{3.3.4}$$

These equations are linear and allow specification of a boundary condition directly, once the equivalent condition is known in the (x,t) plane.

One method for specifying a boundary condition in the physical space is to use the solution of the equivalent linear problem, as given by equation (3.2.6). This is certainly correct to the same order of approximation as (3.3.4). The obvious choice for specifying the boundary condition is the seaward boundary. This is dictated by the requirement to use the linearised form of the transformation at the furthest possible location from the initial position of the shoreline, but at a location where the Carrier and Greenspan formalism is still valid. This is the point $x = X_o$, and it corresponds to the point $\sigma=\sigma_0=4$ in the (σ,λ) space. Then $\eta(X_0,t) = (1/4)\psi_\lambda(4,\lambda)$. The boundary condition $F(\kappa)$ in the (σ,κ) plane is determined from (3.3.3) and (3.2.8) by repeated application of the Fourier integral theorem. Assuming

that $\psi(\sigma_0,\lambda)$ goes to zero at $\lambda = \pm\infty$, then the solution of (3.3.2) follows as,

$$\psi(\sigma,\lambda) = \frac{8i}{X_0} \int_{-\infty}^{\infty} \frac{2\Phi(\kappa)\, J_0(\sigma\kappa X_0/2)\; e^{-i\kappa X_0 + i\kappa\lambda X_0/2}}{\kappa\,\{J_0(2X_0\kappa) - i\, J_1(2X_0\kappa)\}}\, d\kappa. \tag{3.3.5}$$

It is interesting to compare the predictions of the linear and of the nonlinear theories for the maximum runup and minimum rundown. It will be shown that they are identical. The maximum runup according to the linear theory is the maximum value attained by the wave amplitude at the initial position of the shoreline, $x = 0$, or,

$$\eta(0,t) = 2\int_{-\infty}^{\infty} \frac{\Phi(k)\; e^{-ik(X_0 + ct)}}{J_0(2X_0k) - i\, J_1(2X_0k)}\, dk. \tag{3.3.6}$$

In the nonlinear theory the maximum runup is given by the maximum value of the wave amplitude at the shoreline, $\eta(x_s,t)$, where x_s defines the shoreline path and corresponds to $\sigma=0$. Let u_s be the shoreline velocity; then, by definition, $dx_s/dt = u_s$. To find x_s one may use equation (3.3.1d) to obtain :

$$\eta(x_s,t) = \frac{\psi_\lambda(0,\lambda)}{4} - \frac{u_s^2}{2} = 2\int_0^{\infty} \frac{\Phi(\kappa)\, e^{-i\kappa X_0 + i\kappa\lambda X_0/2}}{J_0(2X_0\kappa) - i\, J_1(2X_0\kappa)}\, d\kappa - \frac{u_s^2}{2}. \tag{3.3.7}$$

At the point of maximum runup, the velocity of the shoreline becomes zero. Setting $u = 0$ and $\sigma = 0$ in the transformation equations (3.3.1), reduces them to :

$$u = 0, \quad \eta = \psi_\lambda/4, \quad x = -\eta\cot\beta, \quad t = -(\lambda/2)\cot\beta. \tag{3.3.8}$$

Substitution of these values in equation (3.3.7) reduces it to (3.3.6), proving that *the maximum runup predicted by the nonlinear theory is identical to that predicted by the linear theory.* At the minimum rundown point the shoreline also attains zero velocity, and the same argument implies that the linear and nonlinear theory results for the minimum runup are identical. This behaviour was first noted by Carrier (1971), but had not been previously identified as resulting from the effective linearization of the transformation equations at the maximum and minimum excursion of the wave. This is paradoxical , since the linear and nonlinear theory solution differ most at the initial shoreline. (See, for example, figure (3.5.3)).

3.4 The solitary wave solution. The results of the previous section will now be applied to derive a result for the maximum runup of a solitary wave on a plane beach. A solitary wave centered at $x = X_1$ at time $t = 0$ has the following surface profile :

$$\eta\,(x,0) = \frac{H}{d}\,\mathrm{sech}^2[\gamma\,(x-X_1)], \tag{3.4.1a}$$

where

$$\gamma = \sqrt{\frac{3}{4}\frac{H}{d}}\,. \tag{3.4.1b}$$

The transform function Φ (k) associated with this profile is derived in appendix D. It is given by :

$$\Phi(k) = \frac{2}{3}\,k\,\mathrm{cosech}\,(\alpha k)\,e^{ikX_1} \quad , \tag{3.4.2}$$

where $\alpha = \pi/2\gamma$. Substituting this form in equation (3.3.6) and defining the *dimensional* surface elevation at the initial position of the shoreline as R (t), then the following relationship results :

$$\frac{R\ (t)}{d} = \frac{4}{3}\int_{-\infty}^{\infty} \frac{k\,\mathrm{cosech}(\alpha k)\ e^{-ik\,(\theta + ct)}}{J_0(2X_0k) - i\,J_1(2X_0k)}\ dk\ , \qquad (3.4.3)$$

where $\theta = X_0 - X_1$. This integral can be evaluated with standard numerical methods. However, to obtain physical insight on the quantitative dependence of $R\ (t)$ on H/d and X_0, the integral must be evaluated analytically. To perform the evaluation one can use contour integration techniques.

Consider the integral $\mathbf{I}_c(t)$ defined along a closed contour **C** in the upper half plane, consisting of the semicircle $z = |r|$ and the real axis,

$$\mathbf{I}_c\ (t) = \int_c \frac{z\,\mathrm{cosech}(\alpha z)\ e^{-iz\,(\theta + ct)}}{J_0(2X_0z) - i\,J_1(2X_0z)}\ dz\ . \qquad (3.4.4)$$

The integral $\mathbf{I}_c(t)$ can be broken into two parts, the integral $\mathbf{I}_\theta(t)$ along the semicircle perimeter and the integral $\mathbf{I}_r(t)$ along the real axis segment (-r,r). (Note that $\mathbf{R}/d = (4/3)\mathbf{I}_r(t)$, and it is the desired integral (3.4.3).) $\mathbf{I}_r(t)$ converges for all times, but $\mathbf{I}_c(t)$ converges in the domain **D**, bounded by **C**, only when :

$$0 < (X_1 + X_0 - ct)\ . \qquad (3.4.5)$$

Otherwise it converges in the sector defined by :

$$0 < \alpha\ |Re\ z| + (3X_0 - X_1 + ct)\ |Im\ z| < 0\ . \qquad (3.4.6)$$

To perform the integration (3.4.4), one must define the poles of the integrand in **D**. Since the numerator is an analytic function in **D**, the poles of the integrand are the zeroes of the

denominator. Consider the function $f(z) = J_0(z)-J_1(z)$ defined in **D** and let **N** denote the number of zeroes and **P** the number of poles of f(z) in the same domain. By the principle of the argument,

$$\mathbf{N} - \mathbf{P} = \frac{1}{2\pi i} \int_c \frac{f'(z)}{f(z)} \, dz . \tag{3.4.7}$$

Using Bessel function identities (Abramowitz and Stegun (1970)), this expression becomes:

$$\mathbf{N} - \mathbf{P} = \frac{1}{2\pi i} \int_c \frac{J_0'(z) - i\, J_1'(z)}{J_0(z) - i\, J_1(z)} \, dz = \frac{1}{2\pi} \int_c dz - \frac{1}{2\pi} \int_c \frac{J_1(z)/z}{J_0(z) - i\, J_1(z)} \, dz . \tag{3.4.8}$$

The integral $\int_c dz$ is the integral of analytic function around a closed path inside its domain of analyticity; it is equal to zero. The second integral of the right hand side of the equation cannot be evaluated in closed form. However, an upper limit for its modulus can be obtained. On the circular arc, $z=re^{i\theta}$, and for large r one can easily show that when $Im\ z > 0$:

$$| J_1(z) | \leq | \sqrt{\frac{2}{\pi z}} \sin (z - \frac{\pi}{4}) - \frac{1}{|z|} L_n e^{Im\ z} \tag{3.4.9}$$

and that :

$$| J_0(z) - i\, J_1(z) | \geq | \sqrt{\frac{2}{\pi z}} e^{Im\ z} - \frac{1}{|z|} L_d e^{Im\ z} \tag{3.4.10}$$

L_n and L_d are the remainders in the corresponding asymptotic expansions. All sides in these inequalities are positive definite. Dividing them by parts in the right order and multiplying the resulting expression by $1/|z|$ results in the following relationship :

$$\frac{|J_1(z)/z|}{|J_0(z) - i\,J_1(z)|} \leq \frac{1}{2|z|} \quad \text{as } |z| \to \infty. \tag{3.4.11}$$

An upper bound can also be obtained for the straight line segment of the contour C, where $Im\ z = 0$,. Let $\underline{x} = Re\ z$. Then :

$$\frac{|J_1(\underline{x})/\underline{x}|}{|J_0(\underline{x}) - i\,J_1(\underline{x})|} \leq \frac{1/|\underline{x}|}{\sqrt{(J_0^2/J_1^2 + 1)}} \leq \frac{1}{|\underline{x}|} \ \forall\, \underline{x} \text{ where } J_1(\underline{x}) \neq 0. \tag{3.4.12}$$

The inequality is also valid when $J_1(\underline{x}) = 0$. Noting that the length of the semicircle is πr and of the line segment is 2r, and substituting the upper limits of the moduli along each segment, one obtains that :

$$\frac{1}{2\pi}\int_c \frac{J_1(z)/z}{J_0(z) - i\,J_1(z)}\,dz \leq \frac{1}{2\pi}\left[\pi r\left(\frac{1}{2r}\right) + 2r\left(\frac{1}{r}\right)\right] \leq \frac{2+\pi/2}{2\pi} < 1\,. \tag{3.4.13}$$

Since the function $J_o(z) - iJ_1(z)$ does not have any poles in the upper half plane, then N =0. This implies that the integrand of (3.4.4) has the same poles z_n as the function z cosech(αz). They are $z_n = n\pi i/\alpha$, n = 1,2,3... . The residue of the function at these poles is a_n and it is given by :

$$a_n = (-1)^n \left(\frac{n\pi i}{\alpha^2}\right) \frac{e^{2\gamma(\theta + ct)n}}{J_0(4\gamma X_0 n) - i\,J_1(4\gamma X_0 n)}\,, \tag{3.4.14}$$

where use was made of the relationship $\alpha = \pi/(2\gamma)$. Then, by the Cauchy integral formula :

$$I_c(t) = \frac{2\pi^2}{\alpha^2} \sum_{n=1,\infty} \frac{n\,(-1)^n\ e^{2\gamma(\theta + ct)n}}{I_0(4\gamma X_0 n) - i\,I_1(4\gamma X_0 n)}\,. \tag{3.4.15}$$

By Jordan's lemma, the line integral along the semicircle $\mathbf{I}_\theta$ (t) goes to zero for large r. In the limit as $r \to \infty$, the integral $\mathbf{I}_c$ (t) along **C** is equal to the integral along the real axis, $\mathbf{I}_r$ (t). Then :

$$\frac{R(t)}{d} = 8\frac{H}{d}\sum_{n=1,\infty} \frac{n(-1)^n \; e^{2\gamma(\theta+ct)n}}{I_0(4\gamma X_0 n) - i\, I_1(4\gamma X_0 n)} \tag{3.4.16}$$

This result can be further simplified by using the asymptotic form for large arguments of the modified Bessel functions. For $4X_o\gamma >> 1$, then :

$$\frac{R(t)}{d} = 8\sqrt{\pi X_0}\,\frac{H}{d}\left(3\frac{H}{d}\right)^{1/4}\sum_{n=1,\infty}(-1)^n\, n^{3/2}\, e^{-2\gamma(X_1+X_0-ct)n} . \tag{3.4.17}$$

This form of the solution is particularly helpful for calculating the maximum runup. The series in (3.4.15) is of the form $\sum(-1)^{n+1}n^{3/2}\chi^n$ and its maximum occurs when $\chi = 0.481 = e^{-0.732}$. This value defines the time t_{max} when the wave reaches its maximum runup, i.e., where (3.4.15) has a maximum, as :

$$t_{max} = \left(\frac{1}{c}\right)\left(X_1 + X_o - \frac{0.366}{\gamma}\right) . \tag{3.4.18}$$

The value of the series at t_{max} is $\sum_{max}$ and it is equal to 0.15173. Defining as **R** the maximum value of R (t) and evaluating the term $8\sqrt{(\pi\sqrt{3})}\sum_{max}$ and writing $X_0=\cot\beta$, (3.4.15) becomes :

$$\frac{R}{d} = 2.831\sqrt{\cot\beta}\left(\frac{H}{d}\right)^{5/4}. \tag{3.4.19}$$

This result can also be derived by finding ψ_λ from the nonlinear theory solution (3.3.5) and then using the appropriate shoreline conditions (3.3.8) to find $\eta(x_s,t)$. It is valid when $4X_0\gamma >> 1$, i.e., $\sqrt{(H/d)} >> 0.288 \tan\beta$, and when the series converges as discussed. To derive surface profiles one must use the nonlinear theory and solve the transformation equations (3.3.1) to determine $\eta(x,t)$. The functions ψ_σ/σ and ψ_λ are given by :

$$\frac{\psi_\sigma}{\sigma} = \frac{16i}{3} \int_{-\infty}^{\infty} \frac{\kappa \operatorname{cosech}(\alpha\kappa)\, J_0(\sigma\kappa X_0/2)\, e^{-i\kappa\theta + i\kappa\lambda X_0/2}}{\sigma\, [\, J_0(2X_0\kappa) - i\, J_1(2X_0\kappa)]}\, d\kappa\,, \qquad (3.4.20)$$

and

$$\frac{1}{4}\psi_\lambda = \frac{4}{3} \int_{-\infty}^{\infty} \frac{\kappa \operatorname{cosech}(\alpha\kappa)\, J_0(\sigma\kappa X_0/2)\, e^{-i\kappa\theta + i\kappa\lambda X_0/2}}{J_0(2X_0\kappa) - i\, J_1(2X_0\kappa)}\, d\kappa\,. \qquad (3.4.21)$$

These integrals can be evaluated directly for given (σ,λ) ; then the transformation equations (3.3.1) can be used to evaluate η, u, x, and t explicitly. The function ψ_λ is shown in figure (3.4.1) as a function of σ,λ, for the particular conditions $H/d = 0.0185$, $X_0 = 19.85$, and $X_1 = 37.35$

3.5. Comparison of the theory with experimental and numerical data. This discussion has the objective to determine how well the linear and the nonlinear theory model the equivalent physical phenomenon. This is done in three stages. First, the asymptotic result (3.4.19) is compared with data collected in this and previous studies. Then, surface profiles generated in the laboratory are presented to evaluate the accuracy of the linear and the nonlinear theory. Finally, a comparison between the predictions of the theory with laboratory data is presented for the wavefront path. All the experiments to be referenced were conducted in the wave tank described in chapter 2 using the techniques discussed there. Solitary waves were generated as discussed in section 4.2.3.

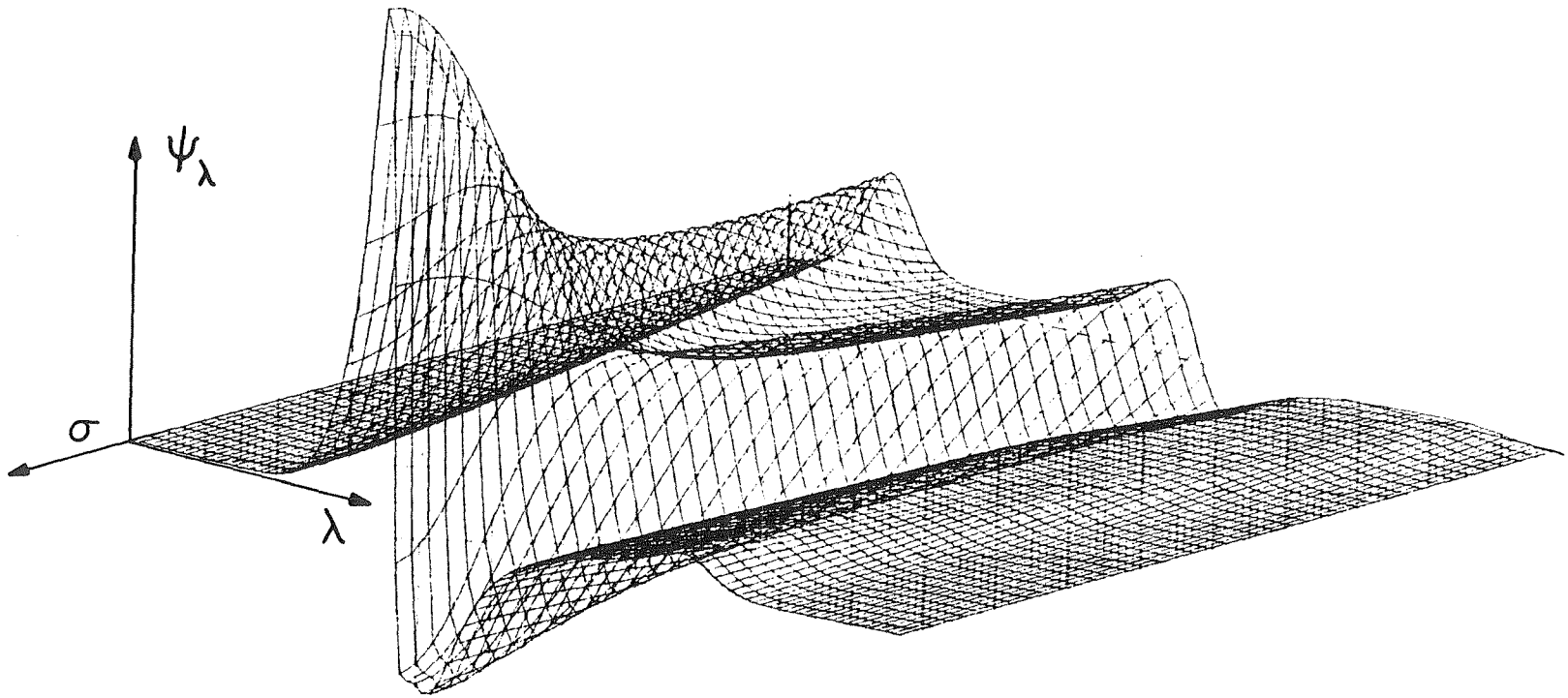

Figure 3.4.1 The function ψ_λ (σ,λ) defined by (3.4.21) for a 0.0185 wave climbing up a 1:19.85 beach.

3.5.1 Maximum Runup. The maximum runup of breaking and nonbreaking solitary waves realized in the laboratory on a 1:19.85 beach is presented in figure (3.5.1); the data included in this figure are listed in table T3.1 .

The abscissa is the height-to-depth ratio of the solitary waves in the constant depth region. It was calculated from the surface elevation time history measured at a distance from the toe of the beach equal to (1/2)L, where L is a measure of the horizontal extent of the wave, and it is defined by :

$$L = \frac{2}{\gamma} \cosh^{-1}\sqrt{(1/0.05)}, \quad \text{where } \gamma = \sqrt{\frac{3H}{4d}} \ . \qquad (3.5.1)$$

This practice was adopted to maintain a constant relative propagation distance (L /2) from the measurement location to the toe of the beach. Refering to figure (3.1.1), $L/2 = X_1 - X_0$. As a consequence, longer waves were measured further form the beach than shorter waves.

The ordinate is the normalised maximum runup **R**/d which is defined as the maximum vertical excursion of the shoreline at the time of maximum runup t_{max}. It should be noted that in the experiments the shoreline usually had a parabolic shape at the time of maximum runup. Its minimum and average position at that time were recorded and the runup distances defined with these lengths exhibited similar dependence on the height-to-depth ratio as the runup distance defined from the maximum position of the shoreline. For example, for the breaking wave data the dependence of maximum runup based on the maximum position of the shoreline is:

$$\frac{\mathbf{R}}{d} = 1.109 \left(\frac{H}{d}\right)^{0.582} . \qquad (3.5.2a)$$

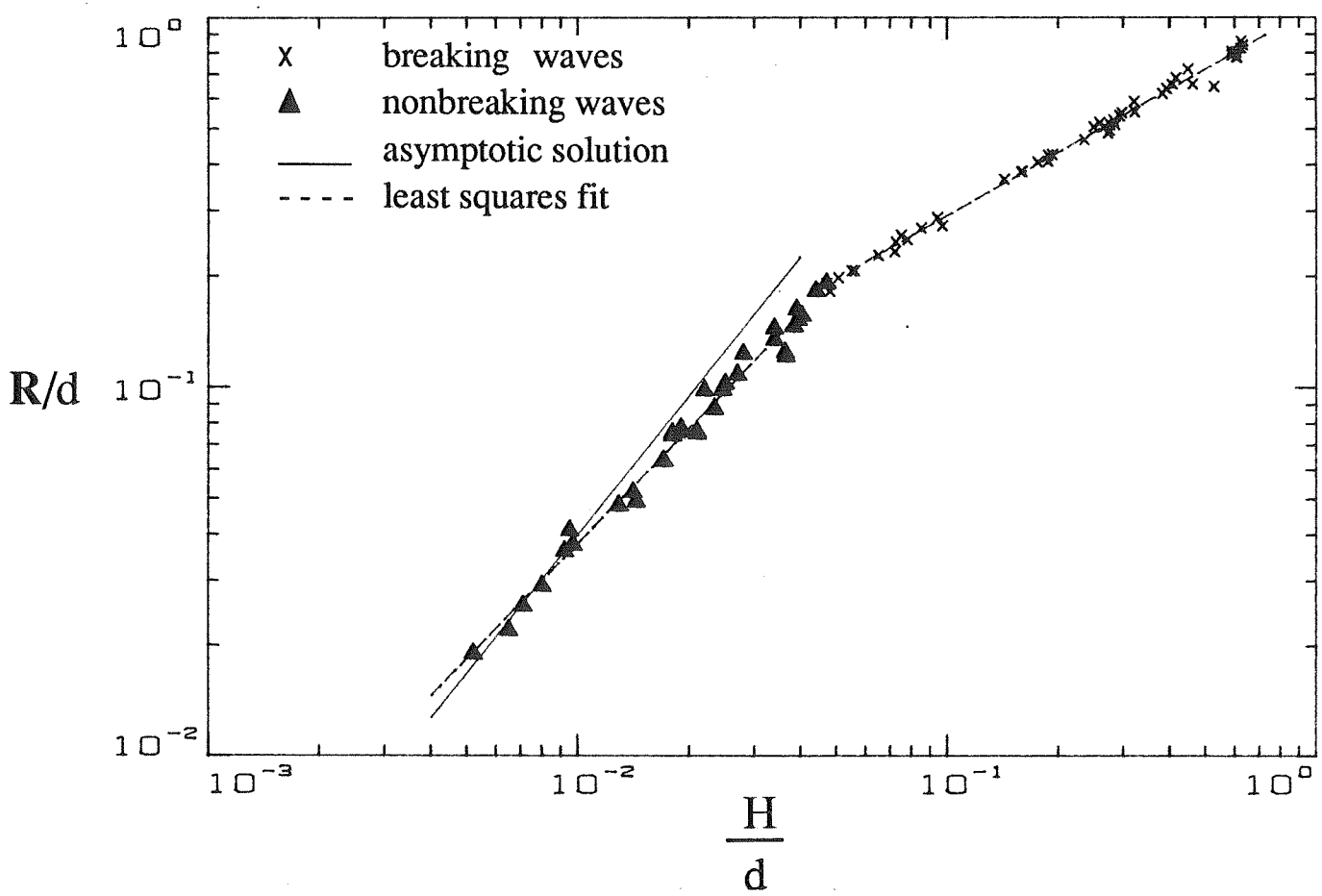

Figure 3.5.1 The maximum runup of solitary waves climbing up a 1:19.85 beach. Comparison between laboratory data and the analytical result (3.4.19). The data shown are listed in table T3.1.

The maximum runup based on the average position of the shoreline takes the form :

$$\frac{R}{d} = 0.918 \left(\frac{H}{d}\right)^{0.606}. \tag{3.5.2b}$$

The two dimensional character of the shoreline was repeatable. It was more prevalent in the breaking wave data than in the nonbreaking wave data, suggesting that it may be a side wall effect.

To generate the data of figure (3.5.1) different flow depths were used, ranging from 6.25 cm (2.46 in) to 38.32 cm (15.08 in), to determine if the depth can be scaled out from the laboratory experiments; Pedersen and Gjevik(1983) had reported experiments where the runup relationship for a given slope was influenced by the depth. In the present experiments a wave of a particular height-to-depth ratio had practically identical normalized runup at different depths. (See, for example table T3.1.) The same conclusion can also be drawn from the Hall and Watts (1953) data. This is exactly what would be expected on dimensional considerations.

Figure (3.5.1) shows two distinct runup regimes, one for breaking and one for nonbreaking waves. Breaking for this particular beach slope 1:19.85 occurs first during backwash when H/d = 0.044; breaking during runup first occurs when H/d = 0.055. Since the theoretical result (3.4.19) is valid even if the wave breaks during the backwash, the qualifier nonbreaking refers to waves that do not break during runup. The solid line represents the asymptotic solution (3.4.19). The asymptotic result appears to be describing the nonbreaking data adequately.

The existence of the two different runup regimes has never been observed previously. One explanation is that most experimental investigations have dealt primarily with breaking solitary waves; it is difficult to generate and measure nonbreaking solitary waves of $H/D < 0.05$ in the laboratory. Even when nonbreaking wave data were examined in the past, they were grouped with breaking wave data for the purpose of deriving empirical relationships. Since no theoretical results were available to suggest a different variation for nonbreaking waves, the phenomenon was overlooked.

To verify this observation and to generalise the asymptotic result for other slopes, the runup law was compared to other published data on solitary wave runup (Hall and Watts (1953), Pedersen and Gjevik (1983), Kim, Liu and Ligett (1984)). In the two latter investigations the authors have done numerical simulations of the runup, so that there is no doubt that their data refers to nonbreaking waves. However, the former investigation includes both breaking and nonbreaking wave data without identifying them. To perform such aposteriori identification, it is neccessary to use a breaking criterion. The criterion, that solitary waves break when $H/d > 0.479\ (\tan\beta)^{10/9}$, has been reported by Gjevik and Pedersen (1981) to be in good agreement with laboratory data for solitary waves. (It is discussed in section 3.6.) This relationship was used for the purpose of identifying the nonbreaking wave data in the Hall and Watts data set. Figure (3.5.2) includes *laboratory* data from the investigations mentioned. (Table T3.2 lists the same data and their sources, while table T3.3 lists the numerical data referenced.) The abcissa is the *runup law*, equation (3.4.19), and the ordinate is the maximum runup. The runup law does seem to explain the data satisfactorily. No data were included for slopes smaller than 1:19.85, because no such data are yet available ; on a 1:100 slope, the highest nonbreaking wave is the wave with $H/d \sim 0.003$ wave. Waves of such small amplitude are difficult to measure in the laboratory and need a long propagation distance to develop fully.

The identification of the nonbreaking wave data in the Hall and Watts data set and its comparison with the runup law (3.4.19) offers some insight why the two regimes in solitary

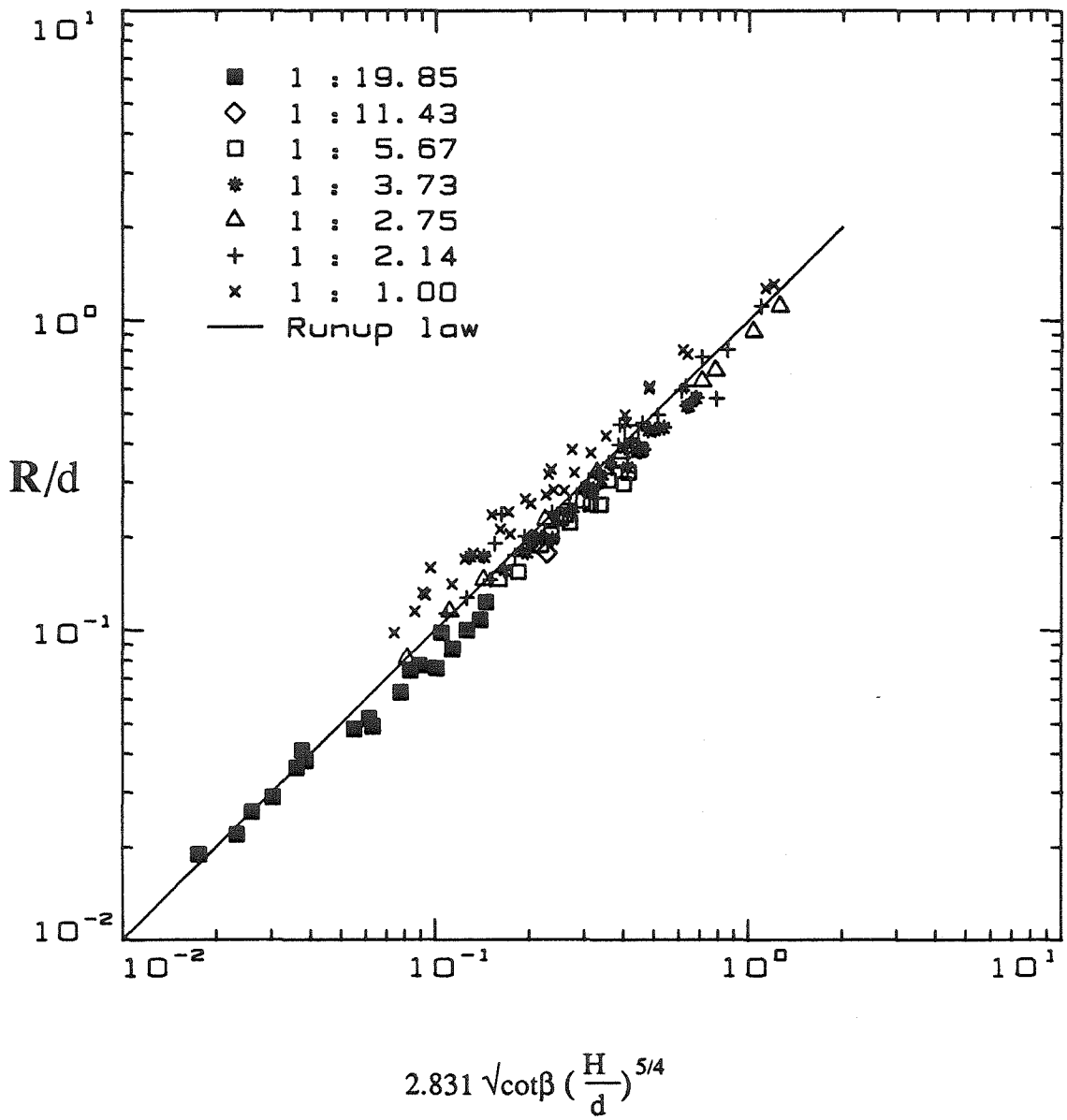

Figure 3.5.2 The maximum runup of nonbreaking waves climbing up different beaches. Comparison between laboratory data from different laboratory investigations. The symbols indicate different beach slopes. The data presented are listed in table T3.2.

wave runup had been overlooked. Kim et al (1983) studied the runup of nonbreaking solitary waves on steep beaches. Their comparison with the data of Hall and Watts (1955) revealed no significant discrepancies because most of the that data for steep slopes refer to nonbreaking waves. In fact, the Hall and Watts data for the 45° angle contain no breaking wave experiments. In the study of Pedersen and Gjevik (1983), the discrepancy of their numerical data for mild slopes from the extrapolated relationships of Hall and Watts is obvious; for mild beaches most of the Hall and Watts data refer to breaking waves. Pedersen and Gjevik reference some other solitary wave experiments which were done in depths of 10 cm (3.93 in), 15 cm (5.09 in), and 25 cm (9.84 in), and they state that their numerical results agree with the 25 cm depth experiments much better than with the 10 cm or the 15 cm depth experiments. They attribute the discrepancy to "*frictional effects (that) become more important in deeper channels* ". It is impossible to comment on this statement, because it has not been possible to obtain the referenced data set. However, it can be hypothesized that their 25 cm depth data set included more nonbreaking wave data than the 10 cm or the 15 cm depth sets, since it is easier to generate nonbreaking waves in the larger depth (25cm) than it is in the shallow depths (10cm). Empirical relationships that include nonbreaking wave data are more likely to agree with numerical simulations than relationships that do not. Table T3.3 lists the data on solitary wave runup derived in the numerical simulations discussed.

3.5.2 Surface profiles. To obtain a better understanding of the validity of the theory described in section 3.4, it is necessary to examine runup profiles in detail and to compare them with the linear and nonlinear models. Two different representations of the data are given : profiles showing the variation with time at fixed locations and profiles showing the variations in space at fixed times.

To derive surface profiles from the *linear* theory solution, equation (3.4.2) can be substituted directly into (3.2.8) and the integral can be evaluated with the contour integration methods presented in section 3.4. Surface profiles for the *nonlinear* theory for given σ,λ are derived explicitly using equations (3.3.1), (3.4.20) and (3.4.21). However, to compare the theory with laboratory data it is neccessary to derive η at specific points in the (x,t) plane, at points where measurements exist. Since the transformation equations define η implicitly in terms of x and t, a numerical scheme is neccessary to derive it explicitly. If one seeks the solution at a particular $x=x$, then one may solve (3.3.1b) with Newton' s method. The iterations take the form:

$$\sigma_{i+1} = \sigma_i - \frac{1}{X_0} \frac{x(\sigma_i) - x}{\sigma/8 - (1/4)\psi_{\lambda\sigma} - (u/\sigma)(\psi_{\sigma\sigma} - u)}, \tag{3.5.3}$$

where the index i refers to the ith iterations. By varying λ in (3.5.3), one obtains complete time histories, albeit not at equispaced intervals. To find the solution for a given t, one may solve (3.3.1c) with the following iteration algorithm :

$$\lambda_{i+1} = \lambda_i + \frac{1}{X_0} \frac{t - t(\lambda_i)}{\psi_{\lambda\sigma}/\sigma - 0.5} \tag{3.5.4}$$

To obtain surface profiles at given times, σ is varied in (3.5.3) from 0 to 4. The iteration schemes involve evaluation of two integrals, $\psi_{\lambda\sigma}$, $\psi_{\sigma\sigma}$, in addition to ψ_λ and ψ_σ which are always needed to calculate the solution at arbitrary x,t. This imposes no further computational complexity, because these quantities are monitored routinely for the calculating the Jacobian of the transformation. The iterations converged rapidly and with little computational effort, usually in less than 10 steps.

In general, when evaluating any of the integrals $\psi_{\lambda\sigma}$, $\psi_{\sigma\sigma}$, ψ_{λ} or ψ_{σ} numerically, care should be exercised because the Bessel functions in the integrands vary rapidly. The argument of the functions is $2X_0\kappa$, and therefore for any given slope $1{:}X_0$ the optimal integration range should be determined to ensure convergence with the least number of steps. This is done easily, either by comparing preliminary integration results with the corresponding series expansion of the form of (3.4.17) or by using standard methods. In this study, the Symbolic Manipulator Program (1983) was used to verify series and integral evaluations. (It was not possible to derive the result (3.4.16) analytically using the SMP.) When numerical evaluation of integrals was performed for the solitary wave with H/d=0.0185, and when X_0=19.85, the integration step $d\kappa$ was set equal to 0.004, the range of κ was [-1.6,1.6], and the number of panels was 800.

Figures (3.5.3a) through (3.5.3f) show the comparison of the linear solution (3.2.8) with the nonlinear theory solution derived from (3.3.5) and with laboratory data for a solitary wave of H/d = 0.0185. The profiles are plotted as a function of the dimensionless time at different locations away from the initial position of the shoreline. For x=19.85, 15.71, 9.95, and 5.10, there is no significant difference among the three profiles. However, closer to the shoreline, at x=0.25 and x= 0.74, the nonlinear effects become important and the linear theory greatly overestimates the wave profile. It is also apparent that dissipation attenuates the wave height close to the shoreline. An interesting feature of these surface profiles is their behavior during the time interval from approximately t=125 to t=138, where there is no data displayed. This is the time of the backwash, or rundown of the wave; the shoreline retreats beyond the particular measurement location, and there is no flow depth to be measured. The shoreline then returns but does not stop moving at its initial position; it continues its motion and behaves as an underdamped oscillator. This is a characteristic phenomenon of the runup process and was observed in all the waves studied.

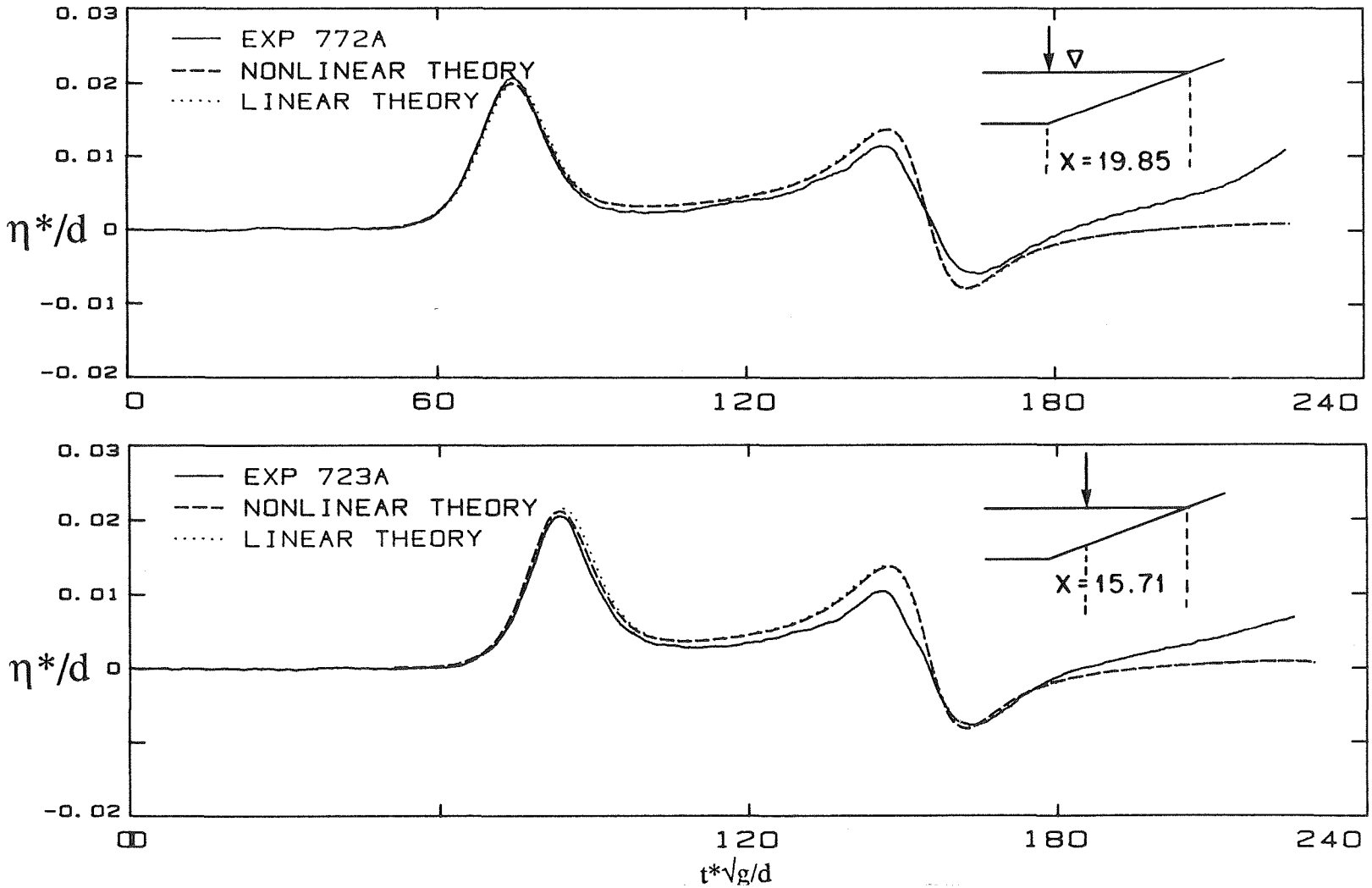

Figure 3.5.3ab Comparison between laboratory data, the linear theory model and the nonlinear theory model for a 0.0185 solitary wave climbing up a 1:19.85 beach at x=19.85 (a) and x=15.71 (b).

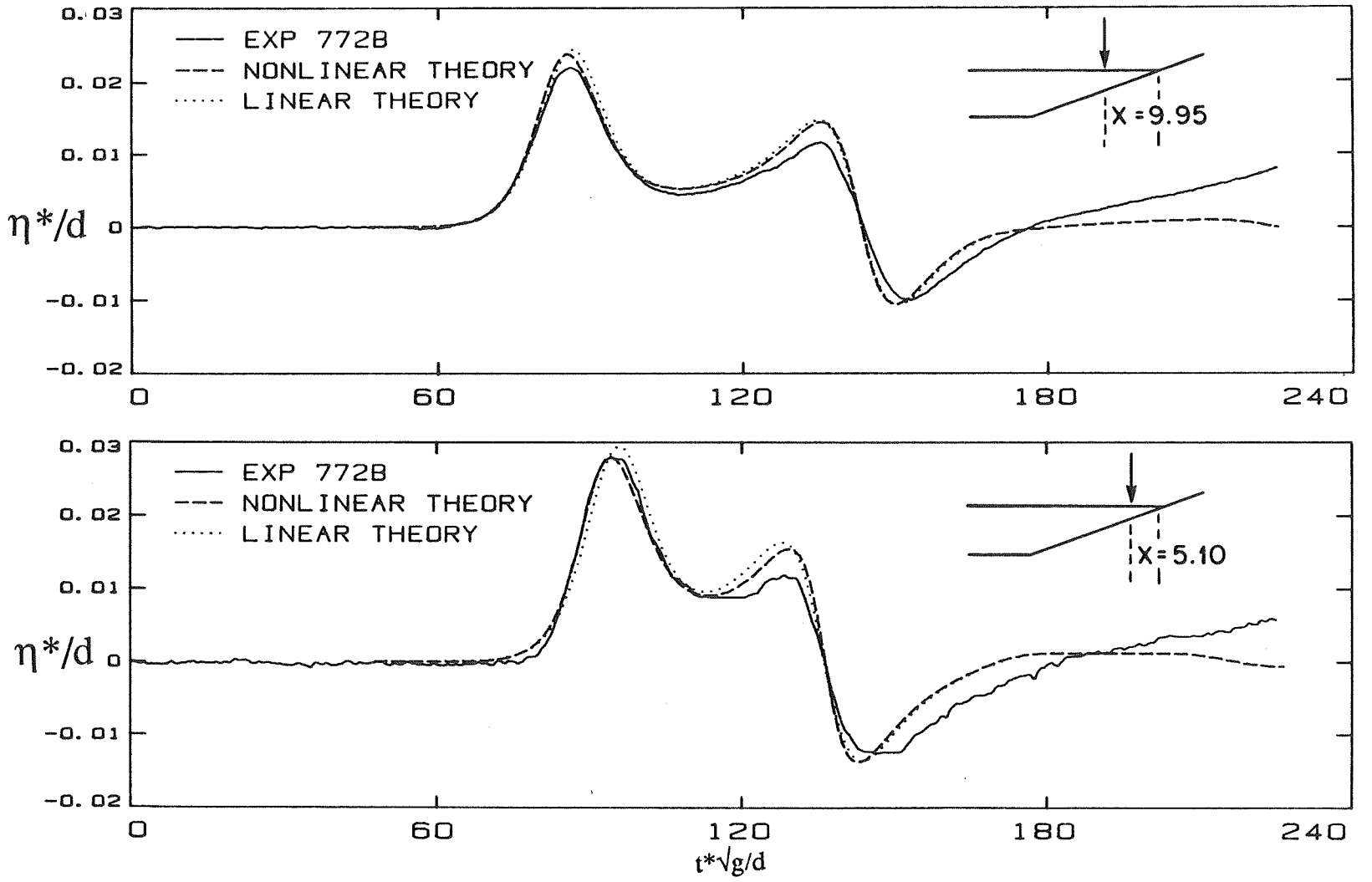

Figure 3.5.3cd Comparison between laboratory data, the linear theory model and the nonlinear theory model for a 0.0185 solitary wave climbing up a 1:19.85 beach at x=9.95 (c), x=5.10 (d).

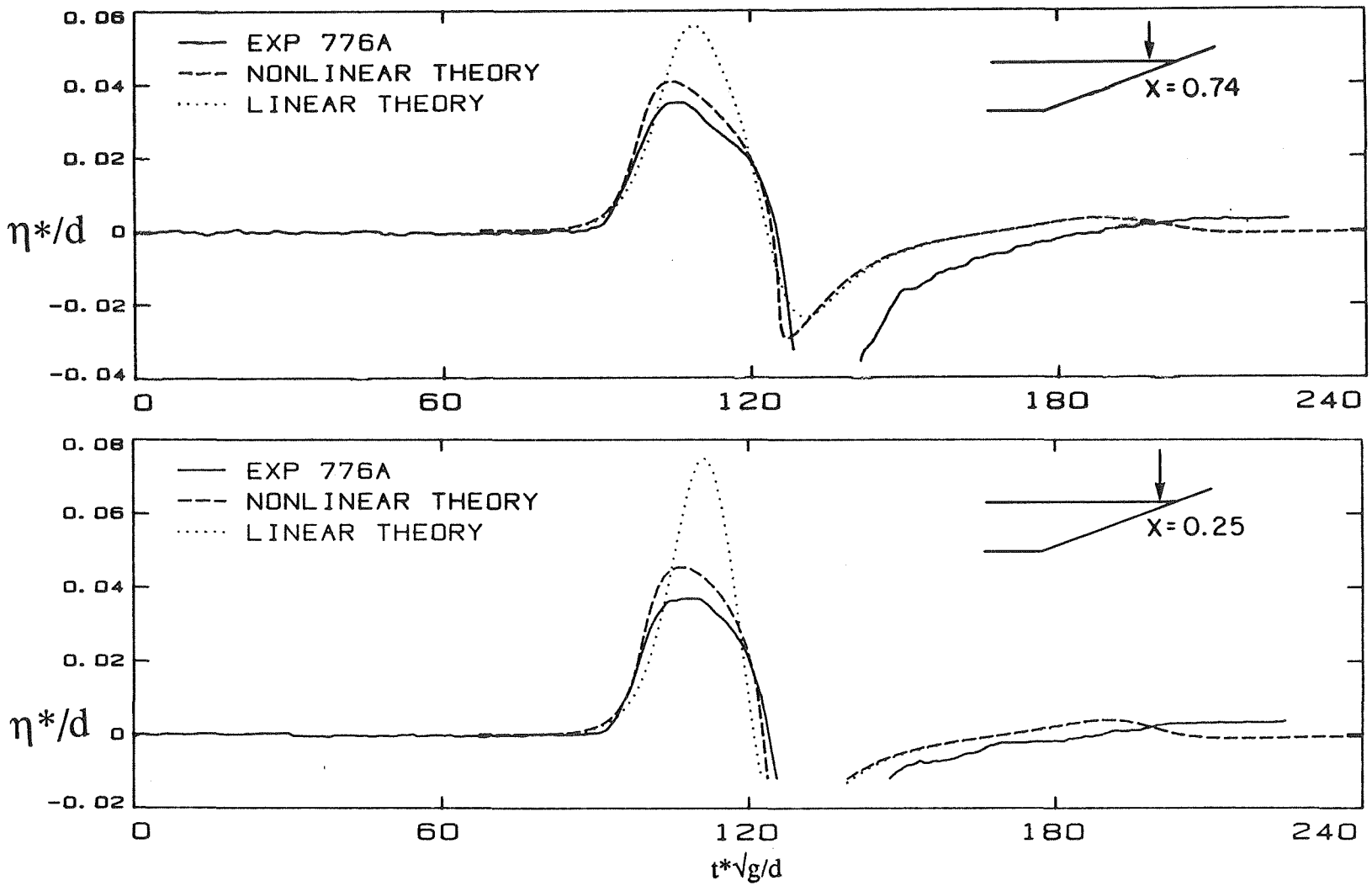

Figure 3.5.3ef Comparison between laboratory data, the linear theory model and the nonlinear theory model for a 0.0185 solitary wave climbing up a 1:19.85 beach at x=0.74 (e), x=0.25 (f).

The data in figure (3.5.3) confirm Carrier's hypothesis. Carrier (1966) hypothesized that far from the shoreline nonlinear effects are small, so that the linear form of the transformation equations can be used. This implies that the term $u^2/2$ can be neglected in (3.3.1b) and (3.3.1d) when $x=X_0$. This is indeed an excellent approximation as can be seen in figures (3.5.3a) through (3.5.3d). It does not limit the application of the theory to "linear" waves. As it can be seen in figure (3.5.2), it predicts reasonable maximum runup values even on the 1:1 slope for waves up to H/d=0.5, waves which are highly "nonlinear".

Figure (3.5.4) is a different representation of the same H/d=0.0185 solitary wave as the wave in figure (3.5.3). It shows the wave at different instants as it climbs up the beach. These profiles shown can be visualised as being 'photographs' of the free surface. Different symbols in the figure identify different realizations of the same wave at different depths. This display is also intented to give a measure of the overall experimental errors associated with this study. The profiles are compared with the nonlinear theory, as derived from (3.3.5) using $\Phi(k)$ from (3.4.2). The nonlinear theory appears to predict the details of the climb of the wave on the beach relatively well. Near the shoreline tip the theory overestimates the wave height, as expected ; viscous effects are more important in this region of the flow.

Figure (3.5.4) contains data from many realizations of the H/d=0.0185 wave. However, when the wave was generated in the laboratory at different depths, the actual H/d ratio $(H/d)_{actual}$ ranged from 0.0177 to 0.0209. To perform the comparison with the theoretical profile, the experimental data were scaled by multiplying with a factor equal to $0.0185/(H/d)_{actual}$. This variation may be due to random experimental error and due to the response of the hydraulic system. If all experiments were run at the same depth, then there would be much less variation in the H/d ratio of the generated wave ; this was not possible due to miscellaneous water leaks around the wave tank.

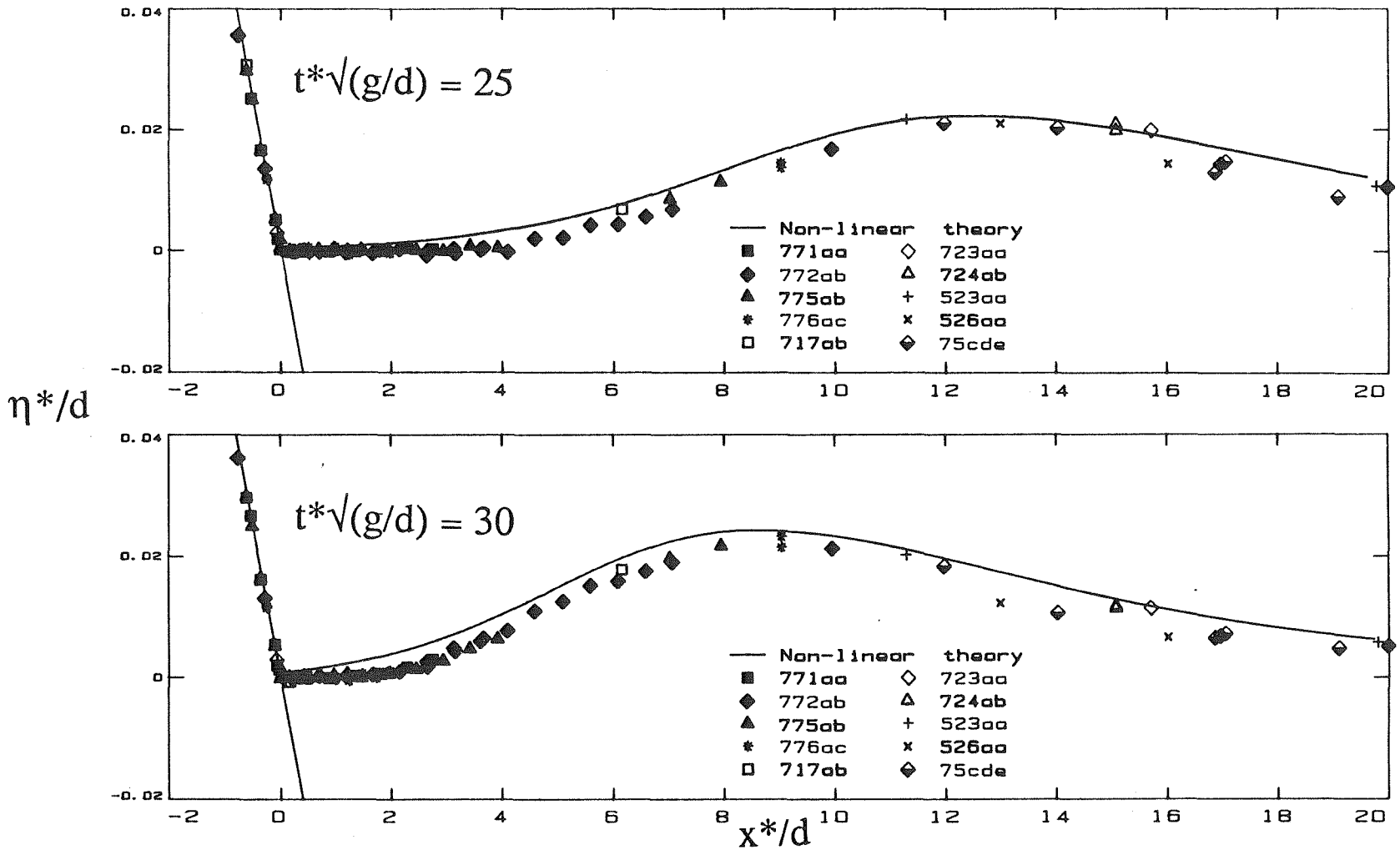

Figure 3.5.4ab Comparison between laboratory data and the nonlinear model for a 0.0185 solitary wave up a 1:19.85 beach. Profiles are shown as functions of x at t = 25 (a) and at t = 30 (b). Different symbols indicate different realizations of the same experiment.

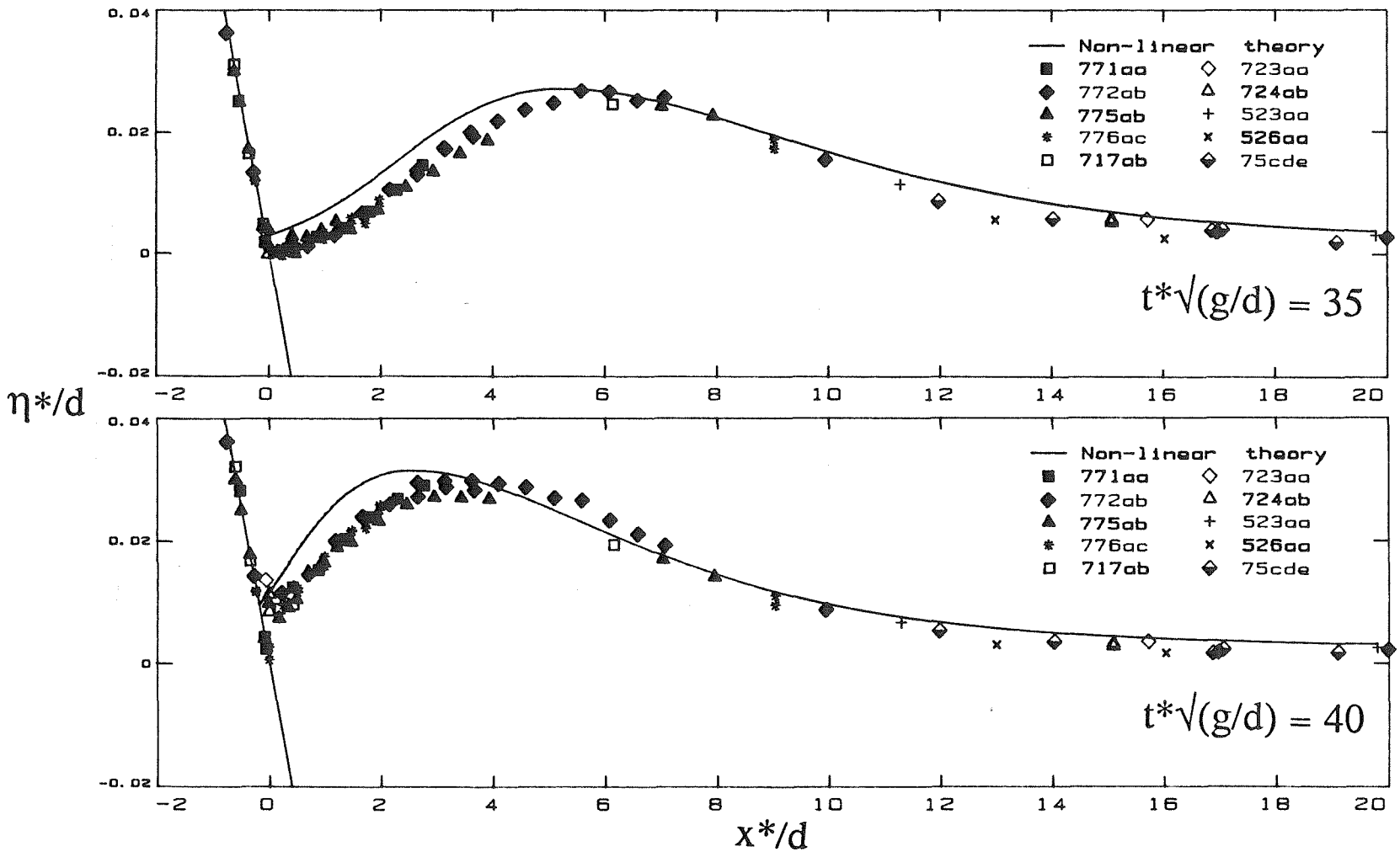

Figure 3.5.4cd Comparison between laboratory data and the nonlinear model for a 0.0185 solitary wave up a 1:19.85 beach. Profiles are shown as functions of x at t = 35 (c) and at t = 40 (d). Different symbols indicate different realizations of the same experiment.

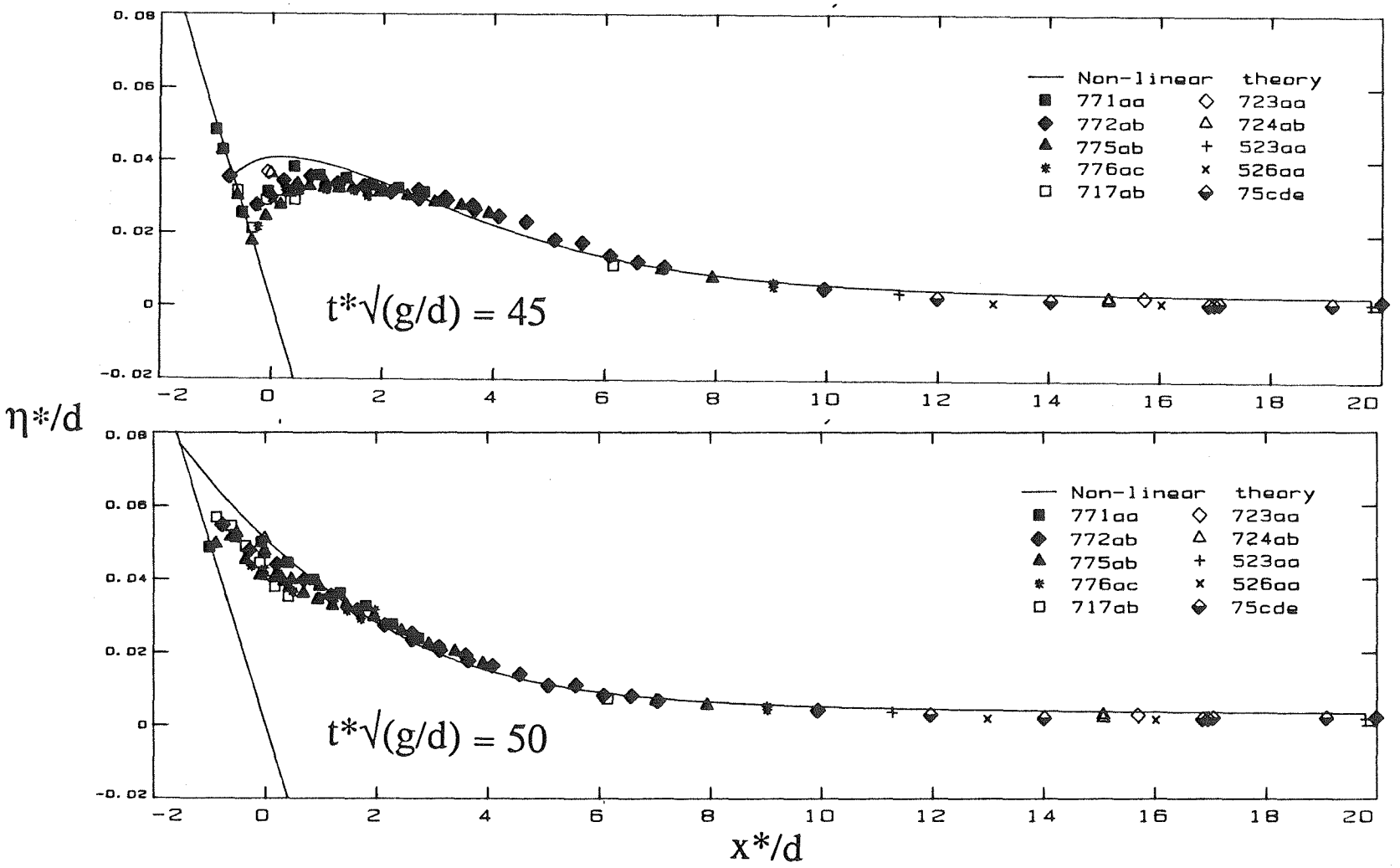

Figure 3.5.4ef Comparison between laboratory data and the nonlinear model for a 0.0185 solitary wave up a 1:19.85 beach. Profiles are shown as functions of x at t = 45 (e) and at t = 50 (f). Different symbols indicate different realizations of the same experiment.

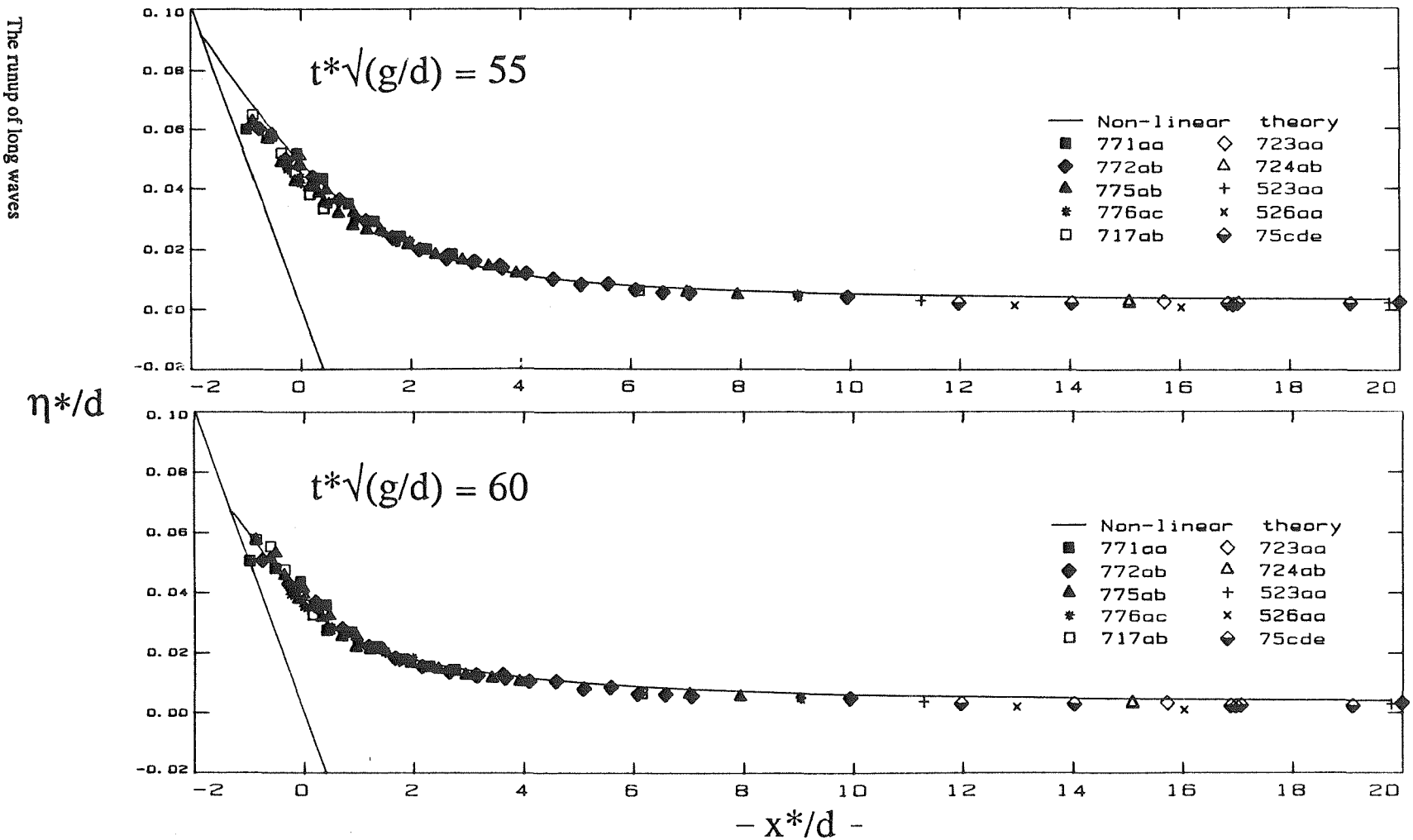

Figure 3.5.4gh Comparison between laboratory data and the nonlinear model for a 0.0185 solitary wave up a 1:19.85 beach. Profiles are shown as functions of x at t = 55 (g) and at t = 60 (h). Different symbols indicate different realizations of the same experiment.

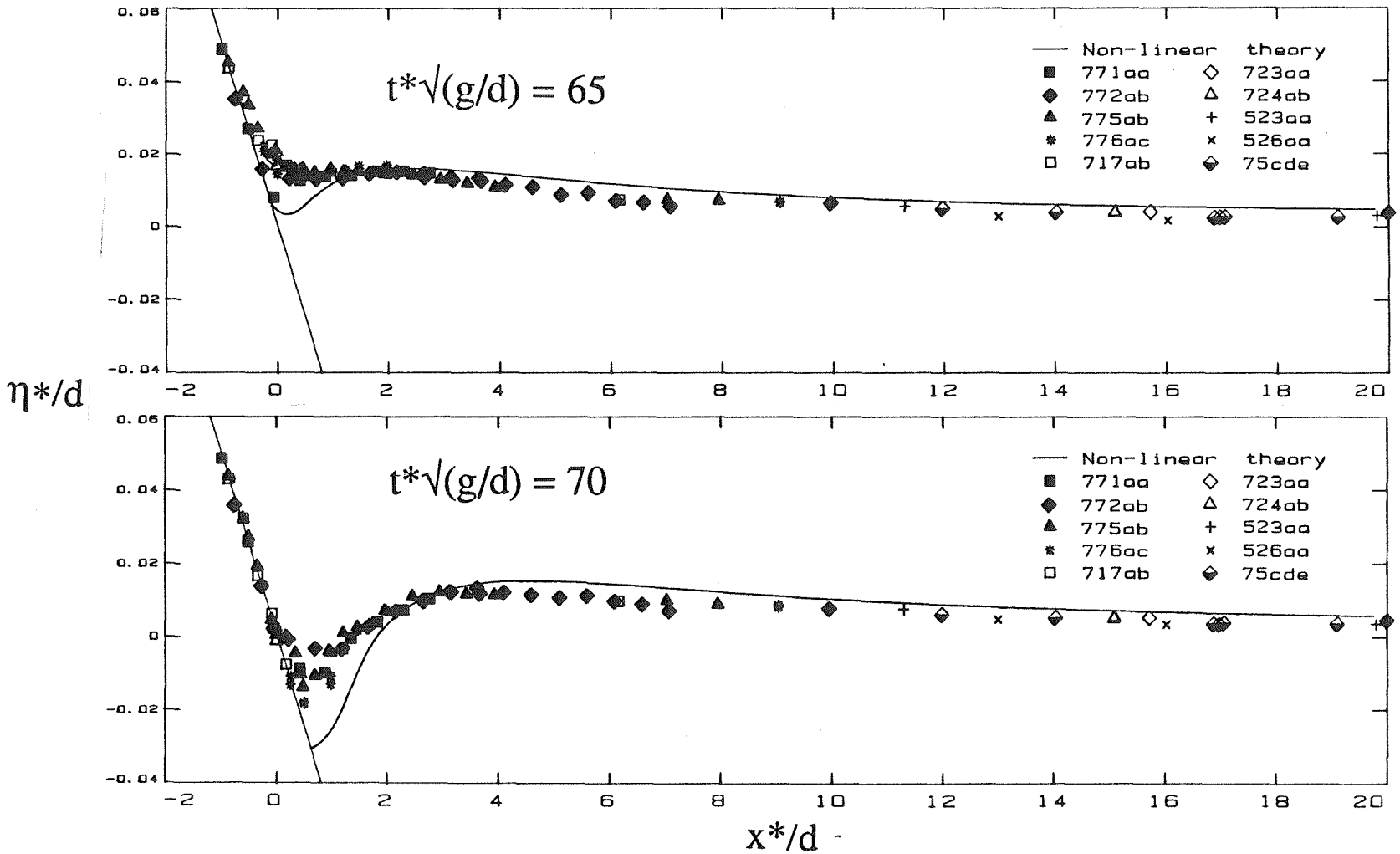

Figure 3.5.4ij Comparison between laboratory data and the nonlinear model for a 0.0185 solitary wave up a 1:19.85 beach. Profiles are shown as functions of x at t = 65 (i) and at t = 70 (j). Different symbols indicate different realizations of the same experiment.

One problem encountered when comparing surface profiles obtained in the laboratory at different depths is time synchronization; waves arrive at the measurement location x_n at different times and the resulting time series cannot be superposed, unless the time origin is shifted. One standard method to synhcronize an ensemble of wave profiles at some reference location x_n, is to transform each wave profile from $\eta_i(x_n,t)$ to $\eta_i(x_n,t+\Delta t_{ni})$, where Δt_{ni} is the difference between the times the crest of the ith wave and that of the reference wave pass through x_n. However, this technique may obscure variations due to local changes in the phase speed. To obtain one single Δt_i for all locations of every run i, a different practice was adopted. The profiles were shifted from $\eta_i(x_n,t)$ to $\eta_i(x_n,t+\Delta t_i)$, where Δt_i is the interval between the time the plate starts moving to generate the ith wave and the time the wave crest passes through $x=X_1$. X_1 is the location where the wave is measured to determine its H/d ratio and is given by $X_1=X_0+L/2$, where L is defined by (3.5.1) By the definition of the boundary condition (3.4.1a) in the theoretical development, t=0 when the wave crest passes through $x=X_1$. This technique simply shifts the time origin of each run so that it corresponds to t=0 in the definition of the solitary wave (3.4.1a).

3.5.3 The wavefront path and the evolution of the tail. The wavefront path is the locus of the points (x_w, t_w), where t_w is the time when the front of the wave passes through x_w. The path over the sloping beach is shown in figure (3.5.5) as a trajectory in the (x,t) space, and the data is compared with the predictions of the nonlinear theory. Away from the shoreline, the wave is seen to propagate slower in the laboratory than in the theoretical development. When the wavefront reaches the initial shoreline position, the velocity of the front decreases dramatically and the theory appears to predict the shoreline path well.

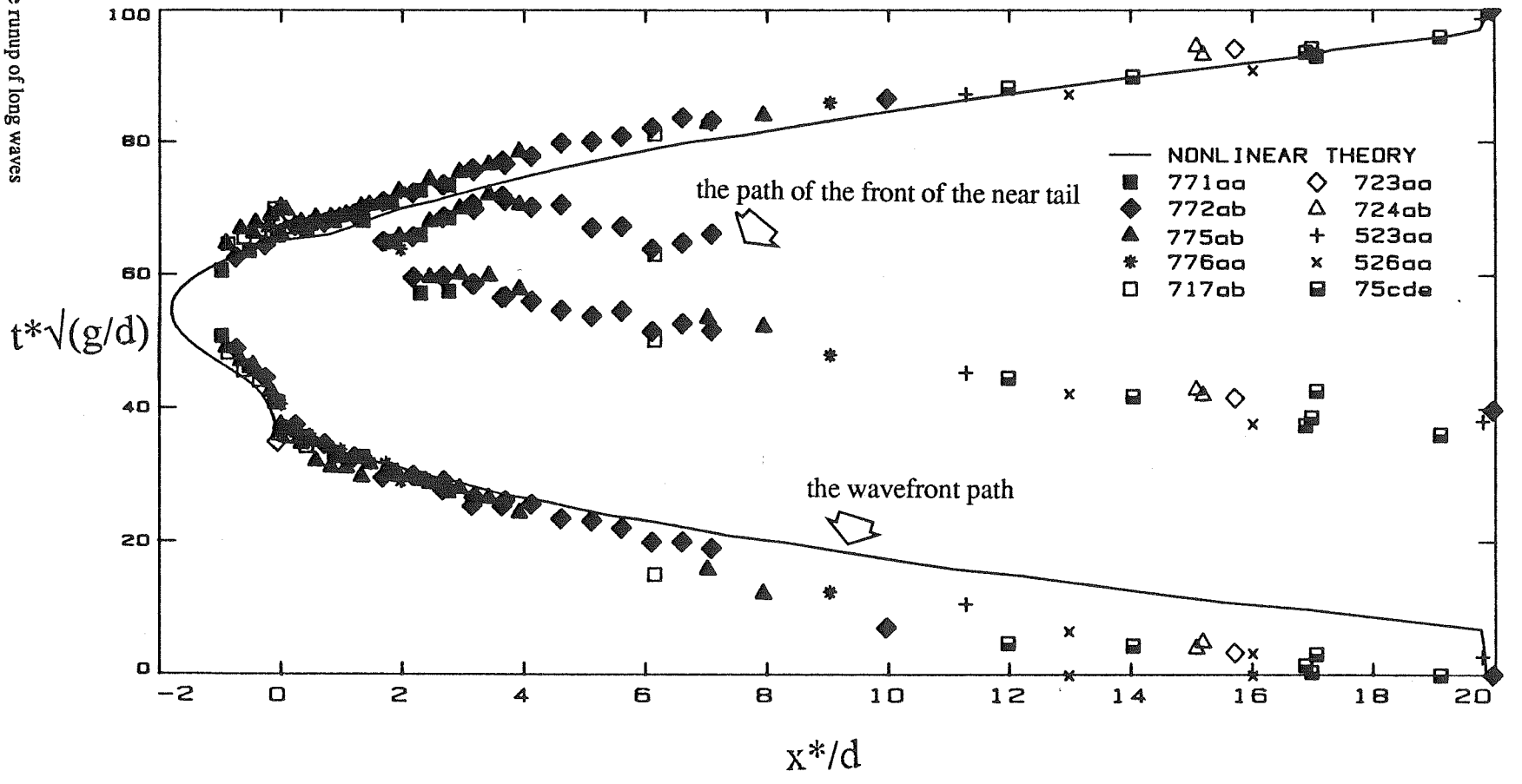

Figure 3.5.5 The path of the wavefront and of the tail of a 0.0185 solitary wave up a 1:19.85 beach. Comparison between the nonlinear model and experiments. Different symbols indicate different realizations of the same experiment.

Figure (3.5.5) also includes data for the tail of the wave. This appears to be the first observation of the evolution of a solitary wave tail in the laboratory. The development of a tail behind a solitary wave propagating over slowly varying topography has been noted in the solution of KdV-type equations by Ablowitz (1971), Johnson (1973) and Ko and Kuehl (1978). The soliton tail generated a lot of interest when Miles (1979) pointed out that, while these solutions conserve the KdV mass, they do not conserve the actual mass; he suggested that a reflected wave be added to the solution to account for the mass deficit. Smyth (1984) observed that, since the KdV equation is restricted in motion in one direction, to study the question of whether a reflected wave exists, the Boussinesq equations must be used to allow motion in both directions. He demonstrated how part of the mass that Miles added to the reflected wave can be accounted for by higher order corrections to the tail expansions.

Figure (3.5.5) shows the path of the beginning of the near tail of the wave and the formation of a " shelf " region separating the incident from the reflected wave. (The term *near tail* is used to distinguish it from the *far tail* ; the latter refers to a group of small oscillatory waves sometimes trailing a solitary wave. In these experiments no far tail was observed to form.) To visualise the near tail one should refer to figure (3.5.6). The figure shows the surface elevation time histories at different locations as the wave climbs up on the beach, as realized in the laboratory. The profiles at x=5.10 and at x=2.76 indicate the formation of a shelf.

An interesting phenomenon is evident in figure (3.5.5). Although the t-wavelength of the incident wave does not change considerably as the wave climbs up the beach, the x-wavelength does. (The t-wavelength is a measure of the duration of the wave at a particular x, i.e., the period. The x-wavelength is a measure of the horizontal extent of the wave at a given t.) This observation is contradictory to the standard practice in asymptotic

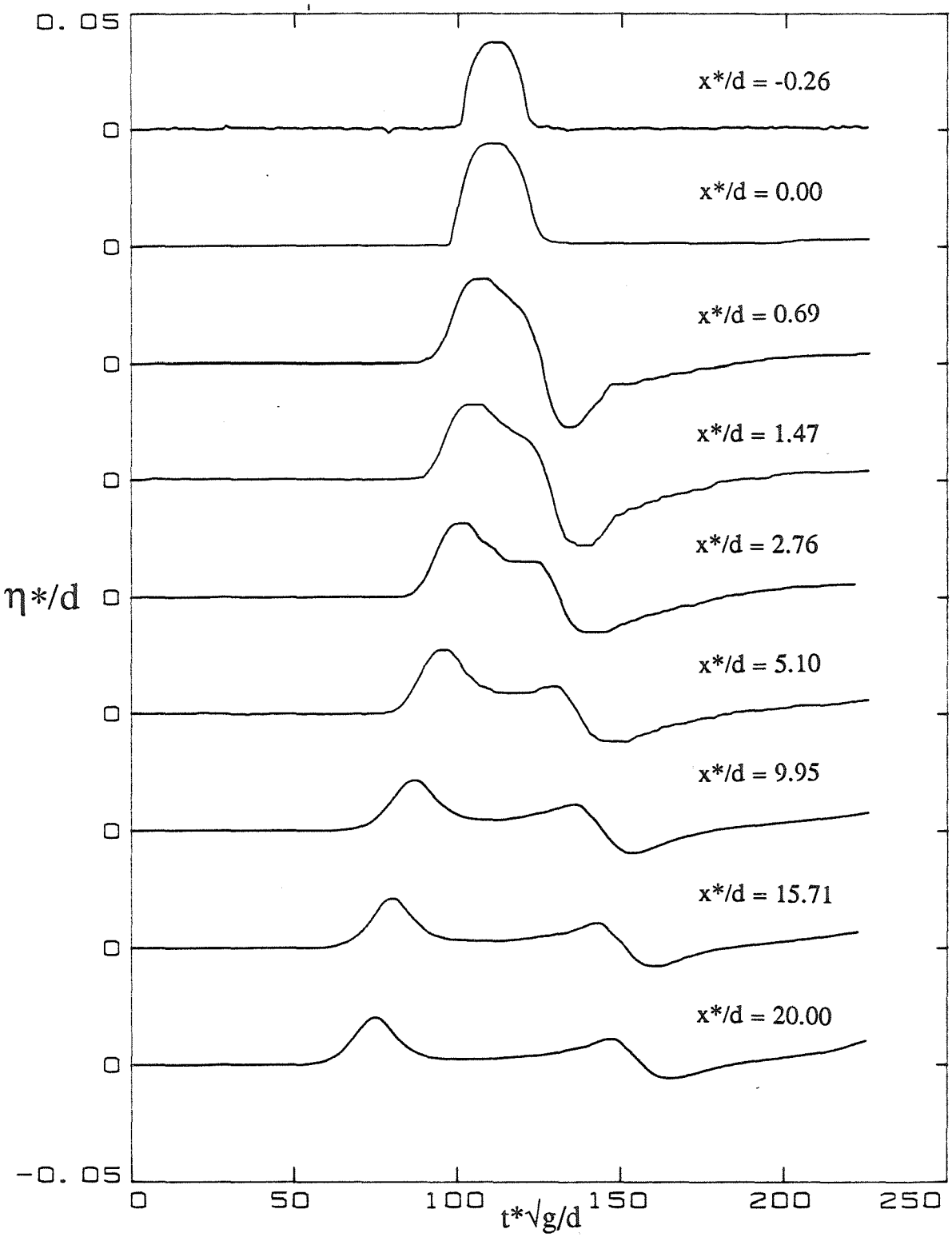

Figure 3.5.6 The climb of a 0.0185 wave up a 1:19.85 beach as realized in the laboratory. Profiles are shown as functions of $t=t^*\sqrt{g/d}$ for different $x=x^*/d$.

models which is to assume that the waveform does not change substantially when a wave propagates over slowly varying bottom, and to use the Boussinesq (3.4.1) or an equivalent profile valid at constant depth to describe the wave over a sloping beach. For the 0.0185 wave climbing up a 1:19.85 beach, this assumption seems reasonable only for the t-description of the wave. However, this is *not* a typical example of a solitary wave over a slowly varying bottom, and caution should be exercised in any attempt to generalise this result.

3.6 Validity of the solution The solution described in section 3.4 is valid for functions $\Phi(k)$ such that the Jacobian of the transformation (3.3.1) is never zero. The Jacobian becomes zero when the surface slope $\partial\eta/\partial x$ in the (x,t) plane becomes infinite. Physically, this point is usually interpreted as the point of wave breaking. In this section a relationship will be derived to determine the limiting H/d for solitary waves climbing up a plane beach of slope $1{:}X_0$ without breaking.

The Jacobian of the Carrier and Greenspan transformation is given by $J = (t_\sigma^2 - t_\lambda^2)$. Since it is anticipated that the tranformation becomes singular close to the shoreline, the Jacobian is expanded around $\sigma = 0$. Substituting (3.3.1c) in the Jacobian and taking the limit as $\sigma \to 0$, then $J = (u_\lambda - 1/2)^2$. When u is given by (3.4.21), then the Jacobian is always regular when :

$$u_\lambda - \frac{1}{2} = \frac{2}{3} X_0 \int_0^\infty \frac{\kappa^3 \operatorname{cosech}\alpha\kappa \, e^{-i\kappa\theta + i\kappa\lambda X_0/2}}{J_0(2X_0\kappa) - i\, J_1(2X_0\kappa)} \, d\kappa - \frac{1}{2} < 0 \qquad (3.6.1)$$

The integral can be evaluated with the formalism described in section 3.4, if one replaces the function $z\operatorname{cosech}\alpha z$ in (3.4.4) with $z^3\operatorname{cosech}\alpha z$. It can be verified by inspection that the

radius of convergence of the resulting contour integral is the same as for (3.4.5). For large values of $4X_0\gamma$, the terms of the Laurent series can be replaced by their asymptotic form. Then,

$$u_\lambda = -12\sqrt{(\pi\sqrt{3})}X_0^{5/2}\left(\frac{H}{d}\right)^{9/4}.\sum_{n=1,\infty}(-1)^n n^{7/2}\chi^{-n}, \tag{3.6.2}$$

with $\chi = \exp\{-\sqrt{3}H/d\ (\theta+\lambda X_0/2)\}$. The series attains its maximum value at $\chi=0.636$ and this implies that the Jacobian first becomes zero when :

$$\lambda = \lambda_c \approx \left(\frac{2}{X_0}\right)\left\{\frac{0.453}{\sqrt{3}H/d} - X_1 - X_0\right\} \tag{3.6.3}$$

The limiting H/d ratio for the validity of the theoretical analysis is then given by :

$$H/d = 0.8183\ X_0^{-10/9} \quad . \tag{3.6.4}$$

This is a weaker restriction than that derived by Gjevik and Pedersen (1981),

$$H/d = 0.469\ X_0^{-10/9}. \tag{3.6.5}$$

There are two major differences between the two results :

1) The breaking criterion (3.6.4) indicates when a wave first breaks during the runup process. The Pedersen and Gjevik criterion (3.6.5) indicates when a wave first breaks during the rundown process. Since, as the wave height is increased, waves start breaking first during rundown forming the so called backwash bore, it is expected that a criterion for breaking during rundown will be a stronger criterion than a criterion that determines when

waves break during runup. An equivalent criterion with Pedersen and Gjevik's cannot be derived with the formalism of section 3.4, because the series expansions of the integrals are only valid during runup. [See equation (3.4.5).]

2) The Pedersen and Gjevik result was derived by using the sinusoidal wave profile that best fits the Boussinesq profile. (See section 1.3.2, page 14) Equation (3.6.4) is based on the actual Boussinesq profile (3.4.1).

It is a well documented phenomenon that the shallow water wave formalism predicts wave breaking earlier than it actually happens in nature. It is interesting to examine what the theory predicts for the climb of solitary waves that are slightly larger what (3.6.4) requires. For the slope used in this study, 1:19.85, wave breaking first occurs in the backwash bore when $H/d = 0.017$, while the breaking criterion (3.6.4) predicts that breaking first occurs during runup when $H/d = 0.029$. Consider the climb of a 0.040 wave. Figure (3.6.1) is a sketch of the Jacobian of the transformation as a function of λ as $\sigma \rightarrow 0$. Figure (3.6.2) shows the wave profile realized in the (x,t) plane when the Jacobian first goes through zero, and it indicates the wave curling over as it starts to break. Note, that the laboratory realization of the same wave does not exhibit breaking.

On intuitive grounds, it is expected that beyond λ_{c1} any analytical results in the (x,t) plane will be meaningless. Also, in numerical simulation of the climb of breaking solitary waves, the solution becomes unbounded soon after the slope of the wavefront becomes infinite. It is therefore surprising to discover that the analytical solution recovers and seems to predict the runup at later times satisfactorily. This is demonstrated in figure (3.6.3). The theory models the laboratory data equally well, before and after the breaking point $t \approx 36$. The same phenomenon occurs during the rundown. The Jacobian goes through zero again at λ_{c2}, which corresponds to $t \approx 62$, but the solution recovers at later times.

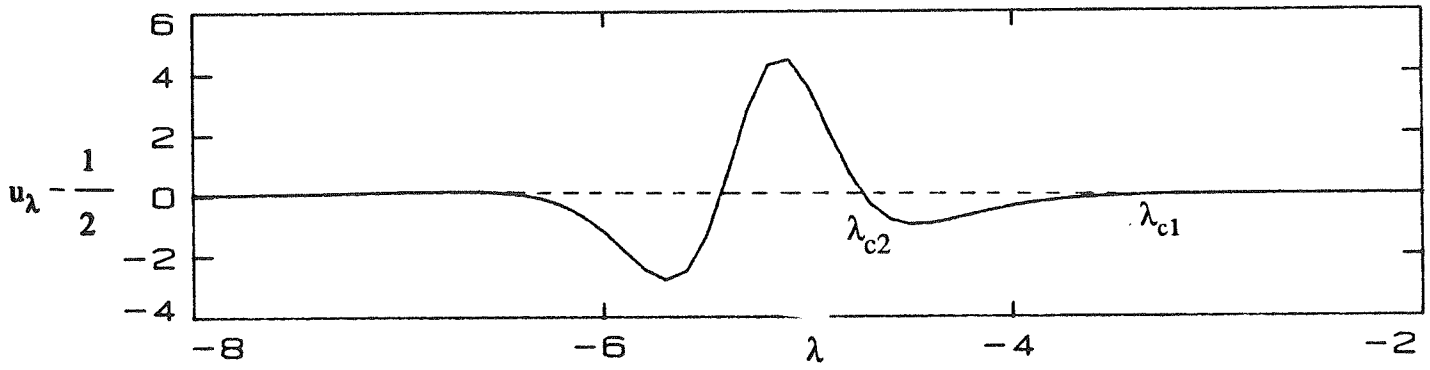

Figure 3.6.1 The Jacobian of the Carrier and Greenspan transformation when H/d=0.040 and $X_0 = 19.85$, expanded around $\sigma = 0$.

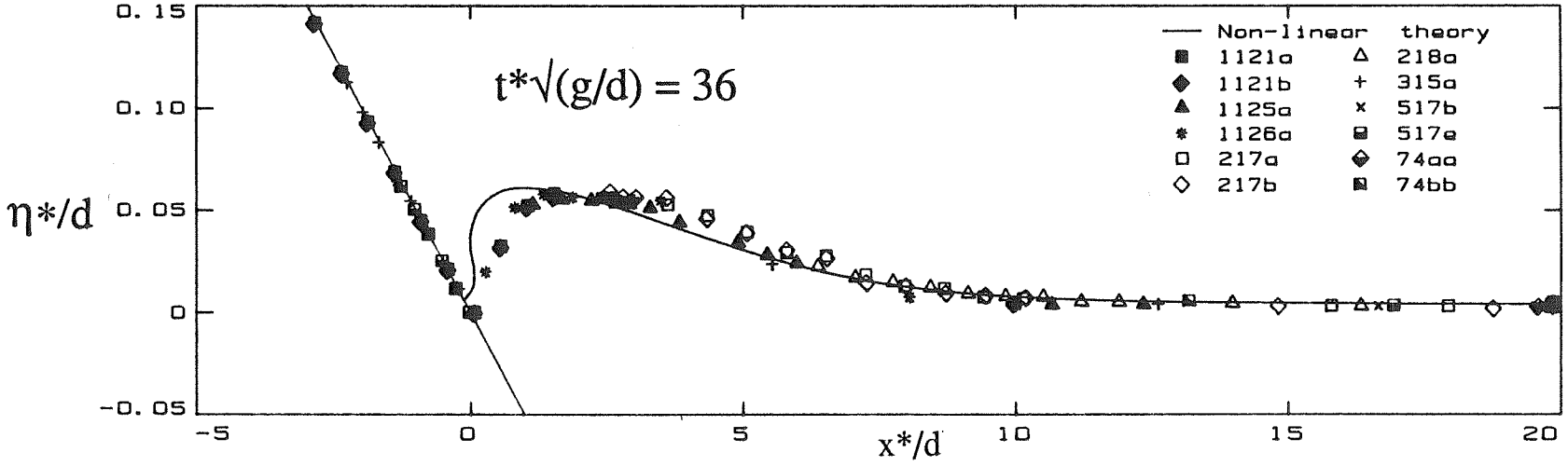

Figure 3.6.2 Comparison between the nonlinear model and laboratory data when the Jacobian becomes singular, for a 0.040 wave up a 1:19.85 beach at t = 36. Different symbols indicate different realizations of the same experiment.

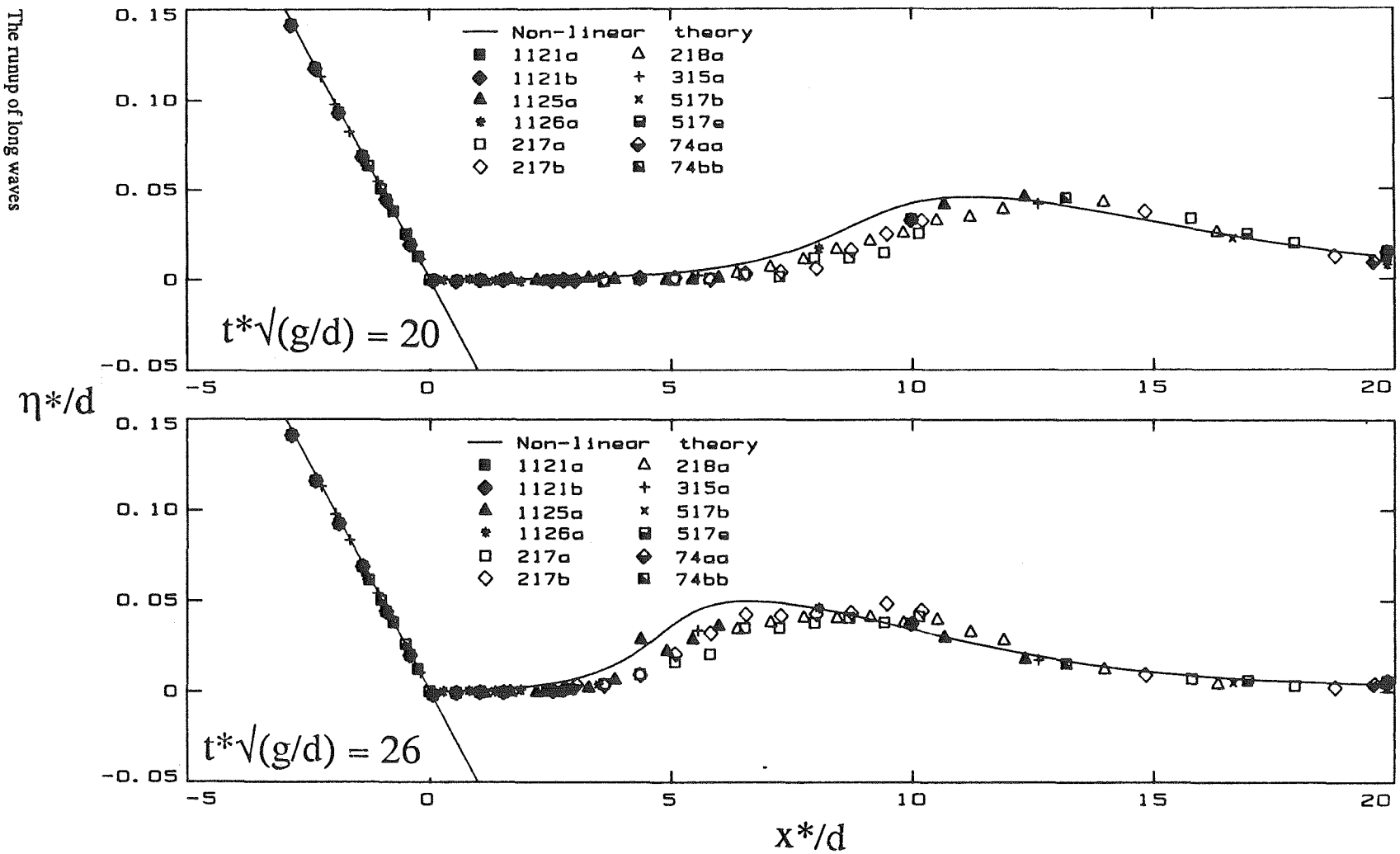

Figure 3.6.3ab Comparison between laboratory data and the nonlinear model for a 0.040 solitary wave up a 1:19.85 beach. Profiles are shown as functions of x at t = 20 (a) and at t = 26 (b). Different symbols indicate different realizations of the same experiment.

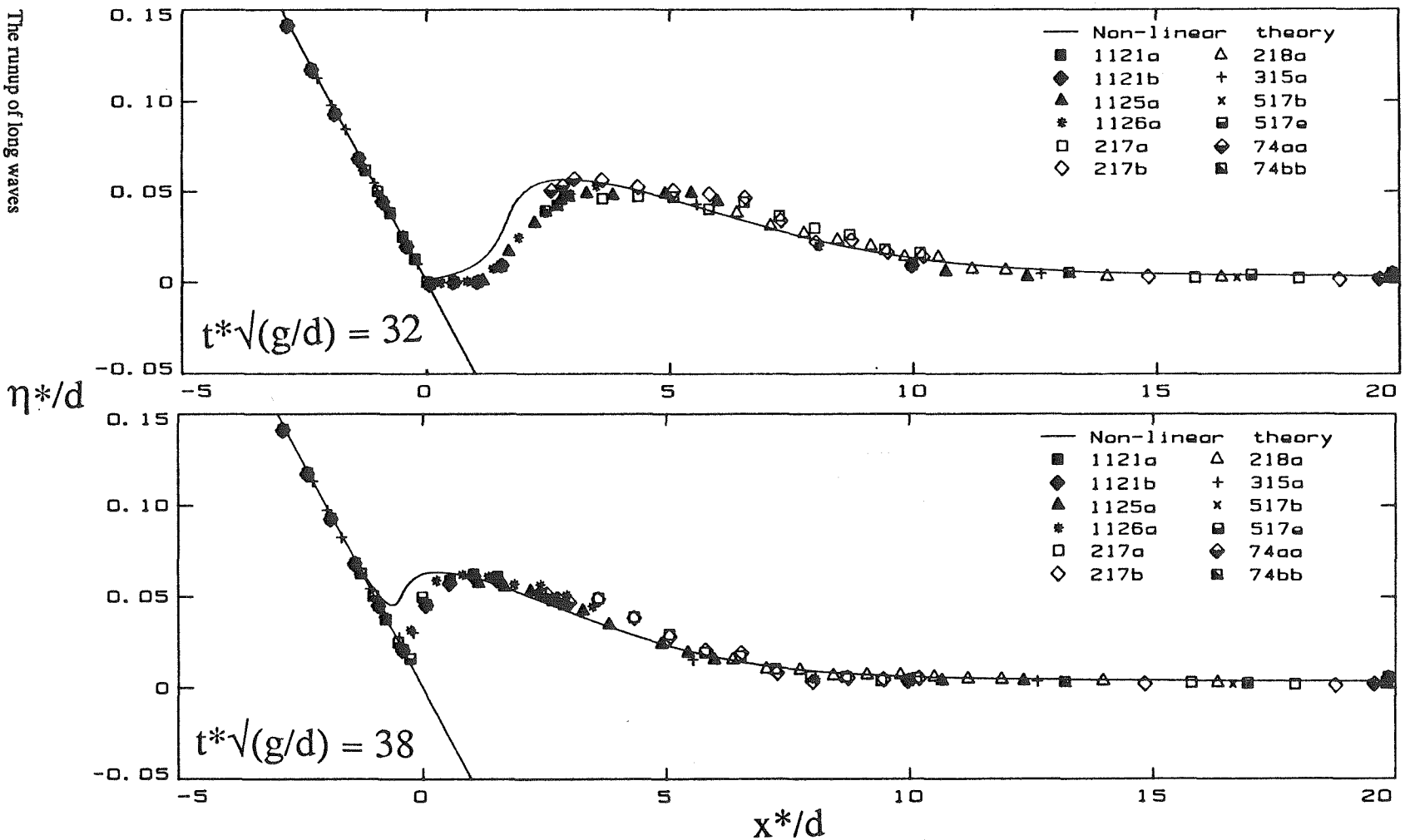

Figure 3.6.3cd Comparison between laboratory data and the nonlinear model for a 0.040 solitary wave up a 1:19.85 beach. Profiles are shown as functions of x at t = 32 (c) and at t = 38 (d). Different symbols indicate different realizations of the same experiment.

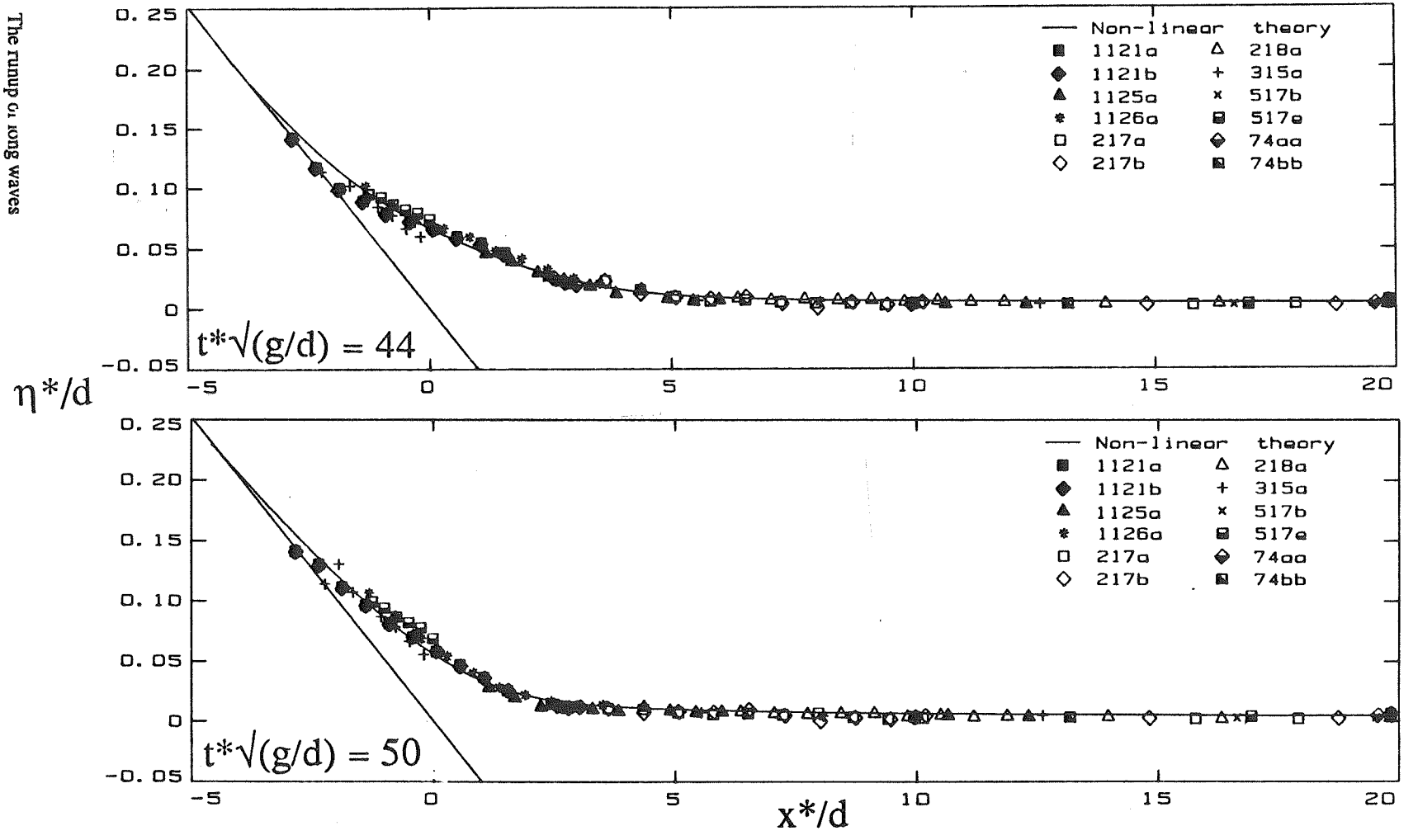

Figure 3.6.3ef Comparison between laboratory data and the nonlinear model for a 0.040 solitary wave up a 1:19.85 beach. Profiles are shown as functions of x at t = 44 (e) and at t = 50 (f). Different symbols indicate different realizations of the same experiment.

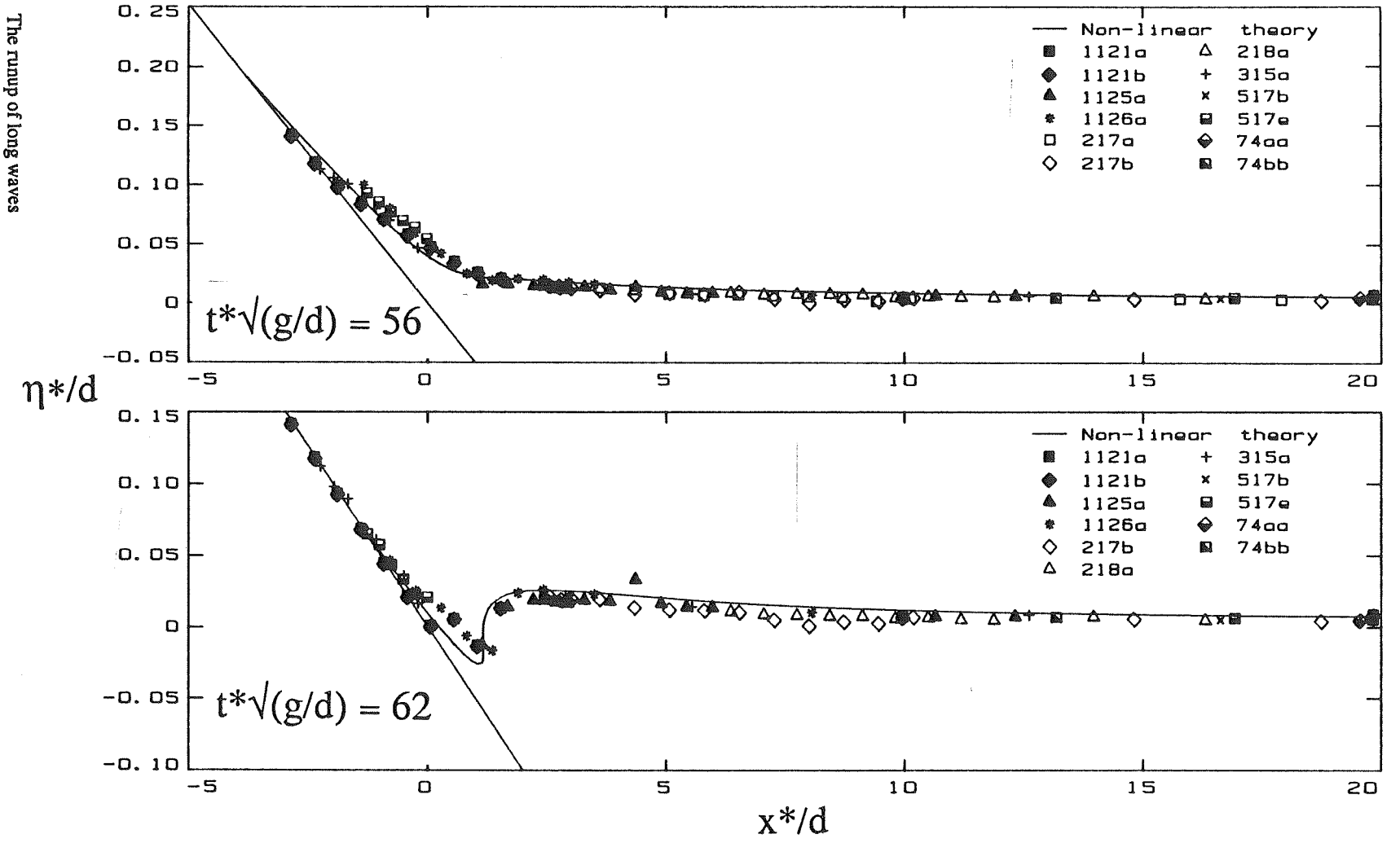

Figure 3.6.3gh Comparison between laboratory data and the nonlinear model for a 0.040 solitary wave up a 1:19.85 beach. Profiles are shown as functions of x at t = 56 (g) and at t = 62 (h). Different symbols indicate different realizations of the same experiment.

To resolve this apparent paradox, one may speculate that although the solution beyond λ_{c1}, for example at $\lambda = \lambda_{c1}+\Delta\lambda$, may not be *the* valid solution to the original boundary value problem, it is *a* valid solution to a new boundary value problem with boundary values specified at $(0, \lambda_{c1}+\Delta\lambda)$. What figure (3.6.3) indicates, is that the solution beyond $(0, \lambda_{c1})$ is relatively insensitive to the actual values at that point, i.e., to the actual shape of the wavefront at the point of breaking. This appears to be another manifestation of the same physical phenomenon that allows for Whitham's bore rule, which postulates that the solution for the problem of the climb of a bore on a beach may be determined by applying the relationships valid at the bore front behind the bore face.

3.7 Surface profiles for breaking solitary waves. The relationship between R/d and H/d is different for breaking and nonbreaking solitary waves, as it is shown in figure (3.5.1). The phenomenology of the climb of breaking wave will be explored in this and the next sections.

Surface profiles as function of x for given times for solitary wave with H/d=0.30 are shown in figure (3.7.1). The time origin is defined in a similar fashion as for nonbreaking waves. Since the experiments included in the figures were performed at different depths, the syncronization of the profiles in figure (3.7.1) was performed as discussed in section 3.5. As can be seen from that figure (3.7.1c) breaking occurs between t=20 and t=25, and is accompanied by a dramatic flattening of the surface profile; this occurs when the wave collapses after plunging. Note the characteristic triangular shape of the wave just before breaking; this shape is often used to depict bores schematically. The maximum runup of the wave is attained between t = 45 and t = 50. At time $t \approx 60$, the wave rushes down the beach and the backwash bore forms.

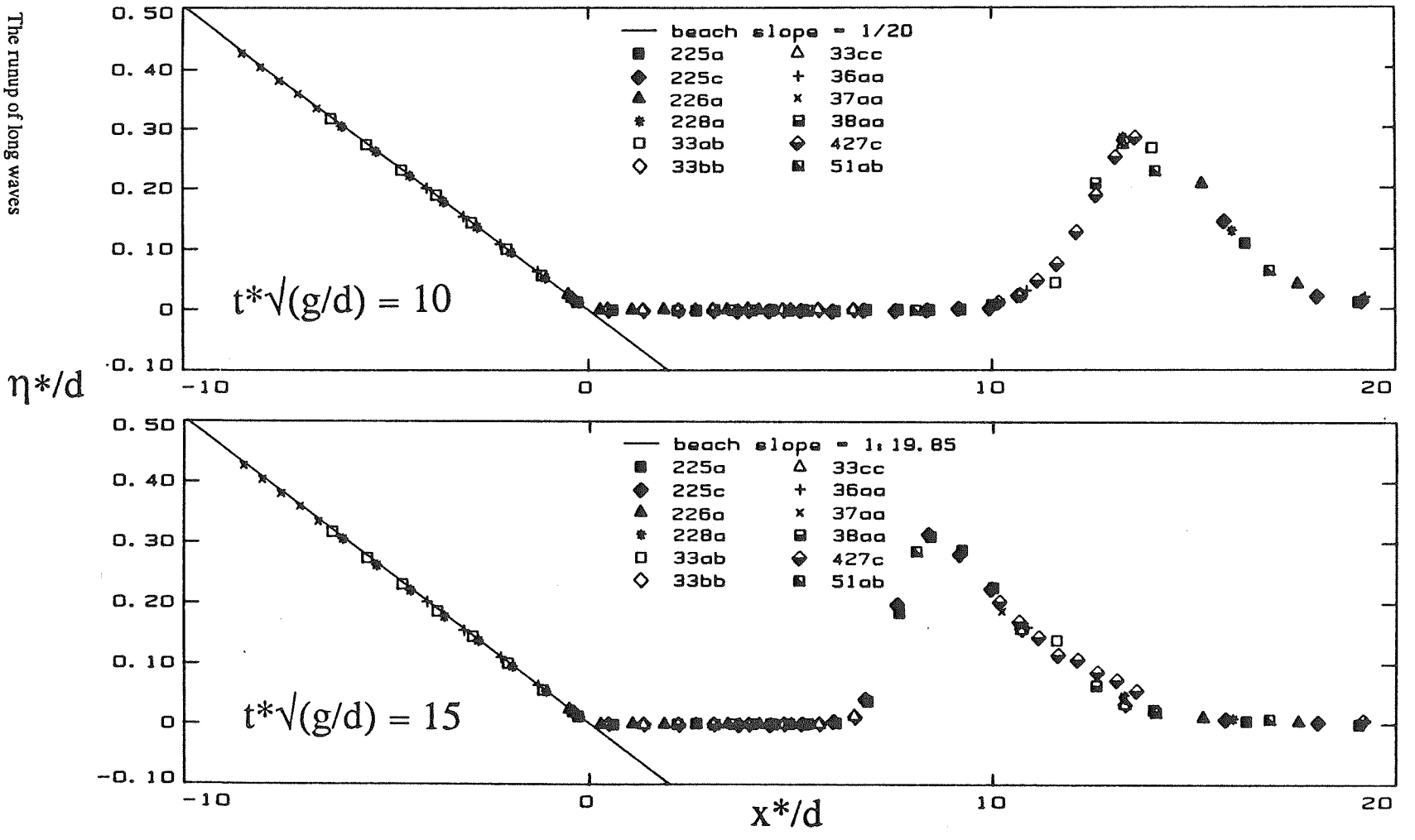

Figure 3.7.1ab Surface profiles of a 0.30 solitary wave up a 1:19.85 beach as a function of x at t = 10 (a) and at t = 15 (b). Laboratory measurements. Different symbols indicate different realizations of the same experiment.

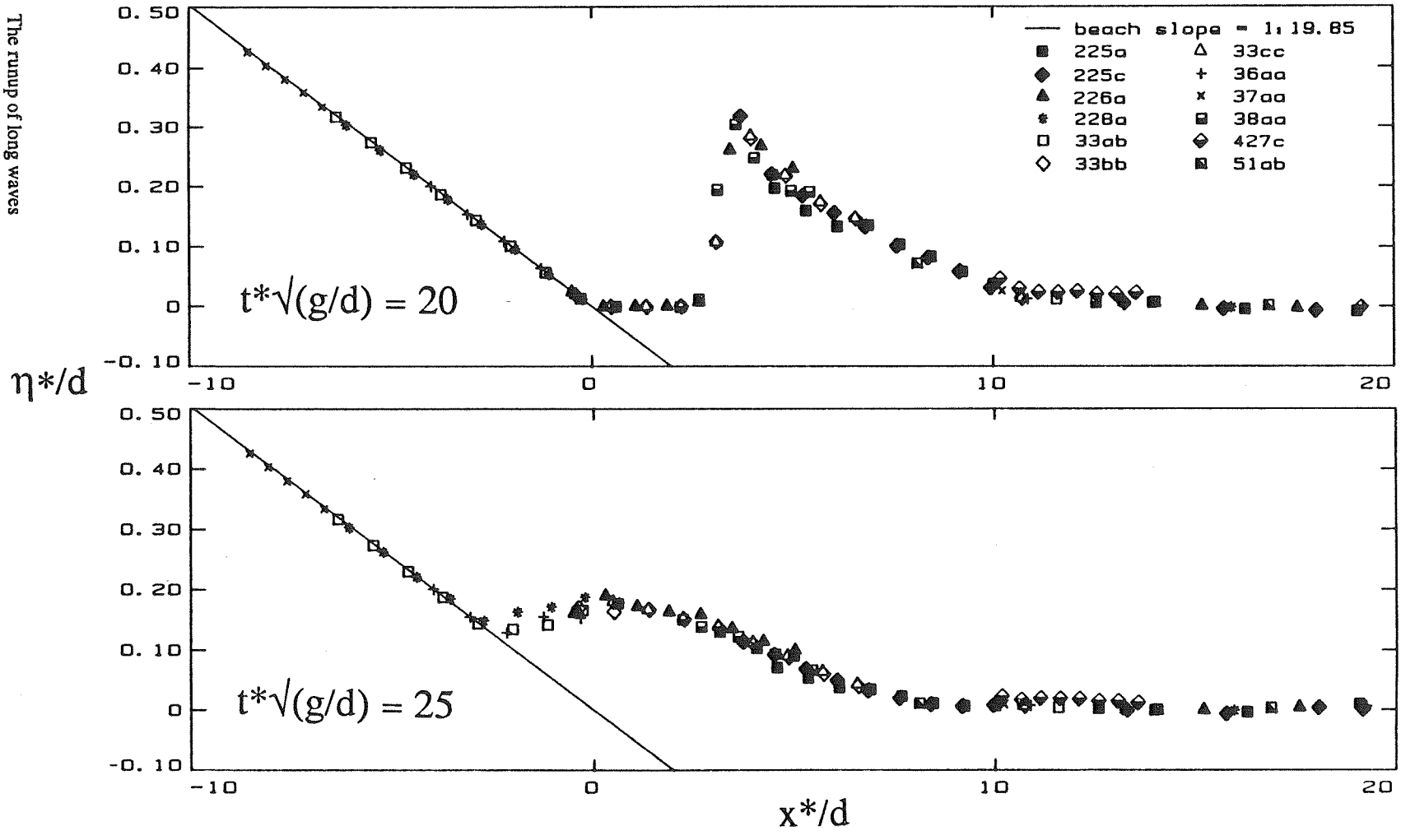

Figure 3.7.1cd Surface profiles of a 0.30 solitary wave up a 1:19.85 beach as a function of x at t = 20 (a) and at t = 25 (b). Laboratory measurements. Different symbols indicate different realizations of the same experiment.

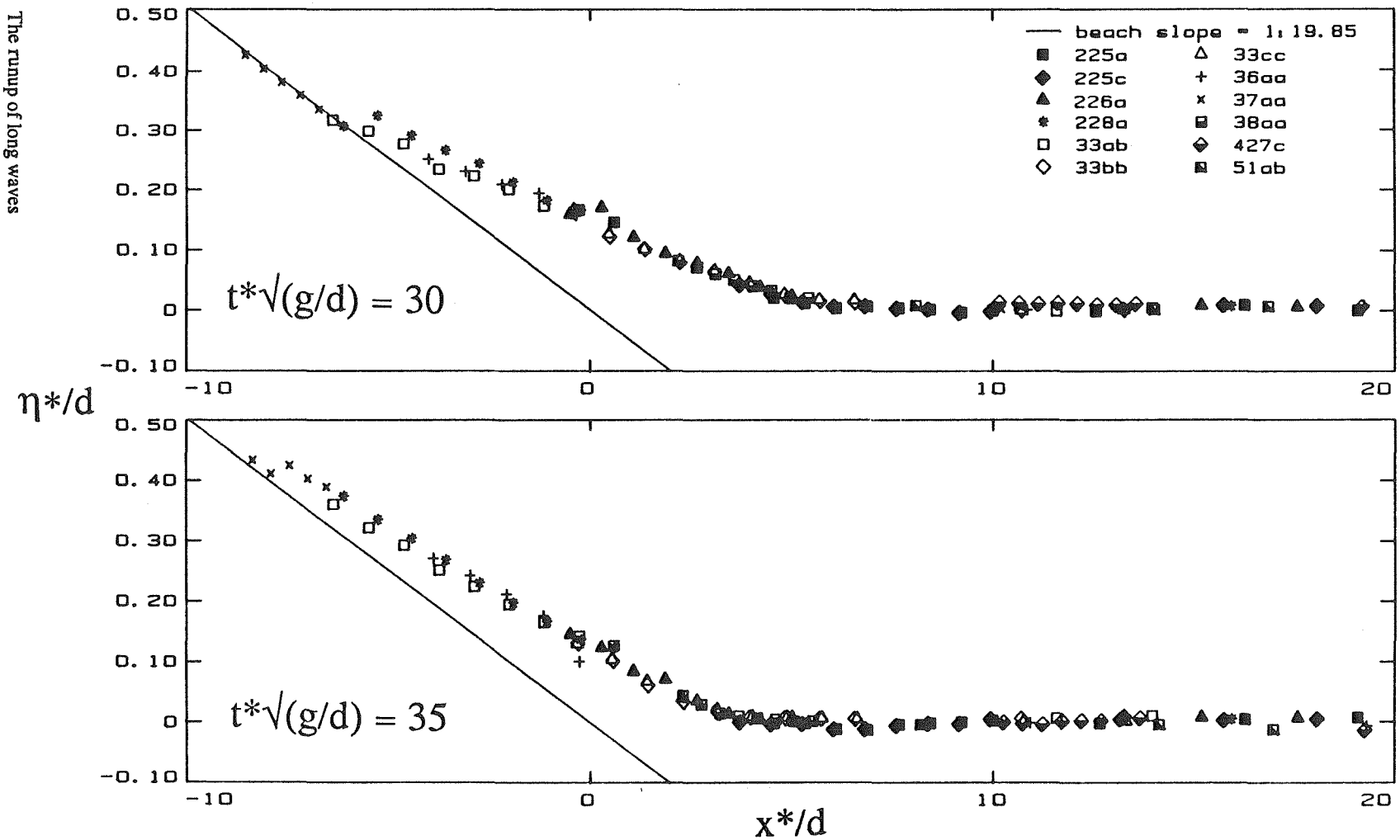

Figure 3.7.1ef Surface profiles of a 0.30 solitary wave up a 1:19.85 beach as a function of x at t = 30 (e) and at t = 35 (f). Laboratory measurements. Different symbols indicate different realizations of the same experiment.

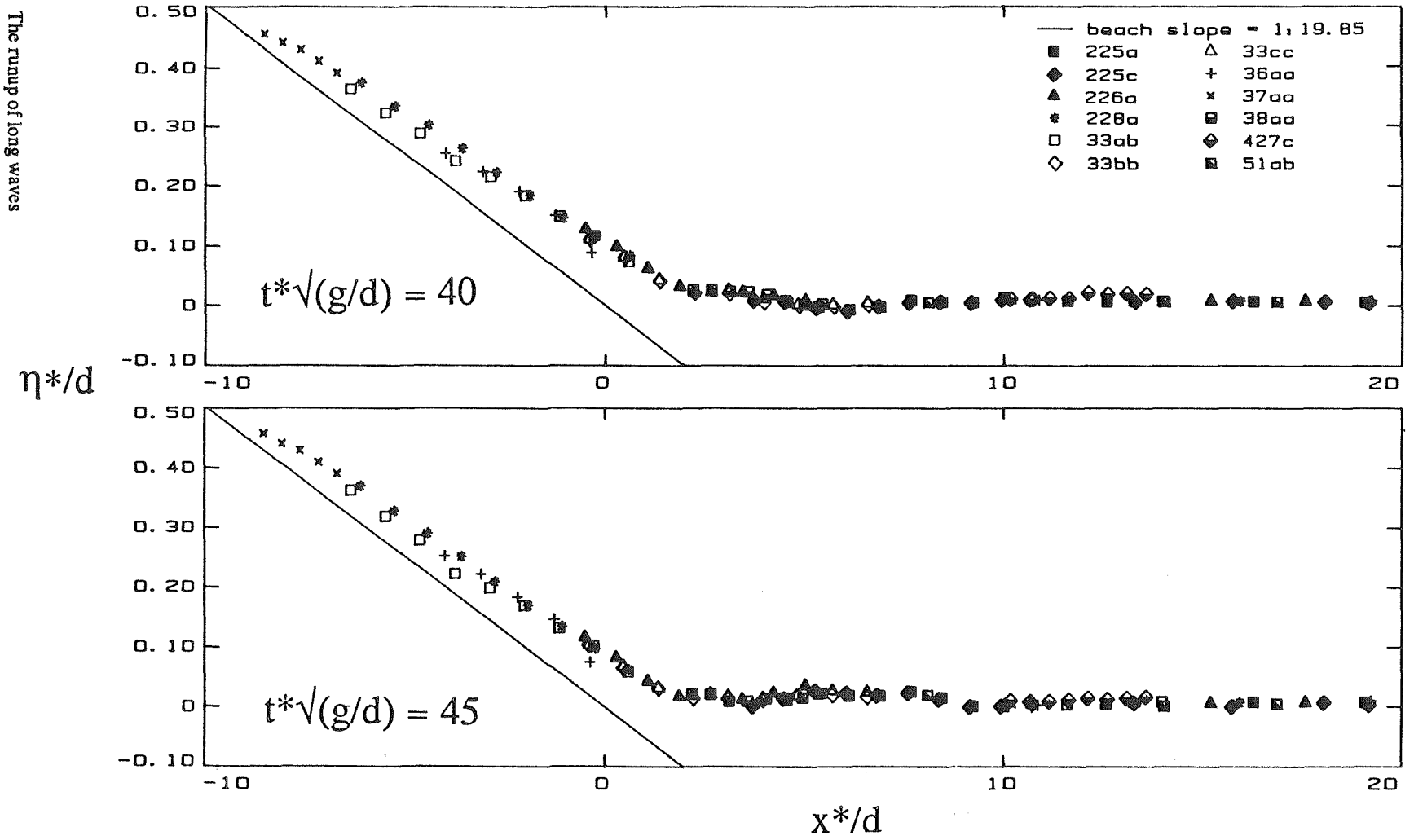

Figure 3.7.1gh Surface profiles of a 0.30 solitary wave up a 1:19.85 beach as a function of x at t = 40 (g) and at t = 45 (h). Laboratory measurements. Different symbols indicate different realizations of the same experiment.

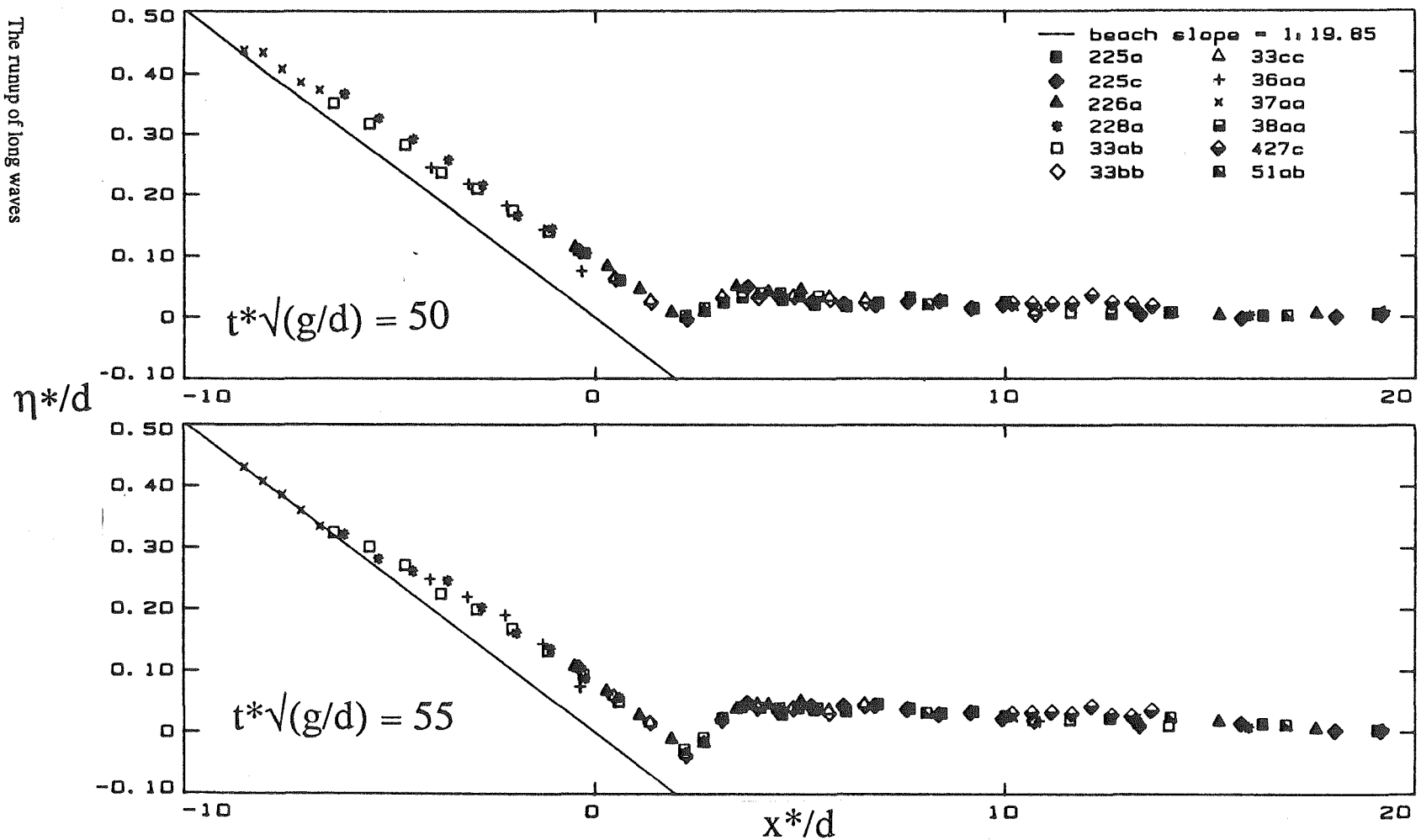

Figure 3.7.1ij Surface profiles of a 0.30 solitary wave up a 1:19.85 beach as a function of x at t = 50 (i) and at t = 55 (j). Laboratory measurements. Different symbols indicate different realizations of the same experiment.

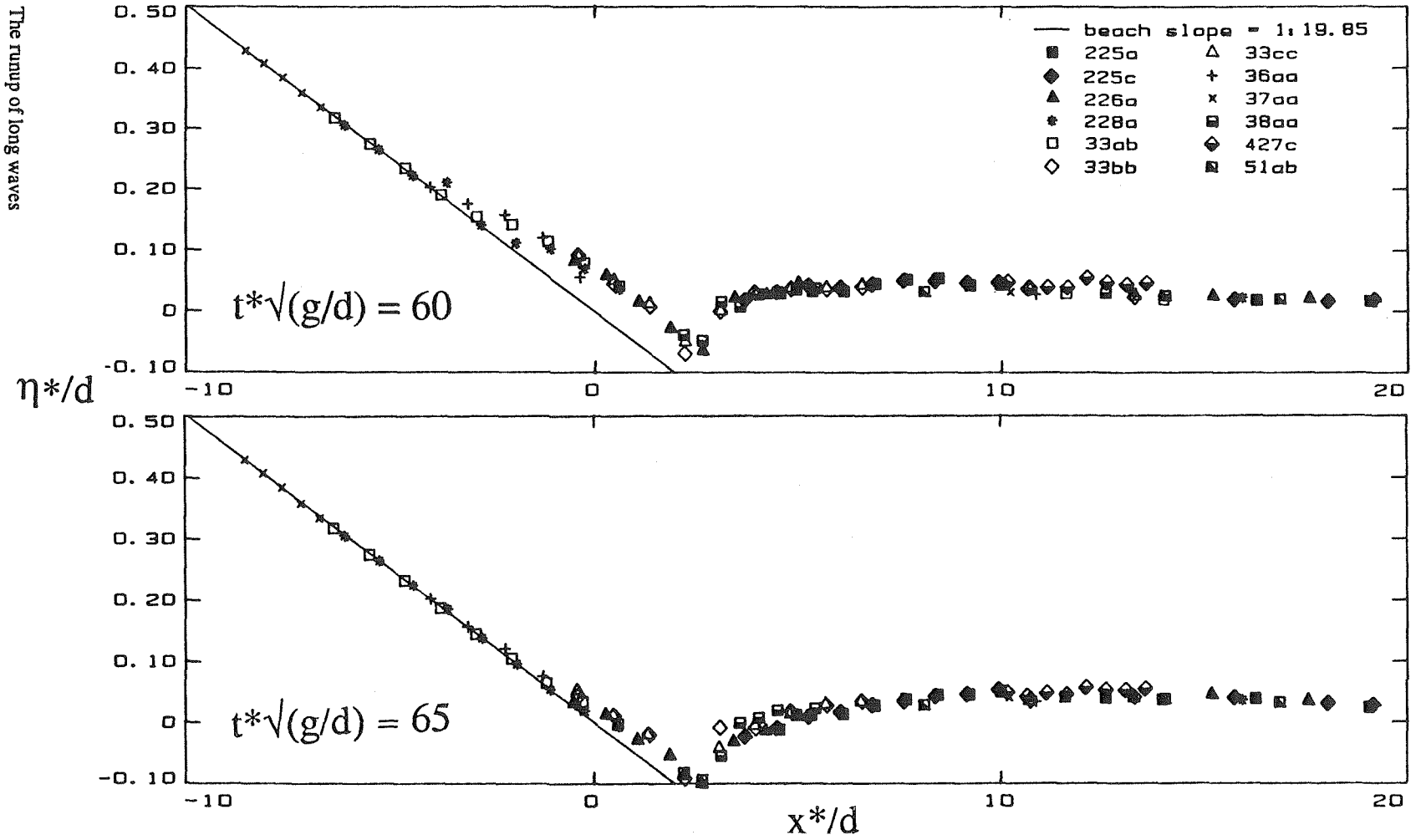

Figure 3.7.1kl Surface profiles of a 0.30 solitary wave up a 1:19.85 beach as a function of x at t = 60 (k) and at t = 65 (l). Laboratory measurements. Different symbols indicate different realizations of the same experiment.

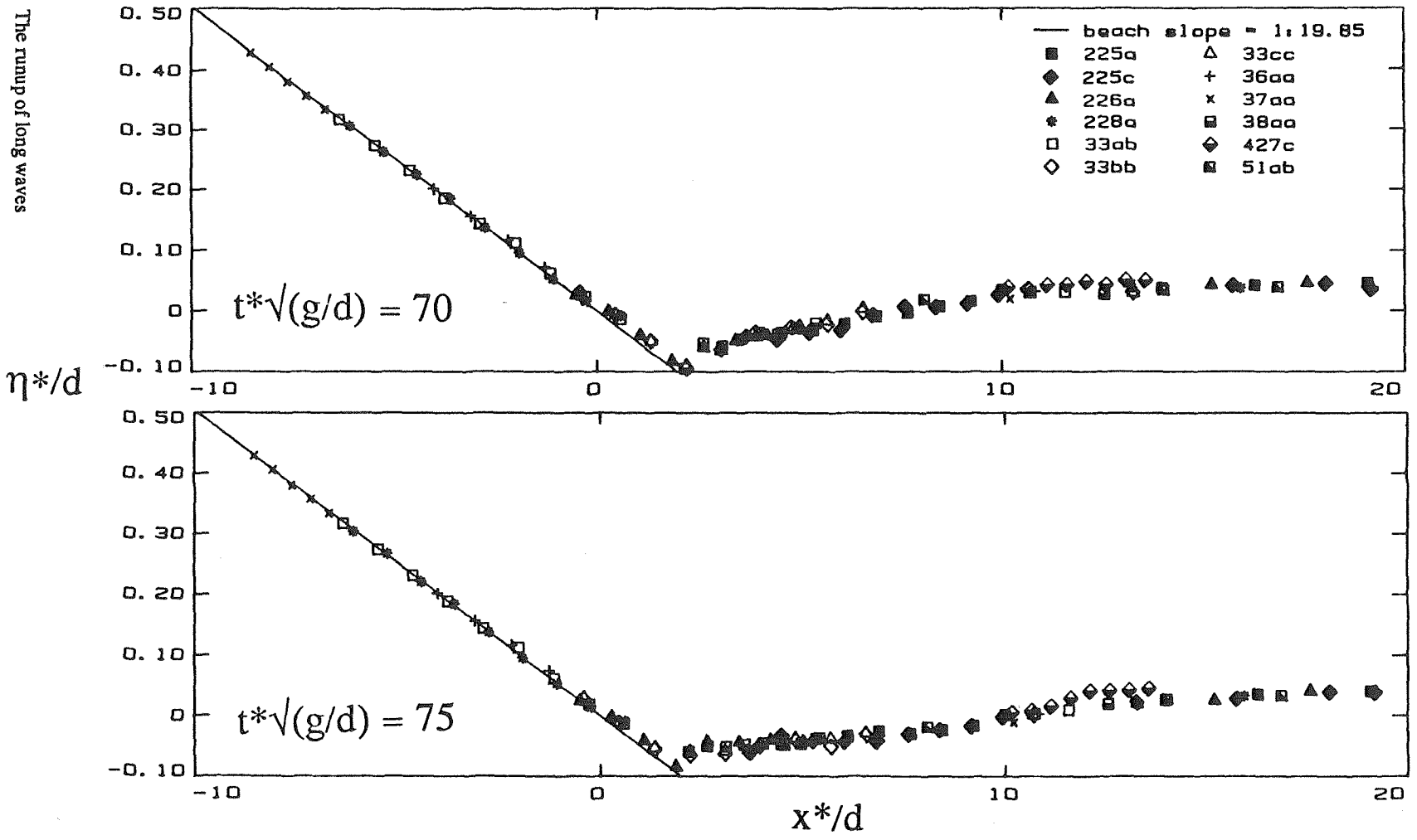

Figure 3.7.1mn Surface profiles of a 0.30 solitary wave up a 1:19.85 beach as a function of x at t = 70 (m) and at t = 75 (n). Laboratory measurements. Different symbols indicate different realizations of the same experiment.

3.8 The reflection process. After waves climb up a beach, the process of the rundown begins and a reflected wave is generated which propagates seaward. Nonbreaking and breaking waves have significantly different behavior during rundown.

Figure (3.8.1) shows the transformation of the 0.040 solitary wave as a function of time at different x-locations. Figure (3.8.2) presents the equivalent data for the climb of a 0.30 solitary wave. In both figures the reflected wave is observed at locations where $2.5<x$. Close to the shoreline, for $x<2.5$, the incident and the reflected wave cannot be identified individually ; they merge into a single wave. Both figures indicate that the reflected wave has a dipole character. This can also be seen in figure (3.5.6) for the 0.0185 wave. This is a very intriguing phenomenon, because it is counterintuitive. When a one-signed incident wave climbs up a beach one would expect a one-signed wave to be reflected. Also, although the linear and nonlinear theory of section (3.1) and (3.2) predict *perfect* reflection for nonbreaking waves, the dipole character is more pronounced for nonbreaking waves. Since both the linear and nonlinear theory agree well with the laboratory data at the toe of the beach (see figure 3.5.4) it is likely that the dipole wave reforms into a one signed wave after propagating over the constant depth region. This dipole character of the reflected wave was also noted by Carrier and Noiseux (1983) in a study of the reflection of long waves off a shelf.

Although both nonbreaking and breaking waves generate reflected waves of similar shape, the process of generation is different. When nonbreaking waves climb up a beach a reflected wave is generated continuously; the continuous reflection manifests itself as a shelf between the incoming and the outgoing waves . It can be seen in figures (3.5.4) and (3.8.1). However the reflected wave generated from the 0.30 wave is negligible, until *after* the wave reaches its maximum runup when the reflection process begins. This behaviour was

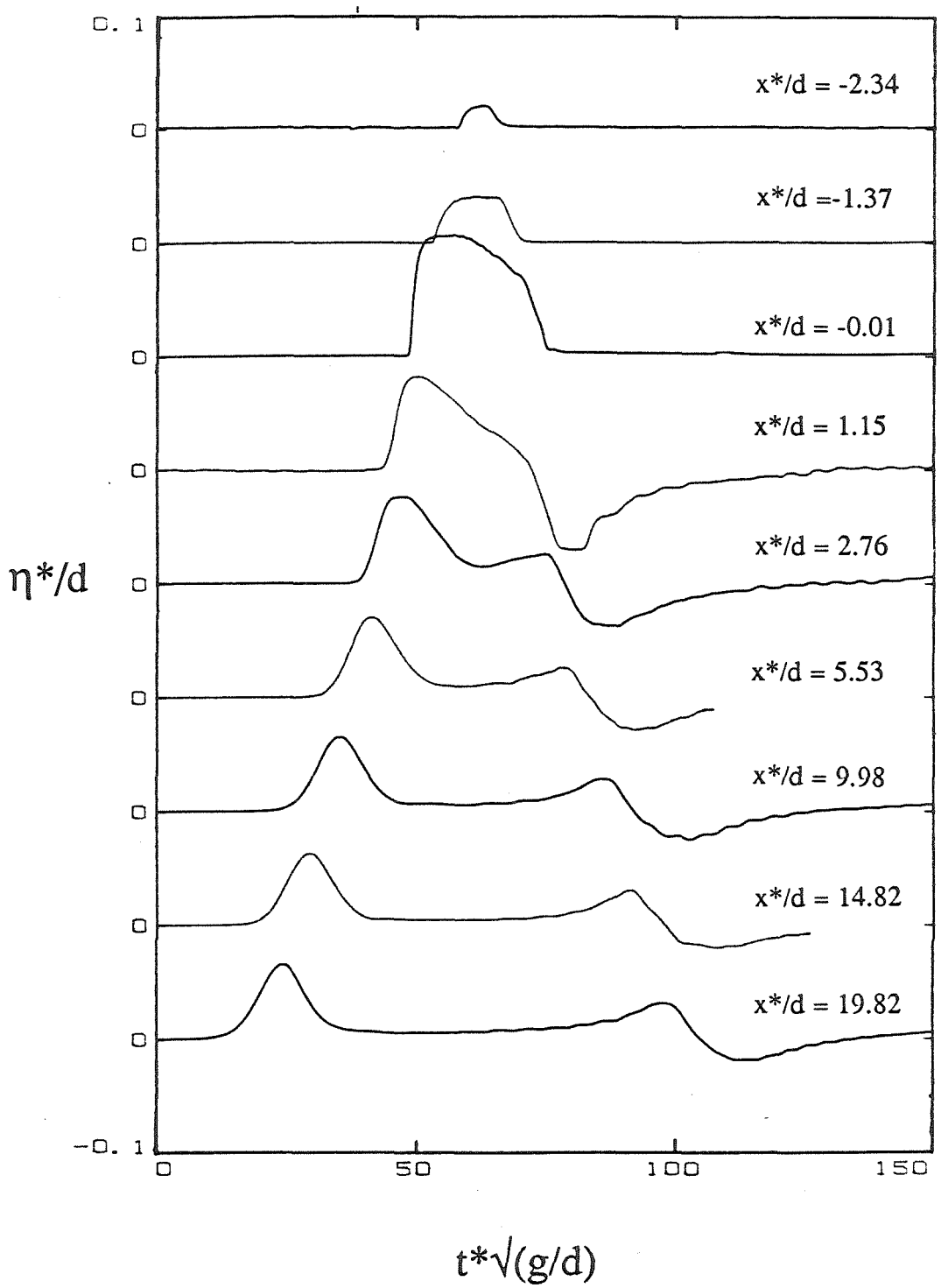

Figure 3.8.1 The climb of a 0.04 wave up a 1:19.85 beach as realized in the laboratory. Profiles are shown as functions of $t=t^*\sqrt{g/d}$ for different $x=x^*/d$.

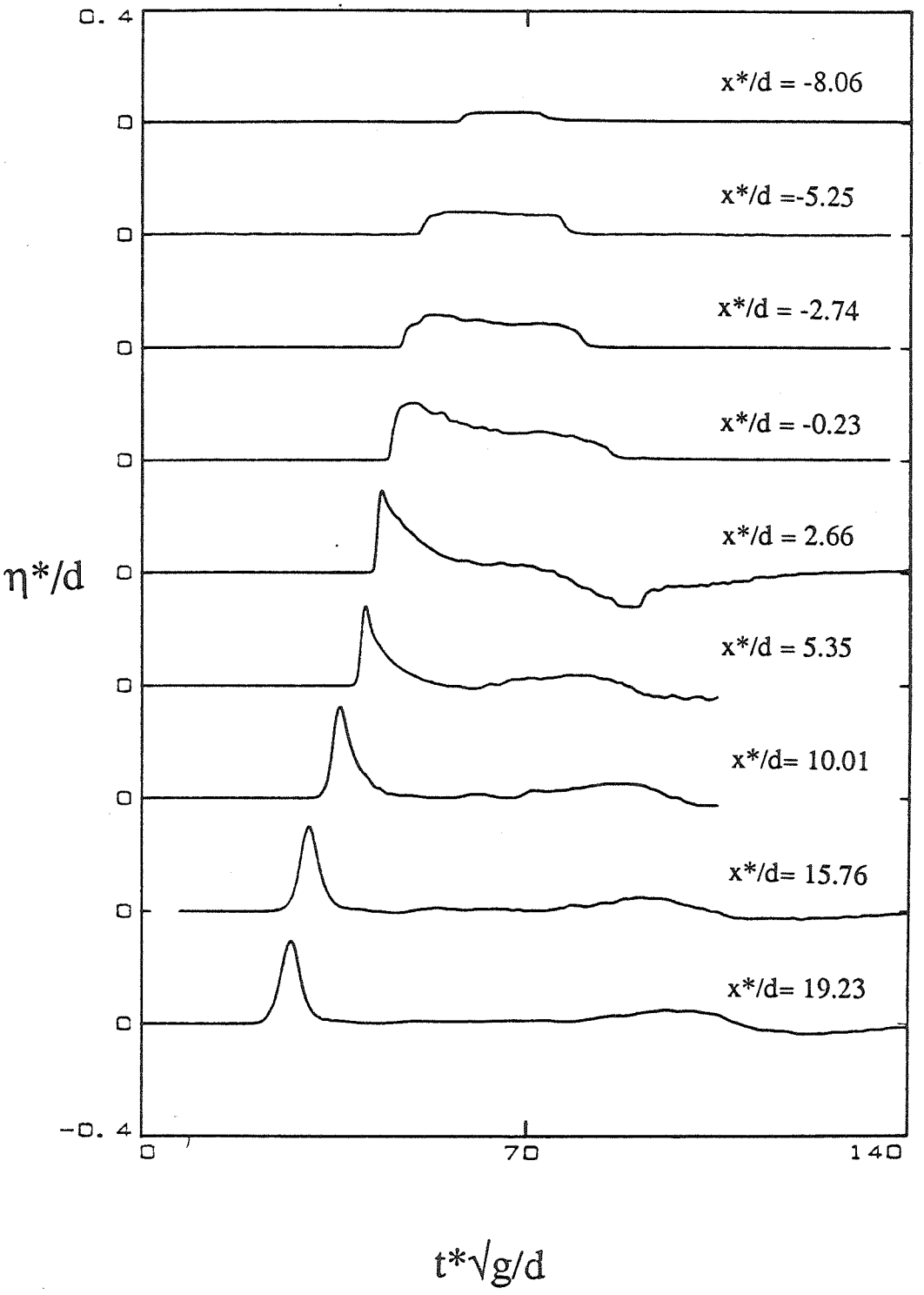

Figure 3.8.2 The climb of a 0.30 wave up a 1:19.85 beach as realized in the laboratory. Profiles are shown as functions of $t=t^*\sqrt{g/d}$ for different $x=x^*/d$.

also observed in experiments with breaking solitary waves with H/d = 0.1, 0.5, and 0.6.

Peregrine (1967) observed the formation of the shelf behind a solitary wave during reflection in a numerical computation of the climb of long waves on a beach. He derived an approximate expression for the height of the shelf at the toe of the beach, η_{rs}. It takes the form :

$$\eta_{rs} = \frac{1}{2}\tan\beta\left(\frac{1}{3}\frac{H}{d}\right)^{1/2} \tag{3.8.1}$$

It is interesting to observe that for a H/d=0.0185 solitary wave climbing up a 1:19.85 beach, η_{rs}=0.0020, while the laboratory data implies that η_{rs} = 0.0029. When H/d = 0.30, the laboratory data do not indicate the formation of a shelf.

The reflection process from a sloping beach is usually characterized with the reflection coefficient, which is the ratio of the incident to the reflected wave. Since the height of the reflected wave cannot be determined accurately because of the dipole nature of the wave, one can define a reflection coefficient from the ratio of the height of the positive wave of the dipole H_{dr} to the height of the incident wave. The following values were derived from the laboratory data for the 1:19.85 beach :

$$\begin{aligned} H_{dr}/H &= 0.52 \text{ when } H/d = 0.0185, \\ H_{dr}/H &= 0.53 \text{ when } H/d = 0.040, \\ H_{dr}/H &= 0.12 \text{ when } H/d = 0.30. \end{aligned} \tag{3.8.2}$$

One can hypothesize that these differences between breaking and nonbreaking waves exist because the breaking and nonbreaking waves have different incident wavelengths. Very long waves see the beach as a vertical wall; the x-wavelength changes rapidly and reflection starts

immediately. The shorter, steeper waves , initially at least, propagate up the beach as if the beach is not present. The wavelength remains constant and reflection starts well after the entire wave is on the beach.

3.9 Summary and conclusions. In this chapter a theory was presented and an exact result was derived for the runup of nonbreaking solitary waves on plane beaches. Detailed measurements of the runup distribution of nonbreaking and breaking solitary waves were presented. There are four major conclusions.

1) *The linear theory predicts that the maximum runup of nonbreaking solitary waves on plane beaches is given by the runup law* :

$$\frac{R}{d} = 2.831 \sqrt{\cot\beta} \left(\frac{H}{d}\right)^{5/4} , \qquad (3.4.19)$$

This relationship models the laboratory data well.

2) *Profiles derived from the nonlinear theory model the climb of nonbreaking solitary waves satisfactorily.* Since a solitary wave initially has dispersion and nonlinearity in balance, this observation implies that nonlinear effects are more important than dispersion during shoaling.

3) *Breaking and nonbreaking waves behave in a different manner during runup and rundown.* The runup variation with wave height is different for breaking and nonbreaking waves. The reflection process is also different; nonbreaking waves generate a reflected wave continuously while the breaking waves generate significant reflection only after the wave reaches its maximum runup.

4) *There are different breaking criteria for determining if a solitary wave of given height-to-depth ratio will break as it climbs up a sloping beach and for determining if it will break during the rundown .*

Waves will break during runup if $H/d > 0.818 \cot\beta^{-10/9}$ (3.6.3)

and

they will break during the rundown if $H/d > 0.469 \cot\beta^{-10/9}$. (3.6.4)

It can also be concluded that, even when the nonlinear theory indicates wave breaking, it may still be possible to continue with the runup calculation, since the flow beyond the point of wave breaking appears to be insensitive to the details of the wave at breaking. However, *extreme* caution should be used in interpeting any results derived in this manner.

Chapter 4

The runup of breaking long waves

This chapter describes some results for the runup of long waves on plane beaches. Different long waves are described by introducing a momentum and an energy scale. One single parameter, the runup number, $R_u = Rg^{1/5}/(S^2d/T)^{2/5}$ derived from the momentum scale may be sufficient to describe the runup process. The energy and momentum scale are shown to represent integrals of motion at generation. Different regimes are derived for waves that break on the beach, waves that break offshore and reform before reaching the beach, and bores of finite volume.

4.1 The runup hypothesis Consider the wave propagation problem defined in figure (4.1.1). The piston PP' moves with trajectory ξ (t) for time **T** and generates the waveform $\eta^*(x,t)$. The wave propagates a distance l and reaches the sloping beach; then it climbs up the beach, reaches the shoreline and runs up on the dry bed.

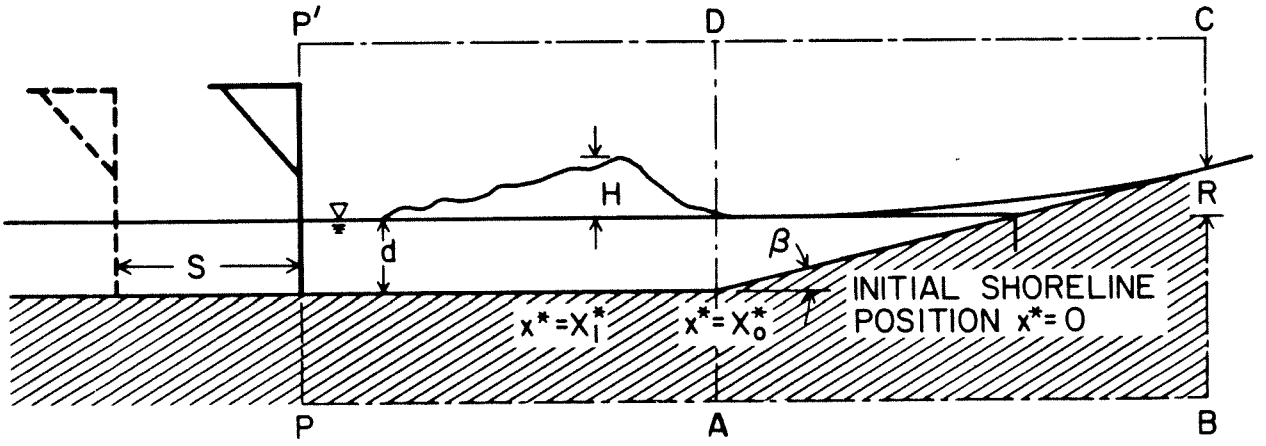

Figure 4.1.1 A definition sketch for long wave generation, propagation and runup.

On physical grounds :

	R	the maximum runup	(L),
is a function of :			
	d	the undisturbed water depth	(L),
	ξ (t)	the piston trajectory	(L),
	ρ	the density of water	(M/L^3),
	μ	the viscocity of water	(M/TL),
	l	the propagation distance	(L),
	g	the acceleration of gravity	(L/T^2)
	ε	the bed roughness height	(L),
and			
	β	the beach slope	(dimensionless).

This formulation is sufficient to describe the problem. Indeed, if the equations of motion were solvable for arbitrary initial conditions, then the specification of the plate motion as a boundary condition and the other physical parameters would be sufficient to define the maximum runup. For nonbreaking waves, the equations of motion can be solved as demonstrated in chapter 3 using as a boundary condition the wave derived with the generation algorithm of appendix C. For breaking waves, the current state of the art permits definition of the jet in front of a plunging wave, but it is unable yet to complete the calculation and provide details for the wave that forms beyond breaking. However, one can hypothesize that, if suitable integrals of the motion could be defined, then it might be possible to solve the integrated form of the equations of motion and use the solution to derive the runup. Ideally, any such integrals should be motion invariants.

This hypothesis is very appealing for three reasons. First, because it has the potential to reveal the fundamental processes that define wave runup. Second, because it

allows runup predictions without knowledge of the details of wave propagation, if the motion invariants are defined in the generation region. Third, because it is easier to define and measure motion invariants during the process of wave generation in the laboratory, and it is potentially easier to estimate them there in the prototype.

Although the assertion that the runup depends on motion invariants at generation seems obvious, it has never been suggested in the past. In fact, no direct connection between wave generation and wave runup has ever been explored. All past investigations have concentrated in relating wave runup with the details of the incident wave, rather than with its generation characteristics. For this reason, it will first be established that such relationship exist, and then possible integral invariants for describing the process will be suggested.

4.2 Dimensional analysis. Consider the propagation problem of figure (4.1.1). Let the piston move with a *specified* trajectory ξ (t), with stroke **S** and duration **T**. Consider the family of waves generated in this manner. The runup of these waves is given by the following relationship,

$$\mathbf{R} = \mathbf{f}\,(d, \mathbf{S}, \mathbf{T}, \rho, \mu, l, g, \varepsilon, \beta) \tag{4.2.1}$$

There are ten independent variables with a total of three physical dimensions ; Buckingham's π-theorem requires that there exist seven dimensionless groups. One particular choice of groups leads to the relationship :

$$\mathbf{R}/d = \mathbf{f}\,(\mathbf{S}/(\mathbf{T}\sqrt{gd}),\ \mathbf{T}\sqrt{(g/d)},\ l/d,\ \varepsilon/d,\ \beta,\ \mathbf{S}d/\mathbf{T}\nu) \tag{4.2.2}$$

The parameter $S/(T\sqrt{gd})$ can be identified as the generation Froude number Fr and it will be referred to as the generation number. The parameter $Sd/T\nu$ is the generation Reynolds number Re. The Reynolds number is of the order of 10^4, a manifestation of the fact that the inertial forces are predominant during wave generation. If viscosity is excluded from the list of variables, then the Reynolds number may be omitted in the preliminary analysis. The bed roughness parameter can also be omitted from the list of parameters, because it does not act to change the wave substantially in the range of l/d considered [Naheer, (1978)]. This reduces the number of dimensionless groups to four. If one considers *fixed* propagation distances and *fixed* slopes, then it follows that :

$$R/d = \mathbf{f}\,(S/(T\sqrt{gd}),\ T\sqrt{g/d}) \qquad (4.2.3)$$

Without experimental data, it is impossible to derive the functional form of this relationship. However, it is possible to identify its qualitative behaviour. Consider waves propagating over a given depth d. For a given generation number $S/(T\sqrt{gd})$, the runup should generally increase as the generation time increases, because then the stroke increases in proportion, thereby generating higher waves. However, this behaviour should not be observed for very large generation times $T\sqrt{g/d}$, because then the process takes place in a quasi-static manner. It is likely that for any given generation number, there is some limiting generation time beyond which there is no further increase in the runup. Conversely, for a given generation time the runup should increase as the generation number increases, since then the stroke increases and larger amplitude waves are generated.

The relationship between the runup and the generation characteristics of a given long wave can also be described by looking at the breaking character of the wave, i.e., whether waves climb up the beach without breaking, whether they break, or whether they propagate

as bores. Such a relationship is suggested from the behaviour of periodic waves. (See section 1.2.) Waves generated at small generation numbers and moderate generation times are small amplitude shallow water waves. They propagate over the constant depth region and then climb up the beach without breaking. Waves generated with very short generation times break during the generation process and reform immediately. Very high wave generation velocities and moderate generation times result in waves that are generated broken and propagate without reforming; they are bores of finite volume. Although it is expected that nonbreaking waves will have shorter runup excursions than waves that break as they climb on the beach and that the latter waves will have smaller excursions than bores, no such relationship has ever been reported.

To determine the functional form of (4.2.3) and to assert how the breaking character of the wave affects its runup, the results from two sets of experiments will be presented. The two sets of experiments differ in the trajectory function used to generate the waves; in the near field, the generated waves also differ and the names *type R waves* and *type S waves* are used to identify the two resulting wave hierarchies. In the first set of experiments the emphasis is on examining the dependence of the runup on the generation parameters, while in the second set of experiments the emphasis is on detrmining how the runup varies as the breaking character of the wave changes.

4.2.1 Waves generated with a ramp trajectory. (Type R waves.) In this set of experiments waves were generated by displacing the plate with constant velocity $v_p=d\xi/dt=S/T$; the dimensionless plate velocity is the generation number. The trajectory is a ramp function, and it is defined by :

$$\xi(t^*) = (S/T)\, t^* \quad , \quad \text{for } 0 \le t^* \le T. \tag{4.2.4}$$

This is the simplest possible piston motion ; it has the distinct advantage that the wave generation process can be entirely defined using two parameters only. Waves generated in this fashion will be referred to as *type R waves*. Examples of these waves are shown in figures (4.2.1), (4.2.2) and (4.2.3).

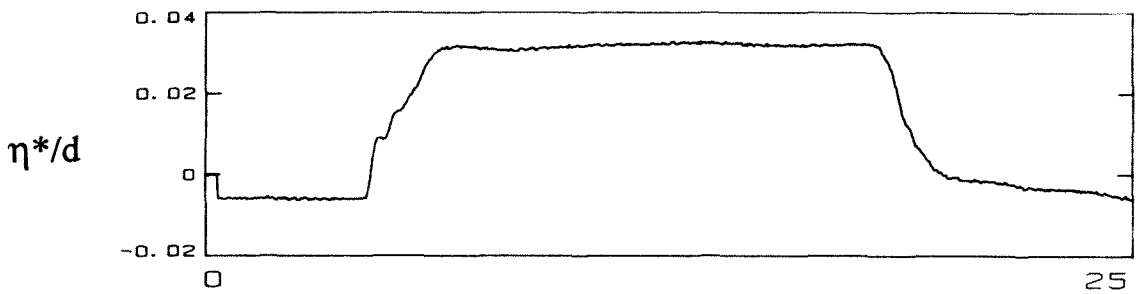

Figure 4.2.1a The wave height at the plate during the generation of a type R waves with $S/(T\sqrt{gd}) = 0.604$ and $T\sqrt{(g/d)}=15.00$

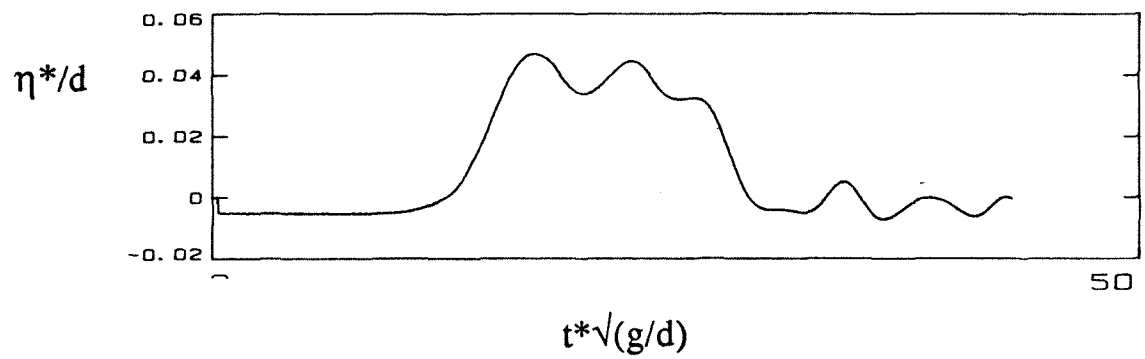

Figure 4.2.1b The resulting wave motion at 20 depths from the toe of the beach associated with the wave motion of figure (4.2.1a).

Figure (4.2.1) shows the wave amplitude at the piston plate and the amplitude of the resulting wave motion measured several depths away from the generation region; the generation number is 0.604. Figure (4.2.2) shows the resulting wave heights when the generation number is increased one order of magnitude to 5.788. Both the amplitude at the plate and the amplitude of the wave downstream increase ten-fold.

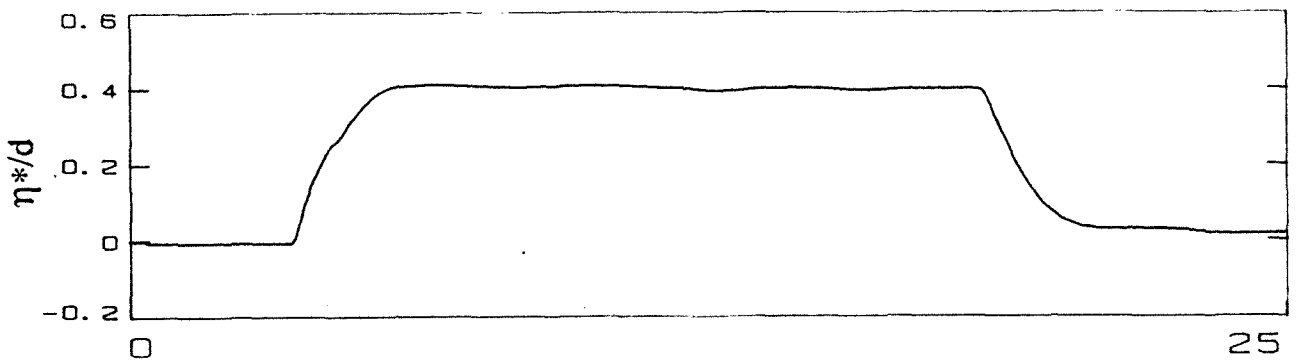

Figure 4.2.2a The wave height at the plate during the generation of a type R wave with S/(T√gd)=5.788 and T√(g/d)=15.00.

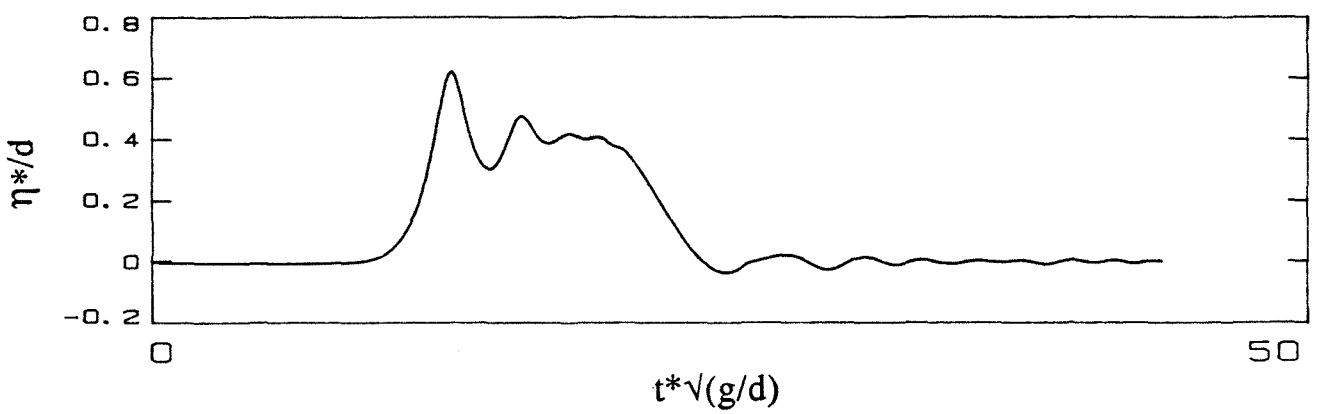

Figure 4.2.2b The resulting wave motion after the generation of the type R wave in (4.2.2a). This wave is a bore of finite volume and propagates to the toe of the beach and beyond without reforming into a nonbreaking wave.

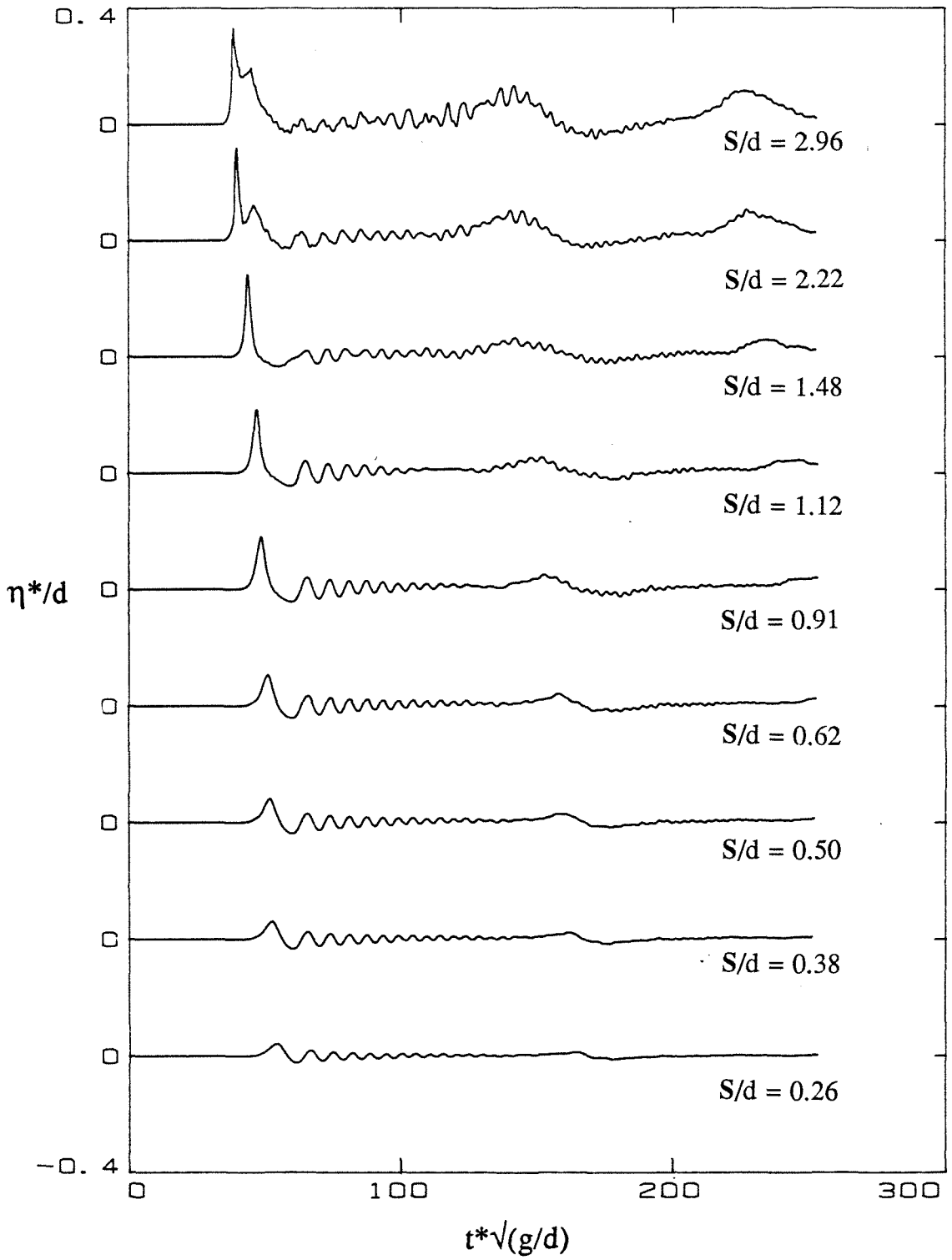

Figure 4.2.3 The wave hierarchy generated with a ramp trajectory with $T\sqrt{(g/d)}=7.2$ and different strokes. (Type R waves.)

The wave shown (4.2.1) is nonbreaking wave, while the wave indicated by (4.2.2) is a wave that propagates broken withour reforming into a nonbreaking wave ; according to the definition of section 1.3.3, it is a bore of finite volume. Both figures show waves generated with $T\sqrt{(g/d)} = 15.0$.

Figure (4.2.3) shows the hierarchy of long waves generated with a generation time of 7.200 and generation numbers $S/(T\sqrt{gd})$ varying from 0.08 to 0.8. All waves were measured at a distance of 20 depths from the toe of the sloping beach. The waves generated with $S/d < 0.38$ are nonbreaking waves, those that are generated with $0.38 < S/d < 2.22$ break only as they climb on the beach, and waves generated with $2.22 < S/d < 2.96$ are bores of finite volume. All waves shown assume the shape of a leading solitary wave with a long tail. (The profiles are not syncronized in time and their relative positions do not necessarily reflect differences in propagation velocities.)

The relationship of the runup of waves generated using the ramp motion (4.2.3) with their generation number is presented in figure (4.2.4). The ordinate of the figure is the maximum runup realized when a wave was generated with the corresponding generation number in the abscissa and with the generation time implied by the symbols. For the range of times $T\sqrt{g/d}$ considered, longer generation times generally produce higher runup for a given generation number. All the data included in the figure refer to waves that break only when they climb on the beach. Note that the runup R/d of these waves is in the range [0.2, 0.78]. Higher runup values are only possible by generating broken waves or bores of finite volume. Smaller runup values can only be achieved by nonbreaking waves. This phenomenon is also observed with the runup of waves that are generated with a solitary wave type trajectory. These waves will be examined in the next section.

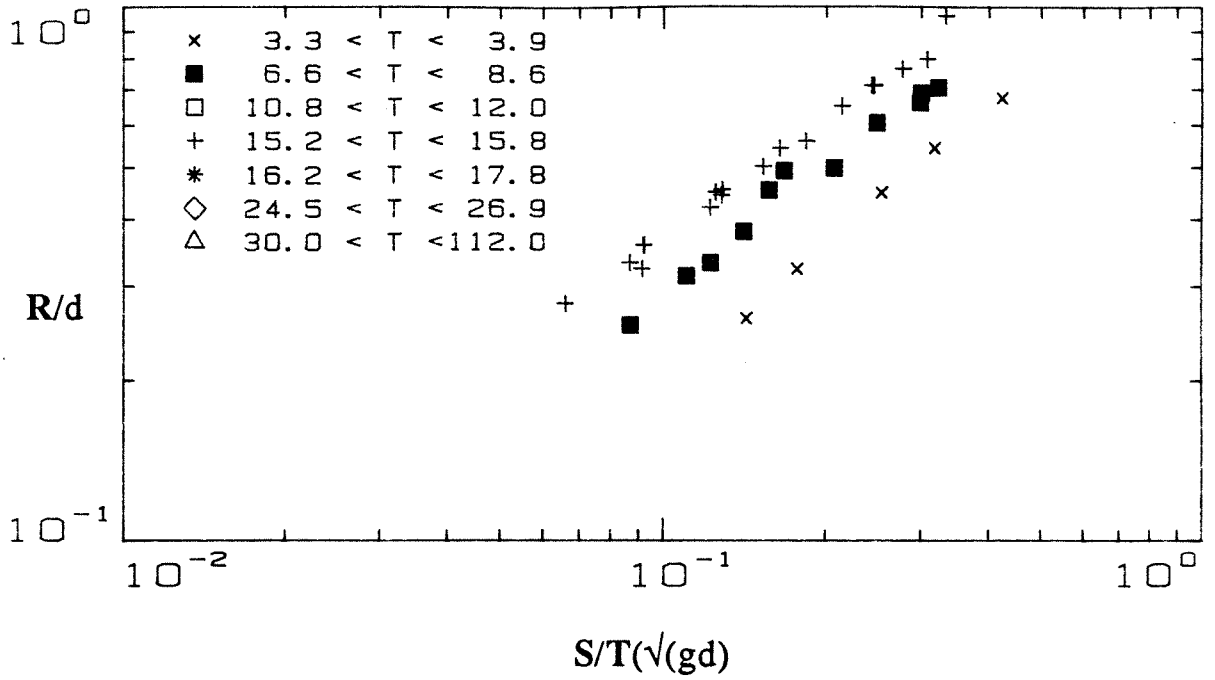

Figure 4.2.4 The runup vs. generation number variation for type R breaking waves.

4.2.3 Waves generated with a solitary wave type trajectory. (Type S waves.) In this set of experiments, waves were generated by using different solitary wave type trajectories. A solitary wave type trajectory is the piston motion that would generate a solitary wave of given H/d, *if the appropriate stroke and time were specified.* This trajectory $\xi(t)$ is defined implicitly by the equation :

$$k\xi(t^*) = H \tanh [\gamma(ct^* - \xi(t^*)/d], \qquad (4.2.4)$$

where γ is the dimensionless wavenumber, and $\gamma = \sqrt{(3/4)}H/d$, $c=\sqrt{(1+H/d)}$, and x and t by (3.1.1). The appropriate stroke S/d and the generation time $T\sqrt{g/d}$ are defined by :

$$S/d = \sqrt{(16/3)}H/d\,, \tag{4.2.5}$$

and

$$T\sqrt{g/d} = (2/\gamma c)\,(3.80 + H/d). \tag{4.2.6}$$

Details of the derivation of these values may be found in Goring (1978). To generate a perfect solitary wave of given H/d, as defined by the Boussinesq profile (3.4.1), the wavemaker must execute a trajectory $\xi(t)$ with S/d and $T\sqrt{g/d}$ specified by (4.2.4), (4.2.5) and (4.2.6) respectively. Such waves will be refered to as *type S waves*.. If different values are specified , a train of long waves is generated.

Figure (4.2.5) shows an example of the wave motion that results when using a solitary wave type trajectory. It shows the plate velocity, the wave amplitude at the plate, and the resulting wave for a generation number of 0.7 and a generation time of $T\sqrt{g/d}$=7.50. Figure (4.2.6) shows the wave hierarchy obtained when the generation time is kept constant at $T\sqrt{g/d}$=15.0 and the stroke S/d is varied as indicated in the figure. The waves in the hierarchy of figure (4.2.6) were generated at depths ranging from 15 cm (5.90 in) to 30 cm (11.81 in). Waves generated with S/d < 0.7 are nonbreaking, while waves generated with 0.7 < 2.0 < S/d are broken waves or bores. (The profiles are not synchronized in time and their relative posititons do not necessarily reflect differences in propagation velocities.)

The relationship of the runup of type S waves with the generation number is shown in figure (4.2.7). (Table 4.2 lists the data used in preparing this figure.) All the data in represented in the figure propagate without breaking in the constant depth region, but break as they climb up the beach. The behaviour is qualitatively similar as in the study of type R waves. However, it is interesting to note that for waves generated with large generation times ($T\sqrt{(g/d)} > 17.00$) the behaviour changes. As the generation time increases, the runup

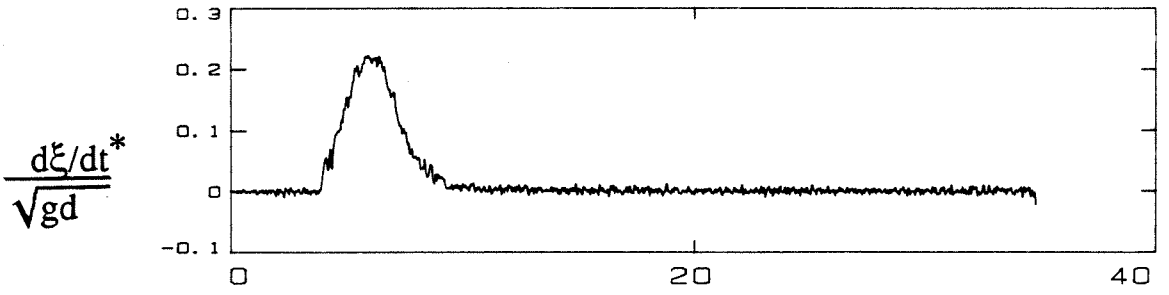

Figure 4.2.5a The plate velocity used to generate a solitary type wave with $S/(T\sqrt{gd})=0.7$ and $T\sqrt{(g/d)}=7.50$.

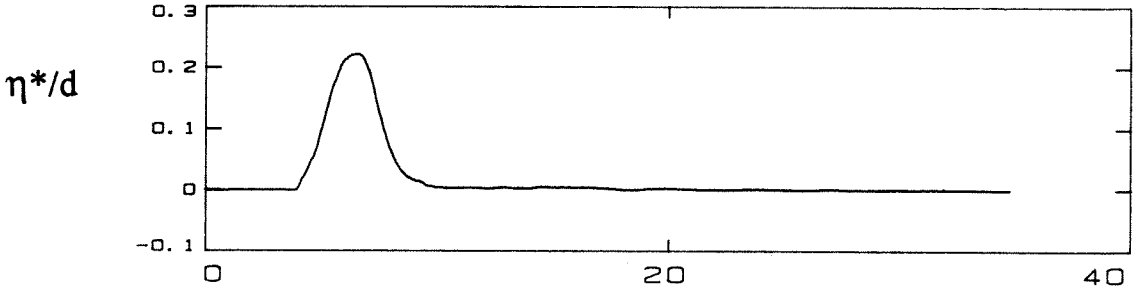

Figure 4.2.5b The wave height at the plate resulting from the morion in figure (4.2.5.a).

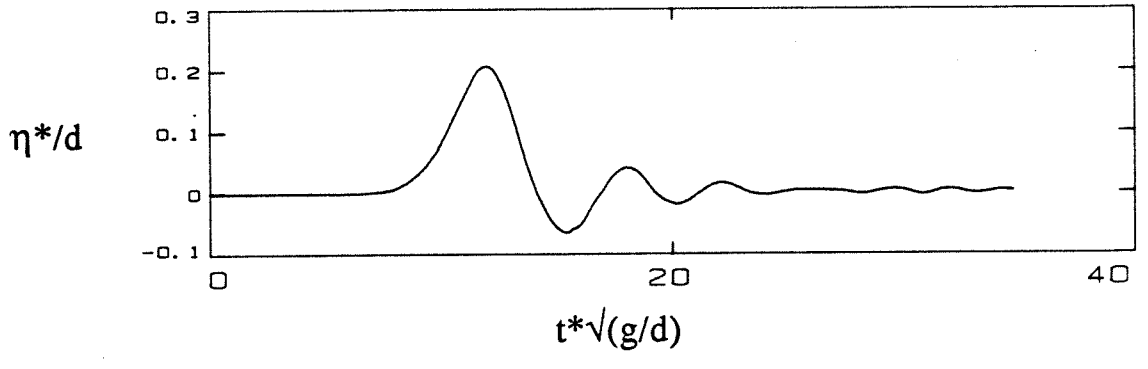

Figure 4.2.5c The resulting wave motion at 20 depths from the toe of the beach. Type S wave. Note that the maximum velocity and maximum wave heights are nearly equal.

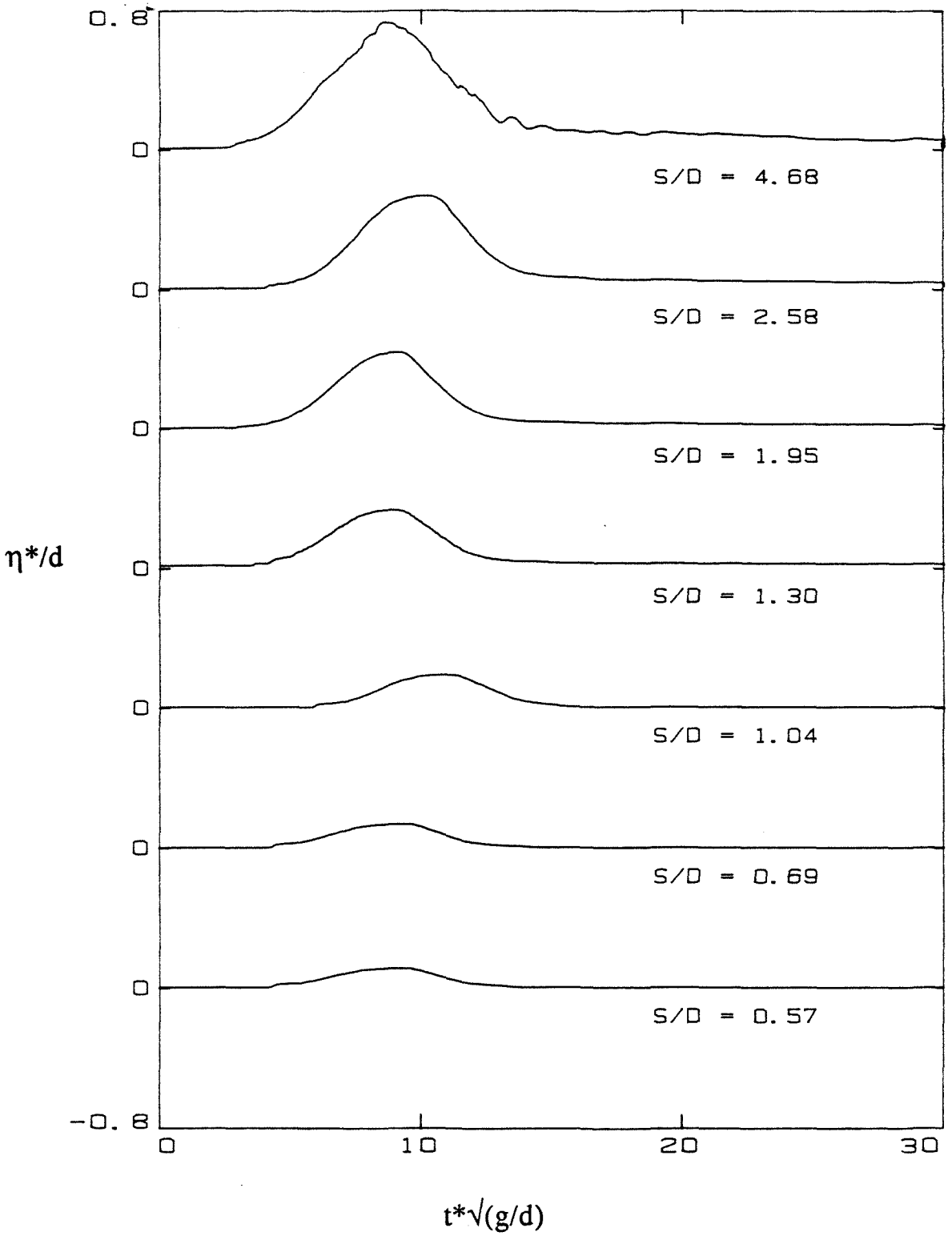

Figure 4.2.6a The wave height at the plate for the wave hierarchy generated with a solitary wave type trajectory with $T\sqrt{(g/d)}=15.00$ and with different strokes. Type S waves.

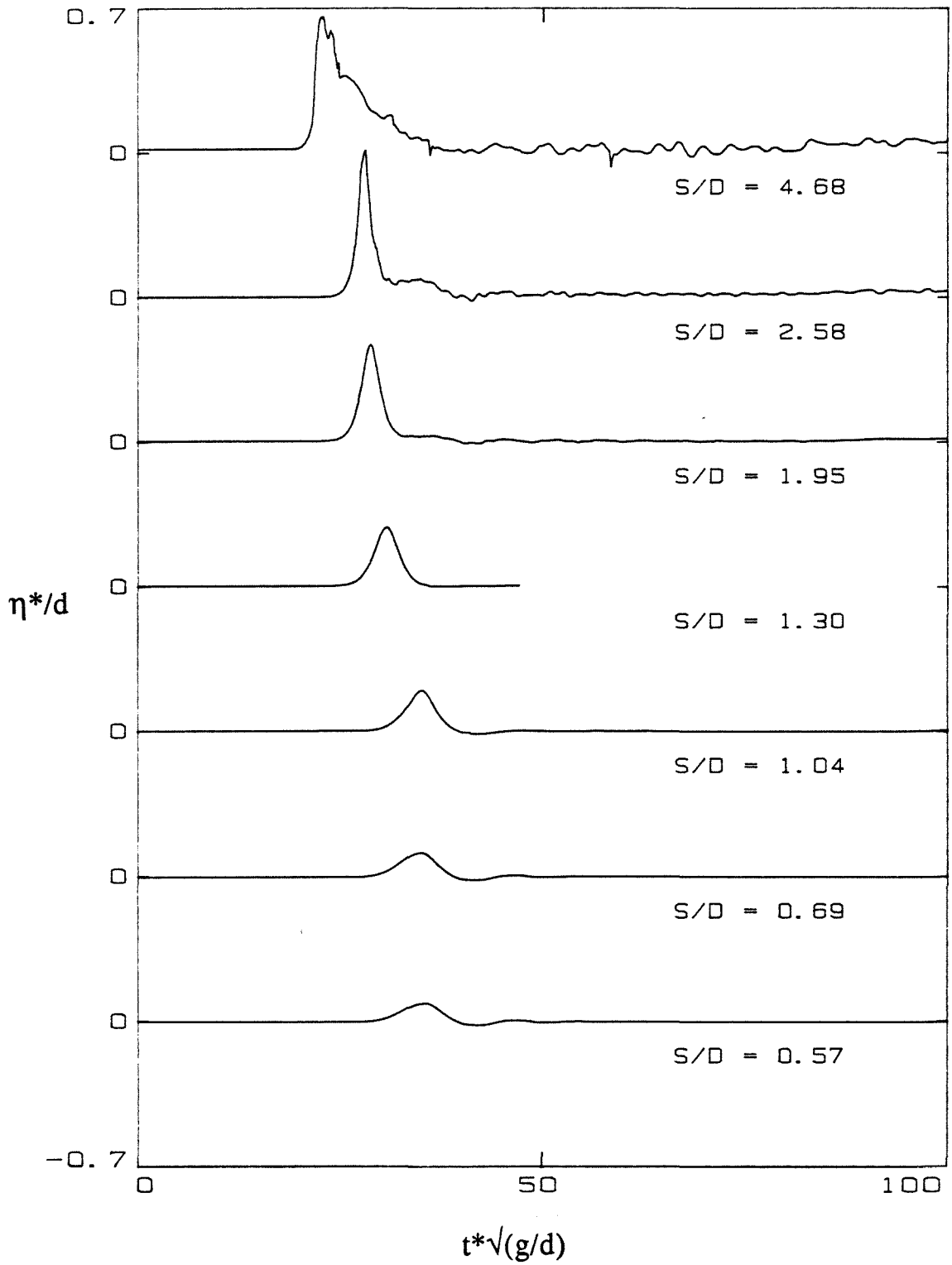

Figure 4.2.6b The wave height 20 depths from the toe of the beach for the wave hierarchy generated with a solitary wave type trajectory with $T\sqrt{(g/d)}=15.00$. Type S waves.

does not increase further, and eventually it decreases. Although there is not enough data to derive the exact form of the functional dependence (4.2.2), one general conclusion can be drawn. For a given piston velocity very short ($T\sqrt{g/d} < 10$) and very long ($30 < T\sqrt{g/d}$) generation times are less efficient in producing beach excursions. Generation times such that $15 < T\sqrt{g/d} < 27$ appear to produce the highest runup.

Figure (4.2.7) also indicates that waves that propagate unbroken and break on the beach can achieve maximum runup in the range of [0.2 , 0.82]. This behaviour was also observed in the experiments for type R waves. Apparently, this is a manifestation of a more general phenomemon; it appears that there is a maximum runup that nonbreaking and breaking waves and bores of finite volume may achieve.

Figure (4.2.8) shows the dependence of the runup **R**/d on the generation number $S/(T\sqrt{gd})$ for waves that break as they propagate over the constant depth region, reform before they reach the toe of the beach and then break again as the climb up the beach, and for waves that propagate broken, i.e., bores of finite volume. The maximum runup range that breaking-reforming waves achieve is [0.63, 0.78], while the maximum runup that bores achieve is [0.72, 1.01].

Figure (4.2.8) suggests that the runup of breaking/reforming waves is independent of the generation number. This observation implies that, although these waves were produced with different generation characteristics, the leading waves that emerge after these waves reform are similar and that they have, initially at least, the same height-to-depth ratio. This conclusion is also suggested by the work of Dally, Dean and Dalrymple (1984), who presented a model for a breaking wave decay. In their model, a long wave propagates up a sloping shelf into a constant depth region. The wave breaks as it climbs up the shelf and

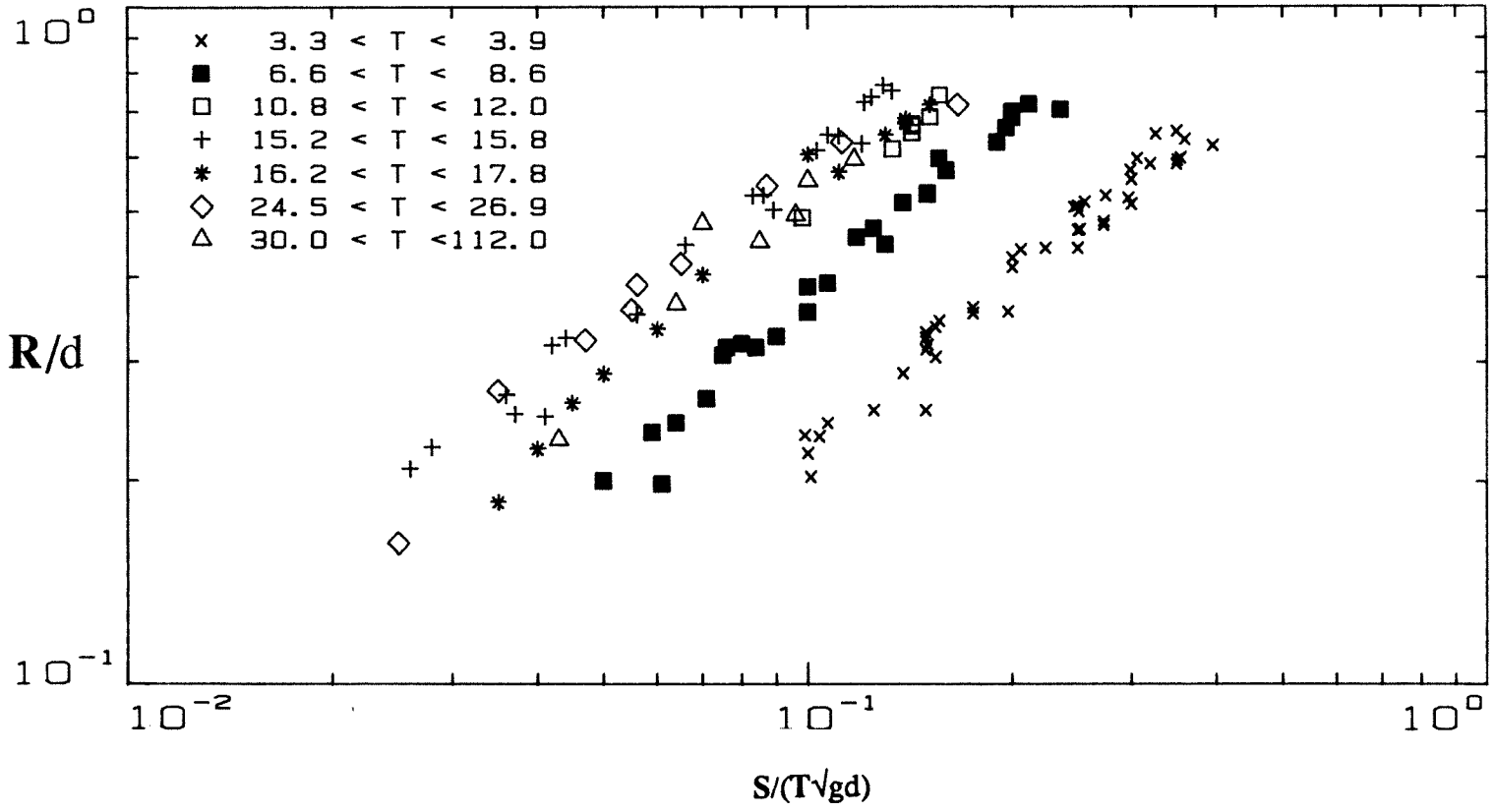

Figure 4.2.7 The runup variation with the generation number. Type S breaking waves.

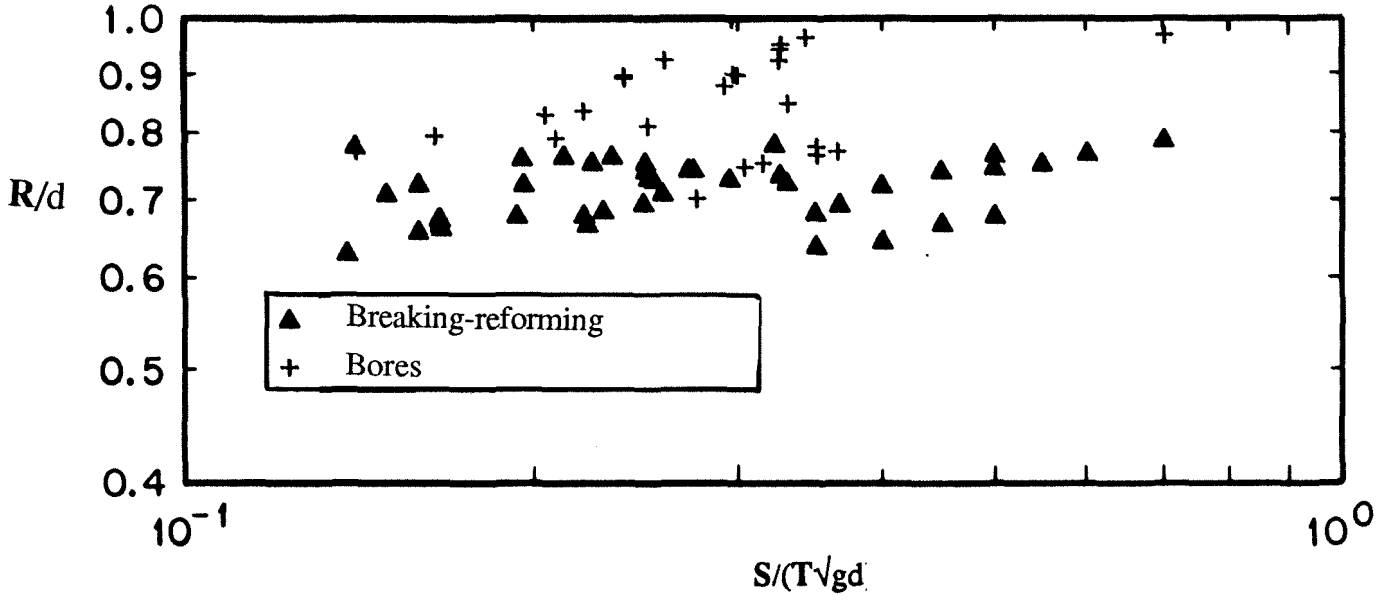

Figure 4.2.8 The runup with the generation number variation for broken waves and bores of finite volume. Type S waves.

reforms into a wave with a "stable wave height". Based on laboratory experiments, they reported an average value for this stable wave height equal to 0.40, apparently independent of the detailed initial conditions of the wave. Since in their work the sloping shelf was introduced in the flow to create a decaying breaking wave, it is reasonable to suggest that a "stable" wave height exists for decaying breaking waves generated by other means, such as moving partitions. It is intriguing to observe that the average wave runup for all broken waves of figure (4.2.8) which is $R/d = 0.714 \pm 0.05$ corresponds to a solitary wave with $H/d = 0.469$, indicating that the leading wave that emerges when breaking waves reform over constant depth is a solitary wave of $H/d = 0.469$.

The figure also shows that the runup of bores is a much stronger function of the generation number. This is expected ; after a bore first forms, any further increase of the generation number at a given generation time produces higher runup. However, there is a practical limit to the maximum runup a bore may attain. Very high generation numbers produce jets of waters sputtering from the wave generator and the resulting bores do not climb up any higher on the beach. The highest runup achieved on the 1:19.85 beach was 1.01. This should be viewed as a limit for the runup of bores of finite volume; uniform bores will attain higher runup. However, it is likely that there is a maximum runup possible for any given beach, since the size of the incident wave is ultimately limited by hydrodynamic stability constraints.

4.3 The runup number. The group of parameters used so far to describe the runup process, R/d, $S/(T\sqrt{gd})$ and $T\sqrt{g/d}$ has two limitations. One is that two parameters are required to describe the runup process uniquely. Two, there are differences between the behaviour of waves generated with a ramp trajectory (type R) and with a solitary wave type trajectory (type S). For example, for any given values of the generation number $S/(T\sqrt{gd})$

and the generation time $T\sqrt{g/d}$, type S waves achieve higher runup excursions than type R waves. This difference may be an artifact of the analysis, since the generation number does not account for differences in the time history of generation. It is conceivable, that another set of independent variables may contain some parameters with values in ranges where they do not significantly affect the runup; then a single dimensionless group may be capable to describe the process. In this section two such groups will be presented and evaluated.

In an attempt to determine one single parameter to describe the process of wave runup, it is instructive to consider the kinematic analogy of a material particle moving up a frictionless inclined plane. Suppose that before the particle climbs on the plane it has acquired momentum mv_i. As it climbs on the inclined plane the component of the gravitational force in the direction of motion acts to change its momentum according to Newton's law, $\underline{\mathbf{F}}=d\underline{\mathbf{M}}/dt$. This implies that its velocity changes like $dv_i/dt^* = -g \sin\beta$,where β is the angle of inclination of the plane to the horizontal. The particle reaches its maximum vertical elevation, **R**, at time T_{max} , when its velocity becomes zero. Then $v_i=gT_{max}\sin\beta$ and hence $\mathbf{R}=v_i^2/2g$. The same result may be arrived at by considering the balance between the potential energy at the maximum excursion and the initial kinetic energy of the particle. Therefore, it is likely that two important parameters that define the runup of a wave are the energy and momentum of that wave before it starts climbing up the sloping beach.

The kinematic analogy cannot be carried any further. When a wave climbs up a beach the process of reflection may reduce substantially the incident wave energy and momentum. Also, energy may be dissipated through other non-kinematic processes, like wave breaking, while momentum can be dissipated through friction and changes in the topography. Nevertheless, appropriate energy and momentum scales will be derived to determine whether they can be used to define wave runup.

Consider a wave of given spatial momentum distribution per unit mass and per unit width in the direction of wave propagation M_x, incident on a given sloping beach and producing a maximum runup height **R**. The basic variables are three : the runup with dimensions of L, the momentum distribution per unit mass and per unit width with dimensions of L^3/T and the acceleration of gravity with dimensions of L/T^2. These three variables can only produce one dimensionless group : $Rg^{1/5}/M_x^{2/5}$. If, instead of the momentum, the incident energy distribution per unit mass and per unit width **E** is considered as one of the variables, then the appropriate dimensionless group takes the form $Rg^{1/3}/E^{1/3}$.

To define exactly the wave momentum distribution M_x, amplitude and velocity data must be available to calculate the integral $M_x = \int_V u^* \, dvol$, over the entire volume V occupied by the wave. In practice this is difficult to accomplish. However, an estimate of the integral, a momentum scale, may be obtained by arguing that one characteristic velocity of the wave is its generation velocity S/T and one characteristic volume is the volume displaced during generation Sd; then the momentum should scale like S^2d/T. The resulting dimensionless group takes the form $Rg^{1/5}/(S^2d/T)^{2/5}$ and it will be henceforth referred to as the runup number R_u. The kinetic energy distribution can also be scaled by the same kinematic analogy ; the energy scale is $(S/T)^2Sd$, and the resulting dimensionless group is $Rg^{1/3}/(S^3d/T^2)^{1/3}$.

To investigate the validity of this preliminary analysis it will be assumed that the two dimensionless groups derived from the momentum and energy scales are equal to the constants C_m and C_e respectively. Then the following relationships are expected to hold :

$$\frac{Rg^{1/5}}{(S^2d/T)^{2/5}} = C_m \quad \text{and} \quad \frac{Rg^{1/3}}{(S^3d/T^2)^{1/3}} = C_e \tag{4.3.1}$$

These relationships may be rewritten in the following form :

$$\frac{R}{d} = C_m \left(\frac{S^2}{dT\sqrt{gd}}\right)^{2/5} \text{(a)} \quad \text{and} \quad \frac{R}{d} = C_e \left(\frac{S^3}{T^2d^2g}\right)^{1/3} \text{(b)} \qquad (4.3.2)$$

The dependence of the maximum runup **R**/d on the momentum (4.3.2a) and the energy (4.3.2b) scales is presented in figures (4.3.1) and (4.3.2) for both type R and type S breaking waves respectively. Figure (4.3.1) suggests that the following relationships exist for breaking waves, i.e., waves that break only as they propagate up the beach :

$$\frac{R}{d} = 1.1016 \left\{\left(\frac{S^2}{dT\sqrt{gd}}\right)^{2/5}\right\}^{0.92} \text{ for breaking type R waves,} \qquad (4.3.3a)$$

$$\frac{R}{d} = 1.1083 \left\{\left(\frac{S^2}{dT\sqrt{gd}}\right)^{2/5}\right\}^{0.937} \text{ for breaking type S waves,} \qquad (4.3.3b)$$

$$\frac{R}{d} = 0.756 \left\{\left(\frac{S^3}{T^2d^2g}\right)^{1/3}\right\}^{0.752} \text{ for breaking type R waves,} \qquad (4.3.4a)$$

and

$$\frac{R}{d} = 0.945 \left\{\left(\frac{S^3}{T^2d^2g}\right)^{1/3}\right\}^{0.657} \text{ for breaking type S waves.} \qquad (4.3.4b)$$

The scatter of the data in the figures (4.3.1) and (4.3.2) suggests that the constants C_m and C_e are both functions of the generation time, although the runup versus momentum relationship is a weaker function than the runup versus energy relationship. Also, the scatter in the type S wave data is larger that with the type R wave data. However, there is one important difference between the runup variation with momentum and with energy. The runup variation with momentum (predicted by (4.3.2a)) conforms well with the fit of the data (4.3.3), but the energy variation (4.3.4) does not conform well with (4.3.2b). The exponent

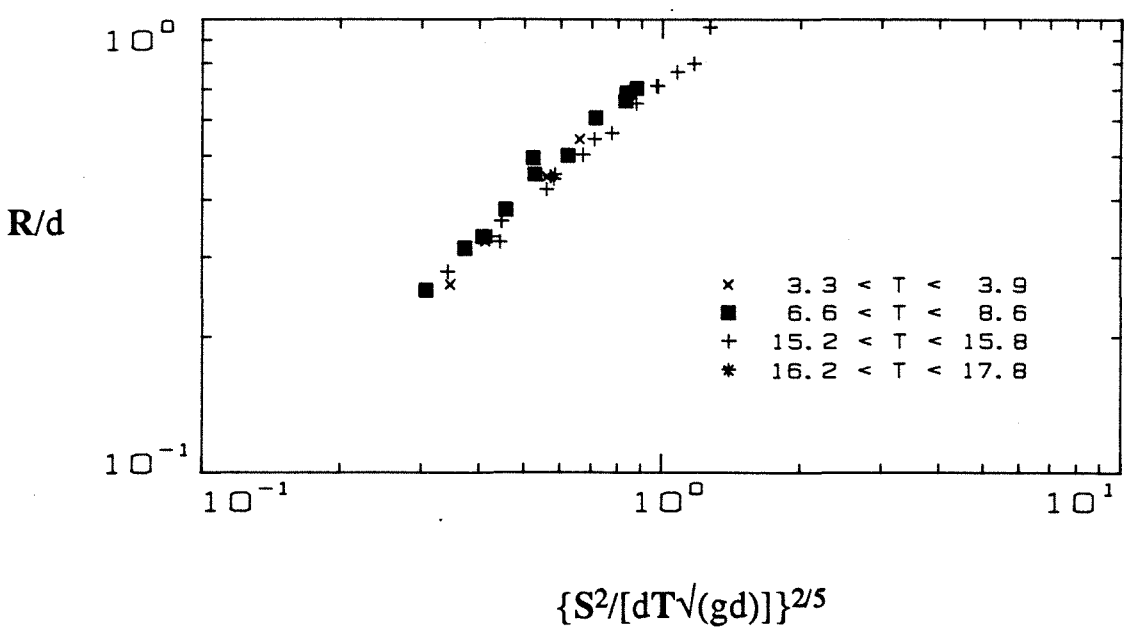

Figure 4.3.1a The runup variation versus the momentum scale for type R breaking waves.

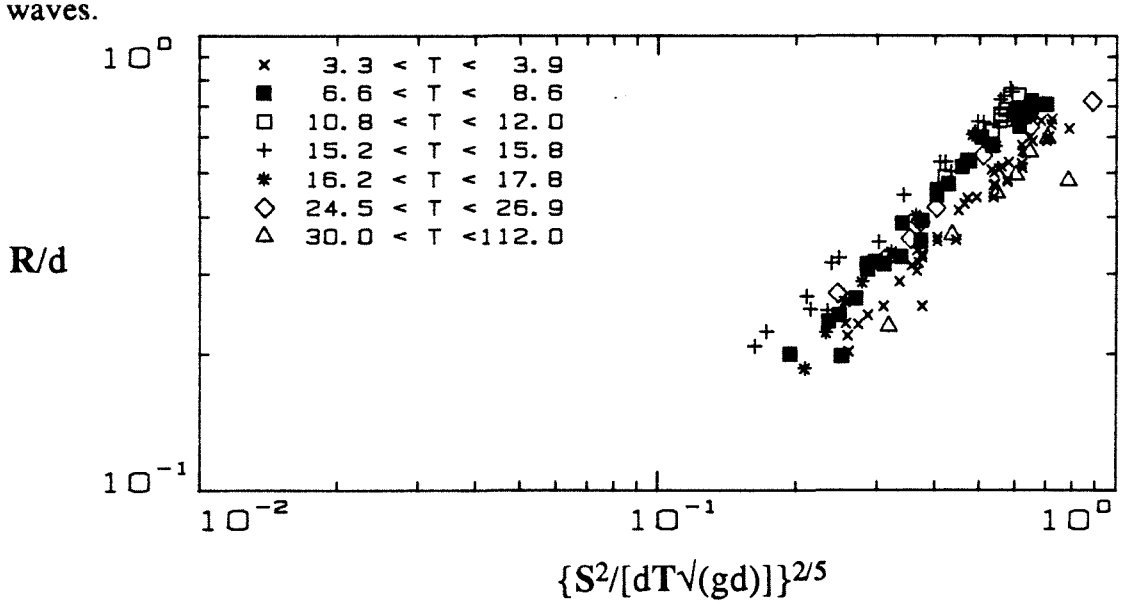

Figure 4.3.1b The runup variation versus the momentum scale for type S breaking waves.

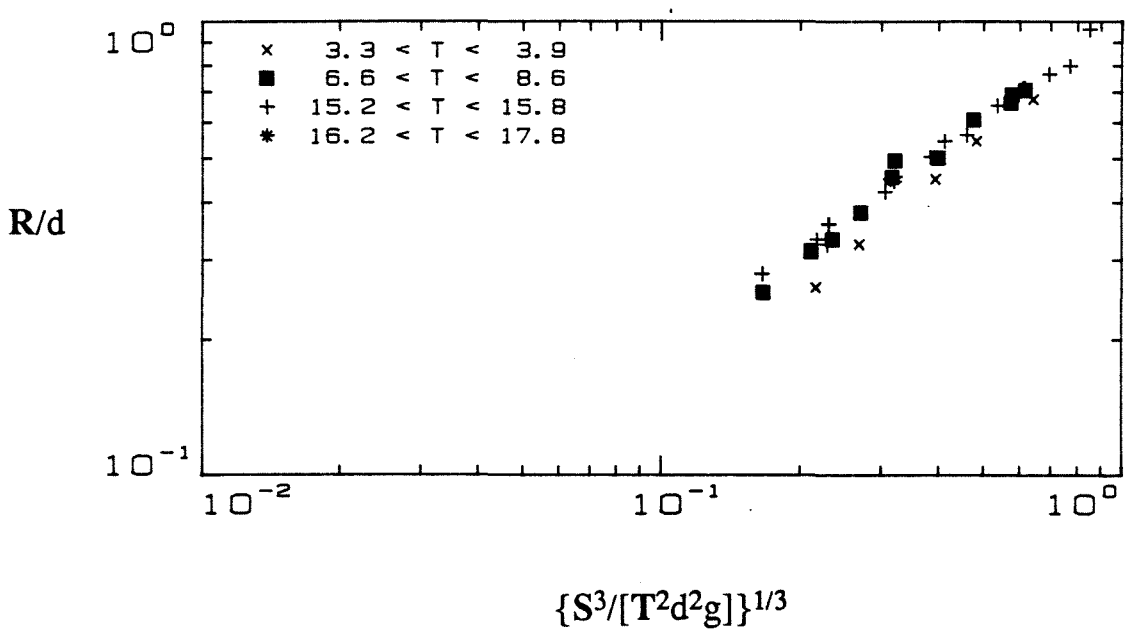

Figure 4.3.2a The runup variation versus the energy scale for type R breaking waves.

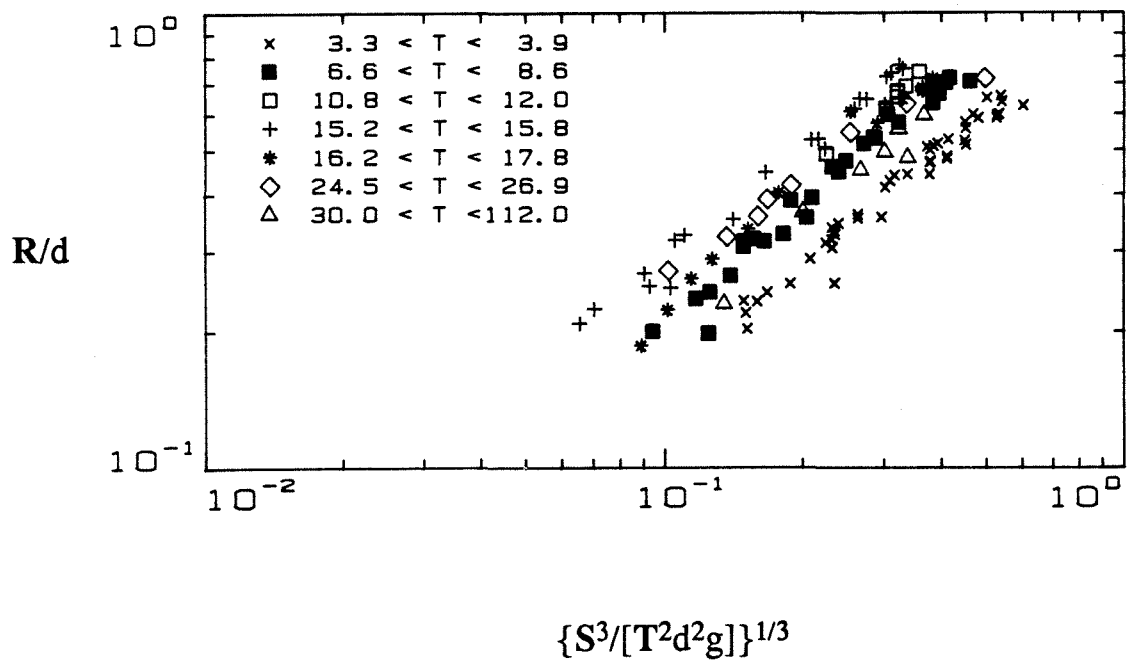

Figure 4.3.2b The runup variation versus the energy scale for type S breaking waves.

in the power law (4.3.4) is less than one, and this implies that the runup is less sensitive to increases in energy than what the kinematic analogy predicts. This behaviour is anticipated because energy dissipation reduces the available energy for the runup; as the energy increases the rate of energy dissipation also increases and the runup increases at a slower rate than if there was no dissipation. Therefore, the momentum relationship (4.3.2a) is more appropriate than the energy relationship (4.3.2b) in modelling runup.

Since the runup number $R_u = \mathbf{R}g^{1/5}/(S^2d/T)^{2/5}$ scales as predicted from the kinematic argument, it is interesting to check whether it is a function of other generation parameters. The dimensional analysis of section 4.2 suggests that the following relationship may exist between the independent variables when the propagation distance and the bed roughness are constant :

$$\frac{\mathbf{R}g^{1/5}}{(S^2d/T)^{2/5}} = f\left(\frac{S}{T\sqrt{gd}}, \frac{S}{d}, \beta, \frac{Sd}{T\nu}\right) \qquad (4.3.5)$$

Figure (4.3.3) presents the runup number plotted as a function of three of the four independent variables of (4.3.5) for type R waves. (No data were available for other beach slopes.) The figures include data from waves that break only as they climb up the beach. It is seen that for the runup number is nearly independent of the S/d, the generation number $S/T\sqrt{gd}$, and the Reynolds number Re. It is also seen that the R_u, is relatively independent of the generation time. The average value of the runup number for breaking type R waves is 0.7437. (See table T4.1) Figure (4.3.4) presents the runup number as a function of S/d, and $S/T\sqrt{gd}$ for type S waves. (See table T4.2, also.) It does appear that the runup number is a weak function of the generation time and that breaking waves have higher runup numbers than nonbreaking waves, breaking-reforming waves and bores of finite volume. The average runup number for type S waves is 1.014 .

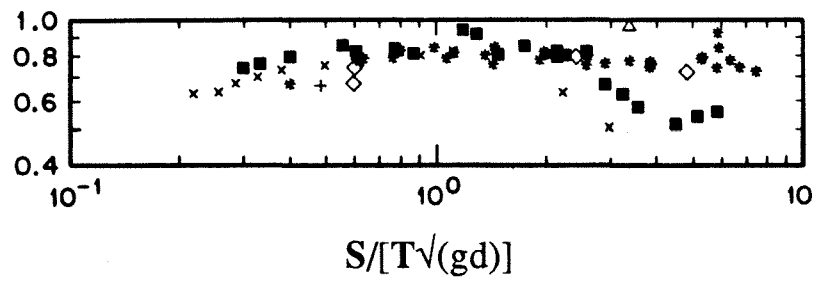

Figure 4.3.3a The runup number variation with the generation number. Type R waves.

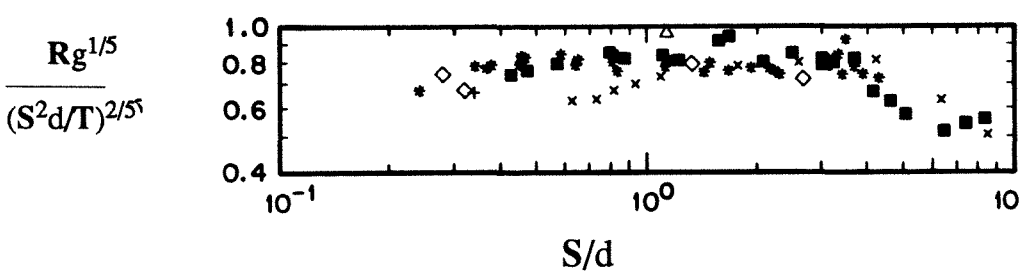

Figure 4.3.3b The runup number variation with the stroke of the generator. Type R waves.

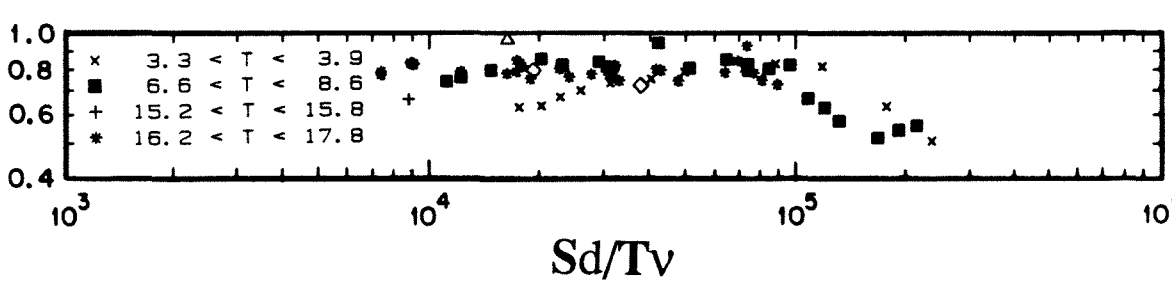

Figure 4.3.3c The runup number variation with the generation Reynolds number. Type R waves.

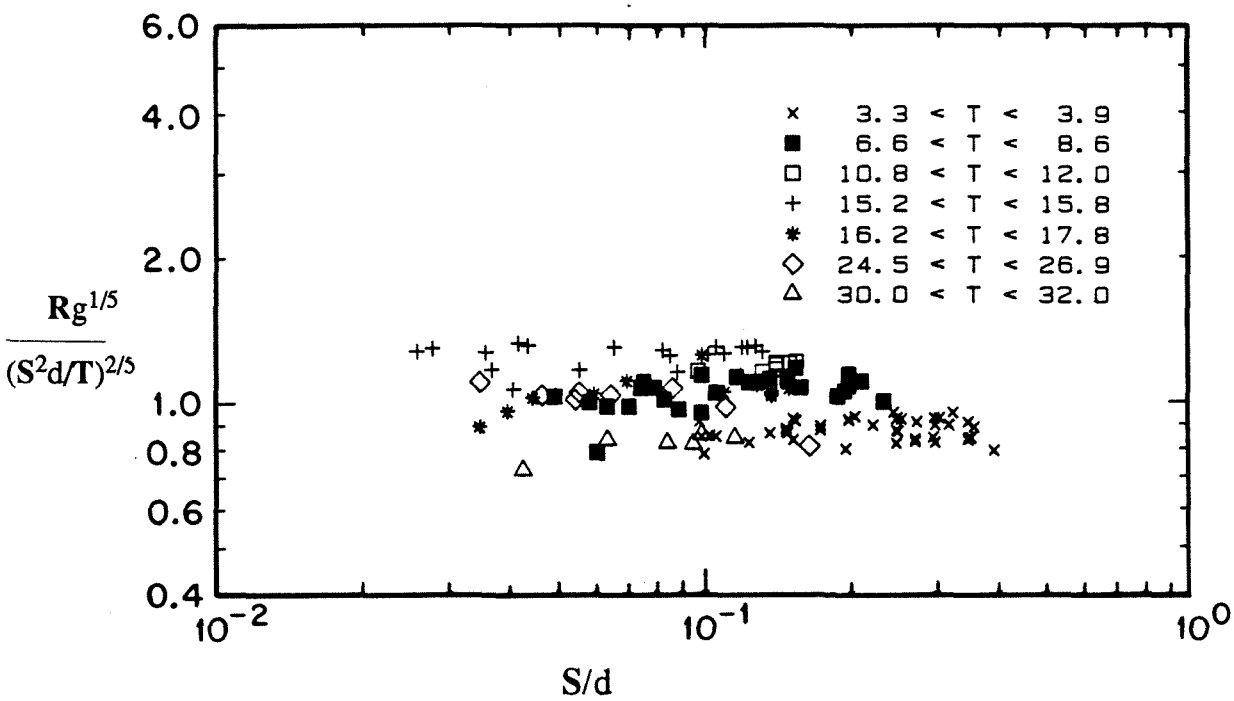

Figure 4.3.4a The runup number variation versus the stroke of the generator. Type S waves.

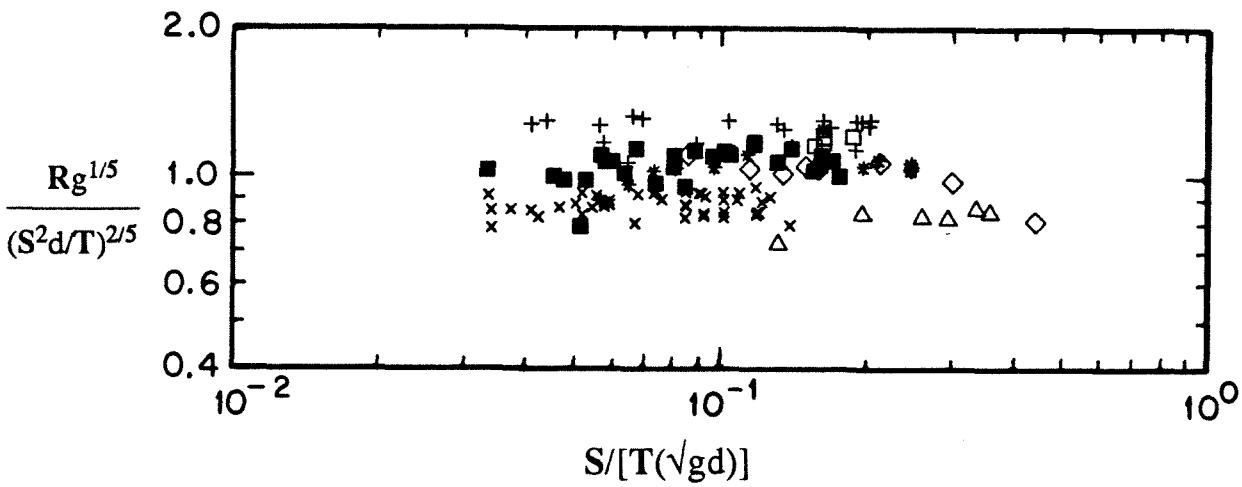

Figure 4.3.4b The runup number variation versus the generation number for type S waves.

Figure (4.3.5) compares the runup number variation with the generation number for three different wave families : type R, type S and type P waves . Type P waves were generated with a parabolic shaped trajectory ; an example of the piston motion and the resulting surface wave motion is shown in figure (4.3.6). Solitary waves are formally type S waves but they are identified in (4.3.5) explicitly. The average runup number for all waves represented in figure (4.3.5) is 1.023 with a standard deviation equal to 0.04675.

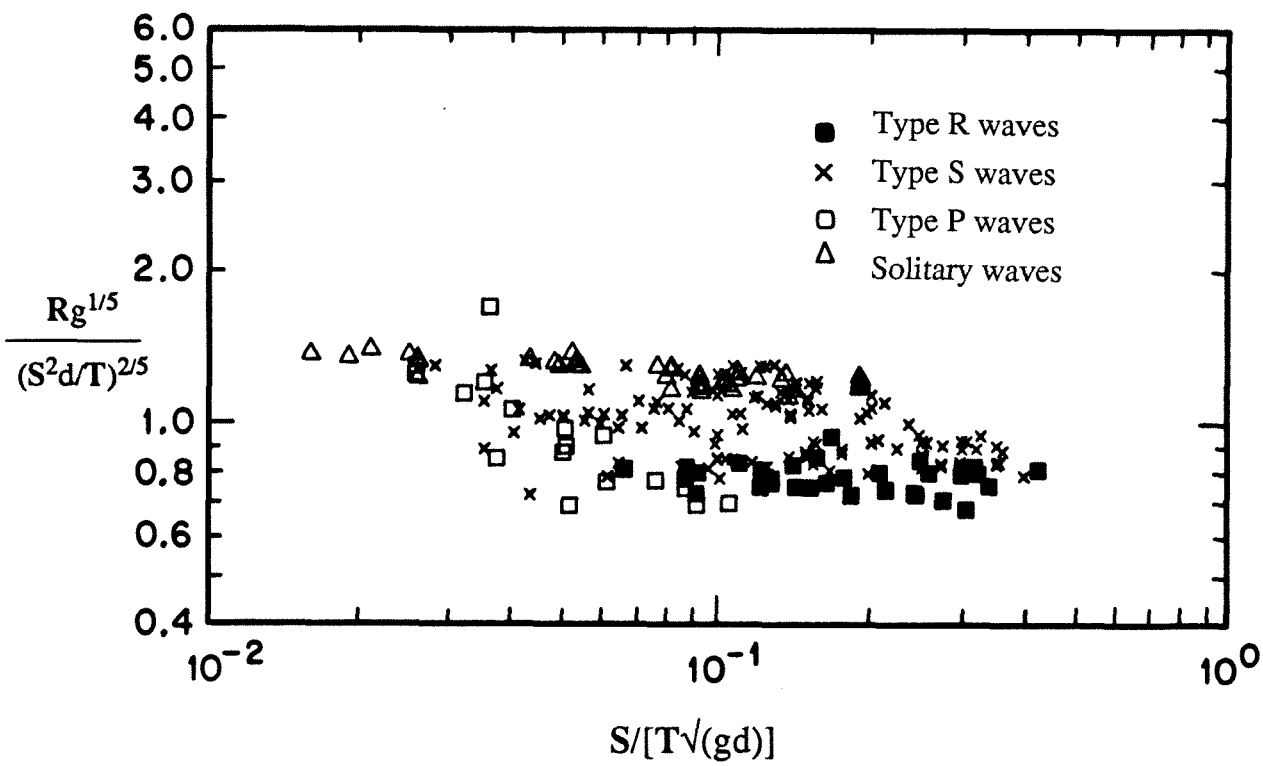

Figure 4.3.5 The runup number variation with the generation number for type R, S and P breaking waves. Type P waves are described in figure (4.3.6). The figure above includes data from the runup of solitary waves (defined by equation (3.4.1).

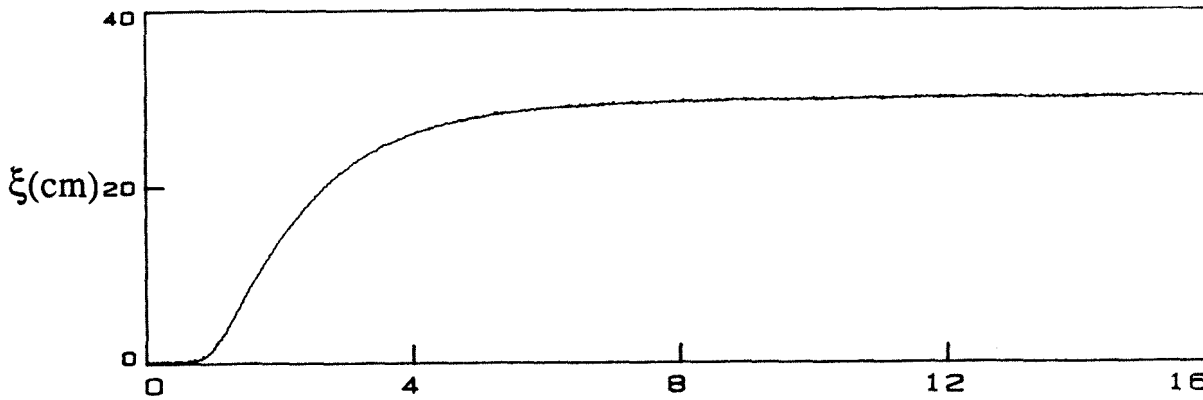

Figure 4.3.6a The trajectory for generating a type P wave.

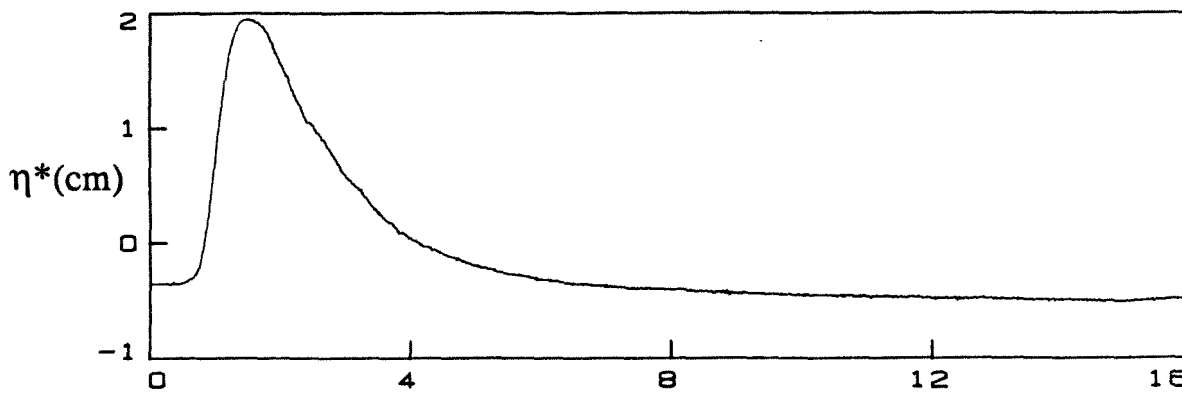

Figure 4.3.6b The wave height at the plate resulting from the morion in figure (4.3.6a).

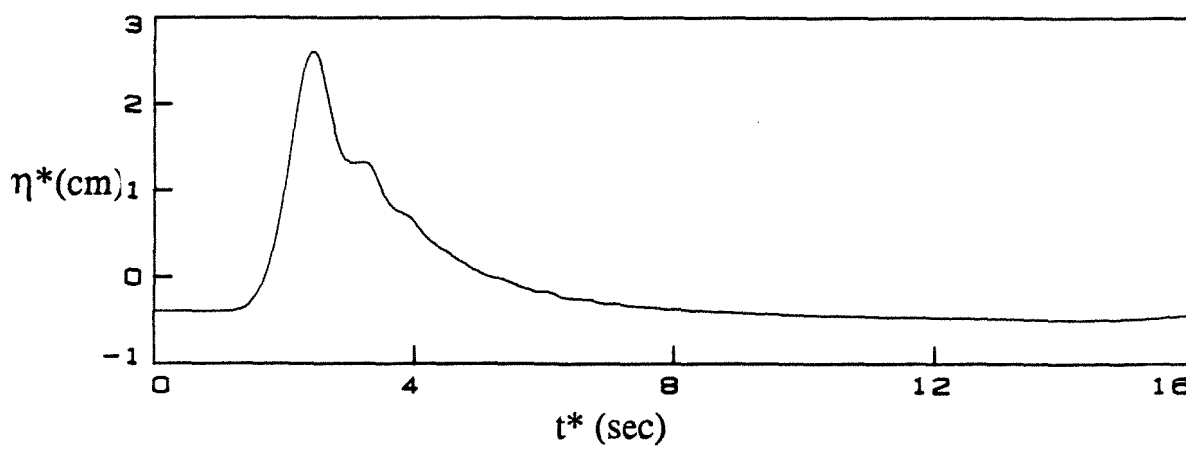

Figure 4.2.1c The resulting wave motion at 20 depths from the toe of the beach.

An interesting observation is suggested by figure (4.3.5). Solitary waves have the highest runup number among all other waves in the figure. This implies that if a solitary wave and another long wave (type R, S or P) have generation characteristics such that the momentum scale S^2d/T is the same for the two waves, the runup of the solitary wave will be bigger or equal to the runup of the other long wave. Only type S waves may have runup numbers as large as solitary waves, and an examination of such S wave data revealed that those waves had generation characteristics similar to solitary wave characteristics.

This phenomenon can be explained if it is realized that arbitrary plate motions usually generate waveforms consisting of one leading wave and a train of oscillatory waves. (See, for example, figures (4.2.3) or (4.2.6b)). It is reasonable to suppose that *the runup of a long waveform will be primarily affected by the momentum of the leading wave that emerges from the long wave group.* This momentum is less that the generated momentum which is partitioned between the leading wave and the tail ; therefore a solitary wave with the same momentum will have higher runup. This conclusion can also be deduced if one recalls that according to the nonlinear dispersive wave theory *any* long wave of arbitrary shape and positive volume will eventually split into a series of solitary waves, analogously to the manner with which the linear dispersive theory predicts that any wave will split into a series of periodic waves with different wavenumbers ; the calculation of the emerging solitary waves at infinity can be performed with the inverse scattering algorithm first developed by Gardner et al. (1967).

This is a very exciting result. It suggests that it may be possible to determine the highest runup number on a sloping beach simply by calculating the runup number of solitary waves on the same beach. It is therefore quite interesting to relate the energy and momentum parameters presented with the energy and mometum integrals of motion at generation and to determine whether similar results can be obtained.

4.4 Integrals of the motion. Impulse, Power, Energy flux and Momentum flux. In this section four integrals of motion will be described, and their relationhip to the maximum runup will be presented for three different wave types, waves generated with a ramp trajectory (type R waves), waves generated with a solitary wave type trajectory (type S waves) and waves generated with a parabolic wave (type P waves). It will be shown that two flux integrals have a relationship with the runup which appears to be independent of the wave type and the generation time. Each integral of motion will be evaluated by reference to two figures. One of the figures will present the variation of the particular integral of motion with the generation time for breaking type R waves. The other figure will include data from experiments with type R, type S and type P waves. The data in this figure will include nonbreaking waves, breaking waves, broken waves, and bores of finite volume.

4.4.1 The impulse integral. The momentum of any two dimensional wave motion generated by a moving partition can be related directly with the impulse of the generating mechanism. In the case of a plane wavemaker generating waves in a frictionless fluid, the generated momentum equals the impulse of the force on the piston.

To calculate the impulse imparted to the wave motion by the generation process, the momentum conservation equation in its integral form will be used. One may consider a material control volume, or a control volume of fixed geometry through which fluid flows. In the first case, one may use the conservation of momentum equation in the form :

$$\underline{F} = \frac{d\underline{M}}{dt^*} \quad , \tag{4.4.1}$$

where $\underline{M}$ is the momentum contained in a control volume . (Symbols with underbars

indicate vectorial quantities.) The momentum is given by :

$$\underline{\mathbf{M}} = \int_{cv(t)} \rho \underline{\mathbf{v}} \, dvol \ . \tag{4.4.2}$$

Consider a control volume cv(t) which always contains the same mass; at the end of the plate motion the control volume coincides with the volume PP'DA of figure (4.1.1). The length of the volume is such that, at the end of the piston motion, when $t^* = \mathbf{T}$, the wave has not yet reached the toe of the beach. Initially, at time $t^*=0$, the fluid is at rest. As the plate moves, momentum is generated due to the action of surface forces. Assume that there is no fluid behind the plate. The total momentum imparted by the plate to the wave motion is calculated by integration of (4.4.1), as follows :

$$\int_0^T \underline{\mathbf{F}} \, dt^* = \int_0^T \frac{d}{dt^*} \int_{cv(t)} \rho \underline{\mathbf{v}} \, dvol \ dt^* = \int_{cv(T)} \rho \underline{\mathbf{v}} \, dvol - \int_{cv(0)} \rho \underline{\mathbf{v}} \, dvol \ . \tag{4.4.3}$$

At $t^*= 0$ there is no momentum in the fluid, and the corresponding integral in (4.3.3) is zero. The first integral represents the momentum in the fluid at time $t^*=\mathbf{T}$. The total force equals the force acting on the plate minus the force on the right boundary of the control volume. Since the wave does not reach that boundary during the generation time, that force arises only from hydrostatic stresses. Then, (4.4.3) reduces to :

$$\int_0^T \mathbf{F}_{px} dt^* - \frac{1}{2} \rho g d^2 \mathbf{T} = \mathbf{M}_x (\mathbf{T}) \tag{4.4.4}$$

where $\mathbf{F}_{px}$ is the force per unit width on the plate in the x-direction and $\mathbf{M}_x$ is the momentum per unit width in the same direction.

Equation (4.4.4) can be used to calculate the momentum imparted to the wave motion by the plate motion. In appendix A an exact theory is derived to determine the force $\mathbf{F}_{px}$ on the plate during wave generation. This theory will now be used to determine the impulse. The law of the plate (A1.16) requires that the force on accelerating vertical plate in a fluid with a free surface with wave height at the plate η_p and depth d is given by :

$$\mathbf{F}_{px} = \frac{1}{2}\rho g\,(\eta_p + d)^2 + \frac{1}{3}\rho\,(\eta_p + d)^2 \frac{d^2\eta_p}{dt^{*2}}. \tag{4.4.5}$$

The wave height on the plate was measured in many of the experiments presented in the previous section and (4.4.5) can be evaluated exactly. The force on the plate was also measured with a load cell. However, only in few cases it was possible to derive $\mathbf{F}_{px}$ directly from the load cell measurements. (See section (2.5)).

Figure (4.4.1) shows an example of the procedure used to calculate the impulse from load cell data. This is one particular motion for which reproducible results were obtained for the tare force on the plate. (This is the force needed to move the piston without any fluid in the tank.) The plate moves in a depth of 13.68 cm (5.38 in) for 4 sec with the ramp trajectory defined by (4.2.4). The force required for this motion is shown in figure (4.4.1a). Note that the increase in the force evident in the first milliseconds of the record is due to the fact that the fluid behind the piston has drained. Figure (4.4.1b) shows a measure of the piston velocity and figure (4.2.1c) shows the wave amplitude at the piston. Figure (4.4.1d) shows the impulse due to the motion of the plate with fluid in the tank which is the integral of the force shown in figure (4.4.1a) and the impulse due to the tare force. Figure (4.4.1e) compares the net impulse derived from the difference of the impulses in figure (4.4.1d) and the impulse derived from the law of the piston (4.4.5). It is seen that the law of the plate predicts the impulse quite well.

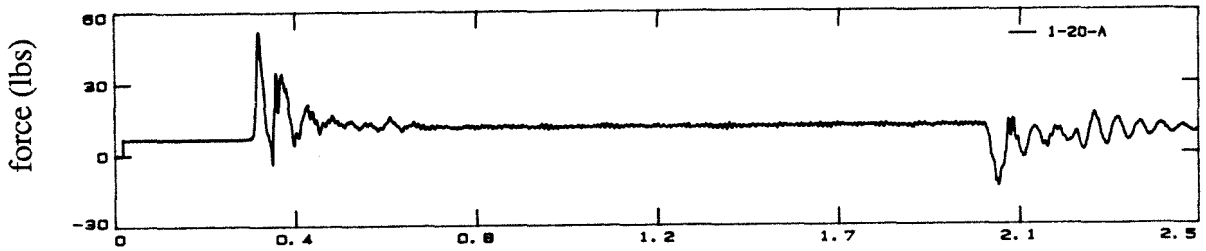

Figure 4.4.1a The force required to produce a type R wave in a depth of 13.68 cm, with generation number $S/[T\sqrt{(gd)}] = 0.24$ and $T\sqrt{(g/d)}=8.46$.

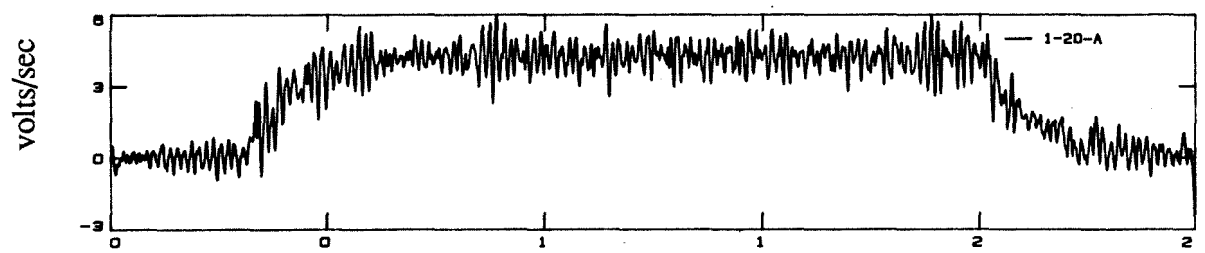

Figure 4.4.1b The plate velocity, in units of volts/sec, used to generate the type R wave described in figure (4.4.1a).

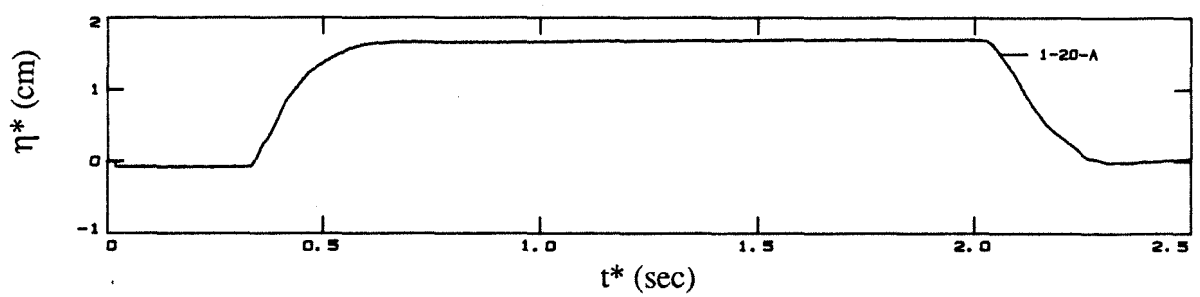

Figure 4.4.1c The wave height at the plate generated with the motion indicated in figure (4.4.1a)

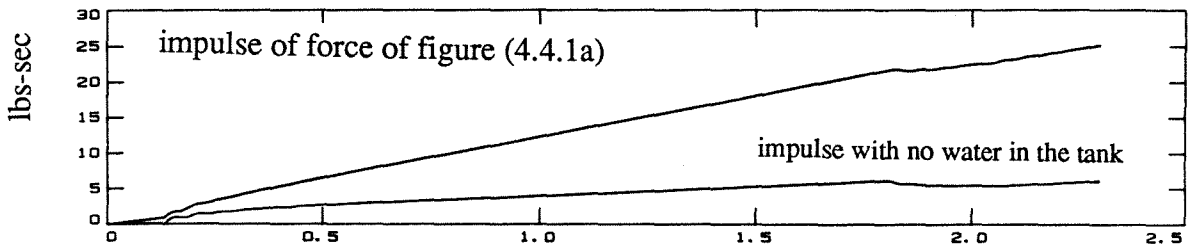

Figure 4.4.1d The impulse derived from the force (figure (4.4.1a)) and from the tare force required to move the plate.

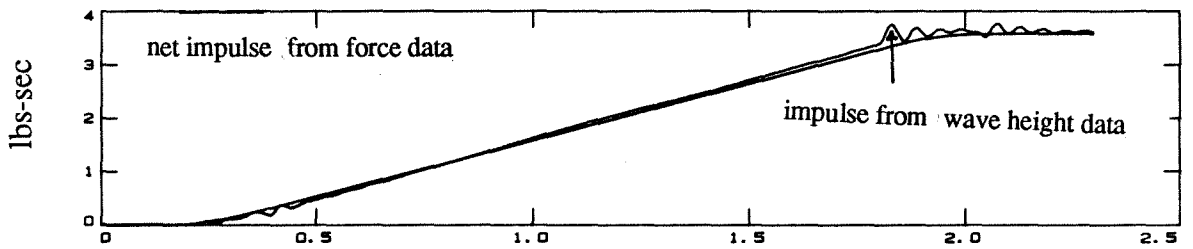

Figure 4.4.1e Comparison between the impulse of the force obtained from the load cell and data derived from equation (4.4.5).

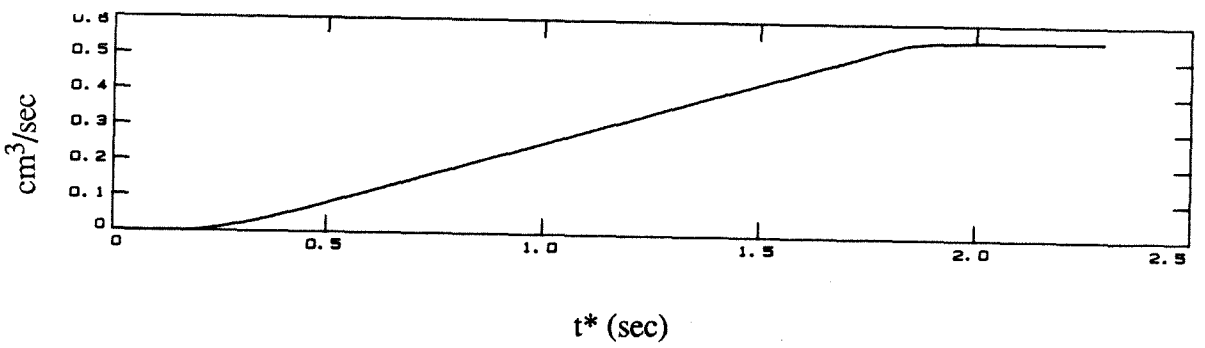

Figure 4.4.1f The integral of the momentum flux derived with the wave data of figure (4.4.1c).

Figure (4.4.2a) shows the maximum runup plotted against the measured impulse for type R waves. Figure (4.4.2b) shows the same variation for type R, S and P waves. For type R waves the relationship takes the form, $R/d = 0.334\ (\int F_p dt)^{0.567}$, where $F_p = F_p/(0.5\rho g d^2)$. Figure (4.4.2a) shows that the runup to impulse relationship exhibits a strong dependence upon the generation time. Figure (4.4.2b) indicates it is also a function of the wave type. It is obvious that the generated impulse is not motion invariant.

It is interesting to reflect why this is the case. If there is no significant reflection before the wave reaches its maximum beach excursion , the generated momentum determines the runup by the relationship $F_{bx} = dM_x/dt$, where F_b is the force on the beach due to the wave motion and M_x is the wave momentum contained in the material volume that includes the entire flow field; this is the volume PBCP' shown in figure (4.1.1). When the wave reaches the point of maximum runup, then $M_x = 0$; otherwise the wave would continue its climb. However, if there is reflection, then there is an additional force due to the generation of the reflected wave should be considered and this force may be responsible for a reduction in the momentum available to the wave. It is also possible that shear forces dissipate the momentum as the wave propagates over the constant depth region, so that the generated momentum is reduced before reaching the beach.

To obtain some insight into the first process, one may use the exact solution derived in chapter 3 to examine the forces acting on a sloping beach during wave runup. Consider the *fixed* control volume ABCD shown in figure (4.1.1). It consists of the volume between two vertical planes, one at the toe of the beach and the other at the point of maximum runup. The conservation of momentum in this volume requires that :

$$F_{Tx} = \frac{\partial M_{vx}}{\partial t^*} + \int_S \rho\, \underline{v}\, \underline{v}\cdot\underline{n}\, ds \ , \qquad (4.4.6)$$

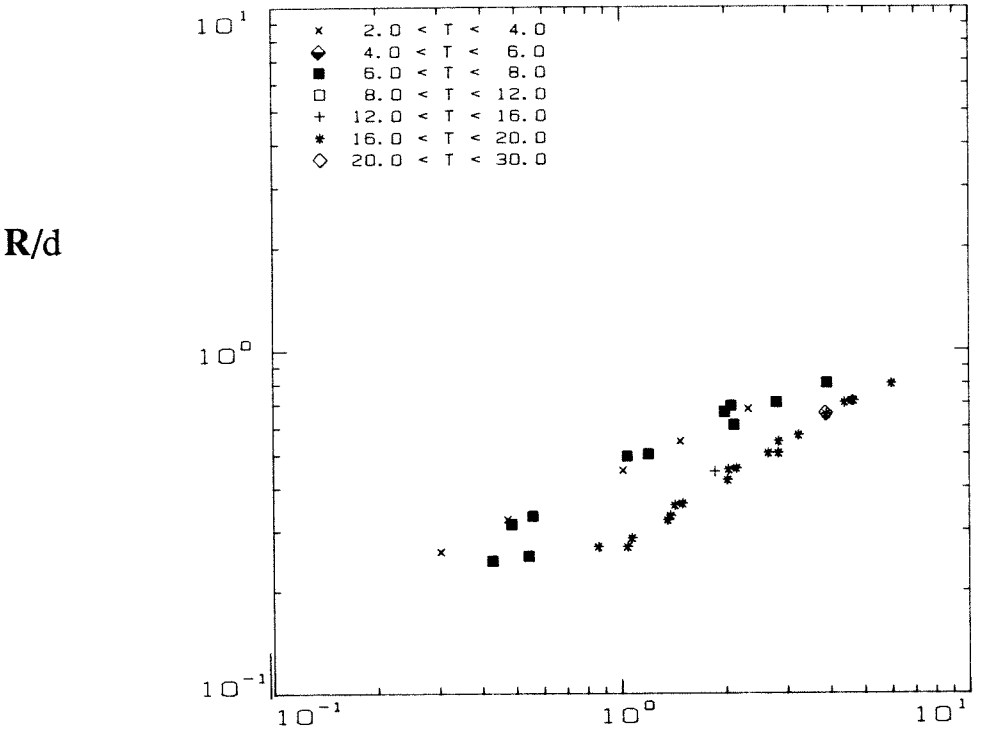

Figure 4.4.2a The runup vs impulse variation for type R breaking waves.

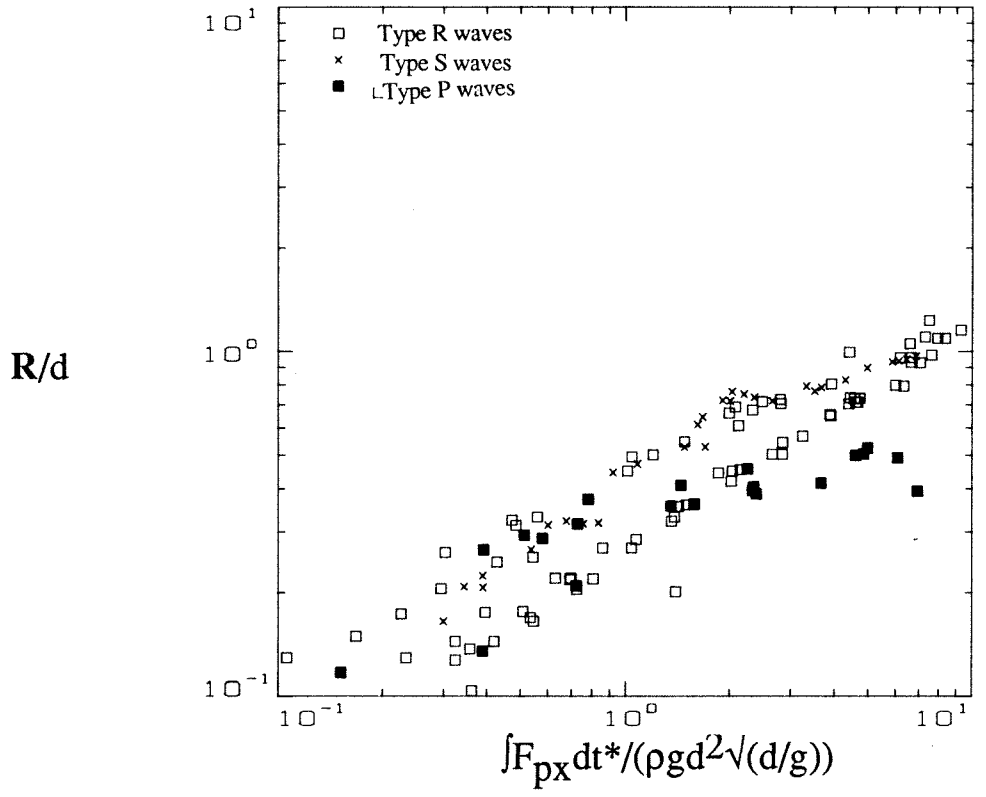

Figure 4.4.2b The runup vs impulse variation for type R, S and P waves.

$\mathbf{F}_{Tx}$ is the sum of all forces acting on the volume in the x-direction, $\mathbf{M}_{vx}$ is the momentum contained inside the volume and S is the surface of the volume. The forces acting on the volume are the reaction from the sloping beach to the hydrodynamic pressure due to the wave motion $\mathbf{F}_{bx}$, the force on the sea boundary of the beach (AB) $\mathbf{F}_{sx}$, and a force arising from shear stresses at the surface of the beach $\mathbf{F}_{dx}$. The forces $\mathbf{F}_{sx}$ and $\mathbf{F}_{bx}$, the integral of the flux, and $\partial \mathbf{M}_{vx} / \partial t^*$ can be evaluated, if one uses the shallow water formalism where the pressure is hydrostatic and where $u^*=c^*\eta^*/(\eta^*+d)$. In particular, the force on the sea boundary $x^*=X_0^*$ is given by :

$$\mathbf{F}_{sx}(t^*) = (1/2)\, \rho g\, [\eta^*(X_0^*, t^*) + d]^2 . \tag{4.4.7}$$

The momentum per unit width inside the control volume is :

$$\mathbf{M}_{vx}(t^*) = \rho \int_{X_0^*}^{x_s^*} u^*(x^*,t^*)\, [\eta^*(x^*,t^*) + d]\, dx^* \quad . \tag{4.4.8}$$

The force on the beach is determined from :

$$\mathbf{F}_{bx}(t^*) = -\, \rho g \tan\beta \int_{X_0^*}^{x_s^*} \eta^*(x^*,t^*)\; dx^* \quad , \tag{4.4.9}$$

and the flux integral is given by the flux of momentum through the sea boundary AB :

$$\int_{AB} \underline{\mathbf{v}}\, \underline{\mathbf{v}} \cdot \underline{\mathbf{n}}\, ds = \rho u^{*2}(X_0^*,t^*)[\eta^*(X_0^*,t^*) + d)] \tag{4.1.10}$$

For example, consider a solitary wave with H/d=0.040 climbing up a 1:19.85 beach. Equations (4.4.7) through (4.4.10) can be calculated as described in section 3.4. Figure (4.4.3) shows the evolution of the various terms of the momentum equation (4.4.6).

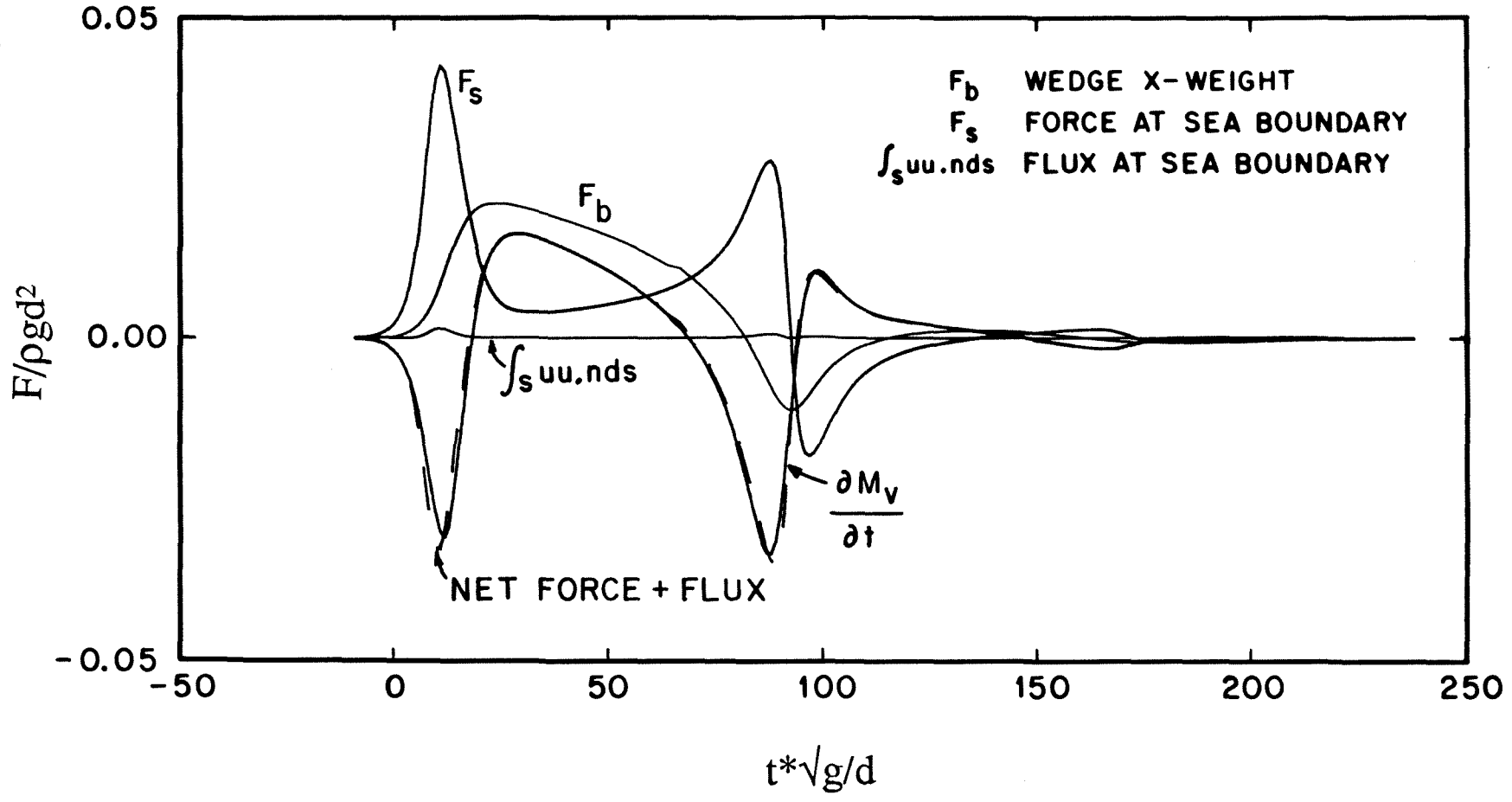

Figure 4.4.3 The evolution of the various forces in the momentum balance of equation (4.4.6).

It is seen that the momentum flux through AB is negligible and that the force on the beach $\mathbf{F}_{bx}$ and the force on the boundary $\mathbf{F}_{sx}$ determine the rate of change of momentum $\partial \mathbf{M}_{vx} / \partial t^*$. The evolution of $\mathbf{F}_{sx}$ clearly indicates continuous generation of a reflected wave; even at the point of maximum runup $t_{max} \sim 48$, there is still finite contribution from $\mathbf{F}_{sx}$ to the rate of change of momentum . Since the reflected wave is usually dependent on the incident momentum distribution, it is unlikely that different momentum distributions with identical momentum will produce the same runup.

4.4.2 The energy of the wave motion. The energy imparted to the wave motion can be calculated by computing the work done by the piston to generate the waves. At every step of the motion, the work, dw, is such that $\mathbf{dw} = \mathbf{F}_p \, dx^*$. The total work done by the piston can be found by integrating over the entire piston motion. If there are only conservative forces acting on the system, then this work is equal to the energy imparted to the wave motion, $\mathbf{E}_p$. This energy is given by :

$$\mathbf{E}_p = \int_0^T \mathbf{F}_{px} \frac{d\xi}{dt^*} dt^* \tag{4.4.11}$$

If data for the plate motion and for the wave height on the plate is available, then this integral can be calculated directly using (4.4.5) . Figure (4.4.4a) shows the runup variation with the energy for breaking type R waves. Figure (4.4.4b) shows the runup to energy relationship for type R, S and P waves. It is seen that the generated power does not describe the runup process in a unique fashion. This is not a surprising result given the non-conservative nature of the energy dissipation during wave breaking.

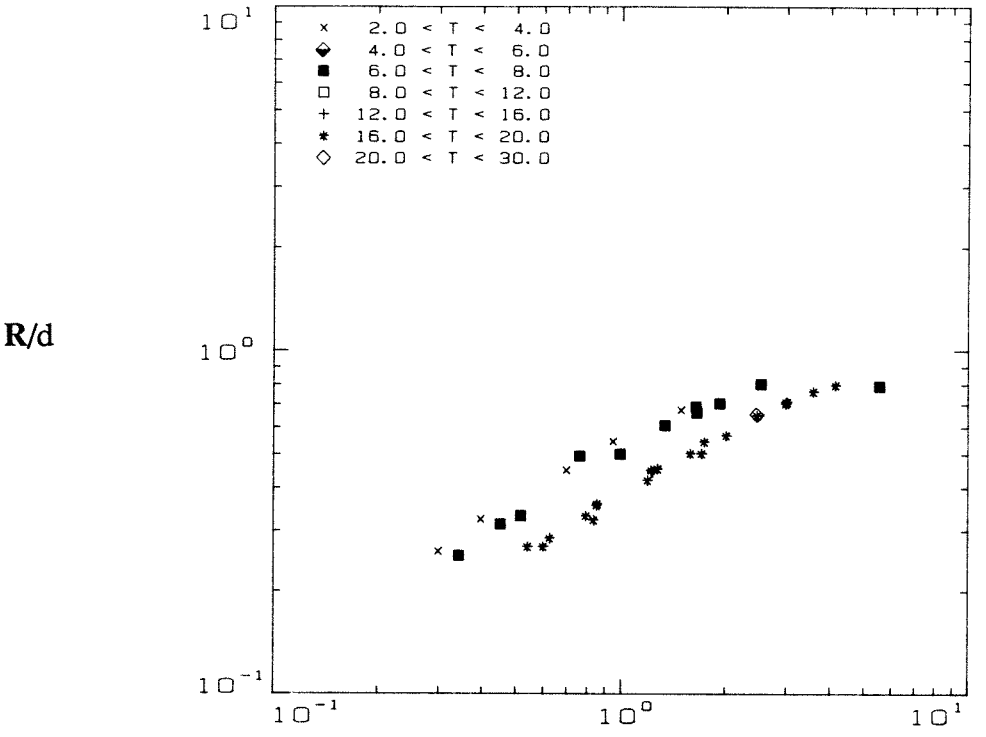

Figure 4.4.4a The runup versus energy variation for type R breaking waves.

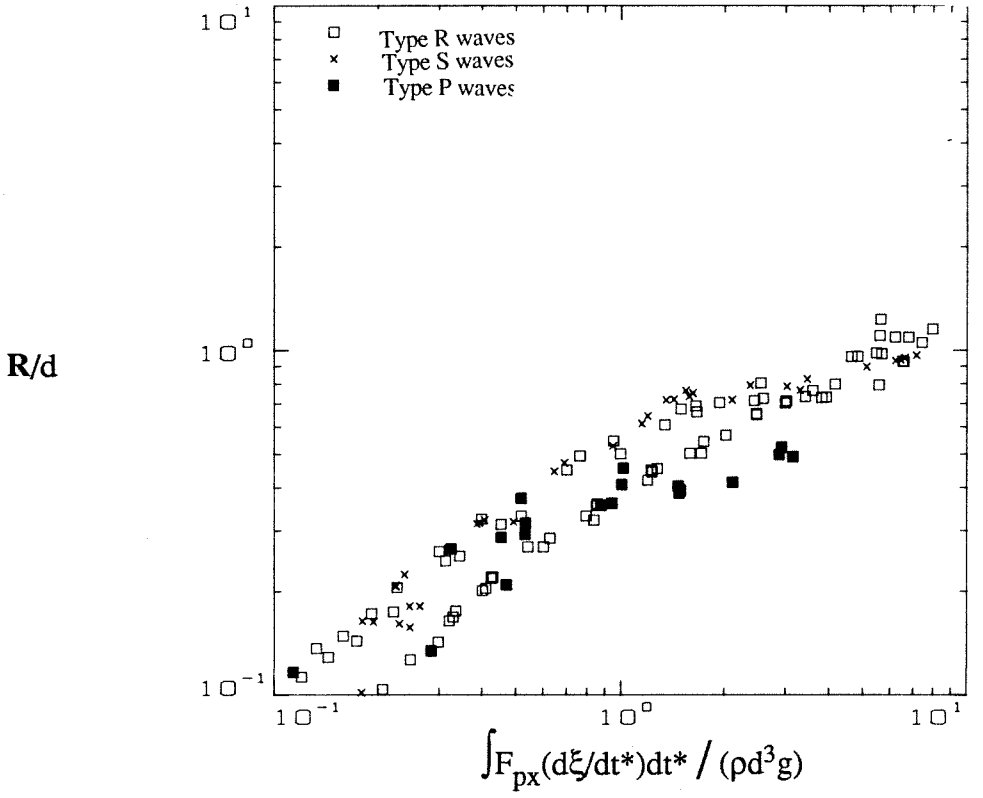

Figure 4.4.4b The runup versus energy variation for type R, S and P waves.

4.4.3. The integral of the momentum flux at the plate. In section 4.3 the runup number was shown to be a powerful concept in modelling the runup; to derive that number a momentum scale was introduced, S^2d/T . The integral of motion that scales in a similar fashion is the integral of the momentum flux at the plate.

The integral of the momentum flux at the plate per unit width and per unit mass is denoted by $\mathbf{P}_f$ and is determined as follows. When the piston moves a distance $d\xi$, it displaces a volume of fluid equal to $d\xi(\eta_p{}^*+d)$, where $\eta_p{}^*$ is the wave height at the front face of the piston. This volume of fluid acquires the piston velocity $d\xi/dt^*$. Then the momentum per unit mass imparted to the adjacent fluid column at every step is given by $d\xi(\eta_p{}^*+d)(d\xi/dt^*)$. Integrating over the duration of motion and using the substitution $d\xi=(d\xi/dt^*)dt^*$, one obtains :

$$\mathbf{P}_f = \int_0^T \left(\frac{d\xi}{dt^*}\right)^2 (\eta_p{}^*+d)\, dt^* \qquad (4.4.12)$$

It is interesting to note that, if the plate motion was generating a permanent form wave, then $\mathbf{P}_f$ would represent the local integral of the momentum flux. This is because, during wave generation, the water particle velocity is $u^*(\xi,t^*)=d\xi/dt^*$. In physical terms, the flux can be thought of as the excess transfer of momentum due to the wave motion and it resembles the radiation stress introduced by Longuet-Higgins and Stewart (1960) to model the wave-current interaction. When vertical accelerations are negligible, Longuet-Higgins (1962) showed that the radiation stress is directly proportional to the energy of the motion. However, the radiation stress formalism was derived for periodic wave motions and it is not obvious how it can be extended readily in solitary wave type propagation problems.

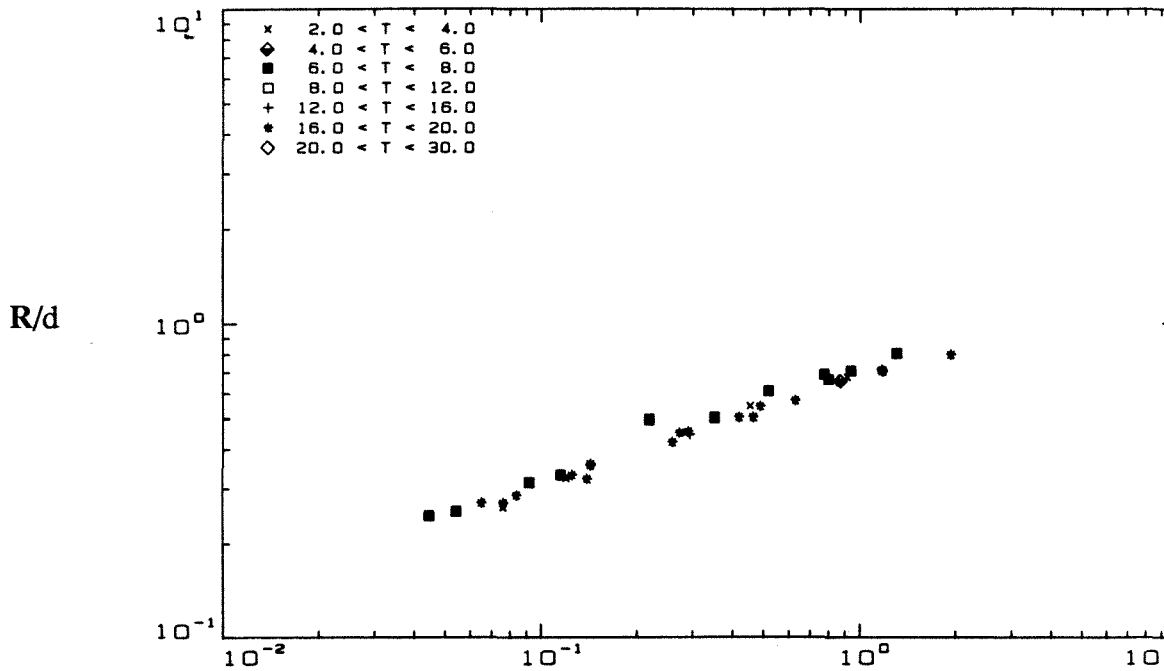

Figure 4.4.5a The runup variation with the integral of the momentum flux for type R breaking waves.

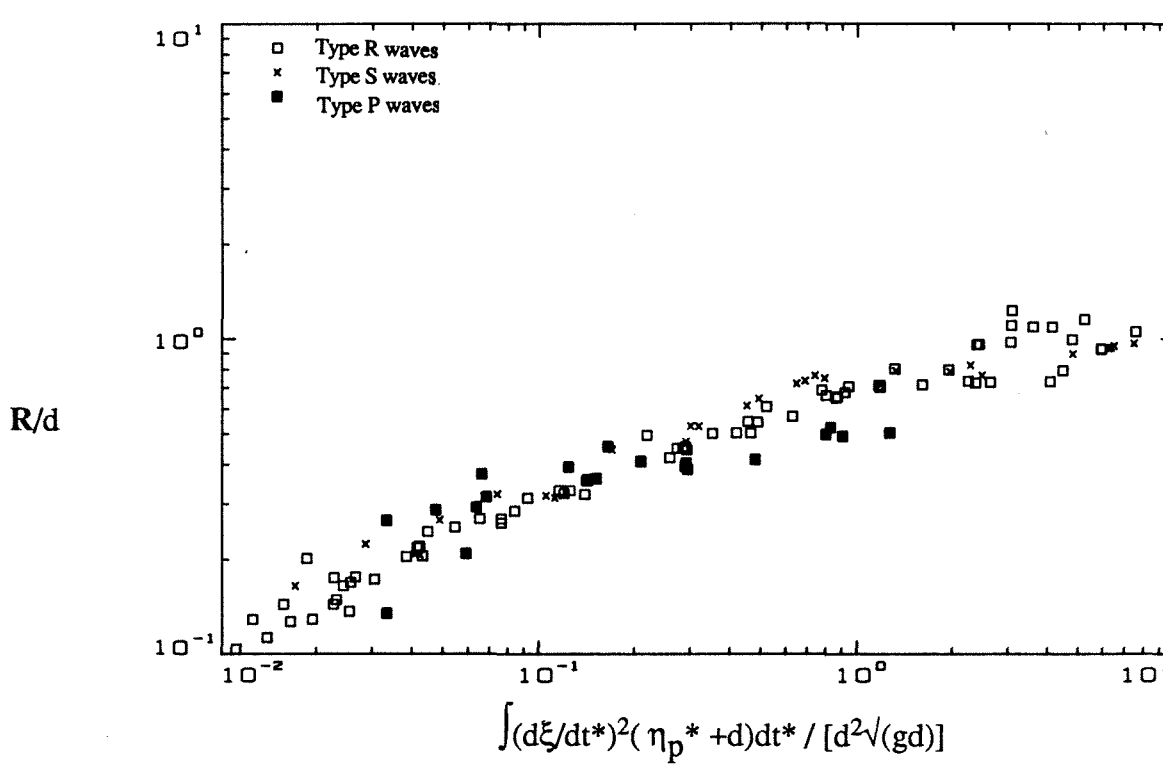

Figure 4.4.5b The runup variation with the integral of the momentum flux for type R, S and P waves.

Figure (4.4.5) shows the relationship between the runup and the integral of the flux for type R, S and P waves. For breaking waves, the integral of the momentum flux does seem to correlate well with the runup ; the relationship between the two variables is given by $\mathbf{R}/d = 0.644\, \boldsymbol{P}_f^{\,0.351}$. ($\boldsymbol{P}_f$ is the dimensionless integral of the momentum flux and is defined by $\boldsymbol{P}_f = \mathbf{P}_f / [d^2\sqrt{(gd)}]$.) It appears that $\mathbf{P}_f$ may be motion invariant.

4.4.4 The integral of the energy flux at the plate. One more flux integral maybe defined at the plate. During generation , the kinetic energy per unit width that the water column next to the plate acquires is $(1/2)\rho d\xi(\eta_p{}^*+d)(d\xi/dt^*)^2$. Then, the energy flux per unit width is given by :

$$2\,\mathbf{E}_f = \rho\int_0^T \left(\frac{d\xi}{dt^*}\right)^3 (\eta_p{}^*+d)\, dt^* \qquad (4.4.13)$$

This integral can be evaluated directly. If the generated wave was a permanent form wave, this integral would represent the integral of the energy flux past one vertical crossection of the flow field. Note that the energy scale derived from the characteristic length and time scales of generation at the piston is $(\mathbf{S}/\mathbf{T})^2\mathbf{S}d$, which is one measure of the mean value of $\mathbf{E}_f$ per unit mass .

Figure (4.4.6a) shows the variation of the runup with the energy flux for breaking type R waves. Figure (4.4.6b) shows the runup variation for type R, P, and S waves. The integral of the energy flux also correlates with the runup well. It is apparent that it is motion invariant, although it is not obvious why this is the case.

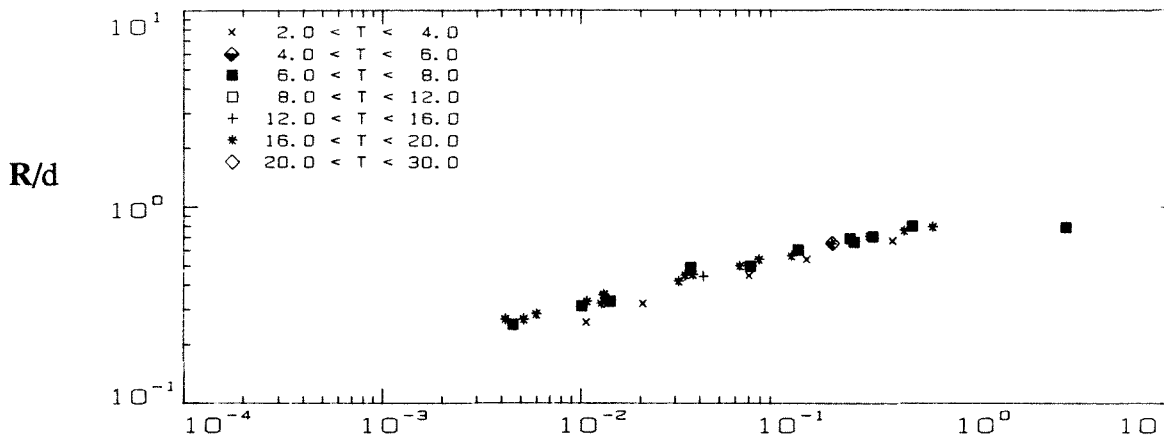

Figure 4.4.6a The runup variation with the integral of energy flux for type R breaking waves.

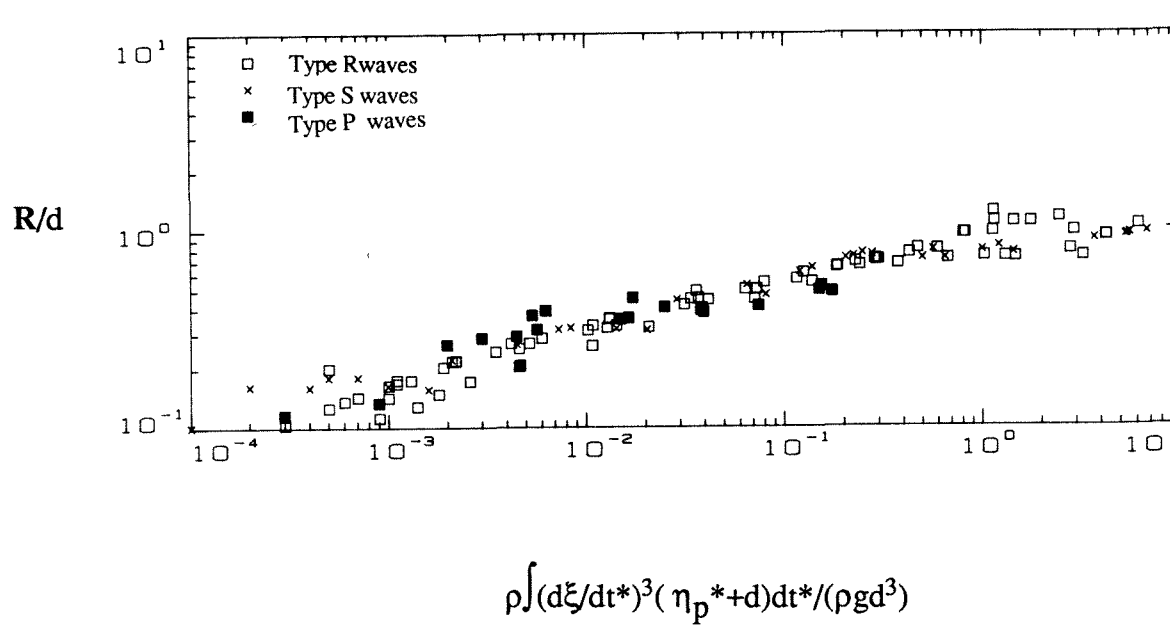

Figure 4.4.6b The runup variation with the integral of the energy flux for type R, S and P waves.

4.5 Summary and conclusions. In this chapter experimental results were presented for the runup of different types of long waves of different breaking characteristics. There are three major conclusions :

1) *There are maximum runup values a wave may attain depending on its breaking character,* i.e., whether a wave is a nonbreaking wave, a breaking wave, a breaking/reforming wave or a bore of finite volume. For the 1:19.85 beach, these values are given by :

Nonbreaking waves		$\mathbf{R}/d < 0.22$
Breaking waves	$0.19 <$	$\mathbf{R}/d < 0.81$
Breaking/reforming waves	$0.64 <$	$\mathbf{R}/d < 0.80$
Bores of finite volume	$0.77 <$	$\mathbf{R}/d < 1.10$

Similar runup regimes should exist for any beach slope. (The ranges will differ for different slopes). This is also suggested by the analysis of chapter 3, where breaking and nonbreaking waves were found to have different runup variations for all slopes where data are available.

2) *The generation characteristics of a long wave determine its runup.* In particular, if the momentum scale is estimated using the generation length and time scales, then the resulting dimensionless group is motion invariant. The runup number based on the momentum scale was introduced and it was shown that for a 1:19.85 beach:

$$R_u = \frac{\mathbf{R}g^{1/5}}{(S^2 d/T)^{2/5}} = 1.0 \pm 0.3 \qquad (4.5.1)$$

The exact value of the runup number depends weakly on the generation time and the wave type. It was also shown that the energy and momentum scales represent measures of the mean values of the integrals of the momentum flux and of the energy flux respectively and that the generated momentum and the generated power are not motion invariant.

3) *Breaking solitary waves have the highest possible runup number among all other wave types studied,* thereby providing a limiting condition for calculating wave runup.

The last two propositions are very intriguing, but it is necessary to obtain more data with long waves climbing up other beaches before drawing any conclusions for the generality of these results. However one may speculate that since the momentum scale is independent of the beach slope, then for any beach of angle β equation (4.5.1) should be replaced by :

$$\frac{\mathbf{R}g^{1/5}}{(\mathbf{S}^2\mathbf{d}/\mathbf{T})^{2/5}} = \mathbf{f}(\beta) \qquad (4.5.2)$$

Since solitary waves always emerge from arbitrary long waves of positive volume propagating over constant depth , it is reasonable to expect that the solitary wave will always represent a limiting waveform for calculating the runup on any given beach.

Chapter 5

Conclusions

The objective of this study has been the investigation of some of the fundamental processes associated with long wave runup on plane beaches. The outcome is an improved understanding of the runup process, an improved ability to predict long wave runup and the resolution of some unresolved questions about the interpetation of runup results.

The runup of nonbreaking long waves has been investigated theoretically and in the laboratory and good agreement has been obtained between the two endeavors. The empirical runup relationships have been explained by asymptotic analysis. Surface profiles during the runup process have been presented for the first time. The runup of breaking waves, waves that break and reform , and bores of finite volume has been investigated in the laboratory ; one momentum and one energy scale have been introduced to describe these waves. A runup number has been derived from the momentum scale and it has been found capable of describing the runup satisfactorily. Two other parallel investigations were conducted to assist the understanding of the phenomenology of long waves; an exact result has been discovered on the hydrodynamic forces on accelerating plate and a technique has been derived to generate arbitrary waveforms in the laboratory.

The following basic conclusions may be drawn from this study :

1) The linear theory predicts that the maximum runup of nonbreaking waves on plane beaches is given by the runup law:

$$\frac{R}{d} = 2.831\sqrt{\cot\beta}\left(\frac{H}{d}\right)^{5/4} \qquad (3.4.19)$$

This relationship models the laboratory data very well. The linear and the nonlinear theory when solved with identical initial conditions predict identical runup heights. The nonlinear theory models the details of the surface elevation of the climb of a long wave on a beach satisfactorily, indicating that dispersion is a much weaker process than nonlinearity during shoaling.

2) Two different runup regimes exist. Breaking and nonbreaking solitary waves exhibit different behaviour at maximum runup and cannot be modelled with relationships derived for nonbreaking waves. Nonbreaking solitary waves reflect continuously as they climb up a beach, while breaking waves reach their maximum shoreline excursion before significant reflection occurs.

3) The maximum runup that a long wave may achieve depends on its breaking characteristics. The following are the limiting values for each breaking category for the 1:19.85 beach :

Nonbreaking waves	$\mathbf{R}/d < 0.22$
Breaking waves	$0.19 < \mathbf{R}/d < 0.81$
Breaking-reforming waves	$0.64 < \mathbf{R}/d < 0.80$
Bores of finite volume	$0.77 < \mathbf{R}/d < 1.10$

4) Long waves propagating over constant depth can be described with the momentum scale S^2d/T. The runup of breaking waves can be modelled uniquely with the runup number based on this momentum scale. For waves climbing up a 1:19.85 beach, the runup number is given by :

$$\frac{\mathbf{R}g^{1/5}}{(S^2d/T)^{2/5}} = 1.023 \pm 0.3$$

The runup number will presumably have different values for different slopes. The momentum and the energy scales are measures of the average values of the integral of the momentum flux at the plate and the integral of the energy flux at the plate respectively ; the generated impulse and energy imparted to the wave motion are not motion invariant.

5) Nonbreaking, breaking, breaking-reforming waves and bores of finite volume have runup numbers that are smaller or equal to the runup number of breaking solitary waves. This allows for the determination a conservative estimate for the highest possible runup on a sloping beach.

6) The force on an accelerating vertical plate in an inviscid fluid with a free surface can be calculated exactly with the law of the plate :

$$F = \rho \frac{1}{2} gd^2 + \frac{1}{3} \rho d^2 \frac{d^2\eta_p{}^*}{dt^2} \qquad \text{(A1.16)}$$

This result is a consequence of the fact that the vertical velocity on the front face of the plate is distributed linearly over the depth. It imposes limits on the range of validity of the classical wavemaker theory when the latter is used to calculate forces.

7) Continously evolving long waves can be generated at any location in a two- dimensional laboratory model using the backwards propagation and generation (BPG) algorithm. The algorithm can reproduce satisfactorily waveforms that would otherwise have evolved after a breaking wave reforms after it propagates over constant depth.

Appendix A

The calculation of the hydrodynamic forces on an accelerating plate in a fluid with a free surface.

Introduction. The problem of determining the forces on an accelerating plate in a fluid with a free surface has been studied extensively in account of its fundamental consequences in two different fields. In earthquake engineering it is of importance in the designing of dams to withstand seismic motions; during strong ground shaking dams move and displace the adjacent reservoir fluid, inducing hydrodynamic pressures that must be properly accounted for in the dam design. In coastal engineering, determination of this force is necessary in designing equipment to generate waves in the laboratory, or when solving wave generation problems. Exact knowledge of the solution of the equations of motion is essential for determining the forces on the plate and for establishing the boundary conditions to be used for calculations of the resulting wave motion.

The classical theory of determining forces on moving plates was developed by Westergaard (1933). He solved the linearized equations of motion and derived an expression for the hydrodynamic pressures exerted on a vertical dam undergoing simple harmonic motion. Von Kármánn (1933) used a heuristic argument to derive an approximation to Westergaard's result, but assumed that the free surface remains undisturbed during the dam motion. Zangal and Heafeli (1952) considered the case of a dam whose upstream face is not vertical and determined the pressure with an electrical analog model. Chwang and Housner (1978) generalised von Kármánn's approach for dams with sloping faces. Chwang (1978) solved the same problem with potential flow. With the exception of Westergaard's work, all other investigations have implicitly assumed that the dam moves with constant acceleration

and that the water surface remains undisturbed during the dam motion. This approach is equivalent to assuming that the hydrodynamic forces during the dam motion are due to the displacement of a fluid confined in a region adjacent to the dam. This is known as the *classical hydrodynamic dam theory*. Chwang (1983) attempted to include the effect of the the motion of the dam to the free surface, but did not include the effect of the free surface to in the calculation of the hydrodynamic force.

Havelock (1929) first solved the problem of forced gravity surface waves in water using the linear theory. Kennard (1948) solved the same problem with a different method. In a series of papers, Biésel (1948), and Biésel and Souquet (1951) derived the solution for a simple wavemaker undergoing simple harmonic motion. In a classic paper, Ursell et al. (1960) verified the linear theory in the laboratory. Gilbert et al. (1971) generalised the wavemaker theory for random small amplitude waves. The small amplitude wave generation theory developed in these investigations is known as *the wavemaker theory*.

Despite this extensive amount of work, there had been no solution to the problem of calculating the forces on a plate moving with variable acceleration, or to that of wavemaker generating finite amplitude waves. The latter problem is discussed in appendix C. A method will be presented next to calculate the hydrodynamic force on a moving plate directly.

A.1 Calculation of the hydrodynamic force on an accelerating plate. The law of the plate. In this section an exact theory will be presented for calculating the hydrodynamic force acting on an accelerating, rigid, vertical plate, given the piston motion and the water depth on the piston during its motion. The derivation proceeds by first deriving a result for the gradient of the horizontal velocity $\partial u/\partial x$. The vertical velocity distribution on the plate is determined, and then it is used in the equations of motion for inviscid flow to evaluate the pressure.

Consider a moving rigid plate PP' as shown in figure (A1.1). The origin of the coordinate system is at the initial position of the plate. The displacement of the plate from its initial position is $\xi(t)$.

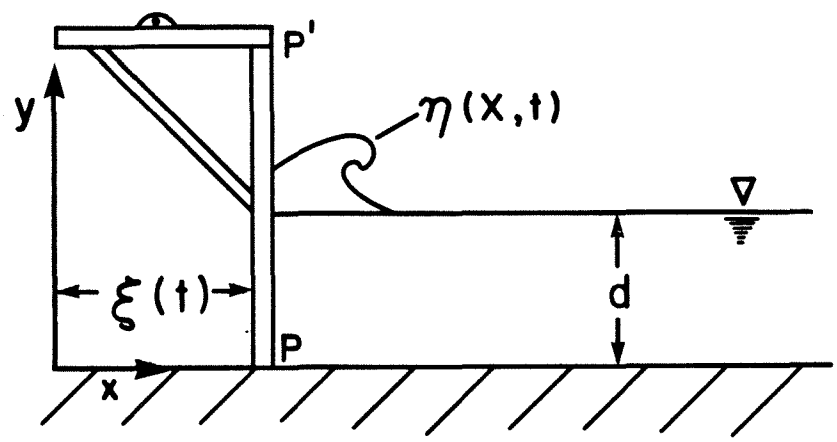

Figure A1.1 A definition sketch for wave generation.

The appropriate boundary condition for the fluid motion is that the fluid adjacent to the plate move with the same velocity as the plate. This requirement can be expressed as :

$$\frac{d\xi}{dt} = u\ (x=\xi(t),\ y,\ t) \text{ for all y such that } 0 \le y \le \eta(x,t) + d \qquad \text{(A1.1)}$$

Note that all variables in this discussion are ***dimensional,*** *unless otherwise stated.*

Differentiating (A1.1) with respect to time, one obtains :

$$\frac{d^2\xi}{dt^2} = \left.\frac{du}{dt}\right|_{x=\xi(t)} = \frac{\partial u}{\partial t} + \frac{d\xi}{dt}\frac{\partial u}{\partial x}, \qquad \text{(A1.2)}$$

since $\partial u/\partial y$ is zero at the plate, a consequence of the rigidity of the plate. Integrating this equation over the entire depth, i.e., from $y = 0$ to $y = \eta(x,t) + d$, one obtains:

$$\int_0^{\eta+d} \frac{d^2\xi}{dt^2} dy = \int_0^{\eta+d} \frac{\partial u}{\partial t} dy + \frac{d\xi}{dt} \int_0^{\eta+d} \frac{\partial u}{\partial x} dy. \tag{A1.3}$$

The integral on the LHS can be integrated directly since the integrand is not a function of y. The first integral of the RHS can be integrated using Leibniz's rule to give :

$$\int_0^{\eta+d} \frac{\partial u}{\partial t} dy = \frac{\partial}{\partial t} \int_0^{\eta+d} u dy - \frac{\partial \eta}{\partial t} u \Big|_{\eta+d} = (\eta + d) \frac{\partial u}{\partial t}. \tag{A1.4}$$

The second integral of the RHS of equation (A1.3), $\int (\partial u/\partial x)\, dy$, can be evaluated by substitution, if one uses the two-dimensional conservation of mass equation for an incompressible fluid, $\partial u/\partial x = -\partial v/\partial y$. This process results into :

$$\int_0^{\eta+d} \frac{\partial u}{\partial t} dy = -\int_0^{\eta+d} \frac{\partial v}{\partial y} dy = -v \Big|_{x=\xi, y=\eta+d}. \tag{A1.5}$$

Then, equation (A1.3) reduces to :

$$\frac{\partial u}{\partial t} = \frac{d^2\xi}{dt^2} + \frac{d\xi}{dt} \frac{v \Big|_{x=\xi, y=\eta+d}}{\eta + d}. \tag{A1.6}$$

Equation (A1.2) can now be used to find $\partial u/\partial x$. Then :

$$\frac{\partial u}{\partial x} = -\frac{v \Big|_{x=\xi, y=\eta+d}}{\eta + d}. \tag{A1.7}$$

(In the equation for $\partial u/\partial x$ the kinematic free surface condition was used to eliminate v.)

Integrating the conservation of mass equation along the path $x = \xi(t)$, one obtains that :

$$v(x = \xi, y, t) = \frac{d\eta}{dt}\frac{y}{\eta + d}. \tag{A1.8}$$

which is the vertical velocity distribution on the accelerating plate. Now, consider the equation of vertical motion for inviscid flow,

$$-\frac{1}{\rho}\frac{\partial p}{\partial y} = g + \frac{Dv}{Dt}. \tag{A1.9}$$

where D/Dt is the material derivative operator. Integrating from 0 to y, one obtains that :

$$-\frac{1}{\rho}[p(x, y, t) - p(x, 0, t)] = gy + \int_0^y \frac{Dv}{Dt}dy. \tag{A1.10}$$

Applying this equation at $y = \eta + d$, assuming that $p_{atm} = 0$, and given the requirement of the continuity of pressure across the free surface, then :

$$-\frac{1}{\rho}p(x, 0, t) = \int_0^{\eta+d} \frac{Dv}{Dt}dy. \tag{A1.11}$$

Substituting this equation into equation (A1.10), the vertical pressure distribution results :

$$-\frac{1}{\rho}p(x, y, t) = g(\eta + d - y) + \int_y^{\eta+d} \frac{Dv}{Dt}dy. \tag{A1.12}$$

To evaluate it, it is useful to calculate the material derivative $Dv/Dt = \partial v/\partial t + u\partial v/\partial x + v\partial v/\partial y$. Let d/dt denote the operator $\partial/\partial t + u\partial/\partial x$ evaluated at $x = \xi(t)$. Then,

$$\frac{Dv}{Dt} = \frac{d}{dt}\left(\frac{y}{\eta + d}\frac{d\eta}{dt}\right) + \frac{\partial}{\partial y}\left[\frac{1}{2}\frac{y^2}{(\eta + d)^2}\left(\frac{d\eta}{dt}\right)^2\right]. \tag{A1.13}$$

where use was made of equations (A1.7) and (A1.8). Evaluating this expression gives :

$$\frac{Dv}{Dt} = \frac{y}{\eta + d}\frac{d^2\eta}{dt^2}. \tag{A1.14}$$

Substituting this result into the equation of motion yields :

$$-\frac{1}{\rho}p(x,y,t) = g(\eta + d - y) + \frac{1}{2}\frac{1}{\eta + d}\frac{d^2\eta}{dt^2}[(\eta + d)^2 - y^2]. \tag{A1.15}$$

Integrating this equation over the entire depth gives the total force acting on the plate, as :

$$F = \frac{1}{2}\rho g(\eta + d)^2 + \frac{1}{3}\rho(\eta + d)^2\frac{d^2\eta}{dt^2}. \tag{A1.16}$$

The pressure distribution result and the total derivative $d\eta/dt$ will now be used to evaluate the derivatives $\partial\eta/\partial x$ and $\partial\eta/dt$ on $x = \xi(t)$. Differentiating (A1.11) with respect to x, one obtains that :

$$-\frac{1}{\rho}\frac{\partial p}{\partial x} = g\frac{\partial \eta}{\partial x} + \frac{\partial}{\partial x}\int_y^{\eta+d}\frac{Dv}{Dt}dy. \tag{A1.17}$$

The integral in this expression can be evaluated by Leibniz's rule. At $y = \eta + d$,

$$\frac{\partial}{\partial x}\int_y^{\eta+d}\frac{Dv}{Dt}dy\bigg|_{y=\eta+d} = \frac{\partial \eta}{\partial x}\frac{Dv}{Dt}\bigg|_{y=\eta+d} = \frac{\partial \eta}{\partial x}\frac{d^2\eta}{dt^2}. \tag{A1.18}$$

The pressure gradient can also be obtained from the conservation of momentum equation in the x-direction $(-1/\rho)\partial p/\partial x = d^2\xi/dt^2$. Then, combining this relationship with (A1.16) and (A1.17) the following relationship is obtained for $\partial\eta/\partial x$:

$$\left.\frac{\partial \eta}{\partial x}\right|_{x=\xi(t)} = \frac{d^2\xi}{dt^2}\left(\frac{1}{g+\frac{d^2\eta}{dt^2}}\right). \tag{A1.19}$$

Substituting this expression into the total derivative of η, $d\eta/dt$, gives $\partial\eta/\partial t$ directly. Then:

$$\left.\frac{\partial \eta}{\partial t}\right|_{x=\xi(t)} = \frac{d\eta}{dt} - \frac{d\xi}{dt}\left(\frac{\frac{d^2\xi}{dt^2}}{g+\frac{d^2\eta}{dt^2}}\right). \tag{A1.20}$$

The name *law of the plate* has been coined as a rubric to describe the theory presented in this section, although it will also be used to refer to equation (A1.16) alone. This name is used to emphasize the fact that the vertical velocity on a moving plate can only vary linearly with depth. It will be used to discuss the linear theory result for calculating the hydrodynamic forces on accelerating plates.

A.2 Comparison with the linear wavemaker theory. In this section the law of the piston results are compared with the predictions of the linear wavemaker theory. In the linear model the advective accelerations are neglected, and the total derivative Dv/Dt in the equation of vertical motion is substituted by $\partial v/\partial t$. Postulating the existence of a velocity potential Φ and integrating the equation of motion over the depth one obtains :

$$\frac{p}{\rho} = -\frac{\partial\Phi}{\partial t} - g(d-y) \ , \tag{A2.1}$$

where $y = y - d$. Integrating (A2.1) gives the total force per unit width on the plate :

$$F = \frac{1}{2}\rho g d^2 - \rho \int_{-d}^{0} \frac{\partial \Phi}{\partial t}\, dy \,. \tag{A2.2}$$

and it is the linear theory equivalent expression of (A1.16). The range of integration is [-d,0]; in using the linear theory the amplitude of the resulting wave motion is assumed to be small, so that the boundary conditions are applied at $y = 0$ rather that $y = \eta$. To estimate the order of the correction term to the hydrostatic force in (A2.2) , assume a plane wavemaker undergoing small amplitude, simple harmonic motion defined by $\xi(t) = S\cos\omega t$. The velocity potential is given by :

$$\Phi = \frac{dS\omega}{\delta}\left[- b_0 \cosh(k_0 y)\, e^{ik_0 x} + i \sum_{n=1,\infty} b_n \cos(k_n y)\, e^{-k_n x}\right] e^{i\omega t} \tag{A2.3}$$

This solution was originally derived by Havelock (1929). δ is defined by $\delta = d\omega^2/g$, and it is the same parameter referred to as α by Gilbert et al. (1971). The dimensional wavenumbers k_o and k_n are defined implicitly by the dispersion relationships,

$$k_n d \tan(k_n d) = \delta \quad \text{and} \quad k_0 d \tanh(k_0 d) = -\delta \,, \tag{A2.4}$$

while the coefficients b_0 and b_n are evaluated directly from the boundary condition at the piston plate, $\partial\Phi/\partial y = d\xi/dt$ at x=0. This procedure results into the following expressions :

$$\frac{b_0 \sinh(k_0 d)}{k_0 d} = 2 \left(\frac{\delta}{k_0 d}\right)^3 \frac{1}{(k_0 d)^2 - \delta^2 + \delta} \,, \tag{A2.5}$$

and

$$\frac{b_n \sin(k_n d)}{k_n d} = 2 \left(\frac{\delta}{k_n d}\right)^3 \frac{1}{(k_n d)^2 + \delta^2 - \delta} . \tag{A2.6}$$

A direct comparison between equation (A2.2) and (A1.16) is now possible. $\partial\Phi/\partial t$ and $\partial^2\Phi/\partial t^2$ can be evaluated at x=0 through (A2.3), for a range of values of δ. Since $d^2\eta/dt^2$ is not known apriori in the generalised theory, the linearised form of (A1.15) will be used. Then:

$$F = \frac{1}{2} \rho g d^2 + \frac{1}{3} \rho d^2 \frac{\partial^2 \eta}{\partial t^2} \tag{A2.7}$$

Figure (A2.1) compares the force on the plate as computed by the linear theory (A2.2), and as computed by the law of the piston (A1.16); the amplitude was calculated from the kinematic free surface condition, $\eta = -(1/g)\partial\Phi/\partial t$. The force is shown as a function of the dimensionless time, for $\delta = 0.1$, 1.0 and 10.0. It is seen that for δ=0.1, the two estimates are almost identical. For the larger δ, the linear theory (A2.2) underestimates the linearised result of the generalized theory (A2.7).

This is certainly a paradoxical a result. If the linear theory was consistent, then the results of the linear theory and of the linearised form of the general theory should have been identical for any value of δ where the linear theory is valid. Apparently the linear theory solution is not valid for values of $\delta \sim O(1)$, although these values are given in the usual wavemaker nomograms, such as those in Gilbert et al. (1971). To prove this assertion, the vertical velocity distribution on the front face of the piston is calculated according to the linear theory, and it will be demonstrated that it violates the continuity equation for large δ.

The vertical velocity distribution at x= 0 is calculated from (A2.3) and it is given by:

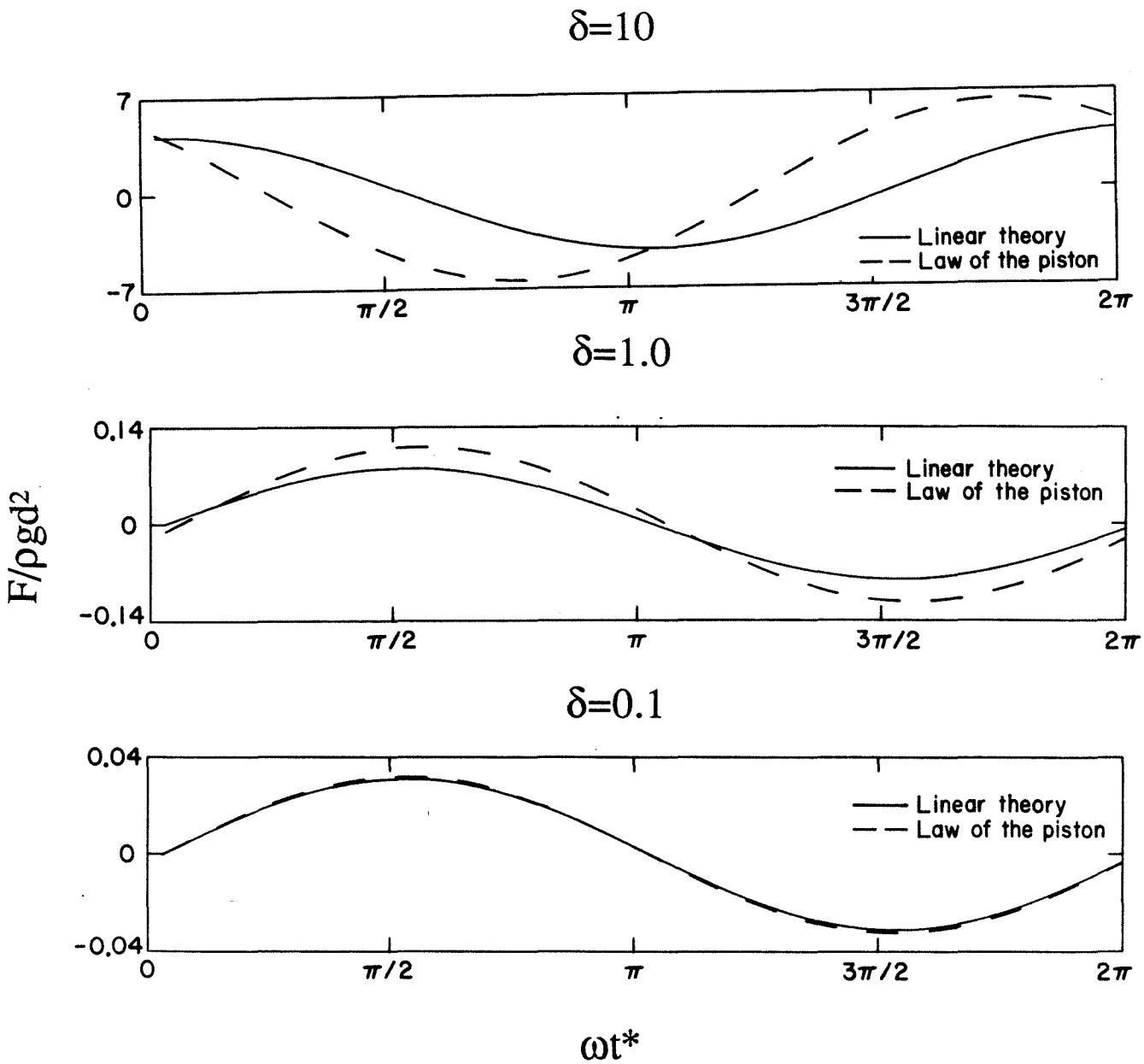

Figure A2.1 Variation of the total force on an plate undergoing simple harmonic motion. for different values of $\delta=d\omega^2/g$.

$$v = \frac{\partial \Phi}{\partial y} = \frac{S\omega}{\delta}\left[- b_0 k_0 \sinh(k_0 y)\cos\omega t + \sin\omega t \sum_{n=1,\infty} b_n k_n \cos(k_n y)\right]. \qquad \text{(A2.8)}$$

For small δ, the vertical velocity distribution is linear over the depth. This can be seen by arguing that for $\sqrt{\delta} << 1$, then $b_o \approx k_o \approx \sqrt{\delta}$. To the same order, $k_n \approx n\pi$, and $b_n \approx 2(-1)^{n+1}\delta^2/(n\pi)^3$. Substituting these approximations in (A2.8) results in a linear vertical velocity distribution, consistent with the conservation of mass equation $\partial u/\partial x = -\partial v/\partial y$, i.e.,

$$v = \frac{Sg}{\omega d}\,\frac{y}{d}\cos\omega t \qquad \text{(A2.9)}$$

This result is also consistent with the law of the plate result, (A1.8), since one can derive from (A2.3) that $\partial\eta/\partial t \approx (Sg/\omega d)\cos\omega t$. This result is shown in figure (A2.2a), where the vertical velocity is calculated according to (A2.8), for different times in the cycle of the oscillatory motion. As the frequency increases, the velocity distribution deviates from the linear distribution, indicating a breakdown of the solution. This is shown in figures (A2.2b,c,d). Based on these results, an approximate limiting criterion for the validity of the linear theory is $\delta < 0.07$. (An exact result can also be derived with some further computational effort.)

It is interesting to note that in the definitive set of experiments [Ursell et al (1961)] when the predictions of the linear theory were "verified", δ was in the range [0.057, 4.974]. The authors compared the measured value of the ratio of the wave height to the piston stroke to the theoretical value, which is given by :

$$\frac{H}{S} = \frac{2(\cosh k_o d - 1)}{(\sinh 2k_o d + 2k_o d)}. \qquad \text{(A2.10)}$$

The agreement was very good and the authors concluded that their experiments " *constituted a close verification of the small-amplitude wave theory... and that this theory may be used with confidence to calculate waves (and probably also forces) in more complex cases...*".

Although, there is no experimental evidence to refute the above statement, it can be speculated that the agreement was partially fortuitous. This hypothesis is suggested by the fact that their laboratory results agree equally well with the theoretical results for steep finite

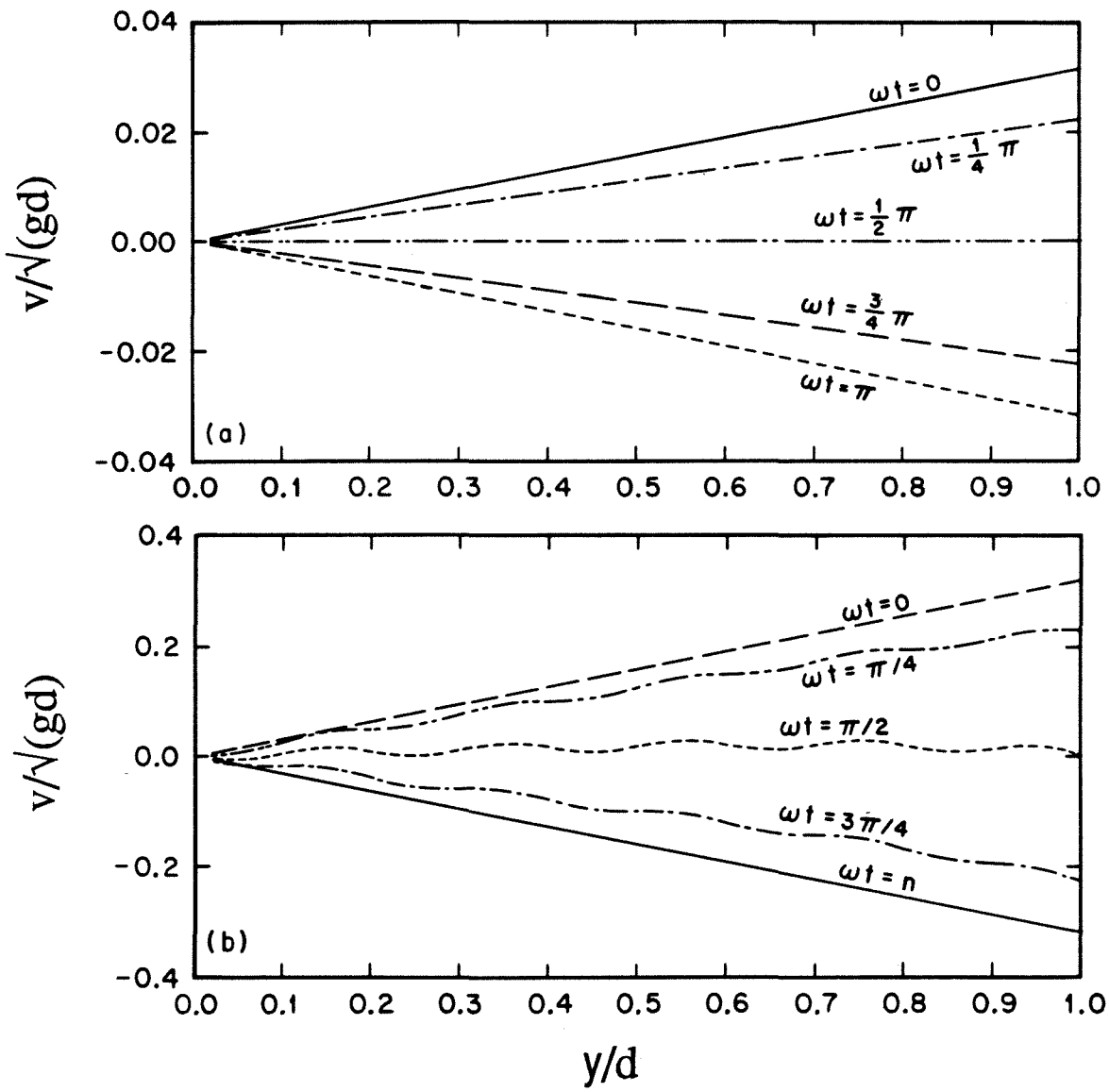

Figure A2.2a,b Variation of the vertical fluid velocity on the front face of the plate, as calculated by the linear theory using equation (A2.8) with $\delta = 0.001$ (a) and $\delta = 0.1$ (b)

amplitude waves, with $0.045 \leq H/L \leq 0.048$ and $0.078 \leq H/d \leq 0.256$, a range where the linear theory is clearly not valid. Since the equation (A2.10) was evaluated by Ursell et al. (1962) several depths away from the wavemaker, it is possible that the linear theory describes the motion well away from the wavemaker, but that it is limited when applied directly in the wave generation region, next to the wavemaker. It is therefore arguable whether the linear theory can be used to calculate forces in the entire range of values as suggested by Ursell et al. (1962).

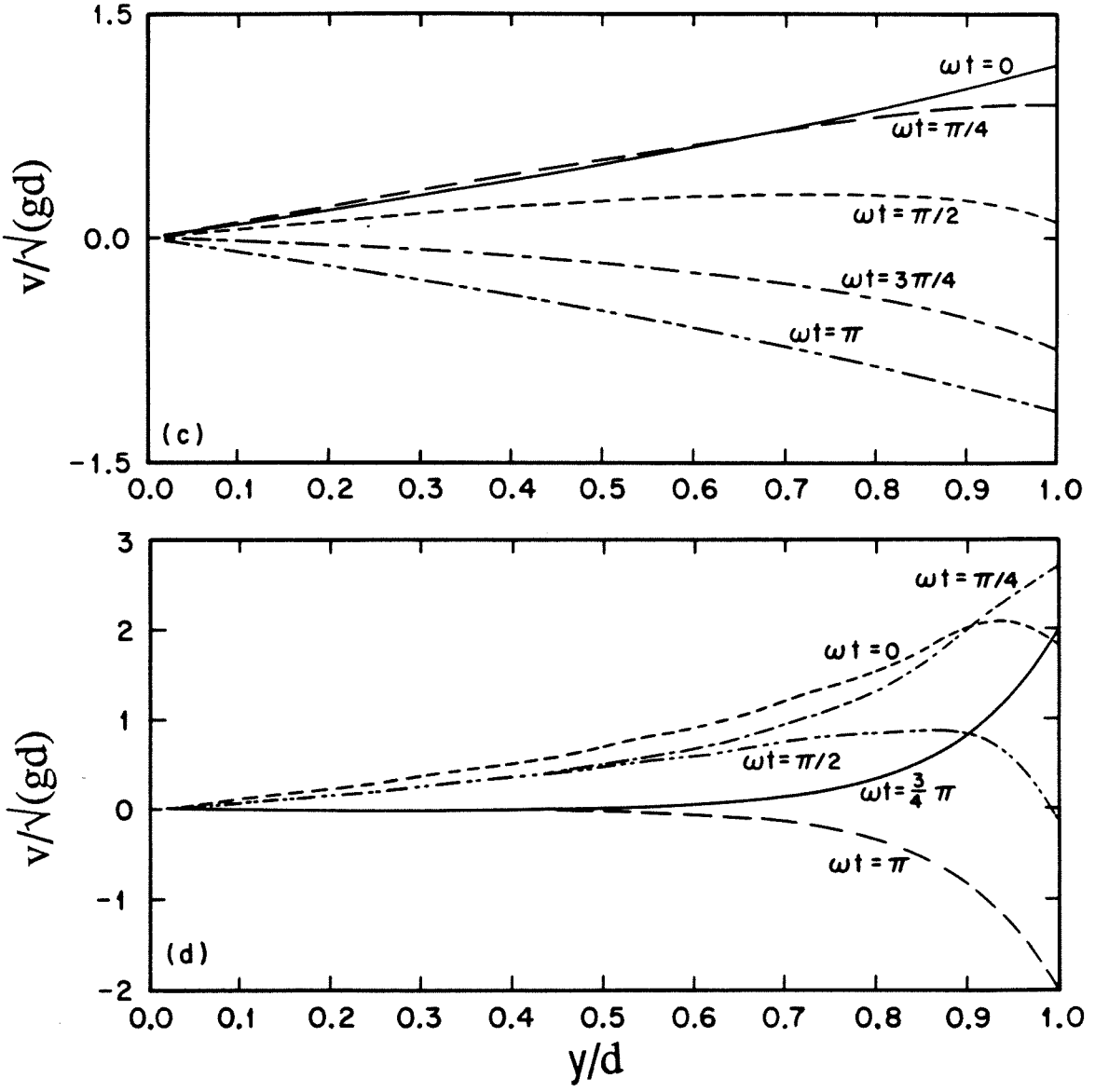

Figure A2.2c,d Variation of the vertical fluid velocity on the front face of the plate, as calculated by the linear theory using equation (A2.8) with $\delta = 1.0$ (c) and $\delta = 9.0$ (d)

On physical grounds, the limitation arises because high frequency plate motions are associated with large plate velocities. Since, to first order, the amplitude on the plate normalized with the depth is equal to the plate velocity normalised with the phase speed $\sqrt{gd}$, it follows that the amplitude on the front face is not negligible. (This is shown in section A.3.) It is therefore no longer permissible to evaluate the free surface condition at $y=0$ rather than on $y = \eta(t)$.

A.3 A note on determining the wave amplitude at the plate. The determination of the wave forces on an accelerating piston requires knowledge of the wave height distribution on the front face of the plate. In many cases this distribution may not be available. However, it can be calculated when generating shallow water by using the method of characteristics. Let v_p denote the *dimensionless* plate velocity given by $v_p=(d\xi^*/dt^*)/\sqrt{gd}$; then the dimensionless wave height at the plate η_p is given by :

$$\eta_p = v_p + \frac{1}{4} v_p^{\,2}. \qquad \text{(A3.1)}$$

One would expect that this relationship is only valid for plate motion such that the shallow water wave theory remains valid, i.e., for motions involving small vertical accelerations. In this sence, the relationship is not expected to be valid when η_p^*/d becomes O (1), since such motions are associated with vertical accelerations, $d\eta^{*2}/dt^{*2} \sim O(g)$. It is therefore remarkable to discover the wide range of amplitudes for which (A3.1) is valid. This is demonstrated in figure (A3.1) which shows the relationship between the maximum wave amplitude at the piston, $[\eta_p^*/d]_{max}$, plotted against the maximum velocity of the plate, $[v_p^*/\sqrt{gd}]_{max}$, for the waves described in chapter 4. It is seen that equation (A3.1) is indeed a good model for the relationship between the two variables.

When the plate generates broken waves and bores, the surface amplitude at the plate can also be calculated with the classical bore theory. Assume that plate is generating a uniform bore of height $\eta+d$, which propagates with speed U. A convenient form for the bore conditions is given by Whitham (1974), and it is :

$$U = u + \sqrt{\frac{g(\eta+d)(\eta+2d)}{2d}} \tag{A3.2}$$

From conservation of mass, one may derive that :

$$u = \frac{\eta c}{\eta+d} \tag{A3.3}$$

Combining (A3.2) with (A3.1), the following expression results :

$$u = g\eta \sqrt{1- \frac{1}{2} \frac{\eta}{\eta+d}} \tag{A3.4}$$

Behind the uniform bore, the fluid velocity is equal to the plate velocity, $u/\sqrt{(gd)} = v_p$, so that (A3.4) may be used to calculate η_p. This relationship is also shown in figure (A3.1) and it is seen that it predicts identical results with the relationship derived from the method of characteristics (A3.1), for plate velocities less than 0.3. This is expected, since for small η_p, (A3.1) and (A3.4) both reduce to $\eta_p \approx v_p$. For larger plate velocities (A3.1) and (A3.4) diverge, but they are not sufficiently different to draw any general conclusions from this set of data.

The relationship between the dimensionless amplitude at the plate and the dimensionless plate velocity is obvious in a comparison of figure (4.2.5.a) with (4.2.5b). It is apparent that the wave amplitude at the plate can be approximated with the plate velocity

in many cases. This result is also consistent with the long wave equations, where the wave amplitude is approximately equal to the depth averaged water particle velocity.

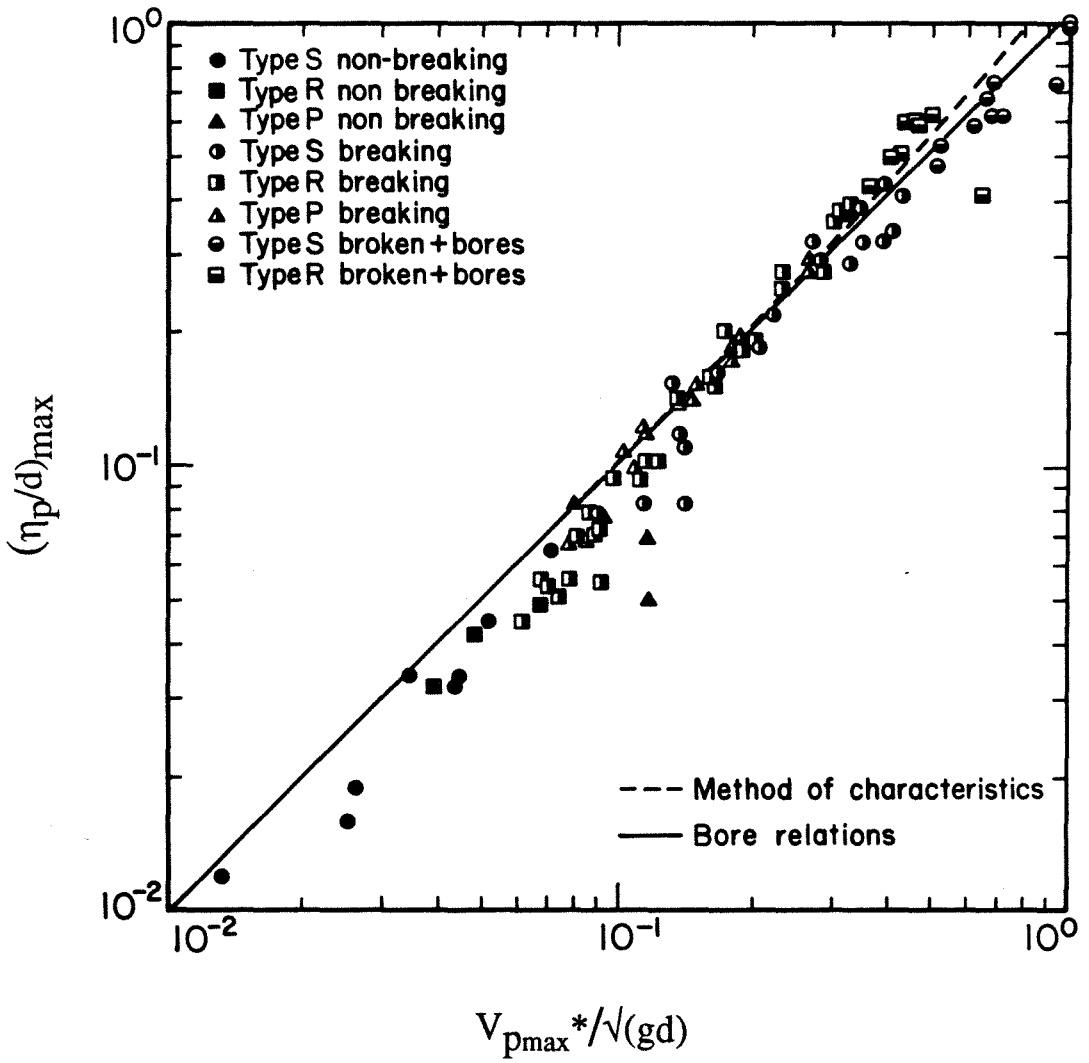

Figure A3.1 The maximum wave amplitude on the front face of a plate as a function of the maximum velocity of the plate.

Appendix B

The runup of a uniform bore

Introduction. Peregrine (1966) describes a uniform bore as a " *transition between different uniform flows of water* ". A bore with a *gentle* transition propagating over constant depth can be modelled using standard methods [Peregrine (1966)]; eventually it transforms into an undular bore, as shown in figure (1.3.2) When a bore climbs on a sloping beach the transition region narrows; the bore evolves into a discontinuity (a shock) in the distribution of the dependent variables. This process imposes a serious impediment in the analysis of the climb of the bore up a beach, since no differential relationships can formally be applied once a discontinuity develops.

Certain approximate analytical solutions that account for discontinuities have been derived since Whitham's (1958) original contribution (see section 1.3.3). There has been no exact solution. However the problem is ideally suited for numerical computation, where flow variables are computed at discrete locations and times. Under certain conditions, shocks may be admitted and higher order solutions can be obtained. One such finite difference procedure was devised by von Neumann and Richtmeyer (1950) permitting shocks to develop in the interior of the flow. This procedure is described in Richtmeyer and Morton (1967) in detail. Another procedure that allows shocks to form and propagate was developed by Lax and Wendroff (1960). This latter procedure has been used with success in free surface problems by Houghton and Kasahara (1968), and by Sielecki and Wurtele (1970). Hibberd (1977) and Hibberd and Peregrine (1979) were the first to

apply the Lax-Wendroff scheme in free surface flows with discontinuities, and they calculated the runup of a uniform bore. Packwood (1980) used the same scheme and included terms for frictional dissipation. Mano (1983) developed a similar Lax-Wendroff type procedure and used the Crank-Nickolson scheme [Gerald, (1983)] to advance the solution.

The Hibberd and Peregrine (1979) algorithm, denoted hereafter as H&P , is now considered the state of the art method for solving the problem of a *uniform* bore climbing on a plane sloping beach. It was reproduced in this study for the purpose of determining whether it is capable to calculate the solution for the runup of a *finite* bore.

B.1 The Lax-Wendroff technique. The Lax-Wendroff (1960) scheme applies to conservation laws of the form :

$$\frac{\partial \mathbf{W}}{\partial t} + \frac{\partial \mathbf{f}}{\partial x} + \mathbf{K} = 0 \quad , \tag{B1.1}$$

where **U** is the conserved vector quantity, **f** is a vector function of **W**, and **K** is a vector. For long waves propagating over a uniformly sloping beach, the shallow water wave equations can be written in the Lax-Wendroff form, if one sets :

$$\mathbf{W} = [h,\ hu] \ ,$$

$$\mathbf{f} = [hu,\ hu^2+h^2/2] = [hu,\ (hu)^2/h + h^2/2], \tag{B1.2}$$

and

$$\mathbf{K} = [0,\ h] \ ,$$

where the following normalization was used :

$$h = (\cos\beta)\, h^*/d, \quad x = (\sin\beta)\, x^*/d, \quad t = (\sin\beta)\, t^*\sqrt{g/d}, \quad u = u^*/\sqrt{gd} \qquad \text{(B1.3)}$$

1: $\cot\beta$ is the beach slope, and h, x, t, and u are the dimensionless water depth, distance, time and depth averaged velocity respectively and are defined as in chapter 3. This choice of dimensionless variables allows for solutions that are independent of the beach slope. To facilitate the finite difference calculation, $\partial \mathbf{W}/\partial t$ is expressed in terms of x-derivatives. This is accomplished by using the Taylor expansion of $\mathbf{W}(x,t)$ in t, by retaining terms of $O(\Delta t^2)$, and by using the relationship :

$$\frac{\partial \mathbf{W}}{\partial t} = \frac{\partial \mathbf{f}}{\partial \mathbf{A}} = \mathbf{A} \quad \frac{\partial \mathbf{W}}{\partial x} \qquad \text{(B1.4)}$$

where

$$\mathbf{A} = \frac{\partial \mathbf{f}}{\partial \mathbf{W}} = \begin{bmatrix} 0 & 1 \\ h - (hu)^2/h^2 & 2\,(hu)/h \end{bmatrix} \quad . \qquad \text{(B1.5)}$$

Equation (B1.1) can now be solved with an explicit finite differencing scheme. Since **W**, **f**, and **K** are vectors and **A** is a matrix, the solution vector of (B1.1) is usually obtained by solving the resulting system of two equations with the two unknowns, h and hu. However, (B1.1) can also be solved directly by defining a complex solution vector, $\mathbf{U} = h + iuh$. This definition takes advantage of complex variable operations that certain compilers allow, and it was used in this study because it simplifies the solution and allows for more compact code. The convergence of the scheme was established by Lax and Wendroff (1960). The stability of the scheme is determined by the Courant-Friedrichs-Lewy criterion which requires that $\Delta x/\Delta t \geq u + c$, where Δx and Δt are the grid size and the time increment respectively.

B2. The Hibberd and Peregrine solution Hibberd and Peregrine used the following initial vector to represent a uniform bore :

$$\mathbf{W}(x, t=0) = \begin{cases} [1, u_o] & \text{when } 1 \leq x \\ [1 - x\tan\beta,\ 0] & \text{when } 1 < x \leq 0 \end{cases} \tag{B2.1}$$

They considered the wave propagation in the region $1 \leq x \leq 0$. To complete the solution , data must be specified for all times at x=1, the sea boundary. They accomplished this by using the characteristic form of the shallow water wave equations to calculate the Riemann invariant $\boldsymbol{\beta}$, defined as follows :

$$\boldsymbol{\beta} = u - 2c - t\ \tan\beta \tag{B2.2}$$

The characteristic form of the equations requires that :

$$\frac{\partial \boldsymbol{\beta}}{\partial t} = -(u-c)\ \frac{\partial \boldsymbol{\beta}}{\partial x} \tag{B2.3}$$

If $\boldsymbol{\beta}$ is known for x = 1, t = 0, then (B2.3) can be used to calculated $\boldsymbol{\beta}$ for all times, and then boundary values can be calculated through (B2.2).

Once seaward boundary values are specified, the Lax-Wenfroff equation (B1.1) can be integrated explicitly. The details can be found in Hibberd and Peregrine (1979). The only difficulty arises when the bore reaches the initial position of the shoreline. Up to this stage in the calculation the shoreline boundary has been assigned the undisturbed flow values, i.e., **W**=[0,0], so as to permit the integration of the solution to the next time step. Now the decision must be made whether this value should be modified, and, if so, whether

new grid points should be introduced in the computational domain. Hibberd and Peregrine proposed a shoreline algorithm that uses linear extrapolation to predict provisional values and then local integration of the equations of motion to correct these values. Iwasaki and Mano (1979) used a different shoreline procedure to introduce new grid points. They modelled the plane sloping beach with a ladder-like topography with small steps. Their algorithm introduces a new grid point in the computation when the water depth exceeded the height of the step at the last grid point.

B3. Implementation of the Hibberd and Peregrine algorithm. The shoreline algorithm was implemented for calculating the runup of uniform bores with mixed results. The solution procedure followed Hibberd's (1977) description. The only detail that may be added to that recounting is the fact that when negative depths values are predicted in the *intermediate* steps of the shoreline procedure they should be retained instead of being set equal to zero; otherwise the algorithm does not converge. [Peregrine (1980)].

The H&P algorithm produced good results when used to calculate the runup of a uniform bore. Figures (B3.1) shows the climb of a uniform bore defined by equation (B2.1) with $u_0 = 0.1$. In these calculations $\Delta x = 0.01$ and $\Delta t = 0.04$, and the x-grid included 100 nodes. (These are also the values used by H&P.) The integration of the solution proceeded smoothly, but could only be advanced up to the point of maximum runup. Beyond that point numerical instabilities developed and floating overflows resulted, even though the H&P rundown procedure was used. Instabilities also developed when calculating the runup of strong bores. This is shown in figure (B3.2) which shows the runup of a bore with $u_0 = 0.6$. This instabilities were not present in Hibberd and Peregrine's solution, so they may be due to incorrect interpretation of the algorithm.

The algorithm was then used to attempt to calculate the runup of a finite bore. A finite bore was generated by propagating a 0.30 solitary wave up a 1:20 sloping beach. The Lax-Wendroff technique was used to solve the propagation problem over the combined topography of a constant depth region joined to a sloping beach. (see figure 1.1.1) The result is shown in figure (B3.3). The figure shows the inital profile as a function of x. The

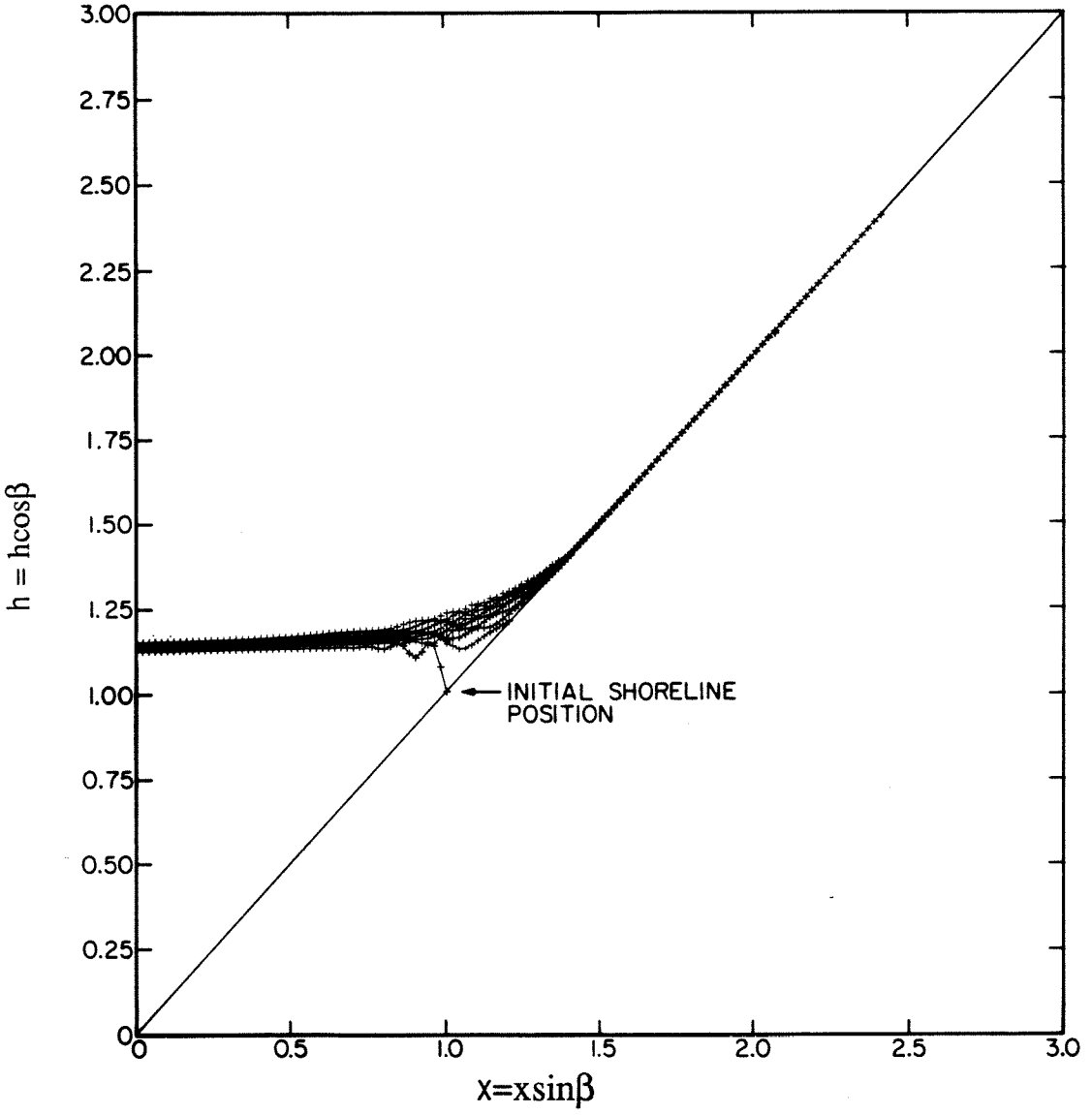

Figure B3.1 The runup of a uniform bore with initial strength u_0=0.1 Δx=0.01 and Δt=0.04

last profile shown has triangular shape and it is very similar to the profiles of *finite* bores realized in the laboratory. When the solution was integrated past this profile the Lax-Wendroff scheme also developed instabilities. This problem was circumvented by smoothing of the solution. Smoothing was used instead of any artificial viscocity terms because the objective was to obtain some representation of a *finite* bore profile at the shoreline instead of deriving the solution for the runup of a solitary wave after

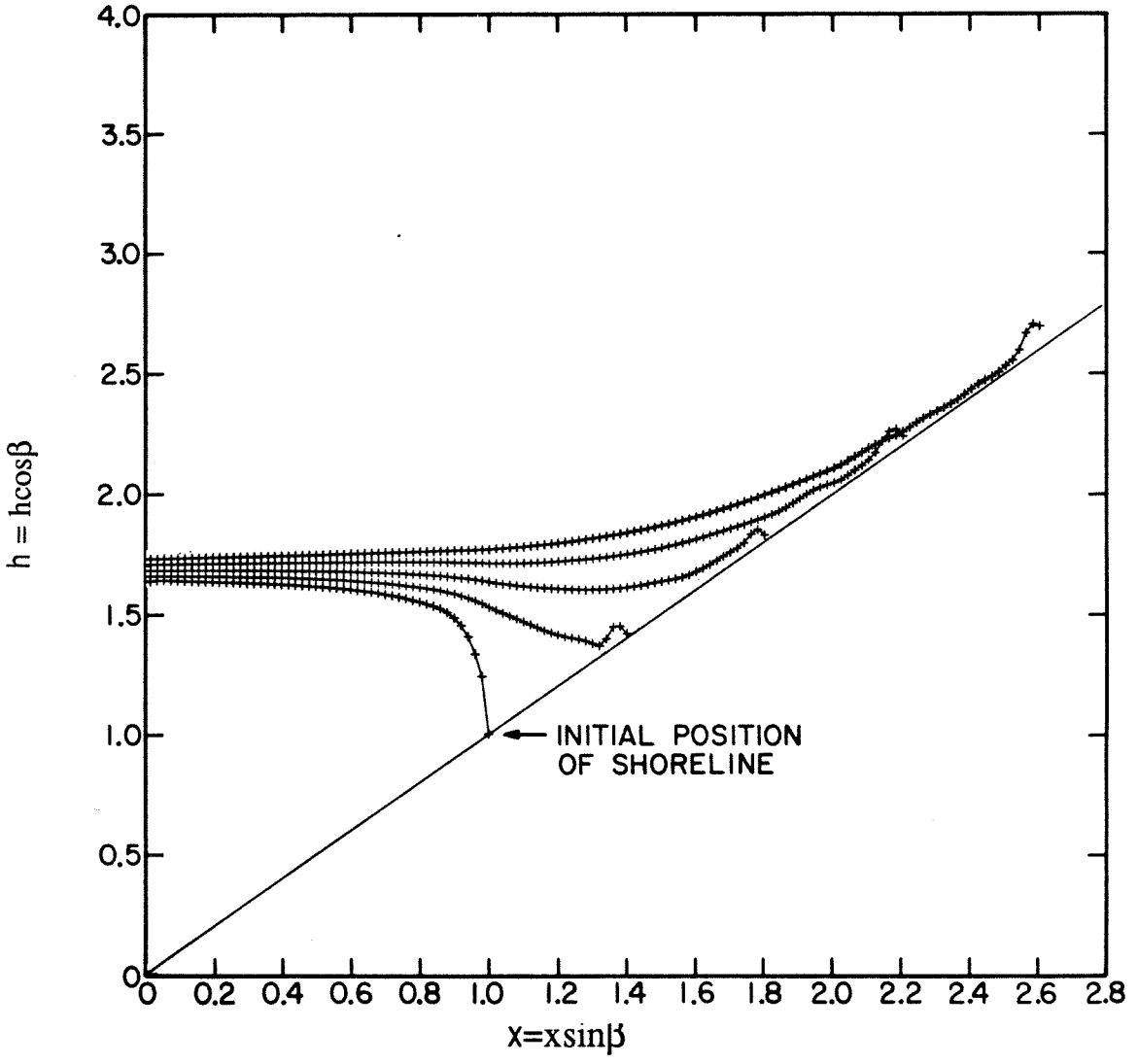

Figure B3.2 The runup of a uniform bore with initial strength u_0=0.6 Δx=0.01 and Δt=0.04

breaking. Once the bore reached the shoreline the H&P algorithm was used to advance the solution. The shoreline algorithm worked well to initiate the motion of the shoreline, but soon thereafter numerical instabilities developed close to the shoreline tip and the integration was stopped. Although it would have been possible to suppress the overflows by different numerical switches, it was felt that the accuracy of the solution would be compromised and that the final code would be of no use other than for the particular case it was developed for. However the calculation did point to the fact that the H&P algorithm in its original form is a powerful but a very sensitive numerical procedure.

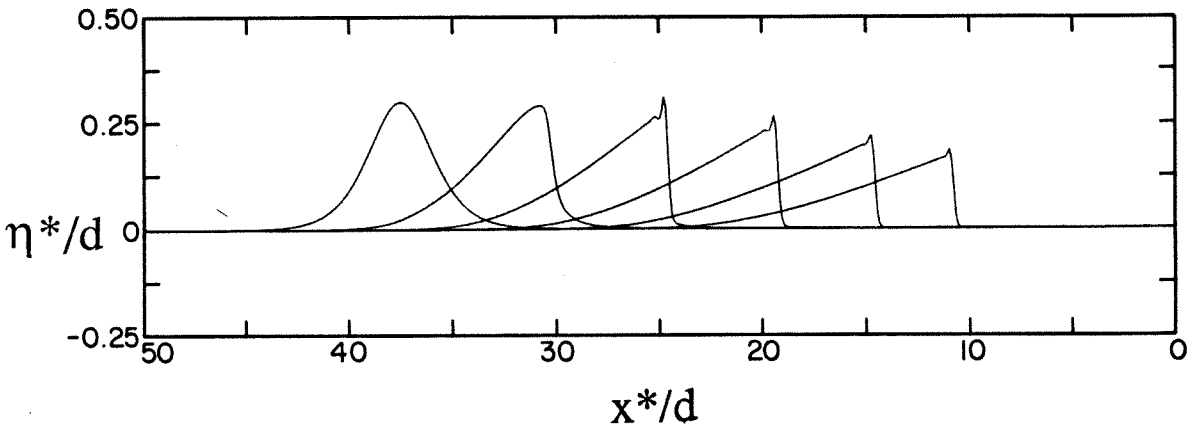

Figure B3.3 The climb of a 0.30 solitary wave up a 1:19.85 beach. The Peregrine (1967) algorithm was used.

Appendix C

The generation of arbitrary long waves in the laboratory

Introduction. In many laboratory investigations it is desired to expose the model of a coastal structure to a particular shape of a finite-amplitude long wave. In nature the prototype wave propagates from the generation region to its destination, and it changes shape through amplitude and frequency dispersion and energy dissipation. Frequently it is not practical to model the entire bottom topography from the generation region to the structure in order to realize similar wave shapes in the laboratory. The problem then arises of how to produce the appropriate wave in the model when it is not possible to scale exactly the natural processes that transform the wave.

In this section a method is presented which allows the creation of any relatively arbitrary *long* wave at a given location in a *two-dimensional constant depth* wave tank. The method is developed in two stages. First, a propagation algorithm is used to determine the wave that must be created by the wave generator to produce the desired wave at the specified location. Then, a generation algorithm is used to calculate the motion of the wave plate necessary to create the wave that resulted from the propagation algorithm.

C.1 The propagation algorithm. Usually, when a particular long wave form is to be realized in the laboratory at a specified location it is neccessary to generate an entirely different wave in the generation region and let this wave evolve into the desired wave. To determine this initial wave one must solve an initial value problem backwards in time, i.e., find the solution at $t = -T$ from the solution at $t = 0$ and then specify a suitable propagation model.

An appropriate propagation model for long waves travelling over constant depth is the KdV equation [Korteweg and de Vries (1895)] ; it can also be derived from the Boussinesq equations. Many variants of this equation exist; the one chosen for this study is the one presented by Peregrine (1966). It has the form :

$$\frac{\partial u}{\partial t} + u\frac{\partial u}{\partial x} + \frac{\partial \eta}{\partial x} = -\frac{1}{3}\frac{\partial^3 u}{\partial x^2 \partial t} + O(\varepsilon^2\sigma^3) \qquad \text{(C1.1)}$$

where ε is the ratio of the wave height to the water depth and σ is the ratio of the water depth to the wavelegth and all the flow variables are normalized as in chapter 3. Both ε and σ are assumed to be small; to the same order as (C1.1), $\eta \approx u$.

Equation (C1.1) was adopted as the propagation model in this study. However, the equation has only two known classes of exact solutions. To use this equation with arbitrary initial conditions a numerical procedure is necessary. Peregrine (1966) presented a robust differencing scheme of this equation and proceeded to calculate the evolution of an undular bore. Hammack (1972) used the same algorithm to calculate the propagation of waves generated by vertical bed displacements. The resulting matrix of the coefficients of the solution vector is tridiagonal so that the system of equations can be solved directly by back substitution. The only difference between the technique used here and Peregrine's (1966) practice was that the time step Δt used in the integration of the equation was negative, since it was desired to advance the solution backwards in time. To determine the appropriate grid size and time step size for the numerical calculation several test runs were executed. The Δx and Δt were halfed until a solitary wave of approximately the same height as the desired waveform propagated in the numerical wave basin without any change in form. (This change is usually a reduction in the maximum wave amplitude and is attributed to numerical dispersion.) For a propagation length of 100 depths and for solitary waves of H/d ratio such that $0.1 \leq H/d \leq 0.5$, the numerical grid parameters that gave the best combination of least numerical dispersion and largest grid size were $\Delta x = \Delta t = 0.01$.

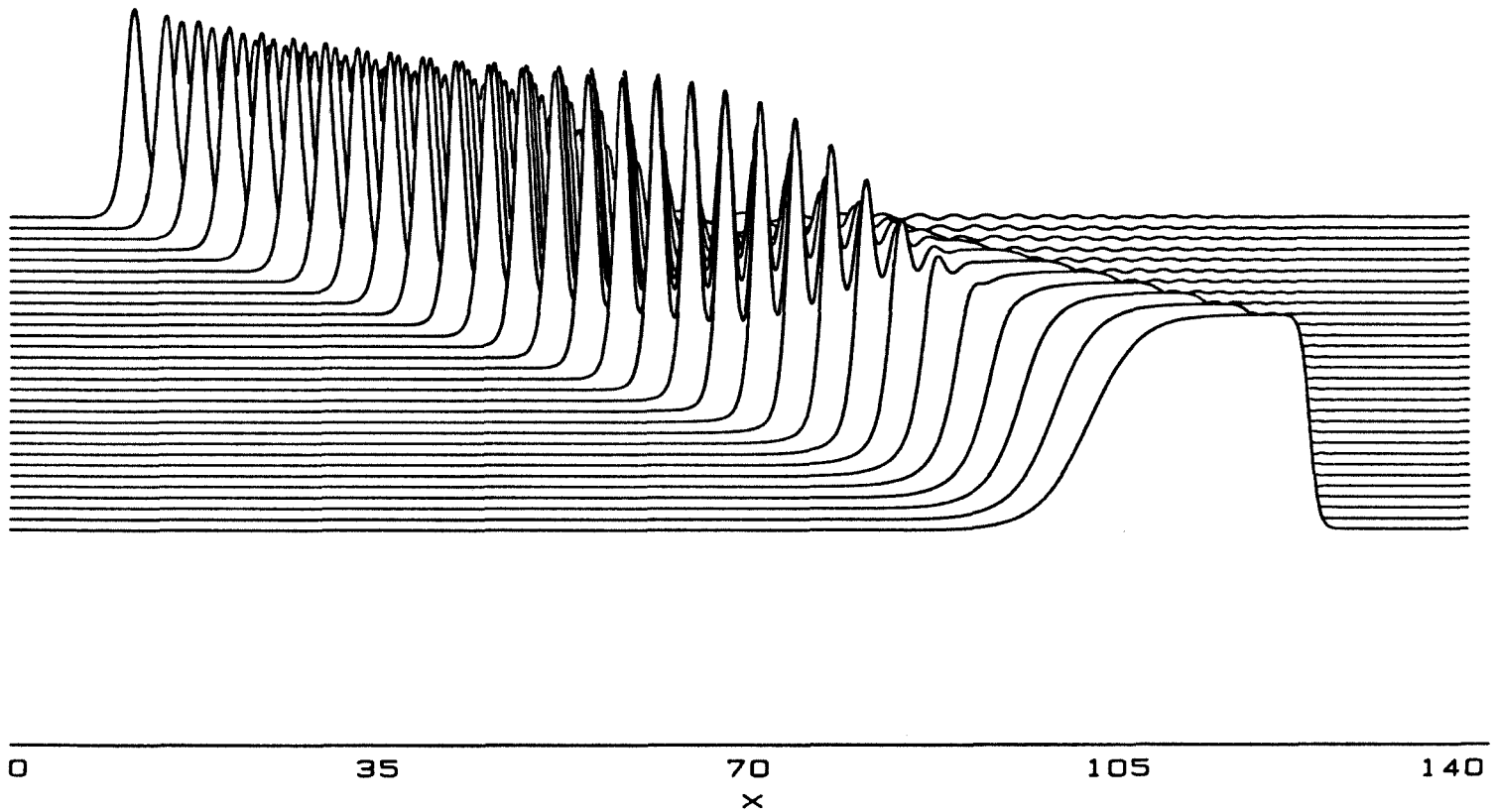

Figure C1.1 The evolution of the wave defined by equation (C1.2) with λ=10 and A=0.3 backwards time. The profiles are shown as functions x and are spaced at time intervals equal to $0.4\sqrt{(d/g)}$. The Peregrine (1966) algorithm was used with $\Delta x=\Delta t=0.01$.

For the purpose of determining whether the propagation model could be used for reasonable, but relatively arbitrary long waves , an initial wave form was defined as follows:

$$u(x, t=0) = \begin{cases} 0.5\,A\,[1 - \tanh(.750x)] & \text{when} \quad 0 \le x \le \lambda \\ 0.5\,A\,[1 - \tanh(.125x)] & \text{when} \quad \lambda \le x \le 2\lambda \end{cases} \qquad \text{(C1.2)}$$

where A is the wave amplitude and 3λ is the wavelength. Different cases were run with A ranging from 0.1 to 0.5 and $\lambda = 10$. The numerical scheme was stable for propagations distances of at least 400 depths; the only limitation on the propagation length was the maximum array size that could be included in the code. (Although the code was of the order of 50 statements, it was executed on a PDP11/60 with 128kbytes of RAM.) Figure (C1.1) is an example of the backwards propagation of the profile defined by equation (C1.2). The profiles shown are the wave amplitude as a function of x at time intervals equal to $40\Delta t$. To interpret the figure, the x-axis may be thought of as the side view of a two-dimensional wave tank and the surface profiles as still photographs of the wave motion superposed on each other.

A more intriguing test of the propagation model is shown in figure (C1.2). This figure shows the numerical propagation, backwards in time, of an initial wave profile derived from laboratory experiments. This profile resulted when a breaking wave , after propagating over constant depth, reformed into a nonbreaking wave consisting of a leading solitary wave followed by a train of oscillatory waves. The propagation model appears to predict that the original wave (that evolved into the laboratory wave) is a nonbreaking solitary wave following an oscillatory train of small amplitude waves. Although it can be argued that this is the expected behaviour since the propagation equation can model only nonbreaking waves, it can also be argued that the propagation model could have produced unbounded solutions to indicate the presence of discontinuities at earlier times. This is quite

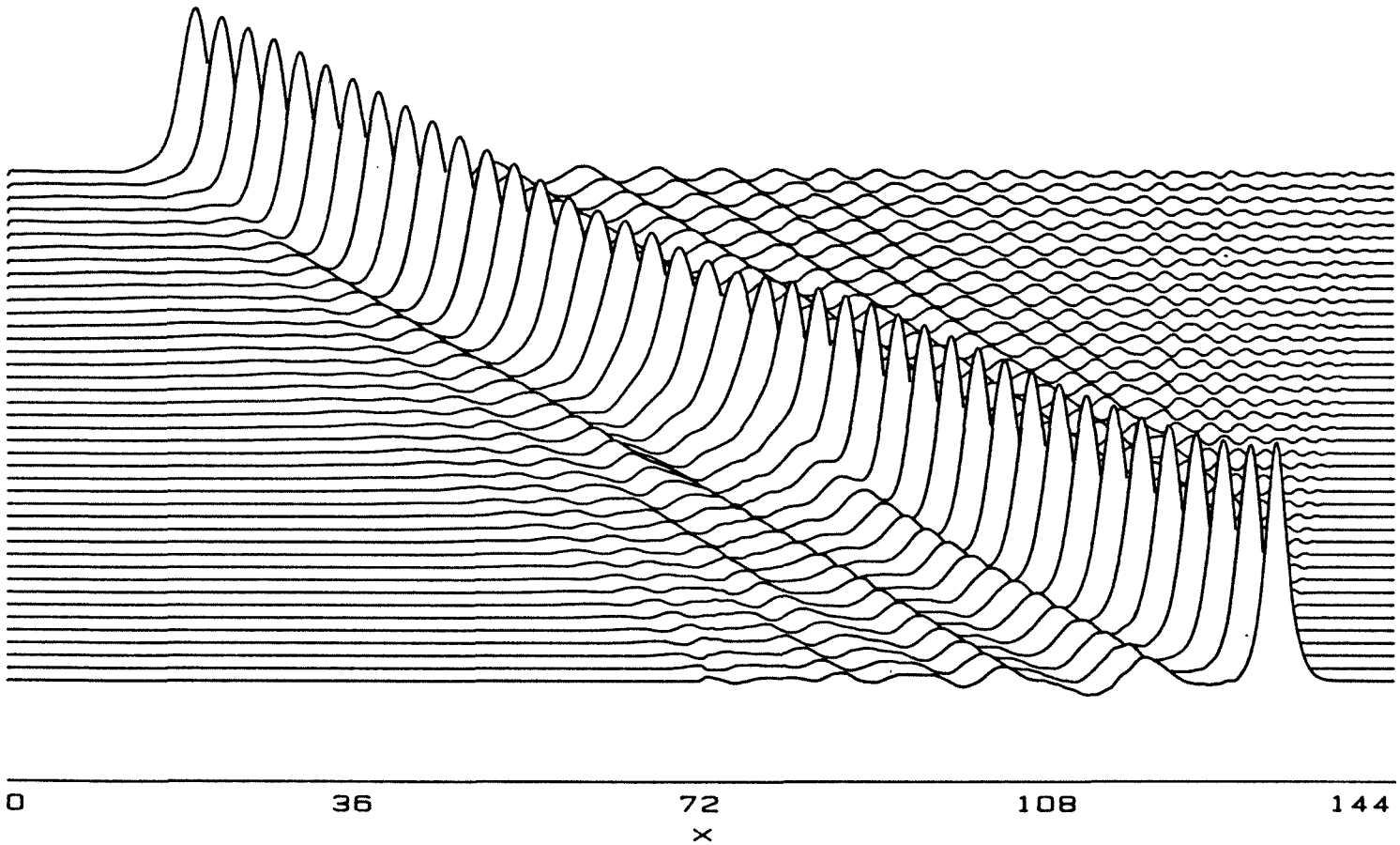

Figure C1.2 The evolution of the a wave that evolves after a broken wave reforms. The profiles are shown as functions x and are spaced at time intervals equal to $0.4\sqrt{(d/g)}$. The Peregrine (1966) algorithm was used with $\Delta x=\Delta t=0.01$.

fascinating because it suggests that it is possible that the same long wave may evolve from two different waves. This assertion will be examined in section C.3.

C.2 The generation algorithm. Long waves can be generated in the laboratory in many ways. Scott -Russell (1844), the first person to describe a solitary wave, suggested some methods for long wave generation ; many of them are still in use. In this study waves were generated by moving a vertical plate, as decribed in chapter 2.

The primary reason for using the vertical plate is that the long wave model (C1.1) refers to the depth averaged horizontal velocity u. Since during wave generation it is attempted to induce the fluid particles to move with a specified velocity, it is sensible to use a wave generation system that forces the fluid particles in a uniform manner across the depth. This means that the trajectory of the plate $\xi(t)$ is defined by :

$$\frac{d\xi}{dt} = u\,(\xi,t) \qquad \text{(C2.1)}$$

This is the *trajectory equation* and it matches the plate velocity with the velocity of the generated wave at each generation step. It accounts for the fact that the wave evolves continuously during generation as it is moving away from the generation area. It is not an easy equation to solve analytically or numerically.

There are two special cases of this equation : one, when the generated wave is a permanent form wave, and two when the wave is a small-amplitude wave :

A. When the wave is one of permanent form, then one can introduce a phase $\theta = x\text{-}ct$, and

write :

$$\frac{d\xi}{dt} = u(\theta) \tag{C2.2}$$

Since for permanent form long waves the amplitude is related to the water particle velocity by the following relationship :

$$u = \frac{c\eta}{\eta + 1}, \tag{C2.3}$$

then the trajectory equation can be solved directly to give :

$$\xi(t) = \int_0^{\theta} \eta(\phi)\, d\phi \tag{C2.4}$$

Goring (1978) developed an algorithm to solve this equation to determine the trajectory to generate solitary waves and cnoidal waves. He verified his technique in the laboratory and obtained excellent results.

B. When small amplitude waves are generated, then equation (C2.1) can be linearised to give the following form of the trajectory equation :

$$\frac{d\xi}{dt} = u(0, t) \tag{C2.5}$$

This equation defines ξ as an explicit function of time and it can be integrated directly to find the trajectory. Equation (C2.5) is used routinely in most laboratory investigations to generate finite amplitude waves because of its simplicity. In most cases the difference between the solutions of (C2.5) and (C2.1) is small. However, when a specific wave must be generated for comparisons with an analytical model, it is necessary to use equation (C2.1).

In the present study the trajectory equation (C2.1) was solved by using the propagation model (C1.1). This is neccessary because the wave to be generated evolves continuously. When the intgeration of (C2.1) begins at t = 0 :

$$\frac{d\xi}{dt}(0, 0) = u\,(0,\ 0) \tag{C2.6}$$

while at time Δt later :

$$\frac{d\xi}{dt}(\Delta\xi, \Delta t) = u\,(\Delta\xi, \Delta t). \tag{C2.7}$$

Since the wave is evolving, $u\,(\Delta\xi, 0) \neq u\,(\Delta\xi, \Delta t)$, and it becomes necessary to employ a propagation model to determine the solution for all times. This is not the case for permanent form waves, because once u (x,0) is known then u (x,t) can be determined explicitly for all x and t.

Let the origin of the coordinate system be at x=0, and let the plate be located at $x=X_p$. Suppose that it is desired to calculate the wave trajectory $\xi(t)$ that will generate a given wave system U(x,t) . Let $\mathbf{V} = d\xi/dt$. By definition,

$$\mathbf{V}\,[t=0] = U[\,X_p,\,0]. \tag{C2.8}$$

To determine $\mathbf{V}\,[t=\Delta t]$, one may use the propagation model defined by (C1.1). At time Δt the plate will have moved a distance $\Delta\xi = \mathbf{V}[t=0]\Delta t$, and its velocity at Δt will be given by :

$$\mathbf{V}\,[t=\Delta t] = U\,[X_p+\Delta\xi,\ t=\Delta t]. \tag{C2.9}$$

For any n, ξ_n is the current plate position and $\mathbf{V}_n=\mathbf{V}(n\Delta t)$ is its current velocity ; the plate position at the next step is $\xi_n+\mathbf{V}_n\Delta t$, and its velocity is given by :

$$\mathbf{V}_{n+1} = \mathbf{V}\ [(n+1)\Delta t] = U\ [\xi_n + \mathbf{V}_n \Delta t,\ (n+1)\Delta t] \qquad \text{(C2.10)}$$

Repeating (C2.10) until the wave is generated determines the required trajectory ξ (t).

There are two practical considerations :

1) It is not possible apriori to determine when to stop the integration procedure, i.e., when the whole wave has been generated. It is reasonable to continue the integration until the time t=T, when **V** =0 and d**V**/dt =0, and then stop. T is then defined as the generation time. When this procedure is used the exact time of ending the integration procedure is immaterial as long as the wave has had sufficient time to evolve. The stroke S is given by the relationship S =ξ(T).

2) The equation (C1.1) is usually solved numerically with Peregrine's (1966) algorithm. His practice is to define an initial condition U (x,0) at M grid point each distant Δx apart, and then to use a central differencing scheme to advance the solution in time and thus determine U (x,Δt). Under these conditions, the solution will not generally be available at arbitrary x, as the use of (C2.10) may require. If this is the case, linear interpolation is required between two adjacent grid points. For example if, m=*Int* {(ξ_n+ $\mathbf{V}_n\Delta t$)/Δx}, then one may interpolate between U[mΔx, (n+1)Δt] and U[(m+1)Δx, (n+1)Δt] to obtain U [ξ_n+$\mathbf{V}_n\Delta t$, (n+1)Δt]. (*Int* is the function that finds the largest integer smaller that the argument of the function.)

C.3 Experimental results. Two sets of experiments will be presented in this section. The first verifies the backwards propagation and generarion algorithm (BPG, for short) for waves assumed to be of permanent form locally, while the second verifies the algorithm for arbitrary waves.

Figure (C3.1) shows the evolution hierarchy of a wave defined by equation (C1.2) with A=0.3. The wave identified in the figure was used as an initial condition for the propagation model (C1.1). The other waves evolve at the distances indicated away from the plate.

Figure (C3.2) shows this profile and the trajectory neccessary to generate it as calculated by using equation (C2.2). (In this particular run it was assumed that the wave is a permanent form wave *locally,* i.e., around the generation region. This is a reasonable assumption ; in this case, the generation region is of the order of four depths and the wave is not expected to change significantly over distances of this order.) Figure (C3.3) shows the comparison between the theoretical profiles and those obtained in the laboratory by using the BPG algorithm. Although the effects of dissipation are more evident in the experiments, the agreement is quite good.

In the next set of experiments a broken wave was generated by the plate in the manner described in chapter 4. The wave reformed and the profile that evolved was recorded. This profile was used as an initial condition to the BPG algorithm and the resulting wave was measured at the same location as the former wave. Then the two waves were compared.

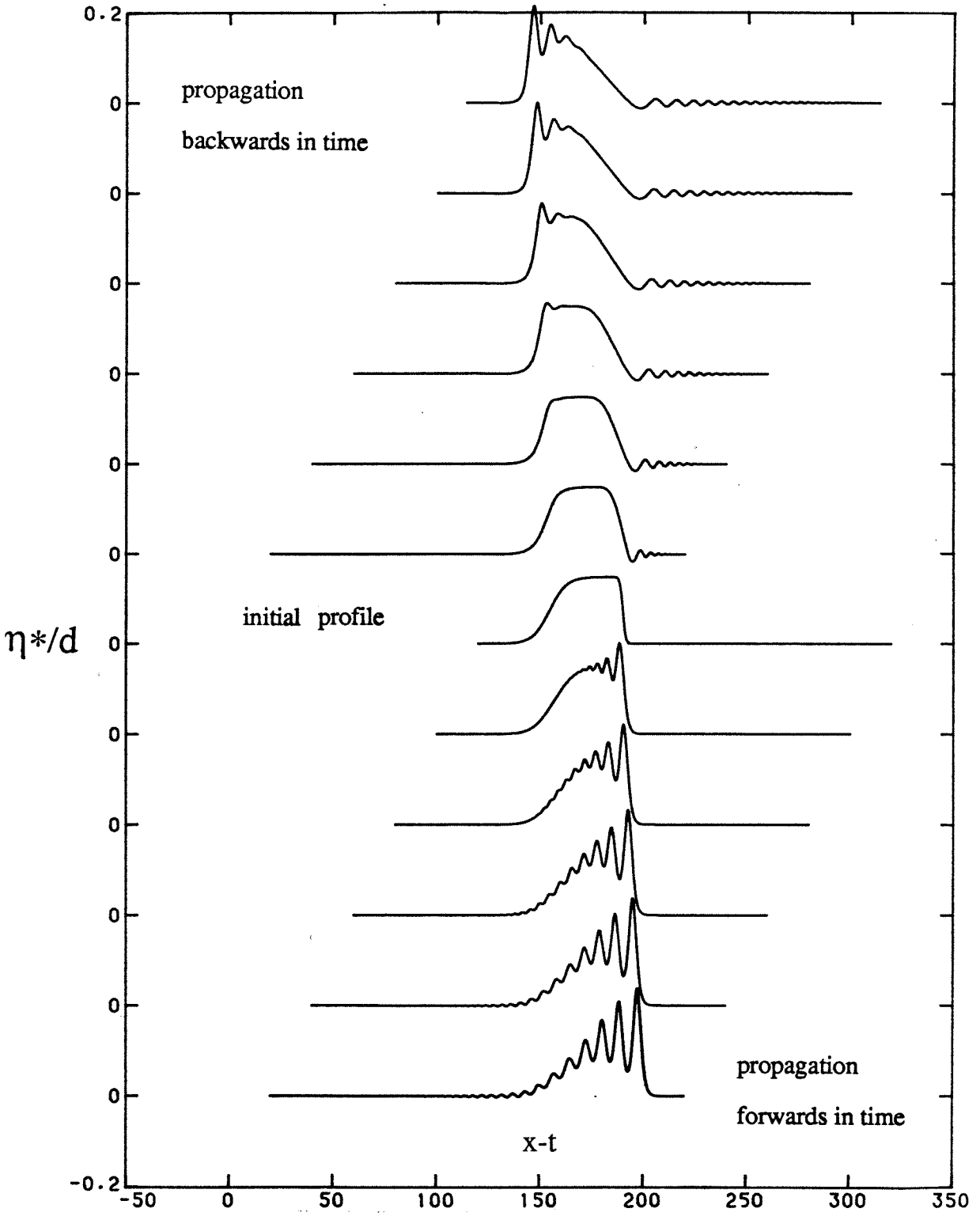

Figure C3.1 The evolution of the wave defined by equation (C1.2) with λ=10 and A=0.3 backwards and forwards in time. The profiles are shown as functions of the *dimensionless* phase and are spaced at intervals of t=20.

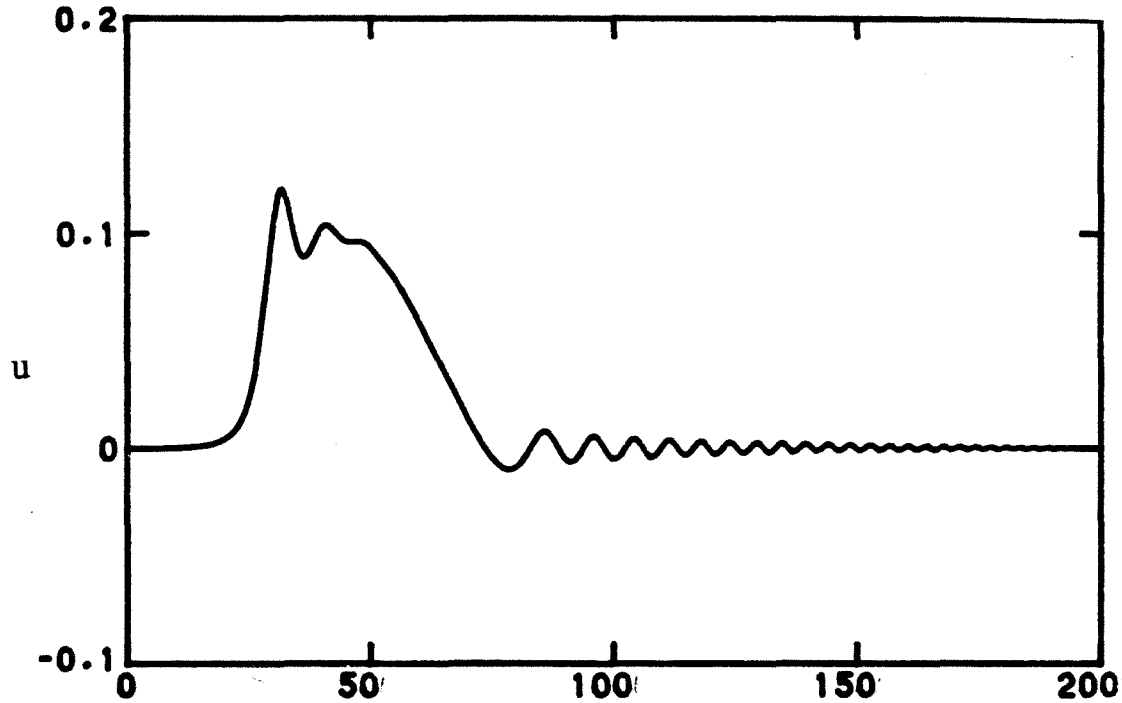

Figure C3.2a The wave that must be created at the generation region so that it may evolve into the desired waveform (marked *initial profile* in figure (C3.1)).

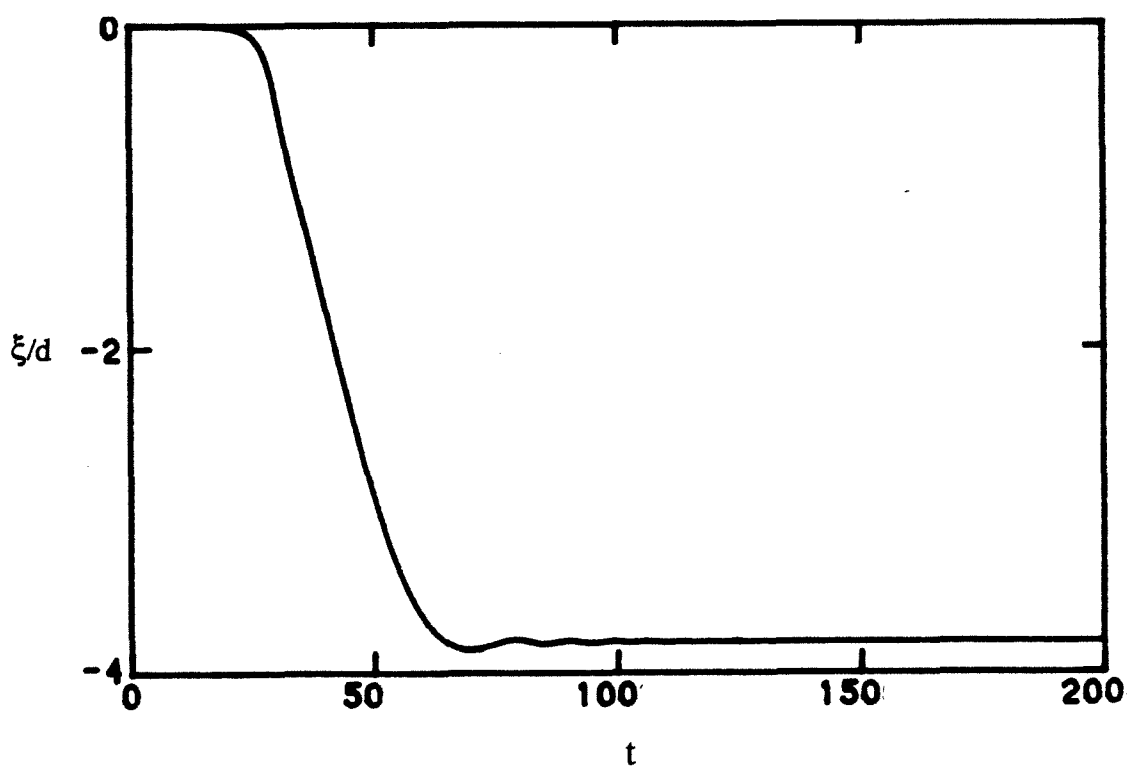

Figure C3.2b The trajectory required to generate the wave of figure (C3.2a).

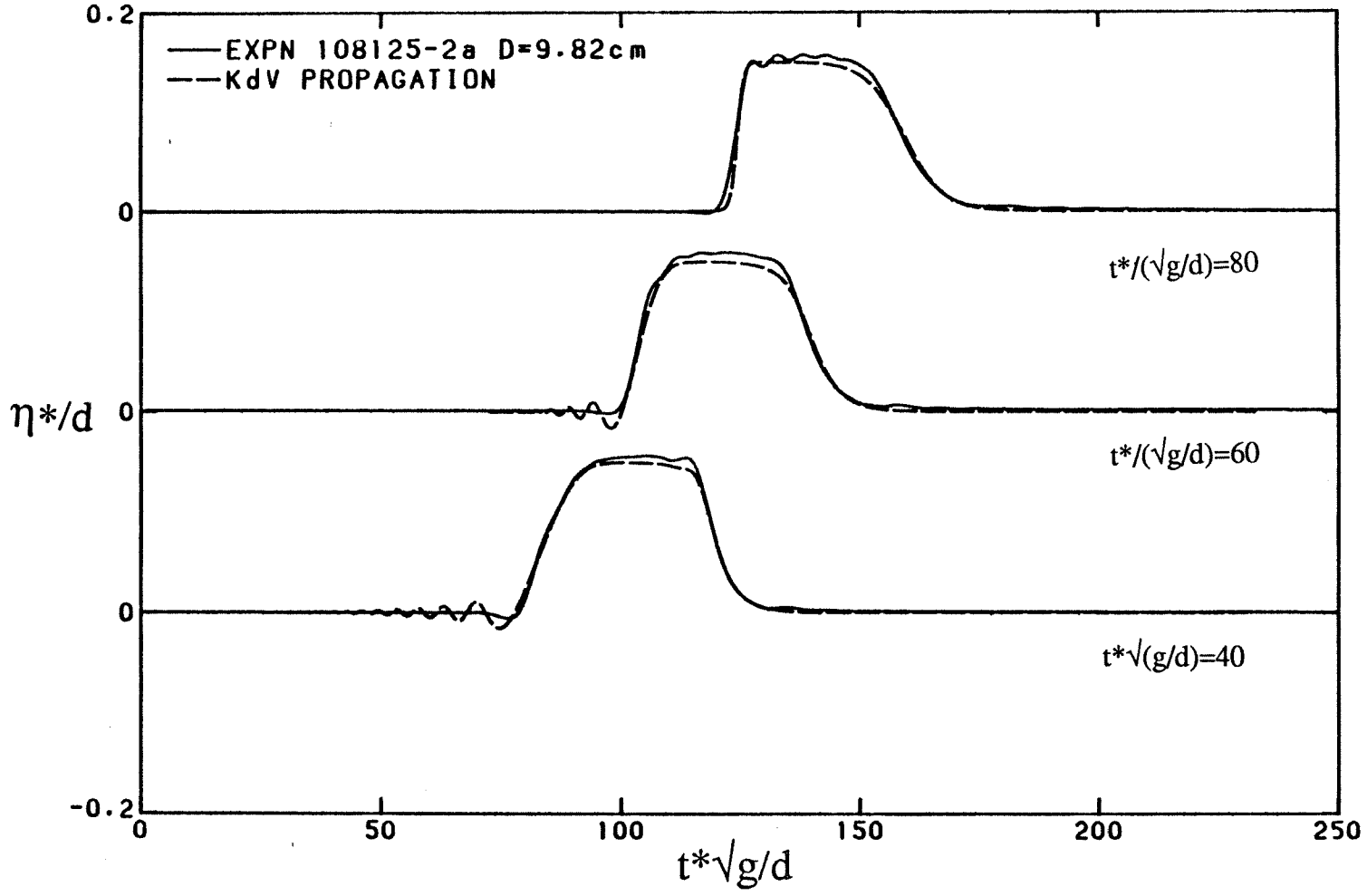

Figure C3.3 Comparison between profiles obtained from the BPG algorithm and from the laboratory experiments for the wave created with the trajectory shown in figure (C3.2b).

The evolution of the wave used as the initial condition is shown in figure (C1.2). Figure (C3.4a) shows the initial wave profile generated after one broken wave reformed. Figure (C3.4b) shows the evolution of that profile backwards in time. Figure (C3.4c) shows the trajectory computed by solving (C2.1) with the algorithm (C2.10) and using the profile in figure (C3.4b) as initial condition.

Figure (C3.5a) shows the comparison of the initial wave (also shown in C3.4a) with the wave obtained from the laboratory experiments after the plate moved with the appropriate trajectory (shown in (C3.4c)). It is seen that the two laboratory profiles agree fairly well with each other, but not as well as the agreement shown in the previous set of experiments, for example in figure (C3.3). One possible explanation is the use of boundary data to initiate the BPG algorithm rather than initial data ; the wave profiles were available only as function of time and the assumption was made that the spatial representation of the initial wave did not differ significantly from the time respresentation.

Figure (C3.4b) shows the comparison between the initial wave profile, shown in figure (C3.4a), and the profile that is generated at the same x-location, if one uses the linearised form of the trajectory equation (C2.5). The generation algorithm produces superior results compared with the linearised trajectory equation.

Conclusion. Given the arbitrary nature of the waves generated in this study, and the fact that it was possible to reproduce a wave resulting after a breaking wave reformed, it is concluded that the BPG alogorithm is a powerful tool for generating long wave in the laboratory.

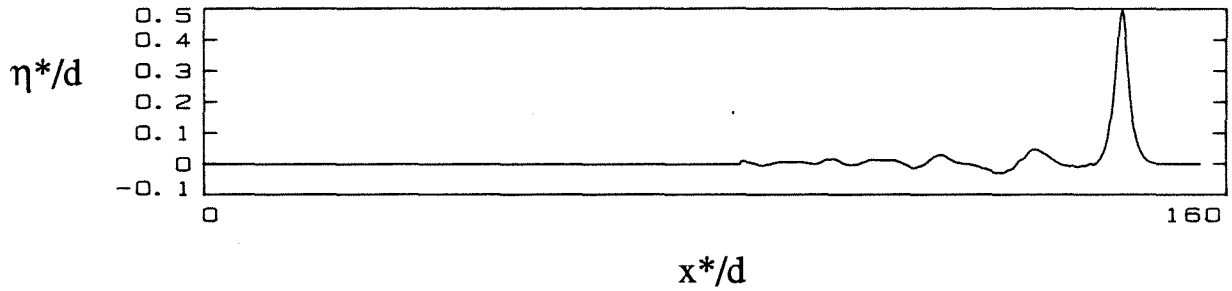

Figure C3.4a The wave that is generated after a broken wave reforms.

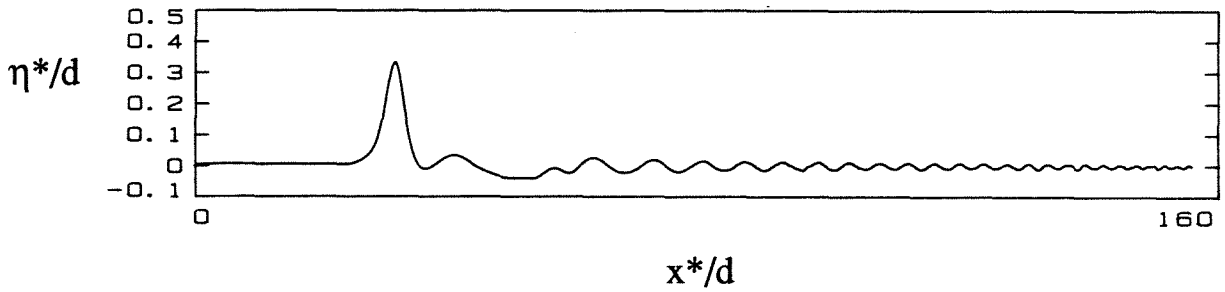

Figure C3.4b The wave that must be created at the generation region so that it may evolve into the wave shown in figure (C3.4a).

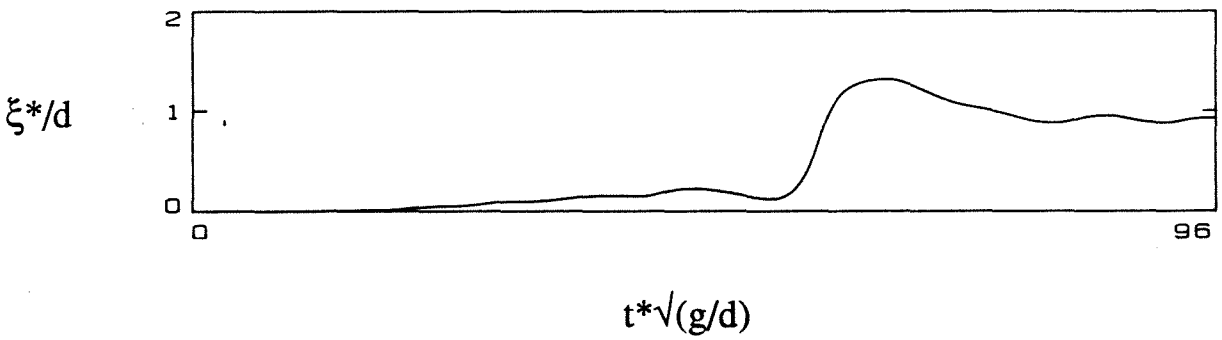

Figure C3.4c The trajectory required to generate the wave motion in figure C(3.4a).

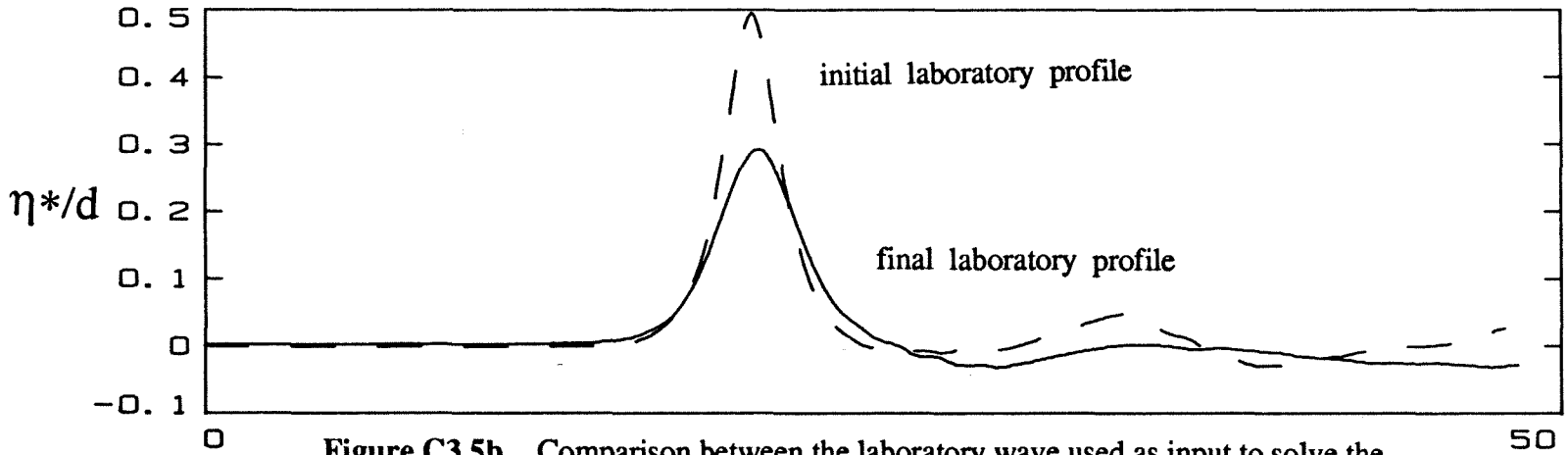

Figure C3.5b Comparison between the laboratory wave used as input to solve the linearised form of the trajectory equation (C2.5) with the laboratory wave that is generated at the same location, x=96.

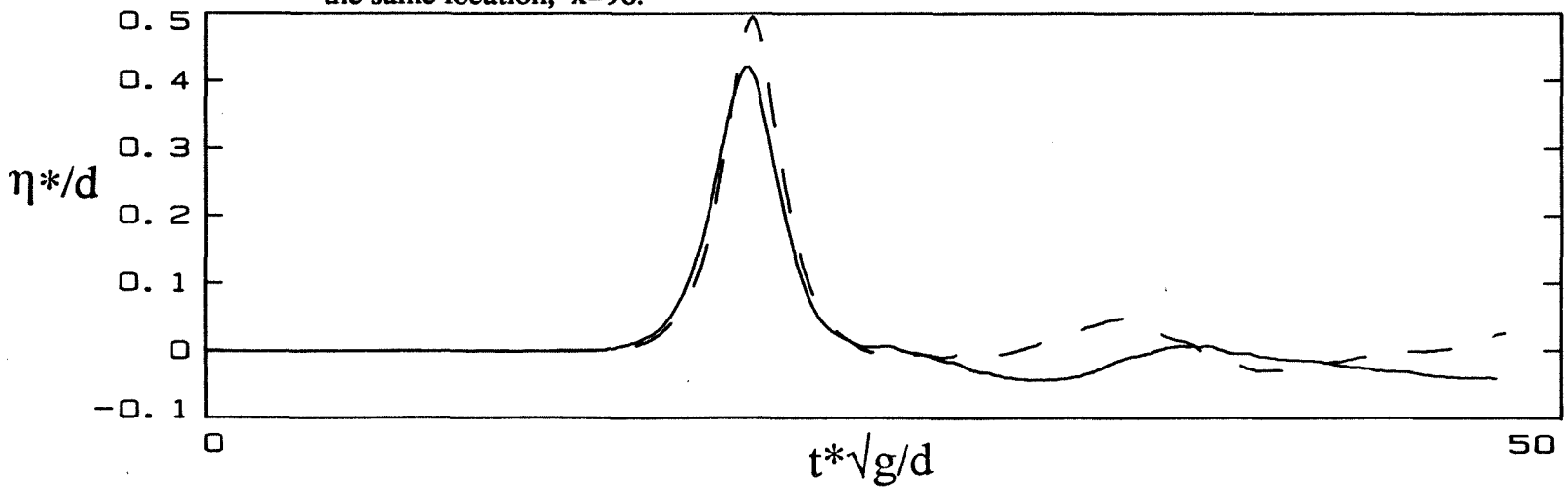

Figure C3.5a Comparison between the laboratory wave used as input in the BPG algorithm with the laboratory wave that is generated at the same location, x=96.

Appendix D

The Fourier transform of a solitary wave.

A solitary wave propagating over constant depth has a velocity profile given by $\eta(x,t) = (H/d)\text{sech}^2\gamma(x-ct)$, where $\gamma = \sqrt{3H/4d}$. To determine the transform of the function $\eta(x,t)$, it is useful to evaluate the following integral :

$$I(k) = \int_{-\infty}^{\infty} \text{sech}^2(\pi x)e^{ikx}dx \qquad (D1.1)$$

The integral converges for all real x. (When $x \to \pm\infty$, then $\text{sech}^2(\pi x) \to 0$).

To calculate the Cauchy principal value of (D1.1) by contour integration consider the function $f(z) = \text{sech}^2(\pi z)e^{ikx}$, where $z = x + iy$ plane, The function $I(k)$ represents an integration of the function $f(z)$ along the entire real axis. Consider the rectangular contour C which extends from $z = R$ to $z = R + i$ to $z = -R + i$ to $z = -R$ to $z = R$. $f(z)$ has one pole of order two inside C at $z = i/2$; it is analytic everywhere else in the strip $0 \leq y \leq 1$. The residue at the pole is $2/\pi k e^{-\frac{1}{2}k}$. Let $I_C = \oint \text{sech}^2(\pi z)e^{ikz}dz$. Then :

$$\begin{aligned} I_C =& \int_{-R}^{R} \text{sech}^2(\pi x)e^{ikx}dx + i\int_0^1 \text{sech}^2\pi(R+iy)e^{-ky+ikR}dy \\ &+ \int_{R}^{-R} \text{sech}^2\pi(\text{x}+\text{i})\text{e}^{\text{ikx}-\text{k}}\text{dx} + i\int_0^1 \text{sech}^2\pi(-R+iy)e^{-ky-ikR}dy. \end{aligned} \qquad (D1.2)$$

The integral over $(R,-R)$ is equal to $-e^-k$ times the integral over $(-R,R)$. The integrals over $(0,1)$ are bounded by $e^{-k}e^{-\pi R}$. In the limit as $R \to \infty$ (D1.2) becomes:

$$\frac{2k}{\pi}e^{-\frac{1}{2}k} = (1-e^{-k})\int_{-\infty}^{\infty} \text{sech}^2(\pi x)e^{ikx}dx. \qquad (D1.3)$$

This equation implies that $\int_{-\infty}^{\infty} \text{sech}^2(\pi x)e^{ikx}dx = (k/\pi)\text{cosech}(k/2)$. The desired transform follows from a change of variable; it is given by :

$$\frac{1}{2\pi}\int_{-\infty}^{\infty} \text{sech}^2(\gamma\text{x})\text{e}^{\text{ikx}}\text{dx} = \frac{\text{k}}{2\gamma^2}\text{cosech}(\frac{\pi\text{k}}{2\gamma}). \qquad (D1.4)$$

Tables of data

Table T3.1

Runup of solitary waves up a 1:19.85 beach

ExpNo	d (cm)	T√(g/d)	Fr	H/d	R/d
116-6 /80	6.25	16.539	0.076	0.250	0.506
116-5 /80	6.25	27.675	0.026	0.072	0.233
1168B /80	8.01	10.015	0.193	0.448	0.723
1219-2 /79	9.79	27.828	0.026	0.078	0.251
1219-5 /79	9.79	11.812	0.142	0.384	0.621
1219-4 /79	9.81	19.430	0.053	0.097	0.274
1219-6 /79	9.84	9.805	0.197	0.462	0.659
1219-8 /79	9.84	10.194	0.189	0.528	0.649
1219-1 /79	9.89	15.547	0.081	0.236	0.467
1027a /84	13.17	13.369	0.105	0.294	0.542
281A /80	14.54	10.012	0.192	0.610	0.780
281C /80	14.54	10.201	0.189	0.591	0.790
281L* /80	14.54	10.201	0.189	0.607	0.805
281E* /80	14.54	10.201	0.189	0.607	0.780
1167C /80	15.50	9.912	0.194	0.601	0.801
122068 /79	15.67	27.851	0.026	0.090	0.270
1220-4 /79	15.72	15.626	0.081	0.259	0.519
1220-3 /79	15.76	12.245	0.133	0.407	0.659
1220-2 /79	15.76	10.193	0.190	0.590	0.810
1029a /84	15.62	13.329	0.105	0.298	0.551
1029b /84	15.65	13.356	0.109	0.322	0.591
1220-5 /79	15.69	19.610	0.053	0.170	0.407
36a /85	16.70	15.329	0.087	0.273	0.487
33b /85	17.53	14.961	0.089	0.276	0.495
221F /80	19.42	10.200	0.189	0.633	0.842
221-6 /80	19.42	10.200	0.189	0.625	0.825
221B /80	19.47	10.200	0.189	0.626	0.862
225c /85	19.56	14.164	0.094	0.283	0.527
225a /85	19.62	14.142	0.094	0.286	0.513
217b /85	20.85	41.498	0.011	0.036	0.124
1220-9 /79	20.92	19.311	0.054	0.188	0.409
122010 /79	20.92	15.545	0.081	0.271	0.513
122011 /79	20.80	11.757	0.109	0.323	0.555
122012 /79	20.92	12.018	0.136	0.416	0.686
626a /84	21.01	19.946	0.049	0.159	0.384
626b /84	21.44	16.955	0.048	0.160	0.384
626c /84	21.47	21.232	0.043	0.143	0.366
218a /85	22.08	41.419	0.011	0.036	0.121
128-1d /80	23.49	13.229	0.110	0.394	0.641
411-2 /83	24.00	38.692	0.132	0.048	0.182
127-1 /80	26.38	16.678	0.076	0.267	0.507
1125a /85	28.43	40.989	0.012	0.039	0.152
1126a /85	28.55	40.947	0.012	0.040	0.156

717a	/84	29.14	61.765	0.006	0.021	0.076
624F	/84	29.34	71.400	0.004	0.014	0.049
624E	/84	29.35	19.032	0.028	0.051	0.198
624D	/84	29.40	30.534	0.021	0.075	0.258
624B	/84	29.62	32.665	0.019	0.065	0.228
624A	/84	29.63	35.387	0.016	0.055	0.207
624C	/84	29.54	30.462	0.021	0.073	0.248
623C	/84	29.72	35.397	0.016	0.056	0.207
623A	/84	29.73	43.456	0.010	0.034	0.144
622A	/84	29.75	61.765	0.005	0.018	0.074
622B	/84	29.77	87.495	0.003	0.009	0.036
621A	/84	29.80	61.764	0.005	0.018	0.075
622C	/84	29.83	49.449	0.008	0.027	0.108
622D	/84	29.86	43.469	0.011	0.038	0.146
410-2	/83	30.00	39.777	0.013	0.047	0.191
410-1	/83	30.48	38.748	0.013	0.047	0.195
25-2a	/80	30.93	19.807	0.052	0.188	0.425
772b	/84	30.97	61.768	0.006	0.019	0.078
772a	/84	31.06	61.746	0.005	0.019	0.076
25-1	/80	31.38	28.526	0.026	0.094	0.288
411-4	/83	33.31	88.001	0.003	0.009	0.041
625K	/84	33.52	113.222	0.002	0.005	0.019
625I	/84	33.55	104.676	0.002	0.006	0.022
625H	/84	33.61	97.922	0.002	0.007	0.026
411-3	/83	33.65	50.246	0.008	0.028	0.123
625G	/84	33.65	92.297	0.002	0.008	0.029
625F	/84	33.76	57.528	0.006	0.023	0.087
625E	/84	33.84	65.143	0.005	0.017	0.063
625C	/84	34.04	53.076	0.007	0.024	0.098
625B	/84	34.24	75.269	0.004	0.012	0.048
624G	/84	34.29	71.395	0.004	0.014	0.052
625A	/84	34.39	79.869	0.003	0.009	0.036
24-1	/80	35.35	19.607	0.052	0.193	0.426
420-3	/82	37.97	41.019	0.012	0.044	0.182
420-1	/83	37.99	54.982	0.007	0.025	0.102
420-2	/83	37.99	58.585	0.006	0.022	0.098
419-2	/83	38.32	43.153	0.010	0.039	0.162

Explanations : a) All waves with H/d>0.055 are *breaking* waves.

b) The data are ordered with respect to the local depth.

c) The values given for the generation time and stroke are not necessarily those specified by (4.2.5) and (4.2.6); to generate the Boussinesq profile (3.4.1) exactly, it is frequently necessary to "tune" the hydraulic system and try different generation times until the desired wave is generated. The values listed are the values actually used.

d) The height-to-depth ratio is measured at a distance (1/2)L from the toe of the beach ; L is given by equation (3.5.1).

Table T3.2

Published data on the runup of nonbreaking solitary waves.

source		slope (cotβ)	H/d	R/d exper	R/d runup law
625k	/84	19.850	0.0052	0.019	0.018
625i	/84	19.850	0.0065	0.022	0.023
625h	/84	19.850	0.0071	0.026	0.026
625g	/84	19.850	0.0080	0.029	0.030
622b	/84	19.850	0.0092	0.036	0.036
411-4	/83	19.850	0.0095	0.041	0.037
625a	/84	19.850	0.0097	0.038	0.038
625b	/84	19.850	0.0129	0.048	0.055
624g	/84	19.850	0.0141	0.052	0.061
624f	/84	19.850	0.0144	0.049	0.063
625e	/84	19.850	0.0170	0.063	0.077
621a/622a	/84	19.850	0.0180	0.074	0.083
772a/772b	/84	19.850	0.0190	0.077	0.089
775c/717a	/84	19.850	0.0210	0.075	0.101
420-2	/83	19.850	0.0220	0.098	0.104
625f	/84	19.850	0.0230	0.087	0.113
625c/420-1	/83/84	19.850	0.0250	0.100	0.125
622c	/84	19.850	0.0270	0.108	0.138
411-3	/83	19.850	0.0280	0.123	0.144
H&W		11.430	0.0460	0.196	0.204
		11.430	0.0500	0.178	0.226
H&W		5.671	0.0500	0.146	0.159
		5.671	0.0560	0.154	0.184
		5.671	0.0640	0.188	0.217
		5.671	0.0680	0.203	0.234
		5.671	0.0720	0.229	0.251
		5.671	0.0740	0.235	0.260
		5.671	0.0760	0.222	0.269
		5.671	0.0820	0.261	0.296
		5.671	0.0860	0.254	0.314
		5.671	0.0880	0.304	0.323
		5.671	0.0910	0.254	0.337
		5.671	0.0950	0.304	0.356
		5.671	0.1040	0.296	0.398
		5.671	0.1070	0.323	0.413
		5.671	0.1090	0.435	0.422
		5.671	0.1140	0.382	0.447

H&W	3.732	0.0500	0.173	0.129
	3.732	0.0540	0.173	0.142
	3.732	0.0610	0.156	0.166
	3.732	0.0680	0.179	0.190
	3.732	0.0700	0.178	0.197
	3.732	0.0720	0.193	0.204
	3.732	0.0760	0.199	0.218
	3.732	0.0810	0.197	0.236
	3.732	0.0910	0.240	0.273
	3.732	0.0980	0.288	0.300
	3.732	0.1010	0.281	0.311
	3.732	0.1020	0.283	0.315
	3.732	0.1030	0.286	0.319
	3.732	0.1080	0.306	0.339
	3.732	0.1240	0.388	0.402
	3.732	0.1260	0.336	0.411
	3.732	0.1340	0.377	0.443
	3.732	0.1360	0.377	0.452
	3.732	0.1380	0.382	0.460
	3.732	0.1420	0.440	0.477
	3.732	0.1480	0.442	0.502
	3.732	0.1560	0.450	0.536
	3.732	0.1780	0.528	0.632
	3.732	0.1810	0.529	0.646
	3.732	0.1880	0.561	0.677
	3.732	0.1890	0.561	0.682
P&G	2.747	0.0390	0.081	0.081
	2.747	0.0500	0.115	0.111
	2.747	0.0610	0.145	0.142
	2.747	0.0880	0.227	0.225
	2.747	0.1370	0.372	0.391
	2.747	0.1190	0.323	0.328
	2.747	0.2210	0.636	0.711
	2.747	0.2390	0.688	0.784
	2.747	0.2980	0.921	1.033
	2.747	0.3480	1.110	1.254
H&W	2.144	0.0540	0.113	0.108
	2.144	0.0610	0.127	0.126
	2.144	0.0700	0.145	0.149
	2.144	0.0720	0.190	0.155
	2.144	0.0750	0.236	0.163
	2.144	0.0810	0.174	0.179
	2.144	0.0860	0.200	0.193
	2.144	0.0960	0.198	0.222
	2.144	0.1010	0.239	0.236
	2.144	0.1040	0.236	0.245
	2.144	0.1120	0.254	0.269
	2.144	0.1210	0.285	0.296
	2.144	0.1220	0.279	0.299
	2.144	0.1320	0.326	0.330
	2.144	0.1410	0.347	0.358
	2.144	0.1430	0.334	0.365

	2.144	0.1440	0.338	0.368
	2.144	0.1490	0.395	0.384
	2.144	0.1500	0.459	0.387
	2.144	0.1560	0.391	0.406
	2.144	0.1620	0.406	0.426
	2.144	0.1720	0.465	0.459
	2.144	0.1880	0.493	0.513
	2.144	0.2160	0.592	0.611
	2.144	0.2220	0.612	0.632
	2.144	0.2440	0.760	0.711
	2.144	0.2650	0.557	0.788
	2.144	0.2830	0.803	0.856
	2.144	0.3440	1.110	1.092
H&W	1.000	0.0540	0.098	0.074
	1.000	0.0610	0.115	0.086
	1.000	0.0640	0.132	0.091
	1.000	0.0650	0.130	0.093
	1.000	0.0670	0.159	0.097
	1.000	0.0760	0.141	0.113
	1.000	0.0820	0.170	0.124
	1.000	0.0860	0.177	0.132
	1.000	0.0920	0.172	0.143
	1.000	0.0960	0.236	0.151
	1.000	0.1010	0.212	0.161
	1.000	0.1060	0.241	0.171
	1.000	0.1070	0.204	0.171
	1.000	0.1170	0.265	0.194
	1.000	0.1210	0.256	0.202
	1.000	0.1320	0.273	0.225
	1.000	0.1340	0.318	0.230
	1.000	0.1360	0.330	0.234
	1.000	0.1380	0.283	0.238
	1.000	0.1470	0.282	0.258
	1.000	0.1540	0.382	0.273
	1.000	0.1560	0.322	0.278
	1.000	0.1720	0.374	0.314
	1.000	0.1880	0.424	0.351
	1.000	0.2100	0.495	0.403
	1.000	0.2120	0.467	0.407
	1.000	0.2420	0.601	0.481
	1.000	0.2430	0.613	0.483
	1.000	0.2960	0.803	0.618
	1.000	0.3040	0.778	0.639
	1.000	0.4800	1.270	1.131
	1.000	0.5040	1.310	1.202

Explanations : a) The column identified as **R**/d runup law refers to the predictions of the asymptotic result (3.4.19). The data on the 1:19.85 slope are data from this study. Nonbreaking data have been identified using the breaking criterion (3.6.3). (See section 3.5.1.)

b) The acronyms are explained after table T3.3.

Table T3.3

Nonbreaking solitary wave runup data from numerical calculations.

source	Slope	H/d	R/d	R/d runup law	R/d exper
H&H (th)	10.000	0.0300	0.100	0.112	
H&H (th)	10.000	0.0500	0.180	0.212	
KLL (th)	3.732	0.0500	0.135	0.129	0.173
KLL (th)	3.732	0.1000	0.308	0.308	0.281
KLL (th)	3.732	0.2000	0.766	0.732	0.599
H&H (th)	3.333	0.0500	0.150	0.122	
H&H (th)	3.333	0.1000	0.310	0.291	
P&G (th)	2.747	0.0500	0.127	0.111	0.115
P&G (th)	2.747	0.0980	0.275	0.257	0.252
P&G (th)	2.747	0.1930	0.599	0.600	0.552
P&G (th)	2.747	0.2940	0.958	1.016	0.898
KLL (th)	1.000	0.0600	0.129	0.084	0.115
KLL (th)	1.000	0.1000	0.159	0.159	0.212
KLL (th)	1.000	0.2000	0.504	0.379	0.454
KLL (th)	1.000	0.4800	1.610	1.131	1.270

0.019

A typ

Explanations: The column identified as **R**/d runup law refers to the predictions of the exact result (3.4.19). The column identified as **R**/d experiments refers to the Hall and Watts (1953) data.

The acronyms in the table refer to the following sources :

H&H : Heitner, K.L. and Housner, G.W. 1970 Numerical model for tsunami runup, *Proc. ASCE,* **WW3**, 701-719.
KLL : Kim, S.K., Liu, P.L-F. and Ligett, J.A. 1983 Boundary integral equation solutions for solitary wave generation, propagation and run-up, *Coastal Engineering*, **7**, 299-317.
P&G : Pedersen, G. and Gjevik, B. 1983 Run-up of solitary waves, *J. Fluid Mech.*, **135**, 283-290.
H&W : Hall, J.V. and Watts, G.M. 1953 *Laboratory investigation of the vertical rise of solitary waves on impermeable slopes*, Beach Erosion Board, US Army Corps of Engineers, Tech. Memo 33, 14pp.

Table T4.1a

Nonbreaking type R waves

ExpNo		d (cm)	T√(g/d)	Fr	R/d	R_u
219-1	/83	19.80	15.725	0.048	0.201	0.765
221-1	/83	19.54	15.723	0.048	0.204	0.764
225-2	/83	16.21	15.730	0.039	0.166	0.735
225-3	/83	16.07	15.728	0.040	0.170	0.747
227-1	/83	15.76	15.732	0.040	0.177	0.766
227-2,3	/83	15.76	15.732	0.050	0.218	0.796
228-1	/83	15.65	15.716	0.026	0.104	0.651
228-2	/83	15.65	15.716	0.039	0.166	0.743
228-3,4	/83	15.65	15.716	0.051	0.220	0.794
120-b,c	/84	13.08	16.056	0.038	0.140	0.638
72-ii	/85	19.01	14.367	0.034	0.127	0.657
71-pp	/85	18.95	7.022	0.057	0.175	0.795
71-xx	/85	18.95	7.022	0.047	0.144	0.755
72-aa	/85	18.91	7.030	0.038	0.106	0.660
72-bb	/85	18.83	7.045	0.070	0.210	0.805
72-ff	/85	19.10	6.995	0.028	0.079	0.627
72-gg	/85	19.06	7.002	0.043	0.129	0.738
72-kk	/85	20.05	3.497	0.063	0.113	0.630
72-ll	/85	20.00	3.502	0.081	0.149	0.672
72-mm	/85	19.90	3.511	0.073	0.129	0.636
72-nn	/85	19.90	3.511	0.093	0.173	0.698
72-oo	/85	20.24	3.481	0.109	0.205	0.732

Table T4.1b

Breaking type R waves

ExpNo		d (cm)	T√(g/d)	Fr	R/d	R_u
217-4	/83	20.02	15.722	0.087	0.332	0.779
217-5	/83	20.02	15.750	0.125	0.450	0.789
218-1	/83	19.97	15.770	0.164	0.544	0.767
221-3	/83	19.54	15.723	0.128	0.455	0.781
223-1	/83	12.99	15.712	0.091	0.323	0.729
223-2	/83	12.91	15.760	0.122	0.421	0.752
223-3,4	/83	12.91	15.760	0.153	0.503	0.750
223-5	/83	12.86	15.729	0.184	0.567	0.730

223-6,7	/83	12.84	15.742	0.214	0.652	0.744
223-8,9	/83	12.80	15.741	0.243	0.707	0.726
223-0	/83	12.72	15.728	0.245	0.712	0.727
223-a	/83	12.68	15.753	0.277	0.765	0.709
223-b	/83	12.70	15.741	0.307	0.798	0.681
224-1,2	/83	16.63	15.760	0.092	0.358	0.801
224-3	/83	16.60	15.728	0.066	0.278	0.814
224-1,2	/83	16.63	15.760	0.092	0.358	0.801
224-3	/83	16.60	15.728	0.066	0.278	0.814
117-a	/84	14.45	8.239	0.157	0.454	0.859
120-a	/84	13.68	15.700	0.128	0.444	0.765
71-cc	/85	18.51	7.105	0.122	0.331	0.812
71-dd	/85	18.41	7.125	0.141	0.380	0.829
71-ee	/85	18.62	7.084	0.168	0.494	0.943
71-ff	/85	18.37	7.132	0.208	0.501	0.803
71-gg	/85	18.41	7.125	0.300	0.689	0.822
71-hh	/85	19.15	6.986	0.323	0.705	0.801
71-ii	/85	19.15	6.986	0.369	0.803	0.820
71-nn	/85	18.40	7.120	0.300	0.662	0.790
72-dd	/85	19.30	6.958	0.087	0.253	0.822
72-ee	/85	19.15	6.986	0.111	0.313	0.838
72-hh	/85	19.03	7.008	0.249	0.608	0.848
72-ss	/85	20.10	3.493	0.142	0.261	0.753
72-tt	/85	20.02	3.500	0.177	0.324	0.785
72-yy	/85	19.89	3.511	0.318	0.546	0.826
72-ww	/85	20.01	3.501	0.423	0.675	0.814
73-cc	/85	19.92	3.509	0.259	0.450	0.802

Table T4.1c

Breaking-reforming type R waves

ExpNo		d (cm)	T√(g/d)	Fr	R/d	R_u
71-kk	/85	19.14	6.987	0.414	0.714	0.664
71-ll	/85	19.08	6.998	0.461	0.733	0.625
71-mm	/85	19.05	7.004	0.507	0.728	0.575
71-oo	/85	19.10	6.995	0.645	0.792	0.516
73-aa	/85	20.02	3.500	0.634	0.724	0.632
73-bb	/85	19.97	3.504	0.846	0.731	0.506

Table T4.1d

Bores of finite volume - type R waves

ExpNo		d (cm)	T√(g/d)	Fr	R/d	R_u
223-c	/83	12.68	15.753	0.339	0.959	0.757
223-d,e	/83	12.60	15.803	0.371	1.024	0.751
224-4	/83	16.57	15.743	0.373	1.123	0.821
224-5	/83	16.45	15.723	0.376	1.102	0.801
224-6	/83	16.46	15.718	0.404	1.091	0.748
120-d	/84	12.82	16.218	0.357	0.993	0.743
224-7	/83	16.44	15.728	0.429	1.091	0.714
224-8	/83	16.40	15.747	0.474	1.151	0.694
225-1	/83	16.22	15.725	0.337	0.957	0.760
71-ss	/85	19.05	7.004	0.738	0.929	0.543
71-tt	/85	19.05	7.004	0.738	0.926	0.542
71-rr	/85	18.94	7.024	0.833	1.052	0.558

Table T4.2a

Nonbreaking type S waves

ExpNo		d (cm)	T√(g/d)	Fr	R/d	R_u
428-1	/85	14.70	3.831	0.048	0.063	0.418
428-2	/85	14.70	3.831	0.059	0.104	0.585
428-5	/85	14.69	3.833	0.064	0.149	0.785
428-6	/85	14.68	3.834	0.069	0.150	0.744
428-3	/85	14.70	3.831	0.075	0.138	0.640
428-23	/85	14.45	3.510	0.080	0.168	0.767
428-245	/85	14.44	3.511	0.086	0.145	0.625
428-4	/85	14.69	3.833	0.091	0.187	0.743
423-2	/82	18.32	3.659	0.100	0.216	0.811
329-2	/82	25.53	6.199	0.010	0.009	0.173
317-1	/82	14.54	8.214	0.020	0.022	0.217
326-2	/82	13.54	8.512	0.030	0.053	0.372
428-17	/85	14.59	7.519	0.030	0.133	0.981
317-3	/82	14.54	8.214	0.033	0.081	0.534
428-8	/85	14.66	7.501	0.039	0.162	0.970
428-9	/85	14.64	7.506	0.045	0.177	0.945
421-abc	/85	16.37	7.741	0.050	0.201	0.974
130-c	/84	16.47	7.502	0.056	0.209	0.937
28-4	/83	22.75	15.734	0.022	0.165	1.161
421-ijk	/85	16.37	15.540	0.025	0.178	1.136
316-3	/82	14.70	24.507	0.025	0.162	0.862

Table T4.2b

Breaking type S waves

ExpNo		d (cm)	T√(g/d)	Fr	R/d	R_u
421-def	/85	16.30	3.388	0.099	0.234	0.914
85-3	/82	15.28	3.397	0.100	0.220	0.851
330-5	/82	21.65	3.366	0.101	0.203	0.782
79-1ab	/82	19.04	3.589	0.104	0.233	0.855
428-7	/85	14.66	3.837	0.107	0.244	0.852
89-3	/82	19.28	3.403	0.125	0.255	0.825
929-4	/82	17.60	3.404	0.138	0.289	0.863
421-23	/85	16.16	3.896	0.149	0.332	0.884
421-24	/85	16.15	3.897	0.149	0.326	0.868
331-2	/82	21.15	3.405	0.149	0.313	0.879
423-1	/82	18.32	3.659	0.150	0.318	0.863
712-3	/82	25.05	3.398	0.154	0.338	0.926
85-4	/82	15.25	3.401	0.154	0.305	0.835
79-3	/82	19.04	3.589	0.156	0.345	0.915
714-4	/82	19.74	3.398	0.175	0.361	0.892
89-2	/82	19.32	3.399	0.175	0.354	0.875
718-4	/82	12.00	3.400	0.197	0.356	0.800
423-3	/82	18.32	3.659	0.200	0.428	0.923
712-4	/82	22.85	3.401	0.200	0.414	0.919
79-4	/82	19.04	3.589	0.206	0.440	0.934
714-5	/82	19.74	3.398	0.224	0.442	0.897
718-3	/82	12.00	3.400	0.247	0.508	0.953
421-3	/82	18.56	3.635	0.250	0.510	0.923
719-4	/82	11.74	3.401	0.250	0.442	0.821
84-1	/82	15.39	3.401	0.250	0.470	0.873
712-5	/82	22.80	3.398	0.251	0.501	0.928
85-1	/82	15.28	3.397	0.252	0.471	0.870
79-5	/82	19.04	3.589	0.256	0.517	0.922
718-5	/82	12.00	3.400	0.273	0.478	0.828
718-6	/82	11.99	3.401	0.273	0.484	0.838
714-6	/82	19.72	3.400	0.275	0.528	0.909
719-1ab	/82	11.74	3.437	0.297	0.524	0.845
85-5	/82	15.25	3.401	0.299	0.576	0.927
718-2	/82	12.00	3.400	0.300	0.558	0.896
718-7	/82	11.99	3.401	0.300	0.513	0.824
79-6	/82	19.04	3.589	0.306	0.599	0.927
88-1	/82	15.07	3.397	0.320	0.588	0.897
714-1	/82	19.81	3.645	0.326	0.651	0.951
421-2ab	/82	18.58	3.633	0.350	0.657	0.908
719-3	/82	18.56	3.401	0.350	0.588	0.835
718-1	/82	12.00	3.400	0.351	0.596	0.844
85-2	/82	15.28	3.397	0.355	0.600	0.842
88-2	/82	15.07	3.397	0.360	0.639	0.887

428-27	/85	14.32	3.526	0.396	0.626	0.793
330-1	/82	22.04	6.672	0.050	0.200	1.028
421-4,5	/85	16.31	7.755	0.059	0.236	1.001
326-3	/82	13.54	8.512	0.061	0.198	0.788
326-3	/82	13.54	8.512	0.061	0.198	0.788
428-10	/85	14.62	7.512	0.064	0.244	0.982
428-112	/85	14.62	7.512	0.071	0.265	0.982
421-no	/85	16.19	7.784	0.075	0.307	1.073
428-15	/85	14.60	7.517	0.076	0.315	1.105
428-14	/85	14.59	7.519	0.080	0.319	1.074
130-a	/84	20.28	7.609	0.084	0.315	1.015
317-4ab	/82	14.54	8.214	0.090	0.327	0.967
330-6	/82	21.65	6.731	0.100	0.387	1.139
326-4	/82	13.54	8.512	0.100	0.355	0.951
428-16	/85	14.59	7.519	0.107	0.392	1.045
428-20	/85	14.52	7.537	0.118	0.458	1.128
130-b	/84	19.59	7.742	0.125	0.472	1.099
329-3	/82	25.53	6.199	0.130	0.447	1.102
428-21	/85	14.50	7.543	0.138	0.515	1.119
428-1	/82	14.70	7.021	0.150	0.530	1.109
331-3	/82	21.15	6.811	0.150	0.532	1.127
428-22	/85	14.47	7.550	0.156	0.598	1.178
317-6	/82	14.54	8.214	0.160	0.574	1.071
317-7ab	/82	14.54	8.214	0.190	0.632	1.028
317-2ab	/82	14.54	8.214	0.196	0.664	1.053
428-2ab	/82	19.90	7.021	0.200	0.687	1.142
326-5	/82	13.54	8.512	0.200	0.701	1.079
216-2	/83	15.27	7.614	0.212	0.719	1.104
815-a	/84	17.52	7.483	0.236	0.706	1.002
126-1	/83	13.23	11.943	0.098	0.489	1.163
121-1a	/83	13.93	11.740	0.133	0.617	1.157
929-1	/82	17.63	11.473	0.142	0.652	1.171
929-2	/82	17.63	11.473	0.142	0.667	1.198
929-3	/82	17.63	11.473	0.142	0.672	1.207
928-1	/82	17.63	10.808	0.151	0.688	1.205
126-8	/83	13.14	11.984	0.156	0.741	1.213
28-1	/83	22.78	15.723	0.026	0.208	1.281
28-5	/83	22.73	15.741	0.028	0.224	1.299
28-2	/83	22.78	15.723	0.036	0.268	1.272
127-a	/84	14.16	15.740	0.041	0.249	1.065
3012	/83	23.95	15.731	0.042	0.317	1.330
28-3	/83	22.75	15.734	0.044	0.325	1.313
421-lm	/85	16.23	15.549	0.037	0.251	1.171
127-b	/84	13.79	15.949	0.056	0.352	1.167
27-4	/83	22.83	15.765	0.066	0.446	1.302
3011	/83	23.96	15.728	0.083	0.527	1.282
217-3	/83	20.02	15.722	0.086	0.528	1.249
129-a	/84	13.45	15.757	0.089	0.502	1.154
27-5	/83	22.83	15.765	0.103	0.614	1.256
216-3	/83	15.27	15.173	0.107	0.647	1.303
216-1	/83	15.29	15.163	0.111	0.645	1.262
129-b	/84	13.25	15.772	0.120	0.628	1.136
28-7	/83	22.73	15.741	0.121	0.723	1.300

3014	/83	23.92	15.741	0.124	0.736	1.298
27-6	/83	22.80	15.775	0.129	0.766	1.308
216-4	/83	15.27	15.173	0.133	0.752	1.273
315-2	/82	14.87	16.245	0.035	0.186	0.891
315-3	/82	14.87	16.245	0.040	0.223	0.960
315-4	/82	14.87	16.245	0.045	0.261	1.023
315-5	/82	14.87	16.245	0.050	0.288	1.037
315-6	/82	14.87	16.245	0.060	0.335	1.043
315-7	/82	14.87	16.245	0.070	0.403	1.109
315-8	/82	14.87	16.245	0.100	0.606	1.254
34-10	/82	14.87	17.753	0.111	0.571	1.049
315-10	/82	14.87	16.245	0.130	0.647	1.085
34-1	/82	12.45	17.753	0.139	0.676	1.037
34-2	/82	12.45	17.753	0.139	0.684	1.049
34-11	/82	12.45	17.753	0.139	0.672	1.031
315-9	/82	14.79	16.288	0.151	0.717	1.066
316-2	/82	14.70	24.507	0.035	0.272	1.106
316-4	/82	14.70	24.507	0.047	0.323	1.037
316-5	/82	14.70	24.507	0.055	0.358	1.014
35-23	/82	12.29	26.803	0.056	0.390	1.050
316-6	/82	14.70	24.507	0.065	0.419	1.038
316-1	/82	14.70	24.507	0.087	0.546	1.071
35-24	/82	12.29	26.803	0.112	0.632	0.977
35-26	/82	12.29	26.803	0.166	0.718	0.811
36-31	/82	9.38	30.680	0.043	0.230	0.725
36-32	/82	9.38	30.680	0.064	0.365	0.837
36-33	/82	9.38	30.680	0.085	0.451	0.824
36-34	/82	9.38	30.680	0.096	0.494	0.819
330-9	/82	21.62	33.680	0.100	0.555	0.858
36-35	/82	9.38	30.680	0.117	0.596	0.843

Table T4.2c

Breaking-reforming type S waves

ExpNo		d (cm)	T√(g/d)	Fr	R/d	R_u
714-2	/82	19.75	3.397	0.351	0.636	0.900
419-1	/82	18.18	3.673	0.368	0.691	0.914
423-5ab	/82	18.32	3.659	0.400	0.717	0.888
88-3	/82	15.07	3.397	0.401	0.642	0.818
423-6	/82	18.30	3.661	0.450	0.738	0.832
88-4	/82	15.07	3.397	0.451	0.665	0.771
423-7	/82	18.30	3.661	0.500	0.743	0.770
89-4	/82	19.28	3.403	0.501	0.762	0.812
88-5	/82	15.07	3.397	0.501	0.675	0.720
423-8	/82	18.30	3.661	0.550	0.749	0.719
423-9	/82	18.30	3.661	0.602	0.765	0.683
423-10	/82	18.30	3.661	0.701	0.785	0.620

430-1	/82	19.41	7.109	0.225	0.750	1.129
326-7	/82	13.54	8.512	0.230	0.682	0.939
430-2	/82	19.41	7.109	0.250	0.750	1.038
326-6	/82	13.54	8.512	0.250	0.738	0.950
329-4	/82	25.53	6.199	0.251	0.727	1.058
130-d	/84	16.19	7.566	0.254	0.724	0.964
129-c	/84	12.99	7.517	0.259	0.707	0.931
430-3	/82	19.41	7.109	0.275	0.740	0.949
428-3	/82	19.90	7.021	0.323	0.778	0.881
130-e	/84	16.05	7.599	0.331	0.721	0.776
326-8	/82	13.54	8.512	0.350	0.679	0.667
216-5	/83	15.27	15.173	0.159	0.719	1.053
3013	/83	23.92	15.741	0.164	0.793	1.118
34-3	/82	12.45	17.753	0.166	0.672	0.894
34-12	/82	12.45	17.753	0.166	0.664	0.883
126-3	/83	13.25	11.934	0.196	0.719	0.981
126-7	/83	13.14	11.984	0.234	0.760	0.900
126-5	/83	13.21	11.953	0.272	0.740	0.777
126-4	/83	13.23	11.943	0.295	0.726	0.714
126-6	/83	13.21	11.953	0.327	0.732	0.664
34-1314	/82	12.45	17.753	0.194	0.676	0.795
217-1	/83	20.02	15.722	0.196	0.757	0.927
216-6,7	/83	15.26	15.178	0.213	0.760	0.884
34-5	/82	12.45	17.753	0.221	0.676	0.715
34-15	/82	12.45	17.753	0.223	0.664	0.699
34-16	/82	12.45	17.753	0.249	0.692	0.666
36-36	/82	9.38	30.680	0.138	0.628	0.778
33-8	/82	7.83	55.966	0.140	0.776	0.747
35-25	/82	12.29	26.803	0.149	0.706	0.867
36-37	/82	9.38	30.680	0.159	0.655	0.724
35-18	/82	12.45	26.630	0.166	0.672	0.761
35-17	/82	12.45	26.630	0.167	0.660	0.744

Table T4.2d

Bores of finite volume - type S waves

ExpNo		d (cm)	T√(g/d)	Fr	R/d	R_u
329-1	/82	25.53	6.199	0.366	0.769	0.829
33-12	/82	7.83	11.193	0.702	0.969	0.490
3015	/83	23.92	15.741	0.205	0.827	0.976
23-1	/83	23.35	15.718	0.209	0.789	0.917
23-2	/83	23.35	15.718	0.251	0.809	0.812
34-6	/82	12.45	17.753	0.276	0.700	0.620
23-3	/83	23.32	15.728	0.292	0.876	0.778
26-1	/83	23.03	15.723	0.297	0.897	0.786

27-3	/83	22.85	15.739	0.300	0.895	0.779
34-7	/82	12.45	17.753	0.304	0.745	0.611
28-10	/83	22.68	15.758	0.326	0.922	0.751
28-8	/83	22.71	15.748	0.326	0.942	0.766
28-9	/83	22.68	15.758	0.326	0.951	0.773
34-8	/82	12.45	17.753	0.331	0.846	0.648
28-11	/83	22.66	15.765	0.343	0.964	0.753
33-9	/82	7.83	55.966	0.140	0.770	0.741
35-19	/82	12.45	26.630	0.221	0.834	0.751
35-20	/82	12.45	26.630	0.239	0.894	0.755
35-21	/82	12.45	26.630	0.239	0.890	0.752
35-22	/82	12.45	26.630	0.260	0.923	0.730
35-27	/82	12.29	26.803	0.296	1.079	0.766
33-6	/82	7.83	22.386	0.315	0.751	0.545
33-7	/82	7.83	22.386	0.351	0.776	0.517
33-14	/82	7.83	22.386	0.351	0.763	0.509

Table T4.3

Breaking type P waves

ExpNo		d (cm)	T√(g/d)	Fr	R/d	R_u
326-a	/84	34.48	34.185	0.026	0.275	1.252
326-b	/84	33.55	34.959	0.026	0.287	1.297
328-c	/84	18.73	41.992	0.040	0.359	1.064
329-a	/84	19.39	32.034	0.050	0.357	0.975
330-b	/84	11.71	51.684	0.050	0.386	0.877
331-a,b	/84	11.79	50.589	0.051	0.400	0.901
331-c	/84	29.94	29.072	0.035	0.316	1.203
41-b	/84	29.81	32.614	0.032	0.293	1.144
415-a	/84	8.76	58.480	0.061	0.415	0.767
415-b	/84	8.68	60.350	0.075	0.504	0.773
415-c	/84	8.40	43.901	0.106	0.524	0.697
415-d	/84	8.30	55.599	0.086	0.524	0.746
415-e	/84	8.13	53.416	0.091	0.500	0.692
415-f	/84	19.60	33.768	0.060	0.406	0.947
416-b	/84	16.68	21.700	0.037	0.209	0.853
416-d	/84	16.34	29.388	0.036	0.456	1.693
416-c	/84	16.48	35.154	0.051	0.266	0.688

Table T4.4a

Integrals of the motion. Type R waves.

ExpNo	d (cm)	T√(g/d)	S/d	Mom flux	Impulse	Energy flux	Power	R/d
72kk /85	20.05	3.497	0.219	0.0139	0.0967	0.0009	0.1205	0.113
72ll /85	20.00	3.502	0.285	0.0231	0.1680	0.0018	0.1586	0.149
72mm /85	19.90	3.511	0.256	0.0194	0.1061	0.0014	0.1437	0.129
72nn /85	19.90	3.511	0.327	0.0304	0.2258	0.0026	0.1910	0.173
72oo /85	20.24	3.481	0.380	0.0430	0.2946	0.0046	0.2261	0.205
72ss /85	20.10	3.493	0.498	0.0762	0.3028	0.0107	0.2993	0.261
72tt /85	20.02	3.500	0.619	0.1201	0.4725	0.0207	0.3972	0.324
73cc /85	19.92	3.509	0.909	0.2839	1.0118	0.0708	0.6985	0.450
72yy /85	19.89	3.511	1.116	0.4538	1.4826	0.1377	0.9500	0.546
72ww /85	20.01	3.501	1.479	0.9163	2.3248	0.3727	1.4935	0.675
73aa /85	20.02	3.500	2.218	2.3570	2.7944	1.4698	2.5796	0.724
73bb /85	19.97	3.504	2.964	4.0701	4.7231	3.2337	3.9153	0.731
72gg /85	19.06	7.002	0.299	0.0125	0.2332	not available		0.129
71xx /85	18.95	7.022	0.332	0.0157	0.3237	0.0007	0.1733	0.144
71pp /85	18.95	7.022	0.401	0.0227	0.3958	0.0013	0.2208	0.175
72cc /85	18.83	7.045	0.558	0.0447	0.4278	0.0035	0.3124	0.245
72dd /85	19.30	6.958	0.606	0.0543	0.5436	0.0046	0.3434	0.253
72ee /85	19.15	6.986	0.773	0.0922	0.4850	0.0102	0.4533	0.313
71cc /85	18.51	7.105	0.870	0.1159	0.5588	0.0142	0.5175	0.331
71ee /85	18.62	7.084	1.187	0.2189	1.0435	0.0361	0.7621	0.494
71nn /85	18.40	7.126	2.141	0.8005	1.9934	0.2390	1.6570	0.662
71ff /85	18.37	7.132	1.481	0.3511	1.2003	0.0721	0.9943	0.501
71gg /85	18.41	7.125	2.140	0.7751	2.0757	0.2276	1.6484	0.689
71hh /85	19.15	6.986	2.256	0.9412	2.8062	0.2976	1.9297	0.705
71ii /85	19.15	6.986	2.574	1.3119	3.9163	0.4700	2.5373	0.803
71kk /85	19.14	6.987	2.894	1.6020	2.4807	0.6684	2.4305	0.714
71ll /85	19.08	6.998	3.229	2.2366	4.4380	1.0218	3.4103	0.733
71mm /85	19.05	7.004	3.554	2.6272	4.5560	1.3074	3.8004	0.728

71oo	/85	19.10	6.995	4.513	4.4600	6.3264	2.7891	5.5604	0.792
71ss	/85	19.05	7.004	5.171	5.9057	6.6547	4.2274	6.5127	0.929
71tt	/85	19.05	7.004	5.171	5.9252	7.0517	4.2424	6.5597	0.926
71rrr	/85	18.94	7.024	5.850	7.5560	6.5877	6.1232	7.3890	1.052
72hh	/85	19.03	7.008	1.745	0.5188	2.1183	0.1251	1.3397	0.608
72ii	/85	19.01	14.367	0.484	0.0165	0.3238	0.0005	0.2468	0.127
120d	/84	12.82	13.311	5.783	4.7736	4.4035	2.9012	5.4620	0.993
221-1	/83	19.54	16.949	0.761	0.0383	0.7241	0.0019	0.4091	0.204
228-1	/83	15.65	16.658	0.400	0.0111	0.3610	0.0003	0.2058	0.104
120b	/84	13.16	18.711	0.595	0.0254	0.3571	0.0006	0.1328	0.137
228-2	/83	15.65	17.814	0.606	0.0243	0.5455	0.0010	0.3204	0.165
225-3	/83	16.07	16.955	0.619	0.0256	0.5340	0.0011	0.3284	0.169
227-1	/83	15.76	16.821	0.633	0.0265	0.5085	0.0011	0.3346	0.176
227-2	/83	15.76	17.184	0.791	0.0414	0.6939	0.0021	0.4267	0.218
227-3	/83	15.75	17.315	0.785	0.0421	0.8057	0.0022	0.4260	0.219
228-3	/83	15.65	16.975	0.791	0.0419	0.6295	0.0022	0.4242	0.220
228-4	/83	15.65	17.402	0.797	0.0421	0.6971	0.0022	0.4290	0.220
228-5	/83	15.64	16.964	0.990	0.0651	0.8579	0.0042	0.5409	0.269
217-4	/83	20.02	16.912	1.363	0.1253	1.3866	0.0108	0.7925	0.331
217-5	/83	20.02	17.220	1.968	0.2722	2.0360	0.0339	1.2230	0.450
221-2	/83	19.54	16.694	1.069	0.0761	1.0411	0.0052	0.5998	0.269
219-2	/83	19.80	17.273	1.120	0.0839	1.0729	0.0060	0.6253	0.285
223-1	/83	12.99	17.224	1.430	0.1395	1.3591	0.0173	0.8334	0.322
224-2	/83	16.61	17.706	1.443	0.1426	1.5023	0.0131	0.8524	0.359
224-1	/83	16.66	17.480	1.451	0.1422	1.4257	0.0130	0.8490	0.355
223-2	/83	12.91	17.103	1.919	0.2585	2.0209	0.0314	1.9370	0.420
221-3	/83	19.54	17.076	2.015	0.2894	2.1433	0.0370	1.2751	0.454
223-3,4	/83	12.91	18.149	2.407	0.4179	2.6495	0.0636	1.5846	0.503
218-1	/83	19.97	17.438	2.587	0.4872	2.8352	0.0792	1.7385	0.544
223-5	/83	12.86	17.346	2.890	0.6273	3.2393	0.1156	2.0129	0.567
223-7	/83	12.83	17.523	3.366	0.8626	3.9000	1.8300	2.4699	0.649
223-8	/83	12.81	16.644	3.816	1.1812	4.3945	0.2903	2.9857	0.703
223-9	/83	12.79	17.849	3.835	1.1694	4.6084	0.2845	2.9911	0.711
223-0	/83	12.72	17.336	3.859	1.1807	4.6571	0.2882	3.0142	0.711
223-B	/83	12.70	18.175	4.832	1.9391	5.9882	0.5922	4.1505	0.797

223-C /83	12.68	17.680	5.338	2.4235	6.6541	0.8157	4.8202	0.959
223-E /83	12.60	17.153	5.840	3.0464	7.6135	1.1279	5.6596	0.975
224-4 /83	16.57	16.866	5.864	3.0600	7.4871	1.1372	5.6206	1.122
225-1 /83	16.22	16.954	5.295	2.3771	6.1709	0.7994	4.6275	0.957
224-5 /83	16.45	17.808	5.906	3.0621	7.2881	1.1490	5.5881	1.101
224-6 /83	16.46	17.293	6.354	3.5887	7.9301	1.4409	6.1814	1.091
224-7 /83	16.44	17.381	6.738	4.1254	8.3417	1.7599	6.7702	1.090
224-8 /83	16.40	17.402	7.461	5.1976	9.2590	2.4511	7.9416	1.151
120a /84	13.68	17.832	2.002	0.2924	1.8563	0.0145	1.2295	0.444
120c /84	13.00	21.556	0.599	0.0226	0.4198	0.0010	0.2975	0.144
223-6 /83	12.85	29.690	3.367	0.8682	3.8761	0.1849	2.4636	0.655
219-1 /83	19.80	33.026	0.746	0.0186	1.3978	0.0005	0.4000	0.201

Table T4.4b

Type S waves

ExpNo	d (cm)	T√(g/d)	S/d	Mom flux	Impulse	Energy flux	Power	R/d
3011 /83	23.96	14.461	1.291	0.3009	1.7030	0.0651	0.9482	0.529
3012 /83	23.95	15.770	0.647	0.0673	0.7566	0.0073	0.3927	0.317
3013 /83	23.92	16.497	2.558	1.3264	3.3253	0.5638	2.3682	0.793
3014 /83	23.92	14.806	1.918	0.6887	2.3530	0.2234	1.5785	0.736
3015 /83	23.92	14.191	1.217	2.2746	4.3059	1.2710	3.4561	0.826
261 /83	23.03	15.820	4.644	4.7983	4.9721	3.7116	5.1267	0.897
274 /83	22.87	17.867	1.016	0.1701	0.9198	0.0288	0.6448	0.446
275 /83	22.83	17.935	1.606	0.4513	1.6198	0.1202	1.1503	0.614
276 /83	22.80	17.684	2.021	0.7388	2.0334	0.2472	1.5431	0.765
281 /83	22.78	16.537	0.403	0.0423	0.3901	0.0045	0.2248	0.207
282 /83	22.78	13.545	0.564	0.0488	0.5383	0.0045	0.3181	0.267
283 /83	22.75	14.447	0.688	0.0741	0.6780	0.0084	0.4058	0.323
284 /83	22.75	14.716	0.341	0.0171	0.2995	0.0010	0.1802	0.165
285 /83	22.73	14.558	0.437	0.0286	0.3897	0.0021	0.2379	0.224

286	/83	22.73	13.776	0.813	0.1055	0.8358	0.0142	0.4925	0.319
287	/83	22.73	15.714	1.904	0.6481	1.9112	0.2044	1.4257	0.722
288	/83	22.71	15.879	5.138	6.2285	5.8662	5.3038	6.2111	0.934
289	/83	22.68	16.521	5.144	6.4891	6.4618	5.5568	6.6032	0.951
2810	/83	22.68	15.942	5.112	6.3468	6.1314	5.4081	6.4264	0.939
2811	/83	22.66	16.897	5.410	7.4836	6.8716	6.7742	7.1430	0.968
2162	/83	15.27	8.849	1.610	1.1848	2.0069	0.6493	1.3542	0.719
2163	/83	15.27	15.421	1.629	0.4920	1.6734	0.1386	1.1975	0.646
2164	/83	15.27	15.389	2.016	0.7926	2.2010	0.2770	1.6186	0.752
2165	/83	15.26	14.977	2.416	1.1913	2.6574	0.4988	2.1006	0.719
2166	/83	15.26	12.139	3.229	2.4761	3.5154	1.4429	3.2952	0.767
2172	/83	20.02	15.400	3.070	1.9653	3.6725	0.9996	3.0207	0.787
2173	/83	20.02	14.420	1.357	0.3189	1.4854	not available		0.528
130a	/84	20.28	9.960	0.636	0.1125	0.6014	0.0204	0.3861	0.314
130b	/84	19.58	10.643	0.967	0.2904	1.0840	0.0810	0.6910	0.472
130c	/84	16.47	11.592	0.418	0.0409	0.3440	0.0045	0.2242	0.208

Table T4.4c

Type P waves

ExpNo		d (cm)	T√(g/d)	S/d	Mom flux	Impulse	Energy flux	Power	R/d
326a	/84	34.48	29.486	0.877	0.0415	0.4069	0.0024	0.4368	0.275
326b	/84	33.55	28.075	0.859	0.0474	0.5797	0.0030	0.4540	0.287
328c	/84	18.73	34.622	1.665	0.1517	1.5831	0.0164	0.9405	0.361
329a	/84	19.39	31.866	1.611	0.1415	1.3577	0.0150	0.8754	0.356
330a	/84	12.84	69.996	2.387	0.1244	6.9502	0.0063	1.4910	0.393
330b	/84	11.71	38.881	2.575	0.2946	2.3880	0.0396	1.4763	0.386
331a	/84	11.85	47.167	2.559	0.2893	2.3276	0.0382	1.4854	0.395
331b	/84	11.73	40.384	2.559	0.2914	2.3461	0.0389	1.4666	0.405
331c	/84	29.94	26.285	1.015	0.0685	0.7296	0.0057	0.5332	0.316

41a	/84	30.21	22.748	1.005	0.0662	0.7809	0.0054	0.5179	0.373
41b	/84	29.81	31.345	1.050	0.0637	0.5137	0.0045	0.5319	0.293
415a	/84	8.76	48.594	3.548	0.4796	3.6608	0.0746	2.1098	0.415
415c	/84	8.40	42.968	4.494	0.8002	4.5981	0.1508	2.8724	0.499
415d	/84	8.30	42.008	4.819	0.8285	4.9810	0.1548	2.9212	0.524
415e	/84	8.13	41.347	4.920	0.9041	6.0824	0.1749	3.1492	0.491
415f	/84	19.60	22.271	2.019	0.2100	1.4483	0.0251	1.0042	0.409
415g	/84	18.36	10.614	0.462	0.0085	0.1521	0.0003	0.1141	0.117
416c	/84	16.48	18.949	1.051	0.0333	0.3921	0.0020	0.3243	0.266
416a	/84	18.02	16.468	0.717	0.0333	0.3892	0.0009	0.2840	0.135
416b	/84	16.68	20.093	0.801	0.0590	0.7242	0.0047	0.4699	0.209
416d	/84	16.34	28.142	1.806	0.1651	2.2531	0.0173	1.0155	0.456

Explanations: The column entries refer to the following integrals :

Mom flux = $\int(d\xi/dt^*)^2(\eta_p+d)dt^*/[d^2\sqrt{gd}]$

Impulse = $\int F_{px}dt^*/[\rho gd^2\sqrt{(d/g)}]$

Energy flux = $\int(d\xi/dt^*)^3(\eta_p+d)dt^*/[gd^3]$

Power = $\int F_{px}\,(d\xi/dt^*)\,dt^*/[\rho gd^3]$

The numerical value of the generation time $T\sqrt{(g/d)}$ indicated in this table may be different from the value of the generation time indicated in table T4.3. When calculating the integrals of the motion, the range of integration was determined by the time instant when the plate velocity first became zero. This range defines one measure of the characteristic generation time and it is listed in the table T4.4. Another measure of the generation time is the time indicated by the function generator ; this value was used in table T4.3. Under ideal operating conditions the two values are identical; however, the response of the hydraulic system often distorts the generation time specified by the function generator. This difference is more prominent in the generation of type P waves.

REFERENCES

Ablowitz, M.J. 1971 Applications of Slowly Varying Nonlinear Dispersive Wave Theories. *Studies in Applied Mathematics* **V**, MIT, 329–344.

Abramowitz, M. and Stegun, I.A.,1972 *Handbook of Mathematical Functions.* Eighth Edition, New York; Dover Publications, 1046pp.

Barker, J.W. and Whitham, G.B., 1980 The similarity solution for a bore on a beach. *Comm. of Pure and Applied Math.* **33**, 447–460.

Battjes, J.A. 1971 Runup distributions of waves breaking on slopes. *Proc. ASCE* **WW1**, 91–114.

Battjes, J.A. and Roos, A. 1971 *Characteristics of flow in the run-up of periodic waves.* Report No. 75–3, Dept. of Civil Engineering, Delft University of Technology, 160 pp.

Boussinesq, M.J., 1872 Theorie des ondes et des remous qui se propagent le long d'un canal rectangulaire horizontal, en communiquant au liquide contenu dans ce canal de vitesses sensiblement pareilles de la surface au fond. *Journal de Mathematiques Pures et Appliquees (Series 2)***17**, 55–108.

Camfield, F.E. 1980 *Tsunami engineering.* Special Report No 6 Coastal Engineering Research Center, Fort Belvoir, VA 222pp.

Camfield, F.E. and Street, R.L. 1969 Shoaling of solitary waves on small slopes. *Proc. ASCE* **WW95**, 1–22.

Carrier, G. F. 1966 Gravity waves of water of variable depth. *J. Fluid Mech.* **24**, 641–659.

Carrier, G.F. 1971 The dynamics of tsunamis. *Mathematical Problems in the Geophysical Sciences.* Proc. of the 6th Summer Seminar on Applied Mathematics, Rennselaer Polytechnic Institute, Troy, NY, 1970. American Mathematical Society.

Carrier, G.F. and Greenspan, H.P. 1958 Water waves on finite amplitude on a sloping beach. *J. Fluid Mech.* **17**, 97–110.

Carrier, G.F., Krook, M. and Pearson, C.E. 1966 *Functions of a complex variable.* McGraw Hill, 438pp.

Carrier, G.F. and Noiseux, C.F. 1983 The reflection of obliquely incident tsunamis.*J. Fluid Mech.* **133**, 147–160.

Chwang, A.T. 1978 Hydrodynamic pressures of sloping dams during earthquakes. *J. Fluid Mech.* **87**, 343–387.

Chwang, A.T. 1983 Nonlinear hydrodynamic pressure on an accelerating plate. *Phys. Fluids* **26**, 383–387.

Chwang, A.T. and Housner, G.W. 1978 Hydrodynamic pressures on sloping dams during earthquakes. Momentum Method *J. Fluid Mech.* **87**, 335–341.

Hall, J.V. and Watts, J.W. 1953 *Laboratory investigation of the vertical rise of solitary waves on impermeable slopes.* Tech. Memo. No. 33, Beach Erosion Board, US Army Corps of Engineers. 14 pp.

Dally, W.R., Dean, R.G. and Darlymple, J.X. 1985 A model for breaker decay on beaches. , *Proc. ASCE*, 19th Coastal Engineering Conference, 1984, Houston, Texas, 82–98.

French, J.A. 1969 *Wave uplift pressures on horizontal platforms.* W.M. Keck Laboratory of Hydraulics and Water Resources, Report No KH-R-19 California Institute of Technology, Pasadena, CA.

Gardner, C.S., Green, J.M., Kruskal, M.D. and Muira, R.M. 1967 Method for solving the Korteweg-de Vries equation. *Physical Review Letters* **19**, 1095–1097.

Gerald, B.F. 1983 *Applied Numerical Analysis*, New York, Addison-Wesley Publishing Company, New York, 570pp.

Gilbert, G., Thompson, D.M. and Brewer, A.J. 1971 Courbes de calcul pour batteurs de houle reguliere et aleatoire. *J. Hydraulics Res.* **9**, 163–196.

Gjevik, B. and Pedersen, G. 1981 *Run-up of long waves on an inclined plane*. Preprint Series Inst. of Math. Univ. of Oslo, ISBN 82-553-0453-3.

Gopalakrishnan, T.C. 1978 *Galerkin finite element analysis of wave shoaling and runup*. Ph.D. Thesis, Center for Marine and Coastal Studies, North Carolina State University, Rayleigh, N.C. 200pp.

Goring, D.G. 1978 *Tsunamis – the propagation of long waves onto a shelf*. Report No KH-R-38 W. M. Keck Laboratory of Hydraulics and Water Resources, California Institute of Technology, Pasadena, CA, 337 pp.

Hammack, J.L. 1972 *Tsunamis – A model of their generation and propagation*. Report No KH-R-28, W.M. Keck Laboratory of Hydraulics and Water Resources, California Institute of Technology, Pasadena, CA, 261 pp.

Havelock, T.H. 1929 Forced surface waves on water. *Phil. Mag.,* **8**,569–576.

Heitner, K.L. 1969 *A mathematical model for calculation of the run-up of tsunamis*. Ph.D. Thesis, California Institute of Technology, Pasadena, CA, 119 pp.

Heitner, K.L. and Housner G.W. 1970 Numerical model for tsunami run-up. *Proc. ASCE* **WW3**, 701–719.

Hibberd, S. 1977 *Surf and run-up*. Ph.D. Thesis, University of Bristol, Great Britain, 124 pp.

Hibberd, S. and Peregrine, D.H. 1979 Surf and run-up on a beach : a uniform bore. *J. Fluid Mech.* **95**, 323–345.

Ho, D.V. and Meyer, R.E. 1962 Climb of a bore on a beach. Part 1. Uniform beach slope. *J. Fluid Mech.* **14**, 305–318.

Houghton, D.D. and Kasahara, X.X. 1968 Nonlinear shallow fluid over an isolated ridge. *Comm. Pure and Applied Mathematics,* **21**.

Hunt, I.A. Jr. 1959 Design of seawalls and breakwaters. *Proc. ASCE* **WW3**, 123–152.

Iribarren, C.R. and Nogales, C. 1949 *Protection de Ports,* **II**, XVIIth Int. Nav. Congress, Lisbon, 31–80.

Kaplan, K. 1955 Generalized laboratory study of tsunami runu-up. Tech. Memo 60, Beach Erosion Board, U.S. Army Corps of Engineers.

Kaplan, K. 1956 Design problems involved in protection from tsunamis. *Trans. ASCE* **WW3**, 968-1–969-1.

Kaup, D.J. and Newell, A.C. 1978 Solitons as particles, oscillators, and in slowly changing media: a singular perturbation theory. *Proc. R. Soc. Lond. (A)* **361**, 413–466.

Keller, H.B., Levine, D.A. and Whitham, G.B. 1960 Motion of a bore over a sloping beach. *J. Fluid Mech.* **7**, 302–316.

Keller, J.B. 1963 Tsunamis – water waves produced by earthquakes. *Proceedings of the Tsunami Meetings Tenth Pacific Science Congress*, Honolulu, August-September 1961. (ed. Cox,D. C.) Monograph No. 24 Paris National Geophysics Institute, 154–166.

Keller, J.B. and Keller, H.B. 1964 *Water wave run-up on a beach.* ONR Research Report Contract No NONR-3828(00), Dept. of the Navy, Washington, D.C.. 40 pp.

Kennard, E.H. 1949 Generation of surface waves by a moving partition. *JMM* **7**, 303–312.

Kim, S. K.,Liu, P.L-F. and Liggett, J.A. 1983 Boundary integral equation solutions for solitary wave generation propagation and run-up. *Coastal Engineering* **7**, 299–317

Kirkgoz, M.S. 1983 Breaking and run-up of long waves in *Tsunamis - Their Science and Engineering.* (eds. Iida, K. and Iwasaki T.) ,Tokyo: Terra Scientific Publishing Co., 467–478.

Kishi, T. 1963 Transformation, breaking and run-up of a long wave of finite height, *Proc. ASCE,* Eighth Conference of Coastal Engineering, Mexico City, November 1962. (ed. Johnson, J.W.), 60–76.

Ko, K. and Kuehl, H.H. 1978 Korteweg-deVries Soliton in a Slowly Varying Medium. *Phys. Rev. Let.* **40**, 233–236.

Korteweg, D.J. and deVries, G. 1895 On the change of form of long waves advancing in a rectangular canal, and on a new type of long stationary wave *London, Edinburgh, and Dublin Philosophical Magazine, Series 5,* **39**, 422–443.

Lepelletier, T.G. 1980 *Tsunamis- Harbor Oscillations Induced by Nonlinear Transient Lonf waves.* W.M. Keck Laboratory of Hydraulics and Water Resources, Report No KH-R-41, California Institute of Technology, Pasadena, California.

Johnson, R.S. 1973 On the development of a solitary wave moving over an uneven bottom. *Proc. Camb. Phil. Soc.* **73**, 183–203.

Lax, P. and Wendroff, B. 1960 Systems of conservation laws. *Communications of Pure and Applied Mathematics* **XIII**, 217–237.

LeMehaute, B. 1962 On non-saturated breakers and the wave run-up. *Proc. ASCE*, 8th Conference on Coastal Engineering,1962, Mexico City,Mexico, 7–92.

Longuet-Higgins, M.S. and Stewart, R.W. 1962 Radiation stresses and mass transport in gravity waves with applications to surf beats. *J. Fluid Mech.* **13**, 529–562.

Longuet-Higgins, M.S. and Cokelet, E.D. 1970 The deformation of steep surface waves on water: I. A numerical method of computation. *Proc. R. Soc. Lond. (A)* **350**, 1–26.

Lynch, D.K. 1982 Tidal bores. *Scientific American,* **247**, 146–156.

Madsen, O.S. and Mei, C.C. 1969 The transformation of a solitary wave over an uneven bottom. *J.Fluid Mech.* **39**, 781–791.

Mano, A. 1983 *Personal communication.*

Meyer, R.E. and Taylor, A.D. 1972 Run-up on beaches. *Waves on beaches and resulting sediment transport* (ed. Meyer, R. E.), New York: Academic Press, 357–411.

Miles, J.W. 1979 On the Korteweg-deVries equation for a gradually varying channel. *J. Fluid Mech.* **91**, 181–190.

Miller, R.L. 1968 Experimental determination of run-up of undular and fully developed bores. *J. Geophys. Res.* **73**, 4497–4510.

Montenegro, L. 1984. *Personal communication.*

Naheer, E. 1977 Stability of bottom armoring under the attack of solitary waves. Report No KH-R-34, W. M. Keck Laboratory of Hydraulics and Water Resources, California Institute of Technology, Pasadena, CA, 256pp.

von Neumann, J. and Richtmeyer, R.D. 1950 A method for the numerical calculation of hydrodynamic shocks. *J. Appl. Phys* **21**, 232pp.

Okoye, J.K. 1970 *Characteristics of transverse mixing in open channel flows.* W.M. Keck laboratory of Hydraulics and Water Resources, Report No KH-R-34, California Institute of Technology, Pasadena, California.

Pedersen, G. and Gjevik, B. 1983 Run-up of solitary waves. *J. Fluid Mech.* **135**, 283–290.

Peregrine, D.H. 1966 Calculations of the development of an undular bore. *J. Fluid Mech.* **25**, 321–330.

Peregrine, D.H. 1967 Long waves on a beach *J. Fluid Mech.* **27** , 815–827.

Peregrine, D.H. 1980 *Personal communication.*

Richtmeyer, R.D. and Morton, K.W. 1967 *Difference methods for initial value problems.*, New York: Interscience Publishers, 405pp.

Russel, J.S. 1845 Report on Waves. *Rep. Meet. Brit. Assoc. Adv. Sci. 14th.* York 1844, 311-390. London : John Murray.

Saeki, H., Hanayasu, S., Ozaki, A. and Takagi, K. 1971 The shoaling and run-up height of the solitary wave. *Coastal Engineering in Japan* **14**, 25–42.

Saville, T.Jr. 1956 Wave run-up on shore structures. *Trans.ASCE* **WW2**, 925-1–925-14.

Shen, C.C. 1965 *Selection and design of a bore generator for the Hilo Harbor tsunami model.*, Hydraulic model investigation, Research Report No 2-5 U.S. Army Engineer Waterways Experiment Station, Vicksburg, MI, 94 pp.

Shen, C.C. and Meyer, R.E. 1963 Climb of a bore on a beach. Part 3. Run-up. *J. Fluid Mech.* **16**, 113–125.

Shuto, N. 1967 Run-up of long waves on a sloping beach. *Coastal Engineering in Japan* **10**, 23–38.

Shuto, N. 1972 Standing waves in front of a sloping dike. *Coastal Engineering in Japan* **15**, 13–23.

Sielecki, A. and Wurtele, M.G. 1970 The numerical integration of the nonlinear shallow-water equations with sloping boundaries. *J. Computational Physics* **6**, 219–236.

Skjelbreia, J.E. 1982 *Personal communication.*

Skjelbreia, J.E. 1983 *Personal communication.*

Smyth, N.F. 1984 *Solitons on a beach and related problems. Modulated capillary waves.* Ph.D. Thesis California Institute of Technology, Pasadena, CA, 146 pp.

Souquet, F. 1951 Les appareils generateurs de houle en laboratoire. *Le Houille blanche* **6**, 723–737.

Stoker, J.J. 1947 Surface waves in water of variable depth. , *Qu. App. Math* **5**, 1–54.

Togashi, H. and Nakamura, T. 1977 An experimental study of tsunami run-up on uniform slopes. *Coastal Engineering in Japan* **20**, 95–110.

Togashi, H. 1981 *Study on tsunami run-up and countermeasure.* English translation of Ph.D. Thesis, Tohoku University, Sendai, Japan, 1976, 295 pp.

Togashi, H. 1983 Shoreline wave height and land run-up height of tsunamis on uniformly sloping beaches. *Tsunamis – Their Science and Engineering.* (eds. Iida, K. and Iwasaki, T.) ,Tokyo: Terra Scientific Publishing Co., 495–509.

Ursell, F. ,Dean, R.G. and Yu, Y.S. 1963 Forced small- amplitude water waves: a comparison of theory and experiment. *J. Fluid Mech.* **7**, 33–52.

von Karman, T. 1933 Discussion of water pressures on dams during earthquakes. *Trans. ASCE* **98**, 434–436.

Warren, P.M. 1985 Minoan Palaces, *Scientific American* **253**,94–103.

Westergaard, H.M. 1933 Water pressures on dams during earthquakes. *Trans. ASCE* **98**, 418–433.

Whitham, G.B. 1974 *Linear and Nonlinear Waves.*, New York: John Wiley & Sons, 636 pp.

Whitham, G.B. 1958 On the propagation of shock waves through regions of non-uniform area of flow. *J. Fluid Mech.* **4** , 337–360.

Zanger, C.N. and Haefeli, R.J. 1952 Electric analog indicates effects of horizontal earthquake shock on dams. *Civil Engineering* **22**, 278–279.